

Volume 1

**A  
R  
O  
D**

**AIRBORNE**

**ANGING**

**and**

**RBIT**

**ETERMINATION**

**DESIGN FEASIBILITY REPORT**

FACILITY FORM 502

N 66-15816

(ACCESSION NUMBER)

365

(PAGES)

CR 69571

(NASA CR OR TMX OR AD NUMBER)

(THRU)

1

(CODE)

09

(CATEGORY)

GPO PRICE \$

CFSTI PRICE(S) \$

Hard copy (HC) 7.00

Microfiche (MF) 2.00

ff 853 July 65

**IBM**

**FINAL REPORT**

5/ 29367

# **AROD Design Feasibility Report**

March 20, 1963

Final Report for NASA Contract No. NAS 8-5098

PREPARED FOR

GEORGE C. MARSHALL SPACE FLIGHT CENTER

NASA

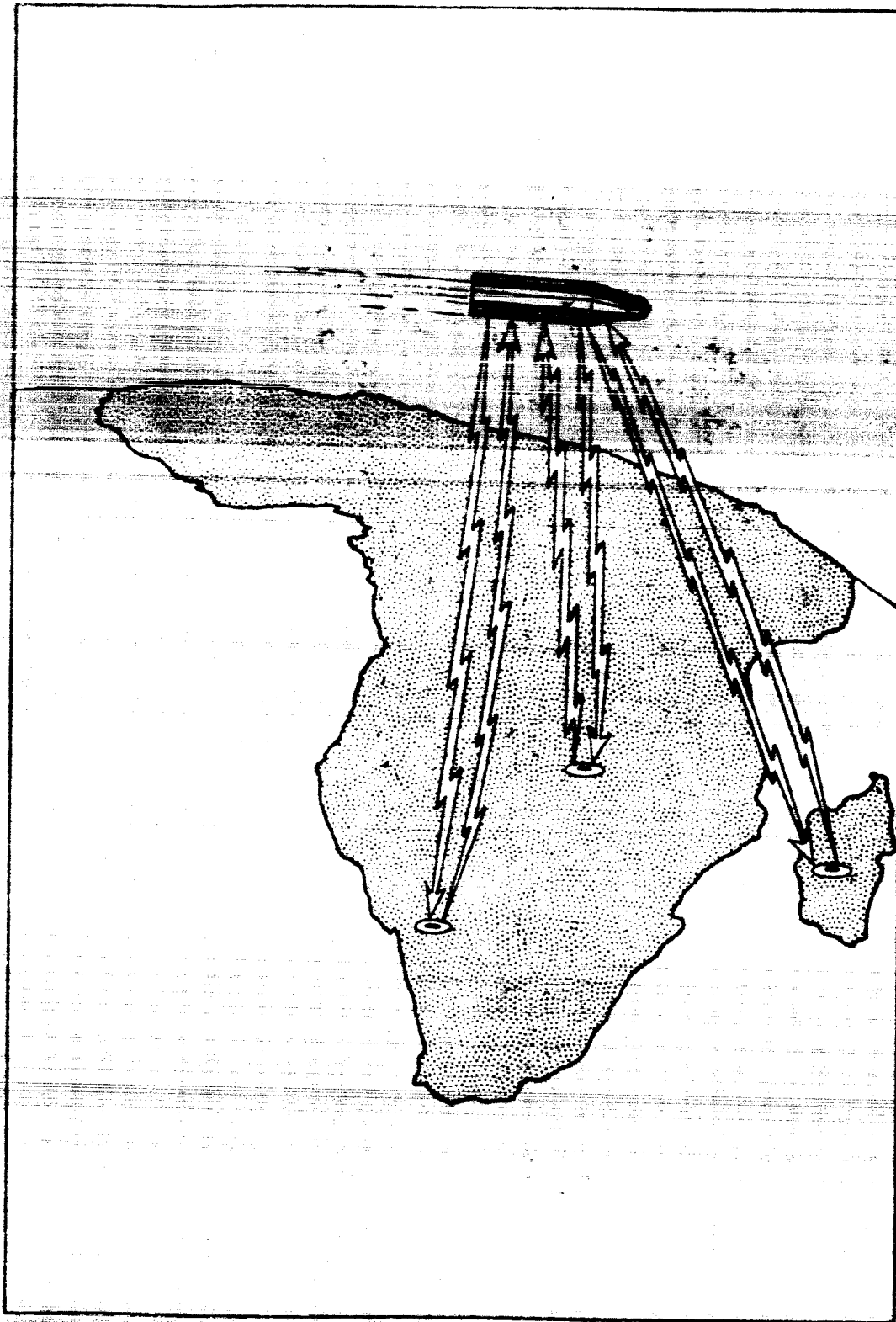
HUNTSVILLE, ALABAMA

PROJECT MANAGER: A. VALAKOS

INTERNATIONAL BUSINESS MACHINES CORPORATION

Federal Systems Division

ROCKVILLE, MARYLAND



*Artist's Concept of the AROD System*

### Abstract

*The Airborne Ranging and Orbit Determination (AROD) system is a precise trilateration system for orbit determination in which range and range rate sensors are located in the spacecraft and transponders are located on the ground. The feasibility and practicality of AROD are demonstrated by means of families of curves indicating the equipment penalties required to achieve various levels of measurement accuracy. To derive these curves, all sources of error in the basic AROD measurements - range and range rate - are considered. In addition, surveying errors and the effects of varying spacecraft-ground station geometries are considered in determining overall system performance. A representative system design is presented with the following parameters: center frequency - 2000 Mc; spacecraft antenna gain-unity; spacecraft transmitter power output - 12.5 watts; spacecraft weight (est.) - 27 pounds; spacecraft input power requirements (est.) - 114 watts; ground transponder antenna gain - 13 db; ground transponder power output - 25 watts; system design margin - 10 db. With these parameters, the representative system provides a range measurement accuracy of 3 meters and a range rate measurement accuracy of .03 meters per second at a range of 1000 miles and an altitude of 500 miles.*

## CONTENTS

### VOLUME 1

	Page
<b>Section 1 INTRODUCTION AND SUMMARY</b>	<b>1</b>
1.1 Introduction	1
1.2 Summary	2
 <b>Section 2 SYSTEM ANALYSIS</b>	 <b>13</b>
2.1 Introduction	13
2.2 Sources of System Errors	14
2.2.1 Uncertainty of the Vacuum Velocity of Light	14
2.2.2 Propagation Errors	15
2.2.3 Equipment Errors	16
2.2.4 Geodetic Errors	26
2.3 Geometrical Dilution of Precision	29
2.4 Smoothing	38
2.5 Equipment Performance Objectives (Error Budget)	40
2.5.1 Uncertainty of the Vacuum Velocity of Light	42
2.5.2 Propagation Errors	42
2.5.3 Equipment Errors	44
2.5.4 Total Errors	52
2.6 Summary	52
 <b>Section 3 SYSTEM DESIGN</b>	 <b>53</b>
3.1 Introduction	53
3.2 Principle of Operation	56
3.2.1 Spacecraft Equipment	56
3.2.2 Ground Station Equipment	65
3.3 Parametric Analysis	68
3.3.1 Signal Parameters	68
3.3.2 Choice of Operating Frequency	70
3.3.3 Range Equation Parameters	71
3.3.4 Signal Tracking Parameters	76
3.4 Comparison of the Transponder Design Approach to Other Approaches	80
3.5 Trade-off Analysis	84

Section 4	EQUIPMENT IMPLEMENTATION	87
4.1	Spacecraft Equipment	87
4.1.1	Spacecraft Transmitter	87
4.1.2	Wideband Receiver	105
4.1.3	Phase Locked Loops	111
4.1.4	Range Rate Measurements	137
4.1.5	Range Measurement Circuit	140
4.1.6	Weight and Power Estimates	145
4.1.7	Equipment Interfaces	149
4.2	Ground Station Equipment	155
4.2.1	Antenna	155
4.2.2	Ground Transmitter	162
4.2.3	Ground Station Signal Processing	168
4.2.4	Multipath Effects	177
Section 5	CONCLUSIONS AND RECOMMENDATIONS	185
5.1	Conclusions	185
5.2	Recommendations for Phase B AROD Study	186
5.2.1	Study Plan	186
5.2.2	System Analysis	187
5.2.3	System Design	190
5.2.4	Investigation of Wide Band Modulation Techniques	192
References		195

## VOLUME 2

Appendices		
A	Geometrical Dilution of Precision	A-1
B	Errors Introduced by the Propagation Medium	B-1
C	Geodetic Aspects of AROD	C-1
D	Mathematical Derivations	D-1

# VOLUME 1

## ILLUSTRATIONS

Figure		Page
1	Range Measurement Performance as a Function of Spacecraft Penalty	4
2	Range Rate Measurement Performance as a Function of Spacecraft Penalty	5
3	Simplified Block Diagram	7
4	Typical AROD System Performance-Position	9
5	Typical AROD System Performance-Velocity	10
6	Propagation-Induced Range Errors at 2 Gc	17
7	Propagation-Induced Range Rate Errors at 2 Gc	18
8	Test Paths	32
9	System Performance at $h = 90$ Nautical Miles	34
10	System Performance at $h = 500$ Nautical Miles	35
11	System Performance at $h = 2000$ Nautical Miles with a 500 Nautical Mile Baseline	36
12	System Performance at $h = 2000$ Nautical Miles with a 1000 Nautical Mile Baseline	37
13	Influence of Range Measurement Errors and Station Coordinate Errors on Positional Accuracy	39
14	Vehicle Equipment Functional Block Diagram	59
15	Block Diagram of Range Ambiguity Resolving Tones Tracking Circuits	64
16	Ground Transponder Block Diagram	67
17	Amplitron Phase Pushing Measurements (QKS997)	90
18	Amplitron Thermal Stability Measurements (QKS997)	92
19	AROD Spacecraft Transmitter R-F Spectrum	99
20	Block Diagram, AROD Vehicle Transmitter-Receiver R-F Section	100
21	Block Diagram AROD Radio Frequency and Range Tone Synthesizer	104

Figure		Page
22	Four Station AROD Spectrum-as seen by Vehicle Receiver (Zero Doppler Assumed)	106
23	Block Diagram AROD Vehicle Receiver, IF and Phase-Lock Section	110
24	Basic Phase-Locked Loop	113
25	Carrier Acquisition and Tracking Loop	115
26	Fine Ranging Tone Phase-Locked Loop	118
27	Low Pass Filter	123
28	Linearized Phase Transfer Model	131
29	Frequency Ramp	136
30	Fine Ranging Tone Down Converter	141
31	Diode Matcher	141
32	Phase Transfer Model	143
33	Ground Antenna Beam Pattern	156
34	Cross Section of the Recommended Antenna	158
35	Antenna Layout	160
36	Radiation Center Errors in Azimuth Plane	162
37	Radiation Center Errors in Vertical Plane	162
38	Differential Phase Shift Between Two Traveling Wave Tubes	167
39	Three Filter R-F Multiplexer	171
40	Single Sideband Up-Converter	176
41	Multipath Interference at Ground Antenna	180
42	Vector Diagram of Multipath Signals	181
43	Design Study Phasing Chart	188

## VOLUME 1

### TABLES

Table		Page
1	Parameters of a Representative AROD System	6
2	Comparative Accuracies of Methods for the Determination of Geodetic Positions Over Extended Land Areas	28
3	Estimated Repeatability of Methods for the Determination of a Ship's Position	30
4	Measurement Error Summary for Various Points in the AROD System	43
5	Parameters of the Representative AROD System	57
6	AROD Signal Parameters	69
7	Trade-Off Table	85
8	Constant Parameter Carrier Loop	120
9	Variable Parameter Carrier Loop	121
10	Fine Ranging Tone Loop	122
11	Spacecraft AROD Equipment Estimates	148
12	AROD Frequency Allocation Table	164

## Section 1

### INTRODUCTION AND SUMMARY

**This document is the final report for the Airborne Ranging and Orbit Determination (AROD) Feasibility Study performed for NASA's Marshall Space Flight Center, Huntsville, Alabama, under Contract NAS 8-5098.**

The Study was conducted by the Federal Systems Division of the IBM Corporation at Rockville, Maryland, with Geonautics, Inc. participating in a special portion as a subcontractor. The period of performance covered by this report is from June 26, 1962 to December 26, 1962.

#### 1.1 Introduction

The AROD System is a precise orbit determination system in which range and range rate sensors are located in the spacecraft and transponders are located on the ground. Range and range rate with respect to three or four ground stations are measured simultaneously and the position and velocity of the spacecraft are determined in real time.

Reversing the location of the sensors and transponders with respect to conventional range and range rate systems results in many significant advantages for the AROD system; the more important of these advantages are:

- Real time orbit determination without the requirement for intercommunications between the ground stations.
- Simple, reliable, unattended ground stations with low initial and operating costs.
- More efficient utilization of the available vehicle power (by a factor of three to four) because a unique r-f transmission to each ground station is not required.

In addition, the AROD system has the good geometrical characteristics of all range and range rate systems, thereby providing a high degree of accuracy in a large volume surrounding the ground stations.

The primary purpose of the AROD Feasibility Study was to determine the technological and practical feasibility of the AROD concept. Toward this end, the general approach of determining the economic factors, or equipment penalties, associated with achieving various accuracies was followed. Spacecraft weight and input power requirements and ground station complexity were assumed to be the penalty factors of greatest concern, and curves were sought relating these factors to the accuracy with which range and range rate could be measured. To obtain the information necessary for these curves, an analysis of all error sources was undertaken and a representative system design was evolved in considerable detail, thereby permitting meaningful estimates of the system penalty factors.

For this study, the only mission requirement established was that the AROD system must be capable of handling spacecraft at altitudes as high as 2000 nautical miles and as low as 90 nautical miles. The modulation techniques that were investigated were restricted to continuous wave "Sidetone Ranging" schemes. From the RFP for the study, position and velocity were taken to be the parameters computed from the range and range rate measurements. Incremental accuracies, which would be much better than the absolute accuracies investigated, were not a primary consideration in the Feasibility Study.

## 1.2 Summary

The principal conclusion of the Feasibility Study is that the AROD concept is feasible. No technological breakthroughs are required to implement the system and, in fact, a representative state-of-the-art system has been designed. This system is discussed in some detail in this report.

The two most important results of the study are the performance curves relating measurement accuracies to equipment penalties and a system design that represents an economical approach to the operational

AROD configuration. Figures 1 and 2 summarize the results of the feasibility investigation in a form that is not restricted to a particular performance objective or a specific system penalty. Rather, the more general approach of indicating the spacecraft and ground station penalty factors required to achieve a given level of measurement capability has been used. From these curves, a potential user can determine whether the penalties for his required accuracy are tolerable, and whether the AROD approach would have a lower overall system "cost" than other approaches.

The second principal result, the representative "design point" system, is summarized in Table 1 (Parameters of a Representative AROD System) and in the block diagram of the representative system (Figure 3). The vehicle equipment, which is entirely solid-state, radiates 12.5 watts of continuous wave power at a nominal carrier frequency of 2000 Mc. Horizon-to-horizon coverage is provided by the vehicle antenna. Included in the transmitted spectrum are supplemental carriers (or "sidetones") differing in frequency from the principal carrier. The sidetone with the largest frequency difference, 5 Mc, is used to determine fine range, and a number of additional tones are provided to resolve all range ambiguities. All of the carrier and range tone signals are harmonically related and are synthesized from an ultra-stable oscillator.

The ground transponder features a multi-beam antenna which provides considerable gain with almost complete hemispherical coverage. A receiver associated with each of the 13 beams of the antenna senses an active beam condition and is switched to the input of a single transmitter chain. Translation of the received signals by 60 Mc (nominally) is effected by an ultra-stable oscillator prior to application to the transmitter chain. The nominal 25-watt output of the transmitter chain is directed by a ferrite switching matrix to the active beam.

The spacecraft receiver amplifies and separates the signals retransmitted from three or four ground stations and applies these signals to tracking filters. Phase locked loops extract the carrier and range tone signals which are then compared to the transmitted spectrum in digital frequency and phase measuring circuits for the determination of range rate

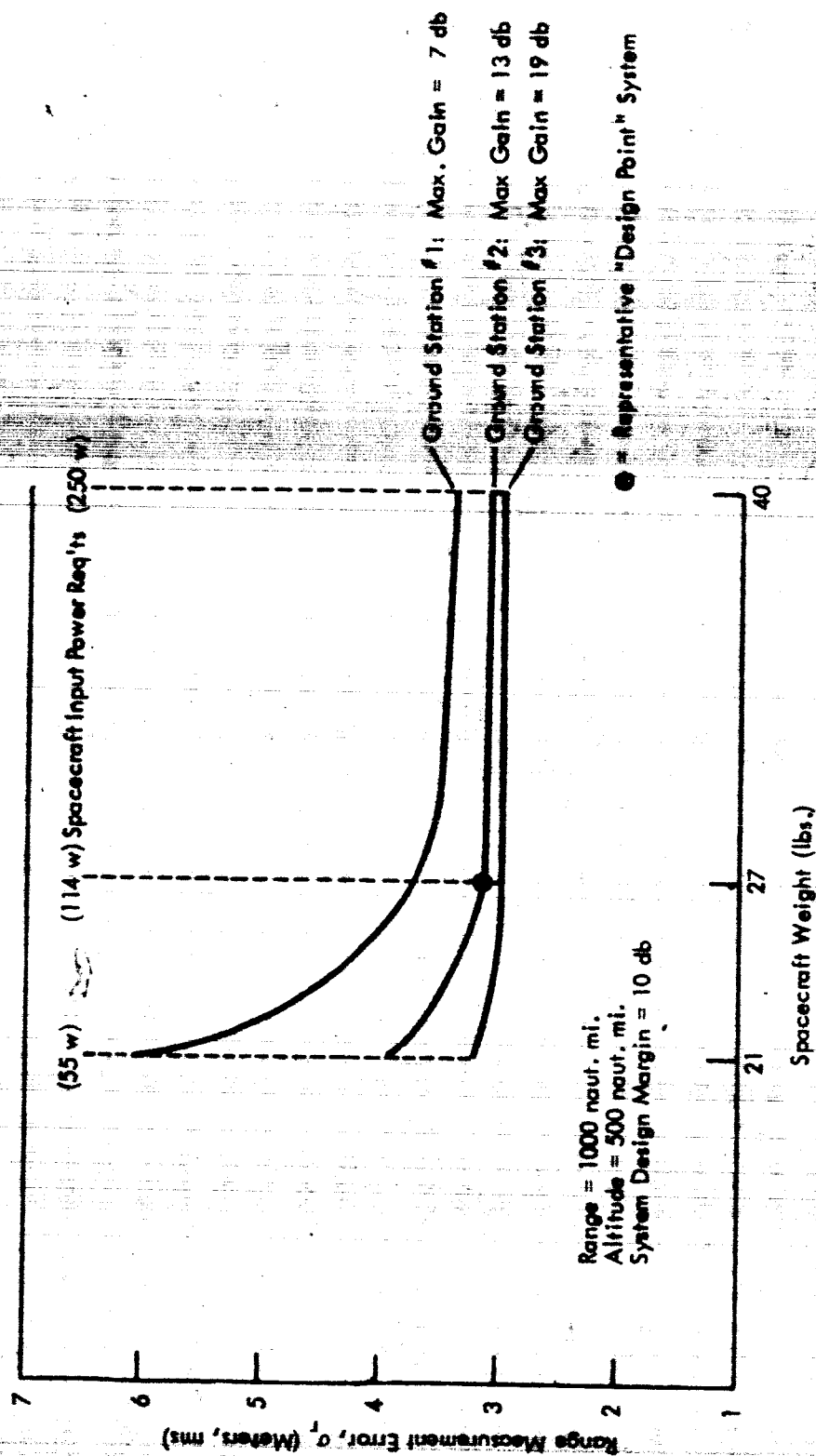


Figure 1. Range Measurement Performance as a Function of Spacecraft Penalty

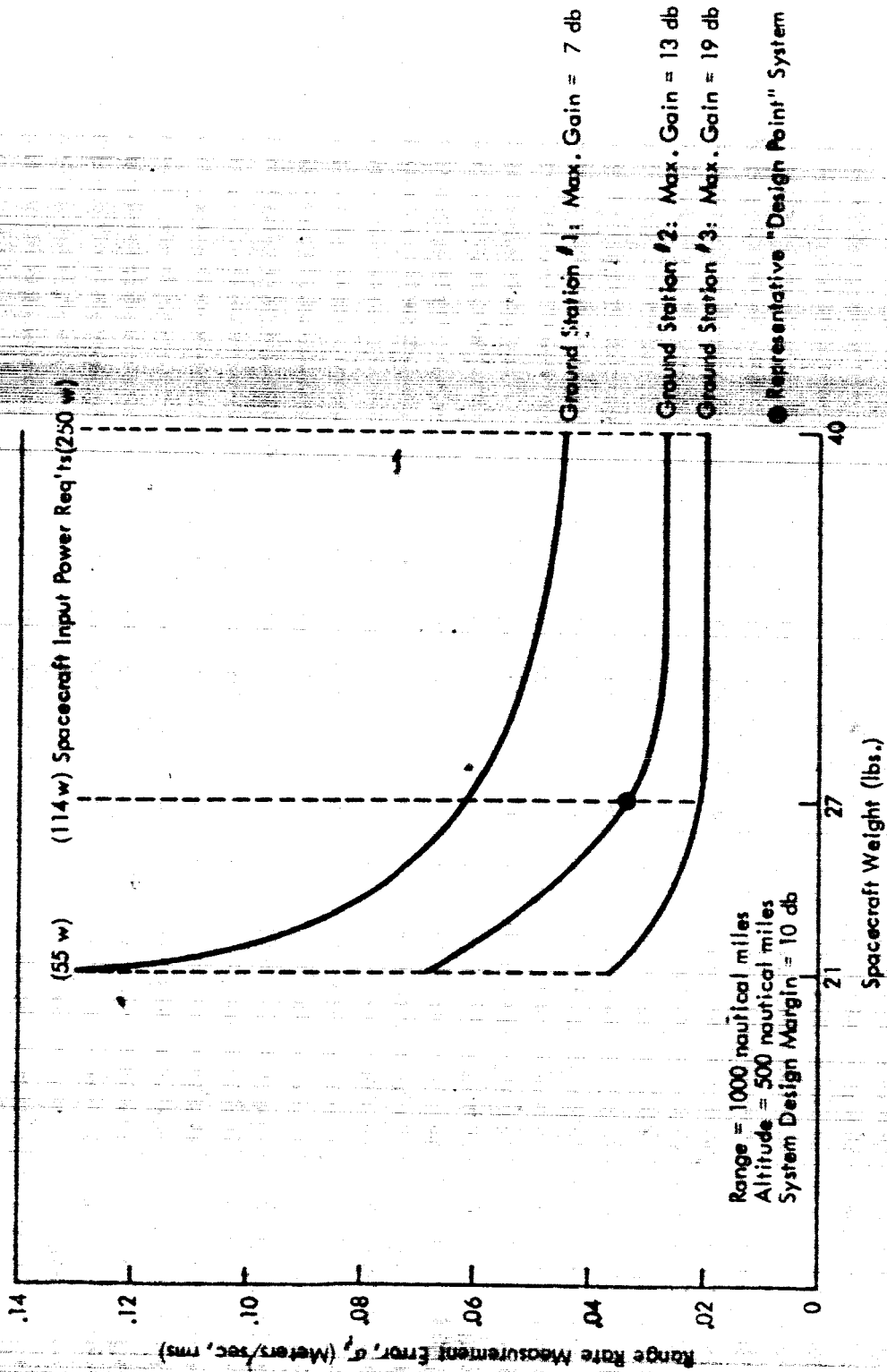


Figure 2. Range Rate Measurement Performance as a Function of Spacecraft Penalty

Table 1

Parameters of a Representative  
AROD System

VEHICLE EQUIPMENT

Center Frequency (Nominal)	2000 Mc
Antenna Gain	Unity
Antenna Coverage	Horizon-to-horizon
Transmitter Power Output	12.5 watts
Equipment Weight (Estimated)	27 lbs.
Equipment Power Input (Estimated)	114 watts
Equipment Volume (Estimated)	800 cubic inches

GROUND STATION EQUIPMENT

Translation Frequency (Nominal)	60 Mc
Antenna Gain	13 db (at 5° elevation angle) 7 db (at 90° elevation angle)
Number of Beams	13
Antenna Coverage	Omnidirectional in azimuth for elevation angles $\geq 5^\circ$
Transmitter Power Output (Nominal)	25 watts

SYSTEM DESIGN MARGIN

10 db

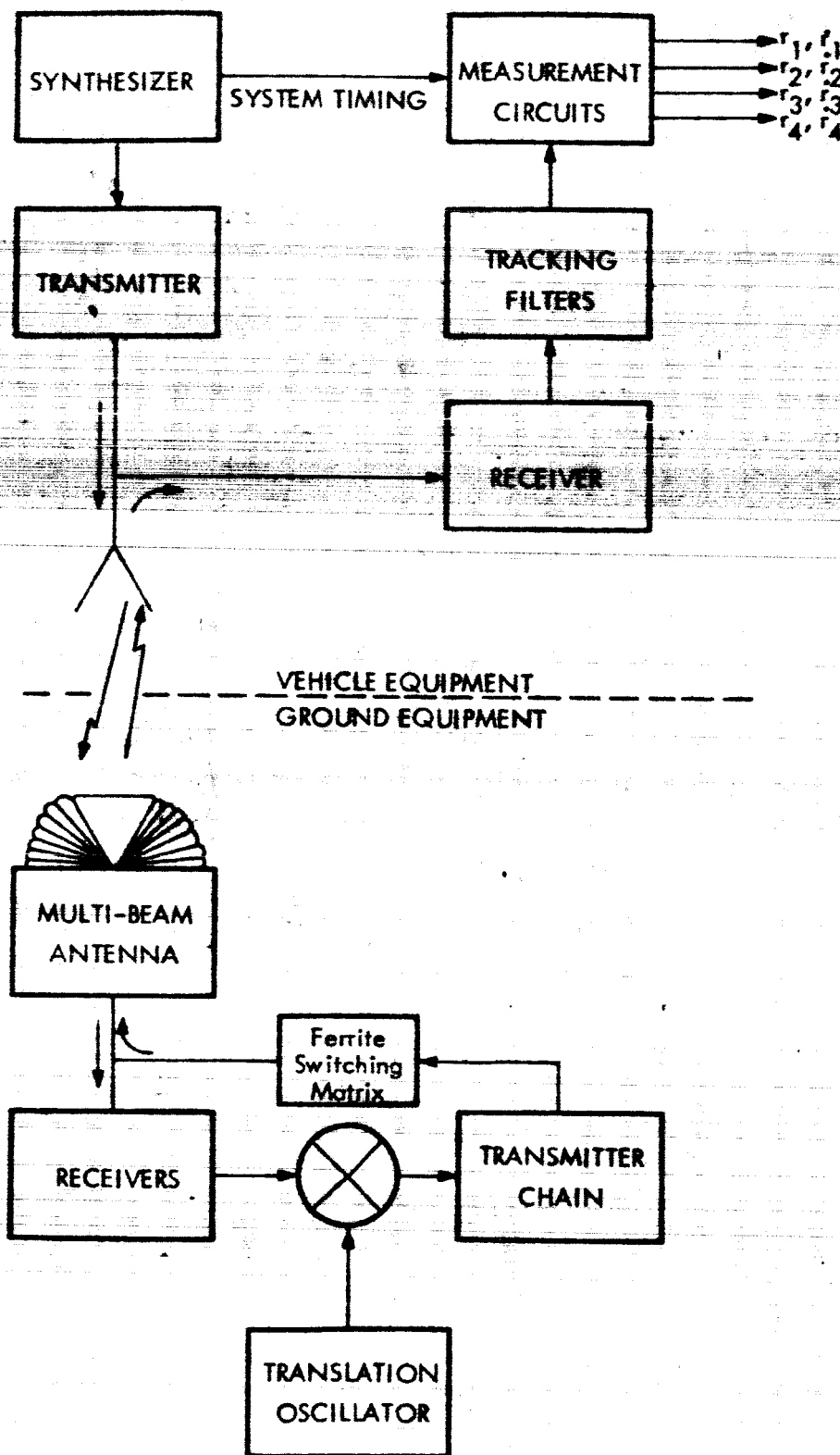


Figure 3. Simplified Block Diagram

and range. These data then enter the vehicle guidance computer where the computations required for orbit determination are performed. The penalties and performance for the representative system are shown in Figures 1 and 2.

The absolute accuracies depicted in Figures 1 and 2 include all error sources that affect the basic AROD range and range rate measurements. In addition to these sources, however, two other factors must be considered in determining the performance of the AROD system: uncertainties in the location of the ground transponders (geodetic errors); and the effects of spacecraft-ground station geometry. The influence of these factors and an estimate of the total AROD system performance can be seen in Figures 4 and 5. Figure 4 shows the radius of the "equivalent sphere"\* within which the true position of the spacecraft is known to a probability of 68%, as a function of the position of the spacecraft over the ground station complex. In Figure 5, the radius of the velocity uncertainty "sphere" for a probability of 68% is shown. Three altitudes covering the entire AROD operating envelope are indicated in these figures, with a range measurement error of three meters (rms) and a range rate measurement error of .05 meters per second (rms) taken as the representative measurement capabilities for the entire pass over the ground station complex. An important additional assumption for generating the curves in Figures 4 and 5 was that a representative value for the geodetic errors was seven meters; this value was determined from a geodetic analysis conducted by Geonautics, Inc. under a subcontract.

As was the Feasibility Study, this report is organized into three major categories: System Analysis, System Design, and Equipment Implementation. The system analysis study (Section 2) was undertaken to analyze the error sources in the AROD system and to establish reasonable equipment performance objectives. Consideration was given to the uncertainty in the vacuum velocity of light, errors introduced by the propagation medium, thermal noise errors, instrumentation errors, quantization errors, multipath

---

\*The sphere containing a volume equal to that of the true error ellipsoid. (See Appendix A).

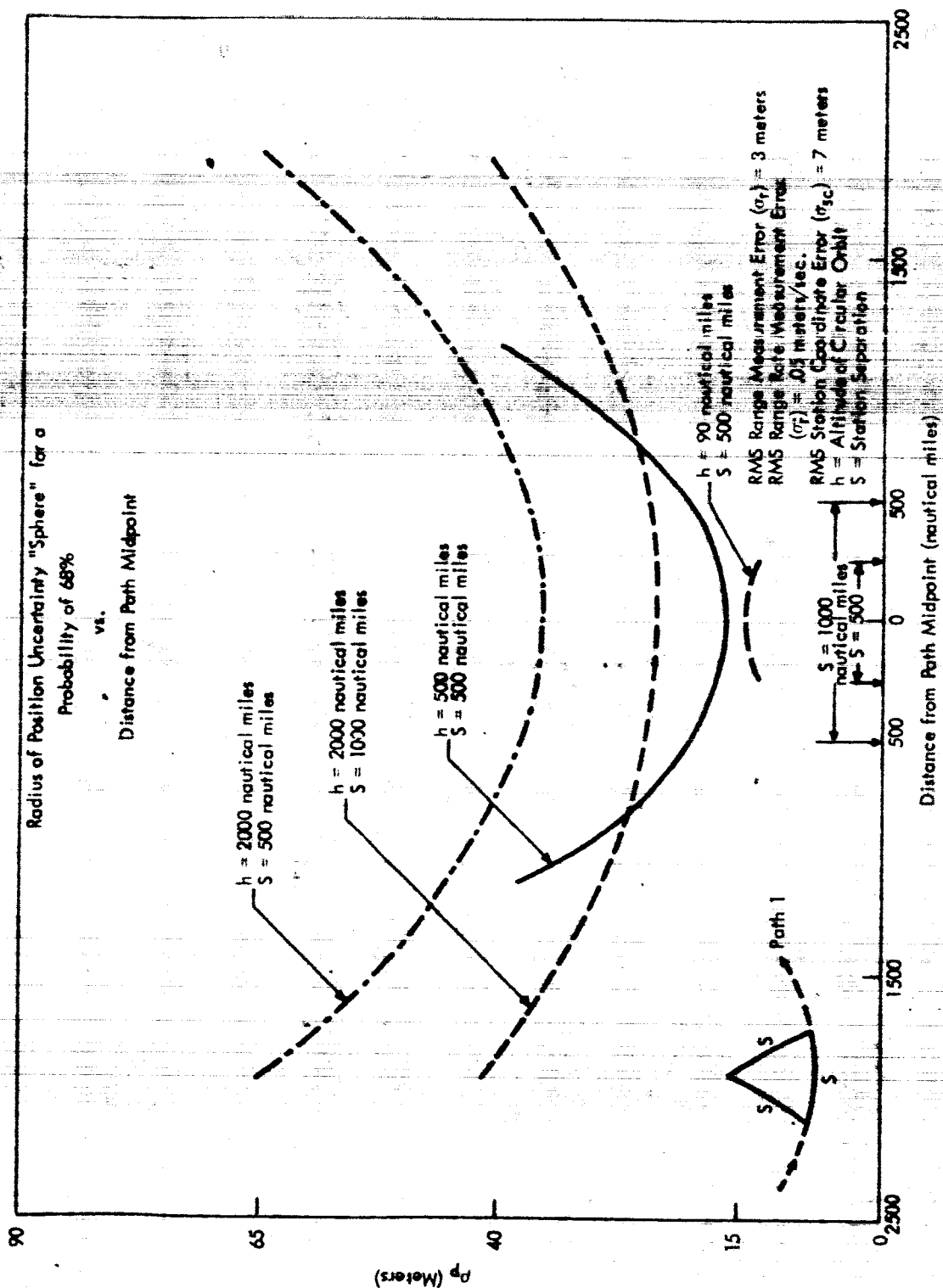


Figure 4. Typical AROD System Performance—Position



errors, and geodetic errors. By taking into account the penalties associated with controlling those sources of error which are affected by circuit and component design, the magnitudes of all the controllable sources of system error were budgeted in an economical manner.

In Section 3, System Design, the basis for choosing the recommended system design approach is presented. A procedure for selecting all the equipment parameters that significantly affect system penalty factors is also included.

The important implementation problems introduced by the recommended system design approach are detailed in Section 4. Major emphasis is given to the selection of the spacecraft transmitter output stage, the design of the ground antenna, and the appropriate characteristics for the phase locked loops.

The conclusions resulting from the study are summarized in Section 5 and a recommended program for the next phase of the AROD program is included.

Four appendices containing analyses that were of considerable importance to the Feasibility Study are contained in Volume 2.

## Section 2

### SYSTEM ANALYSIS

#### 2.1 Introduction

This section summarizes the results of the system analysis portion of the AROD Feasibility Study. The goal of this portion of the study (and of this section) is to determine reasonable performance objectives for the AROD equipment. To achieve this goal, the procedures followed in this section are:

1. The various sources of measurement error in the AROD system are defined and the functional relationships between the magnitudes of the errors and important system parameters are determined.
2. The effects of geodetic errors and various vehicle-ground station geometries on system performance are analyzed.
3. The improvements that can be achieved through the use of smoothing techniques are discussed.
4. Equipment performance objectives, in the form of an error budget, are established on the basis of estimates for the error magnitudes introduced by the various sources, the equipment penalties associated with reducing these errors, and estimates of the effects of geometry and smoothing.

The error budget, which is based upon reasonable measurement accuracy goals, establishes the performance objectives for the major portions of the AROD equipment. These objectives then form the basis for the AROD system design and tradeoff analyses (Section 3) and the equipment implementation considerations (Section 4).

## 2.2 Sources of System Errors

Before proceeding to an analysis of the error sources, a short discussion concerning the terminology used in this report is in order. "Measurement errors" refer to the inaccuracies (usually expressed as standard deviations) in the basic AROD measurements, range and range rate. "System errors" refer to the inaccuracies in the parameters computed from the basic measurements; from the RFP, the parameters assumed for the Feasibility Study were the spacecraft's position and velocity.

Contributing to the measurement errors is a source over which the AROD equipment designer has no control whatsoever (incomplete knowledge of the true value of the vacuum velocity of light), a source over which he has relatively little control (the propagation medium), and sources over which he can exercise strong or complete control (e.g., thermal noise, quantization errors, multipath). This last category is referred to as "equipment errors."

Contributing to the system errors are the uncertainty in the exact locations of the ground stations (geodetic errors) and the vehicle-ground station relative geometry, in addition to the measurement errors.

It is important to note that the errors in range, range rate, position, and velocity investigated in the Feasibility Study are absolute errors. Incremental errors in these quantities from one reading to the next could probably be made an order of magnitude smaller than the absolute errors by removing biased errors (e.g., uncertainty in vacuum velocity of light, geodetic errors) and smoothing thermal noise errors. Although an extensive investigation into incremental errors was beyond the scope of the Feasibility Study, they are a very proper subject for analysis in the next phase of the AROD program.

### 2.2.1 Uncertainty of the Vacuum Velocity of Light

Of all the sources of error in the AROD system probably none is so basic as the uncertainty in our knowledge of the vacuum velocity of light ( $c$ ). The estimate of this uncertainty given by Froome<sup>1</sup> is  $\pm 0.3$  km/sec or one part per million (standard error). Although this uncertainty is expected to be reduced, this well-accepted estimate<sup>2,3</sup> is satisfactory for the purposes of the Feasibility Study.

There is no means of making our measurements more accurately than the uncertainty in the knowledge of  $c$ . Therefore, rather than introducing unwarranted weight, power, volume, and cost penalties for equipment with accuracies an order of magnitude better than the uncertainty in  $c$ , the more practical approach is to set objectives for the equipment errors that are approximately the same order of magnitude.

### 2.2.2 Propagation Errors

The second source of AROD measurement errors to be discussed is the propagation medium. A study of the range and range rate errors introduced by the passage of electromagnetic energy through the atmosphere was conducted as a part of the system analysis portion of the Feasibility Study. The purpose of this study was twofold. First, it was necessary to determine the variation of the propagation errors with frequency and elevation angle\* to aid in the selection of the operating parameters for the AROD system. Second, it was necessary to estimate the errors as a function of elevation angle and vehicle altitude at the operating frequency (2 Go) selected as a result of the system design study summarized in Section 3.

The results of the investigation into propagation errors are contained in Appendix B. As indicated in that appendix, studies that had been performed up to the time of this investigation were not as complete and conclusive as desired for the AROD analysis; however, extensions of the propagation studies were beyond the scope of the AROD Feasibility Study. It is necessary, therefore, to treat the propagation error data as tentative, while awaiting the results of additional experiments currently underway or planned for the near future.

The magnitude of the propagation errors is a function of many variables, and for a general analysis of the errors the reader is referred to Appendix B. However, for the purposes of this section, the results of the propagation study can be summarized by presenting its conclusions and graphs of the magnitudes of the propagation errors at the selected operating frequency.

---

\*Elevation angle is used in its usual sense; see Appendix B, Figure B-7 for a specific definition.

In summary, the tentative conclusions of the propagation study are:

1. Unless a correction based upon the spacecraft's altitude and elevation angle is incorporated into the vehicle computer, propagation errors more than an order of magnitude greater than those due to the uncertainty in  $c$  will be introduced. It is recommended, therefore, that such a correction be included, using a "standard" (worldwide) atmosphere; utilization of local and/or real time atmospheric data is not justifiable. (The next conclusion assumes that a "standard" correction has been employed and refers to the residual errors after the application of such a correction.)

2. To avoid residual propagation errors that are an order of magnitude greater than those due to the uncertainty in  $c$ , it is recommended that the operating frequency be in the kilomegacycle region, and that AROD measurements be restricted to elevation angles greater than  $5^{\circ}$ .

To complete the summary of the propagation error study it is now convenient to anticipate the results of Section 3 and to present, in Figures 6 and 7, the propagation errors encountered at the selected operating frequency, 2Gc. The errors indicated in these figures are the residual errors (standard deviations) remaining after the application of a standard correction.

### 2.2.3 Equipment Errors

In this section, each source of error (in the equipment to be discussed in Sections 3 and 4) that is under the control of the equipment designer is identified and analyzed to determine the functional relationship between the magnitude of the error and the significant parameters of the AROD system. These relationships will be used later (in Section 2.5) to compute the error magnitudes and "budget" errors for the establishment of equipment performance objectives.

#### 2.2.3.1 Thermal Noise

In the range measuring circuits employed in the AROD spacecraft configuration,\* the error due to a finite signal-to-noise ratio can be obtained from:<sup>4</sup>

---

\*By direction of NASA's Contracting Officer's Representative the AROD Feasibility Study was restricted to the sidetone ranging system described in Section 3.

Note: These are residual errors remaining after the application of a "standard" correction.

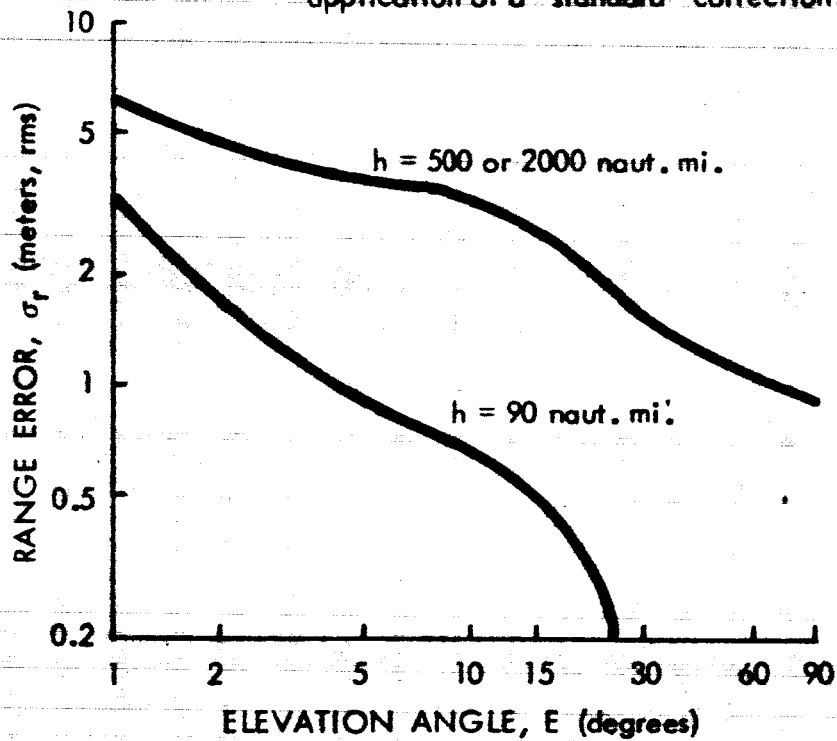
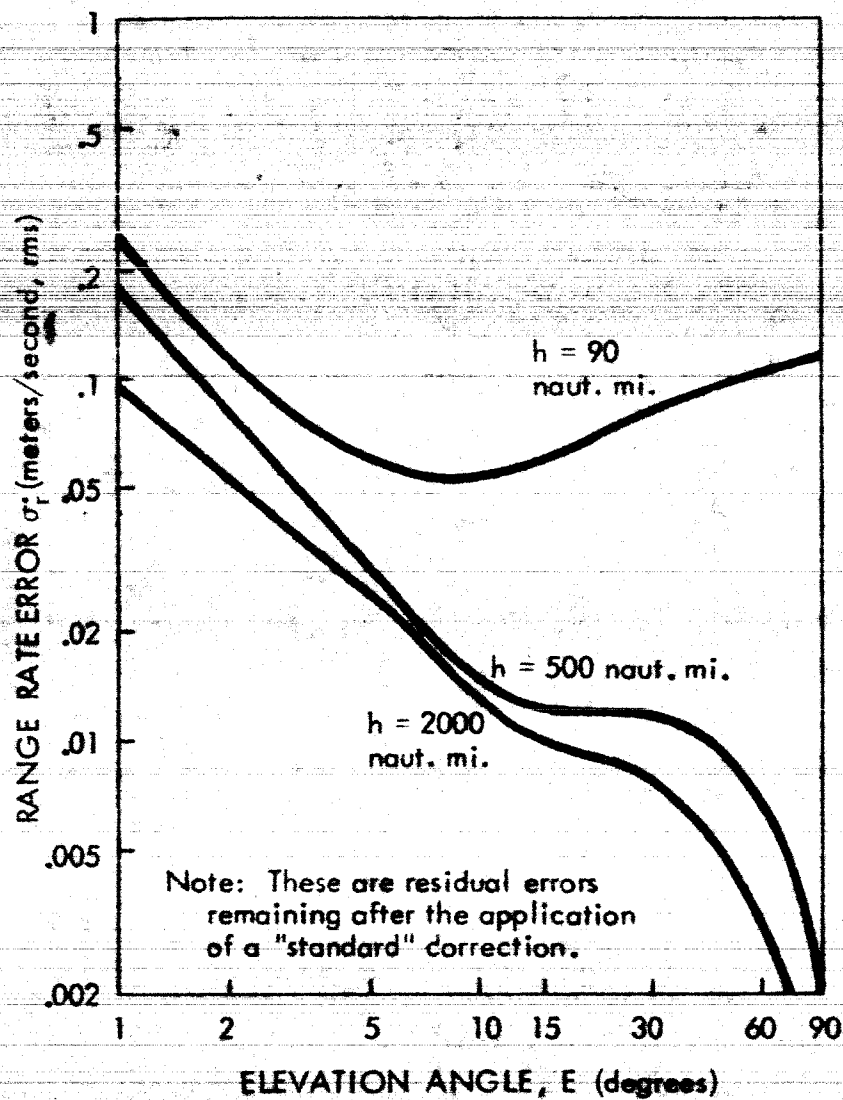


Figure 6. Propagation-Induced Range Errors at 2 Gc



**Figure 7. Propagation-Induced Range Rate Errors at 2 Gc**

$$\Delta R = \frac{\lambda_m^k}{4\pi\sqrt{2} S/N} \quad (1)$$

where:  $\Delta R$  = range resolution or error  
 $\lambda_m$  = wavelength of the range measuring tone  
 $S/N$  = the signal-to-noise ratio in the two-sided phase-locked loop bandwidth.  
 $k$  = a factor related to the probability of a particular  $\Delta R$ ;  $k = 1$  for a probability of 68%;  $k = 4$  for a probability of 99.99%.

A derivation of the most significant part of this equation is contained in Section 4.

In addition to the thermal noise errors introduced by the range measuring tone (fine ranging tone), the errors due to the ambiguity resolving tones (see Section 3) must also be considered. For the ambiguity resolving tones, the general equation given above still holds, but it is desired to insure that the probability of making a mistake in ambiguity resolution is very low. For this reason,  $k = 4$  is recommended for determining the signal-to-noise requirements for ambiguity resolution. Because of the low probability of an error in any ambiguity resolution (.0001), it is deceptive to compute a total rms range error including the errors contributed by the ambiguity resolving tones. Instead, the rms error for the fine ranging tone is used in the error budget with the qualification that this will be the rms error for more than 99.9% of the time. It is expected that a "reasonableness test" performed in the vehicle computer can easily reject the errors introduced by the ambiguity resolving tones for that small portion of the time when these are in error.

With respect to the errors in Doppler due to a finite signal-to-noise ratio, it has been shown<sup>5</sup> that the rms range rate error for measuring equipment similar to that used for the AROD measurements\* can be expressed

as:

$$\sigma_r = \frac{\lambda_t}{4\pi T\sqrt{S/N}} \quad (2)$$

\*See previous footnote

where:

$\sigma_r$  = rms range rate error (in meters per second)

T = cycle counting interval (in seconds)

$\lambda_t$  = transmitted carrier wavelength (in meters)

### 2.2.3.2 Instrumentation Errors

Included in this category are the errors caused by the specific pieces of equipment that have been tentatively specified for the AROD implementation.\*

#### A. Range Errors

##### (1) Oscillator Instability

For the sidetone ranging system specified for AROD, three types of oscillator instability must be considered: long-term instability (days), very short term instability (milliseconds), and random, thermal-noiselike instability. Because the experimental data necessary to determine the exact probability distribution for an oscillator's output are not available, the long term and very short term effects were separated from the thermal noise effects in the Feasibility Study. For the first two effects, manufacturers' data on oscillator stabilities were examined; for the last, the "period of coherence" concept, as defined by Edson,<sup>6</sup> was used.

The effect of long term instability on the range measurement is that the range determination will be in error by the same amount that the fine ranging tone is in error, if a phase measuring device is used. Alternatively, if a digital time measuring circuit is used, the error will be the same proportional error as in the clock generating the digital timing pulses. In either case, it is the proportional error in the basic oscillator in the spacecraft that is the determining factor for the range error introduced by this source.

\*Relativistic effects are not discussed as a source of measurement error because they can be shown to be negligible. Most relativistic effects (e.g., change in length of a ruler and change in clock rate due to relative motion between spacecraft and ground station) are of the order of  $(\dot{r}/c)^2$ , or less than one part in  $10^9$ . To eliminate an error of the order of  $\dot{r}/c$  in the calculation of  $\dot{r}$  from the Doppler frequency ( $f_d$ ) it will be necessary to use the exact formula  $f_d(c - \dot{r}) = 2f_t \dot{r}$  rather than the usual approximation  $f_d \approx 2f_t \dot{r}/c$ .

In operation, the long term stability that will probably be of most interest is that specified for one day. For those AROD missions with a shorter duration, this represents a conservative estimate; while for longer missions, updating or calibrating via ground command should be possible, if it is found to be necessary.

The effect (on the range measurement) of very short term drifts in the fine ranging tone is an error that is equal to the amount of the phase drift during the transit time required for the energy to propagate from the spacecraft to the ground station and return. Since the maximum range that will be encountered for the AROD missions studied is 4000 nautical\* miles (corresponding to an altitude of 2000 nautical miles and an elevation angle of  $5^\circ$ ), the maximum propagation delay will be approximately 50 milliseconds.

For the random thermal-noiselike effects, it has been shown<sup>7</sup> that the phase error in a phase-locked loop due to oscillator instability, assuming that the frequency power spectral density for the oscillator system is white and of zero mean, can be expressed as:

$$\epsilon^2 = \frac{1 + (\omega_n/K)^2}{2\zeta \omega_n T_{ce}} \quad (3)$$

where:

- $\epsilon^2$  = mean square loop error (in radians<sup>2</sup>)
- $\omega_n$  = undamped loop natural frequency (in radians/sec)
- $K$  = open loop DC gain
- $\zeta$  = ratio of actual loop damping to critical damping
- $T_{ce}$  = equivalent coherence time of the oscillator system (in seconds).

As defined by Edson,<sup>6</sup> coherence time, or period of coherence, is the time interval required for the standard deviation of the oscillator phase to increase to one radian (when compared with a perfect oscillator).

\*In some cases, nautical has been deleted from nautical miles for ease of reading; nevertheless, all reference to miles are nautical miles.

Equation 3 has two attendant difficulties. The first is that its derivation is based upon an assumed probability distribution from which "drifts" in the oscillator output frequency are excluded. The second difficulty arises from the fact that practical oscillators do drift; consequently, measuring the coherence time caused by the zero-mean white noise component of the oscillator instability is difficult. For these reasons, use of the coherence time concept in the AROD error analysis has been restricted to the thermal-noiselike instabilities, and theoretical estimates (rather than measurements) of the coherence time due to white zero-mean noise has been used in the error budget (Section 2.5). A highly conservative estimate based upon laboratory measurements has also been included in Section 2.5 to show that coherence time effects are of second order importance.

To convert Equation 3 to a form more useful for the AROD error computations, the assumption is made that the loop gain is large compared with the loop natural frequency. The rms range error can then be expressed as:

$$\sigma_r = \frac{\lambda_m}{4\pi\sqrt{2}B_m T_{oe}} \quad (4)$$

where:  $\lambda_m$  = wavelength of the fine ranging tone.

An additional formula is necessary for determining error magnitudes due to coherence time considerations. This formula relates the coherence time for an oscillator system ( $T_{oe}$ ) used in a typical phase-locked receiving system to other oscillators in the system. It has been shown<sup>5</sup> that:

$$1/T_{oe} = 1/T_{cv} + 1/T_{cr} + 1/T_c \left[ \sum_{k=0}^n a_k \right]^2 \quad (5)$$

where:

$T_{cv}$  = coherence time of the voltage controlled oscillator  
in the loop

$T_{cr}$  = coherence time of received signal

$T_c$  = coherence time of basic oscillator used to derive all other oscillators

$a_k$  = multiplication factor applied to the common basic oscillator to yield the  $k^{\text{th}}$  oscillator frequency.

## (2) Ground Station Equipment

As the propagated energy passes through the signal processing equipment in the ground transponder, a phase error will be introduced which will later be reflected as a range error. The primary sources of error in the ground station equipment are the narrow band filters through which the energy must pass to increase the signal-to-noise ratio at the transmitter output and the phase center shifts introduced by the antenna. Since the fine ranging tone and the ambiguity resolving tones are generated and extracted as the difference between two higher frequencies, it is the differential phase shifts between frequencies that pass through the signal processing circuits that is of importance.

## (3) Spacecraft Receiver Filters

When the (transponded) energy returns to the spacecraft receiver, errors similar to those introduced in the ground station filters are caused by differential phase shifts in the receiver filters. The filters in the spacecraft receiver must be designed to minimize these differential phase shifts.

## (4) Velocity Induced Phase Error

If a standard phase-locked loop is used, there will be a steady phase error due to a constant Doppler frequency on the input signal. As indicated in Section 4.1.3, the magnitude of this phase error (in radians) is:

$$\phi_e = \omega_d / K$$

or

$$\phi_r = \lambda_m f_d / 2K \quad (\text{in meters})$$

where  $\omega_d$  = Doppler frequency (radians/second)

(6)

This tracking error can be reduced by the use of rate aiding (velocity bias compensation). (In Sections 3 and 4, this approach is indicated to be desirable, and a specific implementation is discussed). An alternative approach toward reducing this error is the computation of a correction in the spacecraft computer.

#### (5) Acceleration-Induced Range Errors

If the Doppler frequency on the input signal is changing, a standard phase-locked loop will have an additional phase error. This error will add to that given by Equation 6 and cause a total error that grows with time if the Doppler on the input signal changes at a steady rate. As indicated in Section 4.1.3, the phase error due to the changing Doppler is:

$$\phi_e = \dot{\omega}_d / \omega_n^2 \quad (\text{in radians})$$

or

$$\phi_r = \frac{\lambda_m}{2} \left( \frac{\dot{f}_d}{\omega_n^2} \right) \quad (\text{in meters}) \quad (7)$$

where  $\dot{\omega}_d$  = rate of change of Doppler on the input signal (radians/second<sup>2</sup>)

This error may be reducible by the use of rate aiding. Alternatively, computed corrections may be used to reduce the acceleration induced error.

#### (6) Timing and Controls

Uncertainties in the exact time of occurrence of critical signals in the spacecraft, delays in the spacecraft circuits that have not been accounted for, and other timing and control errors result directly in range errors.

##### B. Range Rate Errors

##### (1) Oscillator Instability

The range rate errors introduced by oscillator instabilities will be discussed in the same manner as the range errors. Three types of instability will be considered: long term instability, very short term instability and random, thermal-noiselike instability.

The range rate errors introduced by the long term drifts of oscillators are primarily due to the translation oscillators (see Section 3). Any

drift of either the translation oscillator on the ground or in the vehicle will cause an erroneous Doppler estimate. The frequency error will be equal to the magnitude of the frequency drift.

Due to very short term instability, the carrier frequency (from which the Doppler is measured) can drift during the propagation time. This drift will be reflected directly as an error in the estimate of the Doppler frequency.

The thermal-noiselike instabilities will again be discussed in terms of coherence time, with the same restrictions and difficulties as in Range Errors. It has been shown<sup>5</sup> that the range rate error (rms) caused by oscillator instabilities of the white zero-mean type is:

$$\sigma_{\dot{r}} = \frac{\lambda_t \sqrt{\tau}}{2 \pi T \sqrt{2 T_{ct}}} \quad (8)$$

where  $\lambda_t$  = wavelength of transmitted carrier  
 $\tau$  = the propagation time for the signal energy  
 $T$  = cycle counting interval  
 $T_{ct}$  = coherence time of the received carrier frequency  
 (in seconds)

and where it has been assumed that  $T > \tau$ . Since the shortest  $T$  anticipated is 0.1 seconds and since the maximum  $\tau$  is 50 milliseconds, the last inequality will always hold.

## (2) Timing and Controls

The total timing error that is anticipated in the spacecraft equipment will result in an erroneous cycle counting time. The range rate inaccuracy will be proportional to the timing error divided by the cycle counting interval.

### 2.2.3.3 Quantization Errors

The rms error in the range measurement introduced by the quantization "box" is equal to the size of the box, in meters, divided by the square root of twelve. The range rate error can be computed in the manner indicated in Section 4.1.4 for the cycle counting method selected for the Feasibility Study.

#### 2.2.3.4 Multipath Errors

The range and range rate errors due to multiple transmission paths are so strongly a function of the system design and the ground antenna design that Section 4.2.4 has been devoted to this subject. In that section the functional relationship between the error magnitudes and the system geometry is derived for the specific ground antenna design selected. (Anticipating the results of Section 4.2.4, the multipath error magnitudes are negligible for all elevation angles except those very close to the horizon).

#### 2.2.4 Geodetic Errors

All of the error sources previously discussed contribute to the AROD "measurement errors," i.e., the errors in the basic AROD measurements, range and range rate. An additional error source that must be considered in determining the "system errors" is the lack of precise knowledge of the locations of the ground stations. This subject is analyzed in detail in Appendix C but this subsection will summarize the information contained in that appendix.

For the purposes of the system analysis portion of the AROD Feasibility Study, the question to be asked concerning these geodetic errors is simple enough: "How precisely are the locations of the ground transponders known?" The answer, unfortunately, is not as simple, but rather depends upon many factors. The most important of these factors are:

1. The surveying technique used to determine the transponder's location (and the number of times the location determination is repeated).
2. The year in which the survey is to be performed (more accurate techniques are a few years away).
3. The general geographic area in which the transponder is located.
4. The relative geometry between the transponder and the network elements used in the surveying technique.
5. Whether the transponder is oceanborne or land-based.

To provide as accurate an analysis of geodetic errors as possible, a subcontract was awarded to Geonautics, Inc. This subcontract was concerned with what were, from the standpoint of the Feasibility Study, the two most important aspects of the general geodetic problem. First, it was necessary to estimate the geodetic accuracies expected from the application of advanced surveying techniques to land-based stations in order to determine the AROD system performance. Second, it was necessary to estimate the accuracy with which the position and velocity of a moving ship could be determined, both for planning purposes for early AROD flight tests, and to serve as a preliminary estimate of the station coordinate errors associated with "fixed" oceanborne transponders for the determination of overall performance of the operational AROD system.

This subsection is principally interested in the problems in determining the locations of the land-based and "fixed" oceanborne stations; the ship's velocity determination problem is discussed in detail in Appendix C.

A summary of the principal results of Appendix C with respect to "fixed" stations is contained in Tables 2 and 3. In Table 2, estimates of the accuracies achievable with various geodetic techniques are presented for fixed ground stations. The accuracies indicated for HIRAN could be considered typical of those that might be encountered in early AROD feasibility flight tests. In later phases of the AROD program, ground stations will be installed in remote areas that do not have very accurate ties to the North American datum. For these stations, therefore, the expected geodetic errors will be greater; for example, current estimates for the Project Mercury tracking stations in Australia indicate an rms error of approximately 60 meters. By the time that AROD becomes operational, however, it is expected that the use of geodetic satellite systems will achieve significant improvements in datum ties.

On the basis of the estimates presented in Table 2, a value for the station coordinate errors of 7 meters (standard deviation) was selected to illustrate the capabilities of the AROD system in the summary portions of this report. Additional data indicating the effects of geodetic errors of different magnitudes are included in Appendix A.

Table 2

**Comparative Accuracies of Methods for the Determination  
of Geodetic Positions Over Extended Land Areas**

Method	Estimated Accuracy (Standard Error)	Remarks
Hiron Trilateration (1962)	1:100,000 to 1:170,000 or 18' - 30' at 500 miles	Suitable for surveys over remote areas on localized datums. Limited inter-continental capability, 500 miles maximum range.
Shiran Trilateration (1965 est.)	1:300,000 to 1:500,000 or 12' - 20' at 1000 miles	Expected to provide accurate control extensions over distances up to 1000 miles.
Photogrammetric Flash Triangulation (1964 est.)	1:1,000,000 or better*	Additional development required to make fully operational.
Geodetic Satellites (1963-64 est.)	1:500,000 or better (electronic trilateration). 1:1,000,000 (photo- grammetric stellar tri- angulation)	Under development.

\* The time at which this accuracy will be achievable is strongly dependent upon the effort expended in improving star catalogs.

The second problem in positional accuracy determination concerns the shipborne stations. This problem is twofold: first, the initial position of the ship must be determined; and second, the ship must maintain this position. A list of the applicable techniques for initial position determination and their expected repeatabilities is presented in Table 3. The problem of maintaining a ship's position was beyond the scope of the Feasibility Study, but is very properly a subject for further investigation in later phases of the AROD program. One technique that appears to hold much promise as an aid for station keeping is the use of sonic buoys whose positions have been determined accurately.

### 2.3 Geometrical Dilution of Precision

Now that the sources of error in the AROD system have been identified, it is necessary to combine their effects in a general analysis for varying spacecraft-ground station geometries. The purpose of this analysis of the Geometrical Dilution of Precision (GDOP) is to determine the errors in the spacecraft's position and velocity\* due to measurement errors and geodetic errors.

In an extensive analysis (Appendix A), a range of values for the measurement errors and station coordinate errors was assumed and the errors in position and velocity were determined. The information contained in that appendix can be summarized by outlining the procedure followed in the analysis and presenting some of the test results. The equations relating the vehicle's position and velocity (and the associated errors) to the range and range rate readings (and associated errors) and the ground station locations (and associated errors) were first constructed. A flexible computer program was then written to determine the position and velocity errors resulting from various measurement and geodetic errors. Representative ground station configurations and vehicle trajectories were then entered into the computer and the resulting errors were calculated. The derivations for the GDOP equations, a description of the computer program, and the results of the computer tests are presented in Appendix A.

\*In the Feasibility Study it was assumed that these were the parameters to be computed from the range and range rate readings.

Table 3

Estimated Repeatability of Methods for the  
Determination of A Ship's Position

Method	Estimated Repeatability (standard deviation)	Approximate Maximum Range (miles)
LORAN C* (1962)	Instantaneous accuracy $\pm 500$ feet (groundwave) or $\pm 1 - 2$ miles (skywave)	1400 (groundwave) 2000 (first-hop skywave)
Omega (operational in 1965)	$\pm 3000$ feet (under optimum conditions) $\pm 1$ mile (average conditions)	6000
Transit (1963)	$\pm 300$ feet or better	Any ship within line-of- sight can utilize the sat- ellite's signals.
Combination (e.g., LORAN- Transit)	$\pm 300$ feet may be achievable over extended areas	A ship within range of a LORAN net could update its position periodically with accurate readings from Transit.
Bathymetric Techniques	$\pm 500$ feet if LORAN C is used for initial tie. $\pm 150$ feet if flash triangu- lation is used for initial tie.	Localized Areas

\* The incremental error between two proximate position determinations is much smaller than the absolute error.

Although it was beyond the scope of the Feasibility Study to perform an extensive system analysis and optimization for all possible AROD configurations, some significant results were achieved through the use of the GDOP program described in Appendix A. The most important of these results were:

1. An estimate of system performance for varying geometries for the measurement errors associated with a representative equipment implementation.
2. An estimate of the optimum relationship between station coordinate errors and range measurement accuracy.
3. A demonstration of the important effects of baseline distance on system performance.

The system performance analysis can best be summarized by presenting the results of the computer tests for trajectories, baselines, measurement errors,\* and station coordinate errors chosen as "representative" of the expected AROD configurations. The three trajectories selected for analysis, and shown in Figure 8, are:

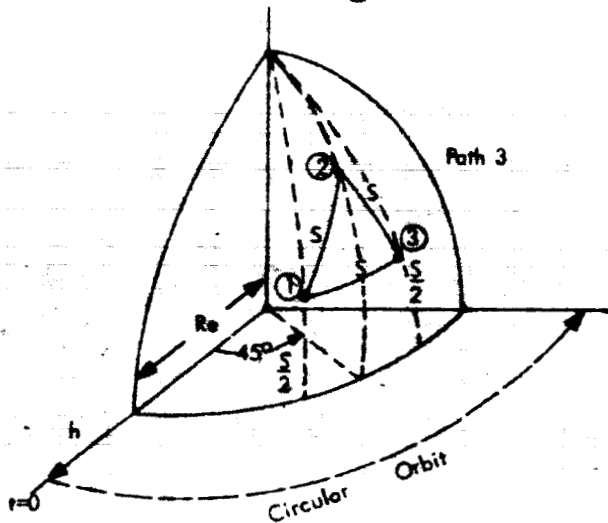
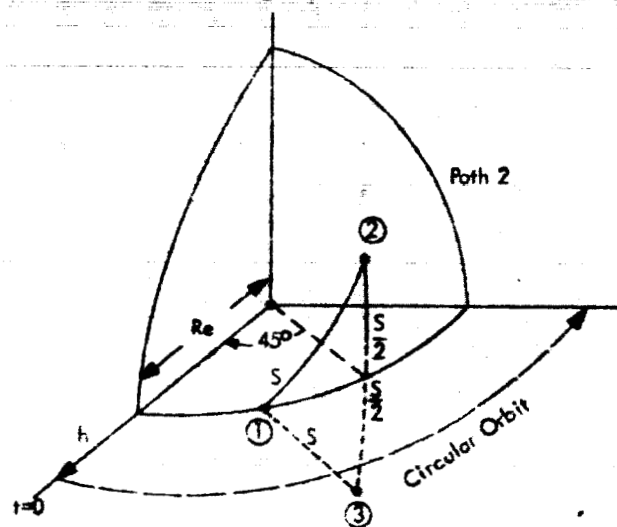
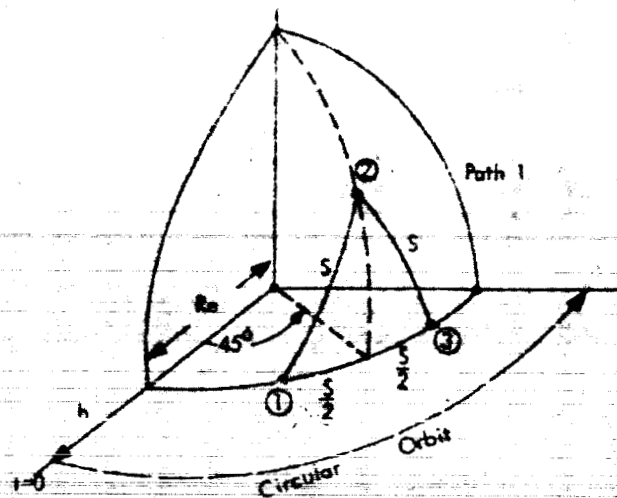
1. A circular orbit over one side of an equilateral-triangular station deployment.
2. A circular orbit over one station and bisecting the other side of the equilateral triangle.
3. A circular orbit parallel to one side of the triangle but outside the triangle by a distance equal to half the length of one side.

The performance of the representative AROD system for these trajectories is indicated in Figures 9, 10, 11, and 12.

The measures of effectiveness used in these figures for indicating system performance are the radius of the uncertainty "sphere" surrounding the vehicle's computed position (for a 68% probability) and the same radius for the computed velocity. The meaning of these measures is discussed in Appendix A and their relationship to the error ellipsoids is also presented.

---

\*The reasons for selecting the measurement error values are discussed in Section 2.5.



$R_e$  = Earth's Radius  
 $h$  = Orbital Altitude  
 ① ② ③ = Ground Stations  
 $S$  = Baseline

Computer tests begin with spacecraft at position indicated as  $t = 0$ .

Figure 8. Test Paths

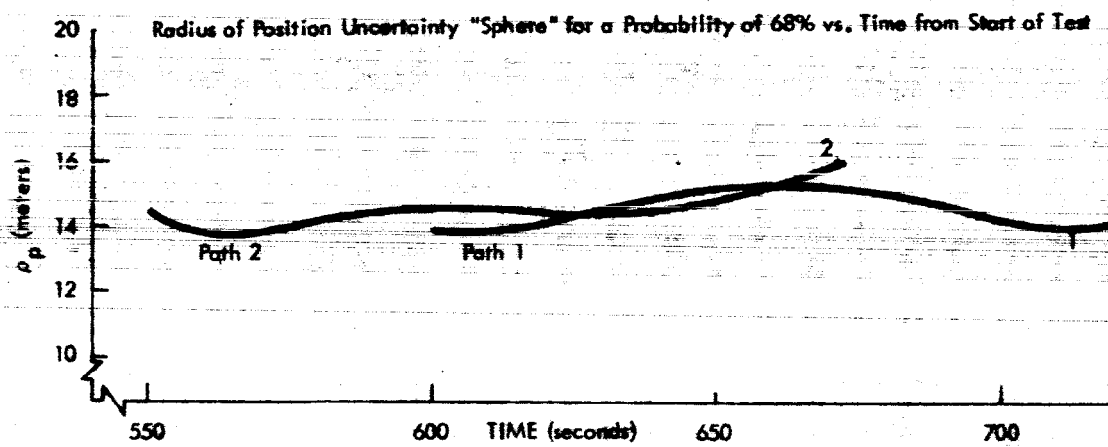
Several aspects of these figures deserve further discussion and clarification. One significant point is that a minimum elevation angle of  $5^{\circ}$  was required in the tests for measurements to be acceptable; since the time scale begins as indicated in Figure 8, the measurement data do not necessarily start at  $t = 0$ . The reason that the coverage intervals do not coincide in time is that the spacecraft comes into full view of the three stations at different times for the three different paths. In Figure 9, no data for Path 3 appear because the spacecraft was never above the  $5^{\circ}$  minimum elevation angle with respect to station 2.

When the data from Appendix A are used to further analyze these results, the position of the spacecraft with respect to the ground stations can be determined and it can be seen that, for the trajectories indicated, the particular path followed by the spacecraft usually has very little effect on system performance. For the summary curves appearing as Figures 4 and 5 in Section 1 of this report, path 1 was selected as being representative of system performance. In those figures the locations of the ground stations are indicated.

The advantage of selecting the baseline (S) as a function of spacecraft altitude can be seen by comparing Figures 11 and 12. For a world-wide AROD network, it is envisioned that stations at 500 mile separations might be installed to track vehicles at altitudes as low as 90 miles; if these stations exist, vehicles traveling at altitudes of 2000 miles should use stations separated by 1000 miles or more.

In the representative system design discussed in Sections 3 and 4, provision has been made for utilizing measurements from four ground stations; with this flexibility the three stations with the best geometry can be selected dynamically in the spacecraft.

To avoid mathematical complexities that were beyond the scope of the Feasibility Study, the usual assumption of constant measurement errors throughout the trajectory was necessary. In actuality, the measurement errors will vary, as indicated later in Table 4. It is therefore recommended that an analysis of the effects of non-constant errors be conducted as a part of the next phase of the AROD program.



Test Conditions  
 Range Measurement Error,  $\sigma_r = 3$  meters  
 Range Rate Measurement Error,  $\sigma_{\dot{r}} = .05$  M/Sec  
 Station Coordinate Error,  $\sigma_{sc} = 7$  meters  
 Station Separation,  $S = 500$  nautical miles

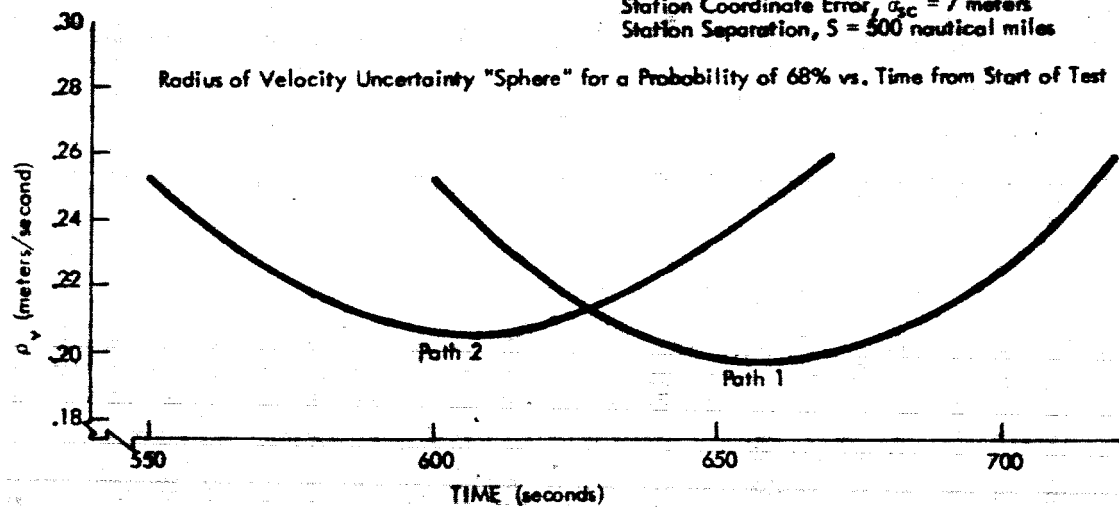


Figure 9. System Performance at  $h = 90$  Nautical Miles

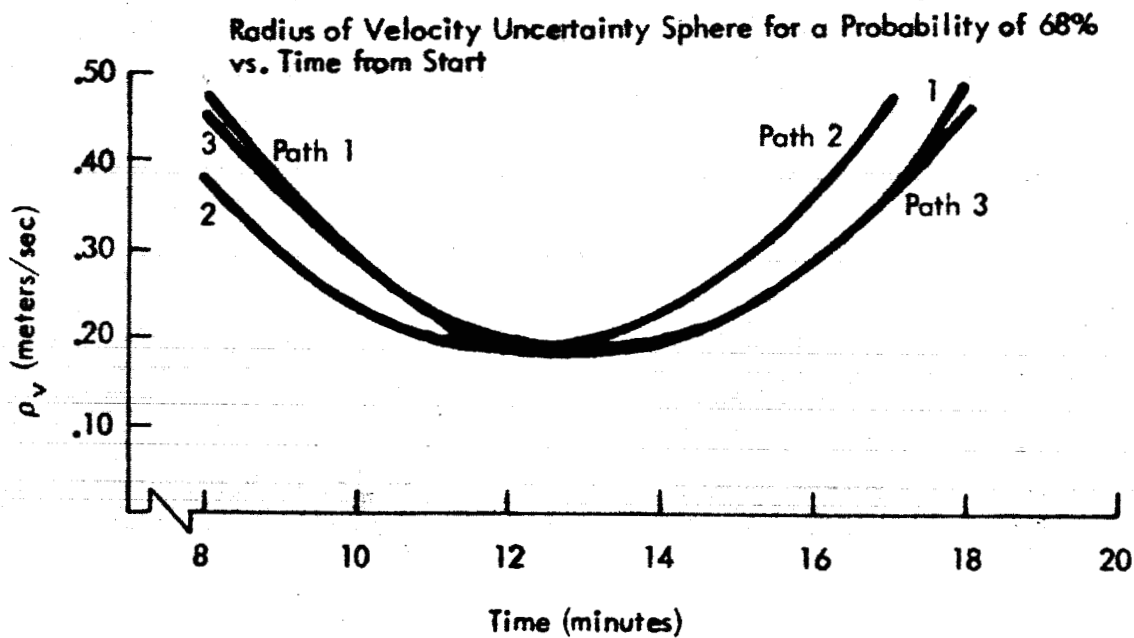
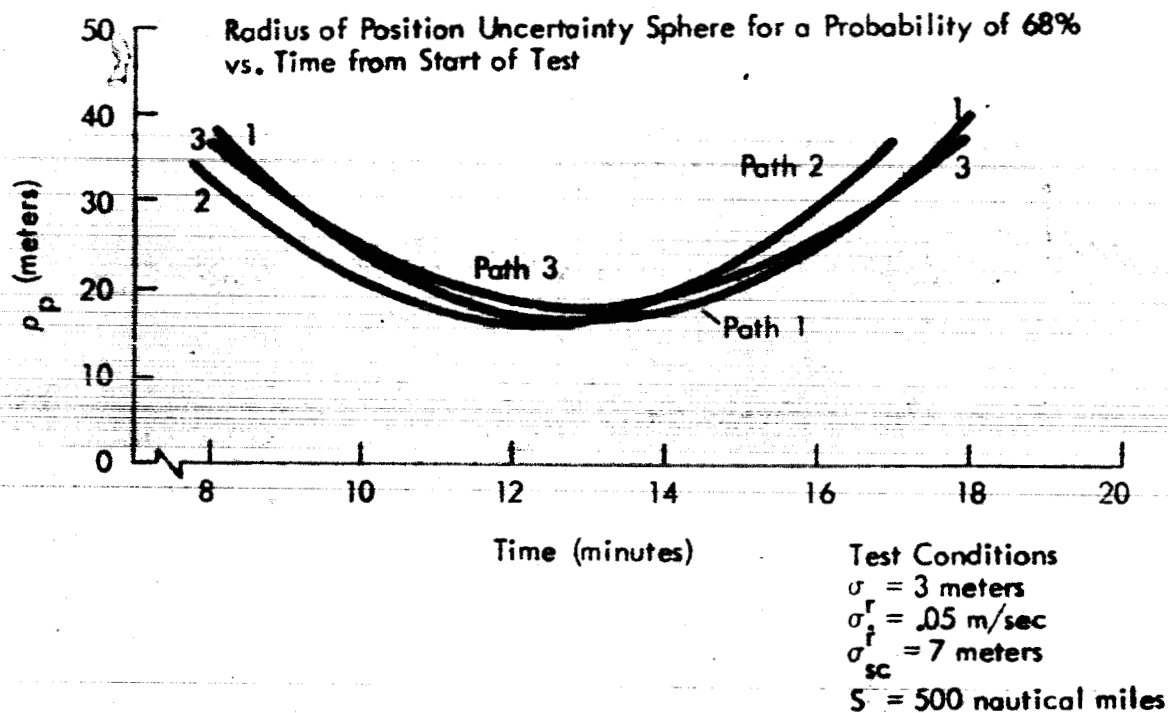


Figure 10. System Performance at  $h = 500$  Nautical Miles

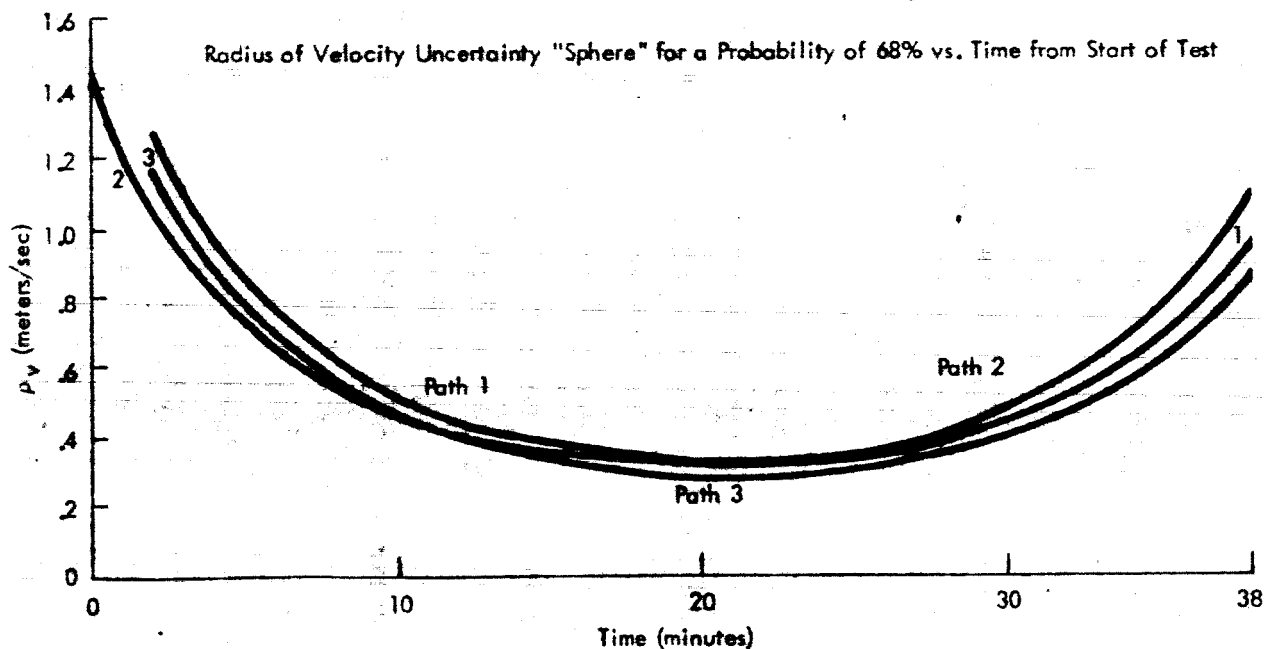
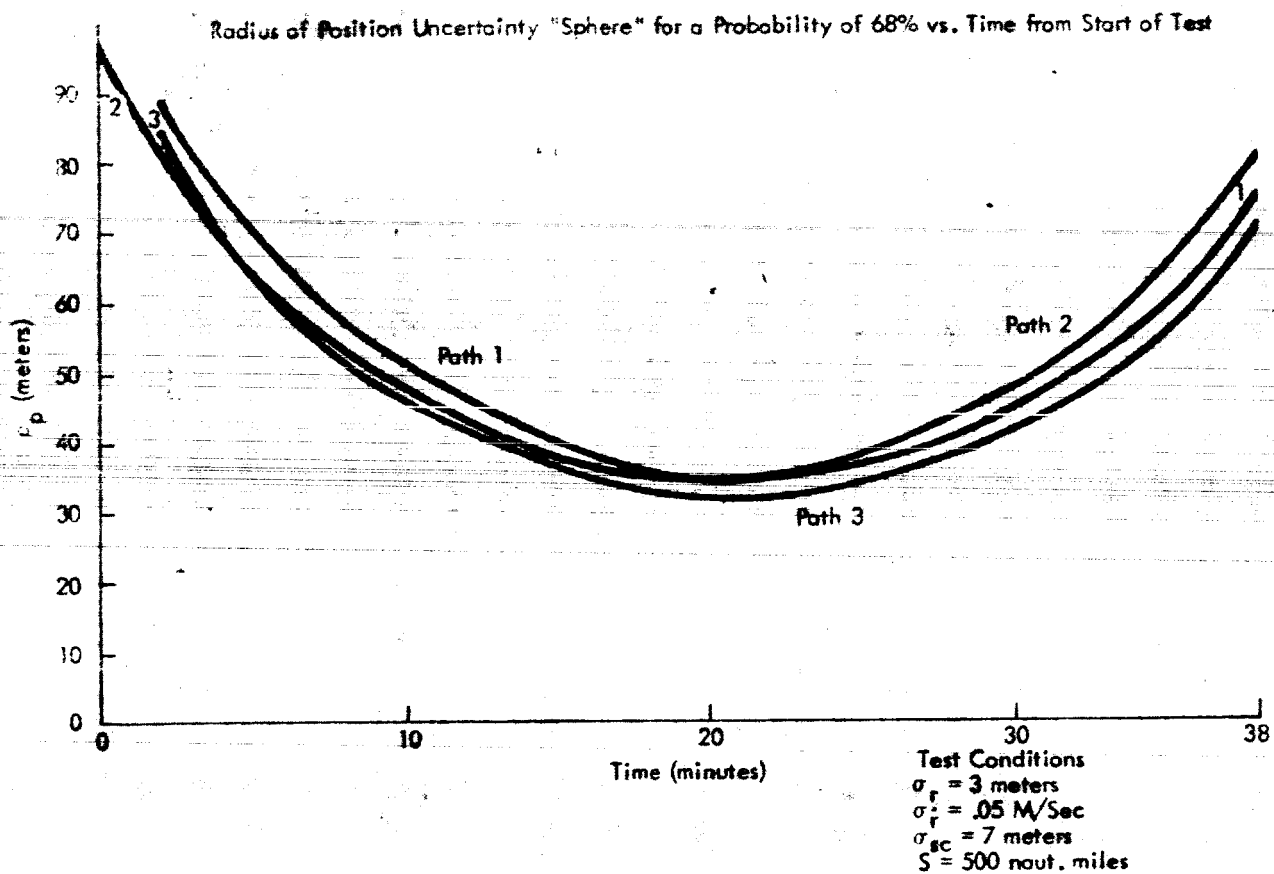


Figure 11. System Performance at  $h = 2000$  Nautical Miles with a 500 Nautical Mile Baseline

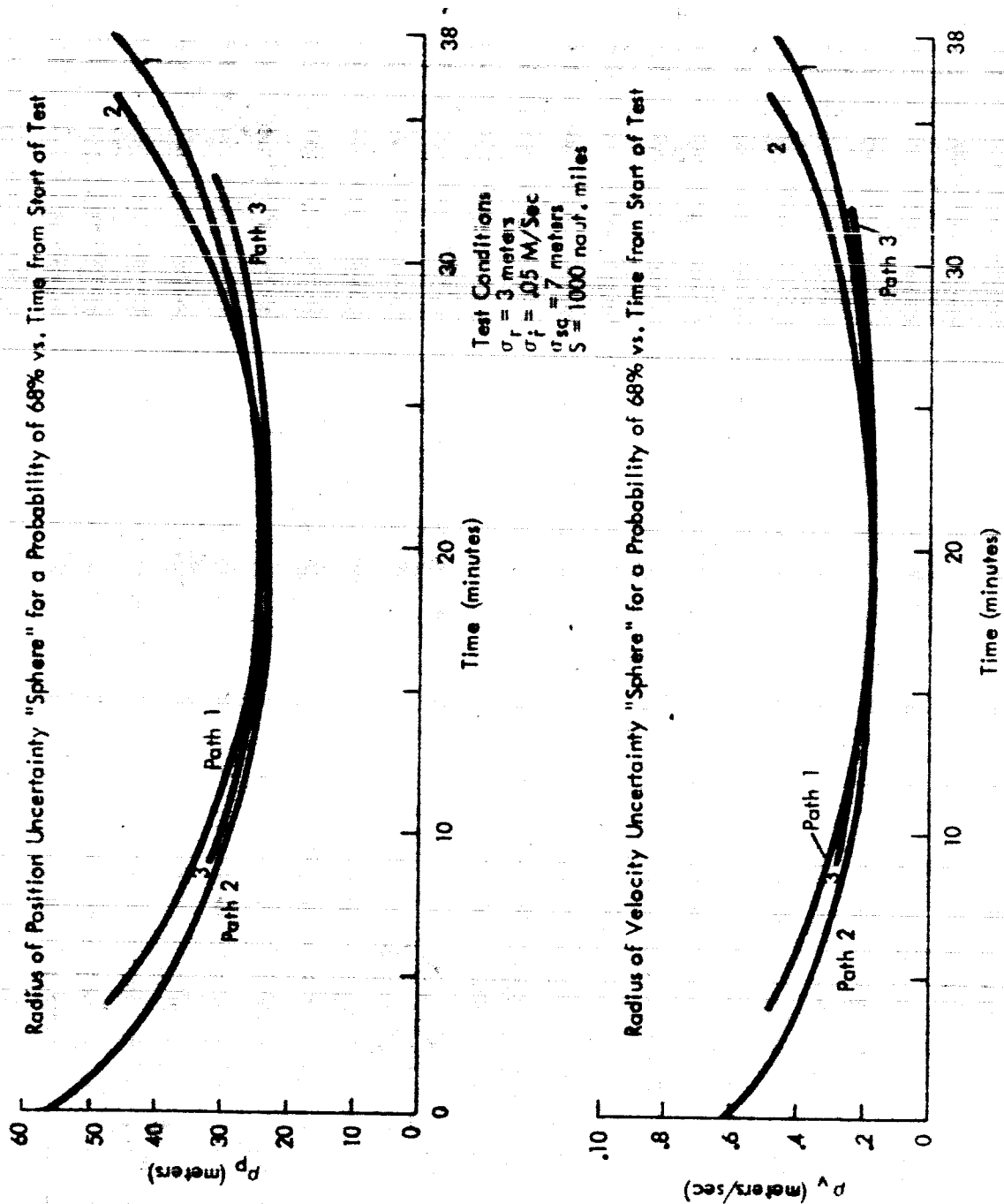


Figure 12. System Performance at  $h = 2000$  Nautical Miles with a 1000 Nautical Mile Baseline

The AROD GDOP program can be an extremely useful tool in the selection of appropriate system parameters as illustrated in Figure 13. In this figure, the radius of the position uncertainty sphere over the center of the ground station triangle (normalized for convenience as indicated in Appendix A) is plotted as a function of the range measurement error for various values of station coordinate errors. The strong dependence of positional accuracy upon the value assumed for the geodetic errors can be seen. Using the data in Figure 13 and the 7 meter station coordinate error selected as "representative" in subsection 2.2.4, a range measurement error of approximately three meters seems to be a reasonable equipment performance objective. Operating at a higher measurement error, for example ten meters, would degrade system performance significantly, while reducing the range measurement error to one meter would not improve system performance appreciably.

In Appendix A, it is shown that the effect of range measurement errors and station coordinate errors on the error in the computed velocity for the vehicle is of secondary importance (for range rate measurement errors as small as .02 meters per second). The primary determining factor for the velocity error is the range rate measurement error, for the error values investigated.

## 2.4 Smoothing

The remaining factor to be considered in determining the performance of the AROD system is the reduction in errors that can be achieved through the use of smoothing in the vehicle. A specific calculation of the error reduction achievable through smoothing must await a detailed analysis of the final equipment implementation and the statistics involved in the error sources. However, it will probably be the case that many of the major error sources are not smoothable. Several examples of errors that will definitely be non-smoothable are the station coordinate errors, the errors due to the uncertainty in  $c$ , and the bias errors introduced by the propagation medium.

(The significance of biased errors would be greatly diminished, however, if incremental errors in range, range rate, position, and velocity were of interest to the user of the AROD system. In this case smoothing of the random,

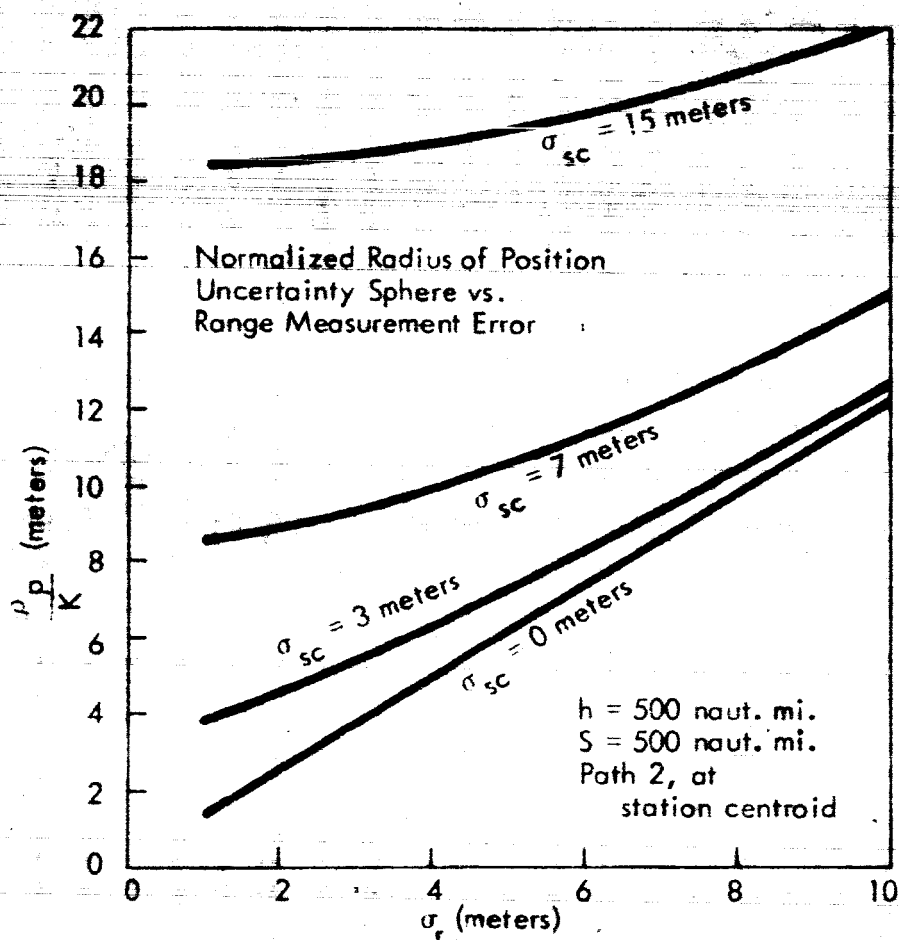


Figure 13. Influence of Range Measurement Errors and Station Coordinate Errors on Positional Accuracy

zero-mean errors could result in substantial improvements in incremental accuracy).

An additional factor that may reduce the utility of smoothing is the possible requirement for computations during powered flight.

## 2.5 Equipment Performance Objectives (Error Budget)

Now that the functional relationships between the error magnitudes and the significant AROD parameters have been established, and the GDOP and smoothing effects have been estimated, a rational approach toward establishing equipment performance objectives can be attempted. Rather than limit the AROD Feasibility Study to one specific performance objective, it was decided to seek results that would provide more general information concerning feasibility. Specifically, two families of curves were sought, one for range and one for range rate, which would present graphically the variation of the AROD measurement errors with spacecraft equipment penalty, using ground station capability as a parameter. Measurement errors were chosen as the measure of effectiveness rather than system errors (in position and velocity) because of the strong assumptions that would have been necessary to utilize the latter. It would have been necessary to assume, for the station coordinate errors, values that would have a strong influence on the system performance. It would also have been necessary to assume that the parameters to be computed were definitely position and velocity, and that orbit extrapolation was not the primary consideration.

From the resulting families of tradeoff curves, the feasibility of AROD could be determined for each application. A potential user could consult the curves and determine whether the combination of AROD spacecraft penalty and ground station "cost" for his required measurement accuracy were tolerable, and whether the AROD approach would have a lower overall system "cost" than other approaches.

To construct the feasibility curves it was decided to perform a fairly detailed design study at one specific point, and then to extrapolate from this point to obtain other points on the curves. Considerable attention was given

to the selection of the appropriate measurement errors and spacecraft penalty for the detailed design study, since the equipment estimates would be most accurate at this point. For several reasons, selection of the design point was based primarily on range measurement errors rather than range rate errors. First, there exist no published data on range rate errors introduced by the propagation medium at all of the frequencies, altitudes and ranges of interest to AROD.\* Second, it is known that the range rate errors vary in a very complex manner as a function of elevation angle and altitude. Third, the completely uncontrollable error source, the uncertainty in  $c$ , becomes zero for range rate errors at certain points in a trajectory; consequently, attempts to keep errors "in balance" become meaningless at these points. Fourth, the cycle counting time cannot be specified definitely at this time.

The desired procedure for selecting an appropriate objective for the range measurement error was to estimate the errors due to all sources and then estimate the region where the decreases in the total range measurement error became significantly smaller as the equipment penalty was increased. Although it was desired to utilize this procedure throughout the AROD operating envelope, the complex variations of the errors with the spacecraft's position necessitated the selection of a particular point in the envelope as representative before the start of the optimization procedure. Since the specified range of altitudes was 90 to 2000 miles, an orbital altitude of 500 miles was selected as representative of the spectrum of system missions. With propagation and multipath considerations limiting the minimum elevation angle to  $5^\circ$  (see Section 3), the maximum range encountered would be 4000 miles; therefore, a range of 1000 miles was selected as representative. The elevation angle corresponding to  $h = 500$  miles and  $R = 1000$  miles is  $23^\circ$ ; this angle is also representative in that it is the angle within which a vehicle in an overhead circular orbit will be for approximately half the time that it is within view of a ground station.<sup>9</sup>

\*Late in the Feasibility Study, personal contacts provided some data planned for publication by Mr. V. A. Counter of Lockheed in 1963. These data form the basis for the range rate errors presented in Appendix B and Section 2.2.2.

It must be emphasized that the "representative" point was only used to aid in selecting appropriate performance objectives for the various portions of the AROD equipment; it was not used to determine the limits of system performance. The system which was designed and "implemented" as indicated in Sections 3 and 4 can operate satisfactorily at all points throughout the AROD operating envelope. It can provide satisfactory signal-to-noise ratios at the maximum range as well as track the rapidly changing Doppler that occurs at the minimum range. However, the selection of a representative point was necessary for choosing an "optimum" range measurement error and also for illustrating the tradeoffs pertinent to the question of feasibility.

Having discussed the reasons for the selection of the representative point and having introduced the procedure to be followed in budgeting errors to the various sources, we will now proceed with the analysis leading to the establishment of the error budget shown in Table 4. It is important to note at the outset of this discussion that the error budget was not established on theoretical considerations alone. Rather, continuous feedback from the equipment designers was used to allocate errors and revise the budget. Thus, the error budget indicated in Table 4 is the result of many iterations.

A discussion of each of the error sources will now be undertaken, with continual references to Table 4 and Section 2.2.

#### 2.5.1 Uncertainty of the Vacuum Velocity of Light

Using the value of one part per million indicated in Section 2.2.1 for the uncertainty in  $c$ , the errors in the range and range rate measurements due to this uncertainty are those listed in the appropriate rows in Table 4. The values for range and Doppler for the various points in Table 4 were obtained from standard tables.<sup>9</sup> At the representative point located in the center column the (standard) errors due to this source are 1.9 meters and .006 meters per second.

#### 2.5.2 Propagation Errors

In establishing performance objectives, the basic principle of keeping "in balance" those errors whose reduction requires large equipment penalties

Table 4

## Measurement Error Summary for Various Points in the AROD System

Measurement Error Source	Magnitude of rms error for circular orbits with height (In nautical miles), range (In nautical miles) and elevation angle shown.				
	h = 90 R = 90 E = 90°	h = 90 R = 600 E = 5°	h = 500 R = 1000 E = 23°	h = 2000 R = 2000 E = 90°	h = 2000 R = 3940 E = 5°
<b>RANGE ERRORS:</b>	(meters)	(meters)	(meters)	(meters)	(meters)
Uncertainty in c.	0.17	1.1	1.9	3.7	7.3
Propagation (residual at 2Gc)	<.1	0.9	1.9	0.9	3.7
Thermal Noise (unsmoothed)	0.16	0.52	1.2	1.6	1.6
Instrumentation:					
Oscillator Long Term Stability	< 0.00017	< 0.0011	< 0.0019	< 0.0037	< 0.0073
Oscillator Very Short Term Stability	< 10 <sup>-3</sup>	< 10 <sup>-3</sup>	< 10 <sup>-3</sup>	< 10 <sup>-3</sup>	< 10 <sup>-3</sup>
Oscillator Coherence Time	< 0.09	< 0.09	< 0.09	< 0.09	< 0.09
Ground Station Filters, etc.	< 0.5	< 0.5	< 0.5	< 0.5	< 0.5
Spacecraft Receiver Filters	< 0.5	< 0.5	< 0.5	< 0.5	< 0.5
Velocity and Accel.-induced errors	0.4	0.01	0.01	0.008	0.005
Timing and Controls	< 0.9	< 0.9	< 0.9	< 0.9	< 0.9
Quantization	0.29	0.29	0.29	0.29	0.29
Multipath	< 0.01	< 0.2	< 0.01	< 0.01	< 0.2
<b>Total Range Error</b>	< 1.3	< 1.9	< 3.2	< 4.3	< 8.5
<b>RANGE RATE ERRORS:</b>	(m/sec.)	(m/sec.)	(m/sec.)	(m/sec.)	(m/sec.)
Uncertainty in c.	0	0.008	0.006	0	0.004
Propagation (residual at 2 Gc)	0.12	0.06	0.012	0.002	0.025
Thermal Noise (unsmoothed)	0.0039	0.013	0.030	0.039	0.039
Instrumentation:					
Oscillator Long Term Stability	< 0.005	< 0.005	< 0.005	< 0.005	< 0.005
Oscillator Very Short Term Stability	< 0.0015	< 0.0015	< 0.0015	< 0.0015	< 0.0015
Oscillator Coherence Time	< 0.0005	< 0.002	< 0.002	< 0.002	< 0.003
Timing and Controls	0	< 0.0005	< 0.0005	0	< 0.0005
Quantization	0.0075	0.0075	0.0075	0.0075	0.0075
Multipath	< 0.001	< 0.04	< 0.001	< 0.001	< 0.02
<b>Total Range Rate Error</b>	0.12	< 0.074	< 0.034	< 0.040	< 0.051

was followed. For the propagation induced range errors to be in balance with those due to the uncertainty in  $c$ , and to avoid the high spacecraft equipment penalty associated with operation at higher frequencies, the nominal AROD carrier frequency was chosen to be 2000 Mc.\* At this frequency the residual propagation errors remaining after the application of a correction based upon a standard worldwide atmosphere are those shown in Figures 6 and 7. As recorded in Table 4, the propagation induced errors at the representative point are 1.9 meters and 0.012 meters per second.

Since a propagation correction table or formula must be stored in the vehicle computer, a "quantization" error may also exist due to a limited number of storage locations (for a table) or an approximation (for a formula). The magnitude of this error is difficult to determine because it depends strongly on how well the altitude of the vehicle will be known. It will probably be possible to make this error negligible, however, because even in the worst case of an unknown vehicle altitude, a table of approximately 300 six-bit entries would result in a range correction quantization "box" of one meter. The rms error due to this box size is  $1/\sqrt{12}$  meters or less than 0.3 meters, which will have a negligible effect when added in a "square root of the sum of the squares" manner to the other errors. This error has therefore been assumed to be negligible in the error budget.

### 2.5.3 Equipment Errors

The primary purpose of the system analysis portion of the Feasibility Study—the establishment of appropriate equipment performance objectives—can now be fulfilled. The basic approach followed in allocating equipment errors was to keep the errors compatible with those from other sources and to allocate the largest errors to those sources requiring the greatest penalty for further error reduction.

\*See Section 3 for an extensive discussion of the reasons for selecting this frequency.

### 2.5.3.1 Thermal Noise

The estimates of thermal noise errors presented in the error budget (Table 4) ignore the reductions that might be achievable by smoothing because of the possibility that smoothing may be prohibited by mission requirements (e.g., position determination during powered flight).

#### A. Range Errors

The basic formula for computing the range error due to a finite signal-to-noise ratio is Equation 1 in Section 2.2.3.1. However, because the fine ranging tone is derived as the difference between two phase-locked signals (see Sections 3 and 4), three phase-locked loops must be considered. These loops operate at frequencies of 2000 Mc, 2005 Mc and 5 Mc and it is necessary to take into account the thermal noise errors caused by all three loops. The errors will add in an rms fashion since they are uncorrelated.

To determine reasonable objectives for the thermal noise errors, the first consideration is that they should be approximately equal to the relatively uncontrollable errors, those contributed by the uncertainty in  $c$  and the propagation medium. If the thermal noise errors are much larger, they dominate the other errors and the total measurement errors increase rapidly. If the thermal noise errors are much smaller than the others only a slight improvement results.

On the basis of threshold considerations in the phase-locked loops, available transmitting components, spacecraft limitations, ground antenna design considerations, and other feedback from the equipment design study, an objective of 1.2 meters rms was established for the thermal noise error at the representative point. The performance objective was also established for the ambiguity resolving tones that the probability of an error in ambiguity resolution be less than .001 at the maximum range of 4000 miles.

The signal-to-noise ratios that exist in each of the phase-locked loops are computed in Section 4.1.3, and presented in Tables 9 and 10. As

indicated there, the range of variation possible in the signal dynamics requires the use of phase-locked loops with a switchable  $\omega_n$  for tracking the 2000 Mc signal and the 2005 Mc signal. The altitude chosen in 4.1.3 for switching loop characteristics is 500 miles, the same as that for the representative point. Consequently, two answers are possible when computing the thermal noise errors for the representative point. For Table 4 the larger error was (arbitrarily) selected; if the smaller  $\omega_n$  (and, consequently, the smaller loop noise bandwidth) had been used in the computation, the thermal noise errors in range and range rate at the representative point would have been smaller, 0.58 meters in the case of the range error.

#### B. Range Rate Errors

For the reasons cited earlier, primary attention was given to the range measurement errors in the establishment of the equipment performance objectives. Sufficient information was obtained to achieve the study's primary goal—the generation of the family of feasibility curves for the range rate (and range) measurement errors—but optimal selection of a range rate design point was not emphasized. For those missions in which the range rate errors are the primary consideration, the frequency selection, r.f. spectrum design, and the entire error budget may have to be re-evaluated. At that time, additional data may be available to increase the knowledge of, and confidence in, the range rate propagation errors. It should also be possible to specify the cycle counting time when specific missions are decided upon.

In designing the r.f. spectrum, a primary consideration was the desire to minimize the range error due to thermal noise for a given total input signal power. This minimization is achieved by providing equal signal powers in the 2000 and 2005 Mc signals that are mixed to extract the 5 Mc fine ranging tone. With this factor automatically establishing the signal-to-noise ratio in the range rate phase-locked loop, Equation 2 yields a range rate measurement error of 0.030 meters per second at the representative point for the minimum cycle-counting time of 0.1 seconds.\*

---

\*Specified in conversations with NASA's Contracting Officer's Representative.

Increases in this time will result in proportional decreases in  $\sigma_T$ , and it may be desirable to exploit this approach, if possible, to bring the thermal noise error more into balance with the other errors.

As before, the larger of the two possible range rate errors at the representative point (due to the switchable loop characteristics) is presented in Table 4. If the smaller  $\omega_n$  had been used in the computation the thermal noise error would have been smaller by a factor of  $\sqrt{5}$  and would have been more in balance with the other errors.

### 2.5.3.2 Instrumentation Errors

The definitions of, and formulas for, the instrumentation errors given in Section 2.2.3.2 will now be used to establish equipment performance objectives. In establishing these objectives, care has been taken not to seek an accuracy that would cause a high vehicle equipment penalty unless the accuracy was required to be compatible with other error sources in the AROD system. In some cases, however, it is possible to reduce the instrumentation errors to negligible levels without incurring an excessive penalty.

#### A. Range Errors

##### (1) Oscillator Instability

With respect to the long term stability of the basic frequency source used in the AROD system, range rate considerations discussed in a subsequent paragraph (under Range Rate Errors) invoke the requirement that the stability be better than one part in  $10^9$ . This requirement results in a range error that is three orders of magnitude smaller than that due to the uncertainty in  $c$ , and that is, therefore, negligible.

The very short term oscillator drifts must be less than one part in  $10^{11}$  in the 50 milliseconds maximum transit time to make the range rate errors negligible. This requirement ensures that the range errors are also negligible.

A computation of the effects of random thermal-noiselike instabilities (described by coherence time in Equations 3, 4, and 5) is hampered by difficulties in measuring or theoretically estimating the coherence time

for an oscillator. Edson<sup>6</sup> estimates the coherence time, or period of coherence, produced by thermal noise alone to be  $1.45 \times 10^{14}$  seconds at  $10^7$  radians per second; converting this number to a 5 Mc system (for reference) by the formula<sup>7</sup>  $T_{c2}/T_{c1} = (f_1/f_2)^2$  yields a coherence time of approximately  $10^{13}$  seconds. Alternatively, if the formulas of Reference 6 are applied to manufacturers' data<sup>10</sup> concerning the physical parameters of a 5 Mc oscillator, an estimate for  $T_{ce}$  of approximately  $10^{12}$  seconds is obtained.

To ensure that zero-mean instabilities will have a negligible effect on the measurement errors, an objective of  $10^8$  seconds has been established for the coherence time of the basic 5 Mc oscillator in the vehicle. If the design indicated in Sections 3 and 4 is analyzed in detail, it is seen that only the 2000 Mc and 2005 Mc signals are significant in computing coherence times; the contributions of the translation oscillators and voltage controlled oscillators are negligible because of the "inverse-frequency-squared" relationship. Since both the 2000 Mc and 2005 Mc signals are used to derive the 5 Mc fine ranging tone, and since three local oscillators are involved in the processing of each of the S-band signals, the equivalent coherence time for the entire system is approximately  $1/8 (10^8) (5/2000)^2 \approx 10^2$  seconds (from Equation 5). To determine the rms range error resulting from this coherence time, Equation 4 is applied to the fine ranging tone phase-locked loop. The resulting maximum range error is approximately 0.09 meters, indicating that this effect is negligible.

(Measurements by one manufacturer<sup>8</sup> on an existing oscillator at 2295 Mc yield a coherence time estimate of about 5 seconds; converting this to 5 Mc indicates a coherence time estimate of approximately  $8 \times 10^5$  seconds. However, this estimate is ultra-conservative because the measurement included the effects of non-zero-mean frequency drifts. Even if this ultra-conservative estimate is used, the resulting range error—less than one meter—does not markedly affect the total range error at the representative point. However, this indicates the necessity for obtaining a meaningful estimate of the coherence time for the oscillators selected for AROD at an early time in the design analysis).

## **(2) Ground Station Equipment**

In making the error introduced by the ground station equipment compatible with that introduced by the spacecraft equipment, it was recognized that the ground station equipment could bear the burden of a tighter error budget because it did not have the weight and power penalty problems associated with the spacecraft equipment. The performance objective was therefore established that the total error introduced by all of the ground station equipment (e.g., differential phase delays in filters, phase center shifts, etc.) should not exceed 0.5 meters rms.

## **(3) Spacecraft Receiver Filters**

Since the filtering problem in the spacecraft receiver is difficult, a substantial portion of the range measurement error budget should be allocated to this source. Consequently, the performance objective was established that the filters in the spacecraft receiver should not introduce a range measurement error of more than 0.5 meters.

## **(4) Velocity and Acceleration Induced Errors**

The signal dynamics of the missions analyzed in the AROD Feasibility Study are computed in Appendix D; the results of this analysis were a primary factor in determining the parameters of the phase-locked loops employed in the measuring equipment. When Equations 6 and 7 are applied to the 5 Mc phase-locked loop that had been designed to keep the thermal noise error within the budgeted value, it is found that the combined phase error due to the velocity and acceleration terms, assuming that velocity bias compensation has reduced the effective  $f_d$  by a factor of 100, is 0.01 meters for the representative point. For the other operating points in the system, the combined error has the values indicated in Table 4. In this computation, it has been assumed that the Doppler and Doppler rate terms have the same sign; for half of a pass over a station they will actually have opposite signs and tend to cancel. The phase errors in the 2000 Mc loop and the 2005 Mc loop are not considered because they will effectively cancel each other in the mixing process. (If desired, the velocity and acceleration induced error could be essentially eliminated by incorporating a correction in the spacecraft computer since the error is deterministic).

#### (5) Timing and Controls

It is definitely desirable to keep the error contribution from this source as small as possible. To achieve this, the delays in the spacecraft circuits will be carefully calibrated and precautions taken to reduce the "jitter" and drift in control pulses. The equipment performance objective, assuming that these actions have been taken, was established as 6 nanoseconds, or 0.9 meters, as an upper bound.

#### B. Range Rate Errors

##### (1) Oscillator Instability

The long term stability requirement for the basic frequency source is established by the requirement that the ground translation oscillator (approximately 60 Mc) and the spacecraft translation oscillator be sufficiently close in frequency after a drift of days, weeks, or even months so that no excessive error is introduced in the Doppler measurement. The availability of VLF transmissions to maintain the ground based oscillator frequency very accurately, and the capability of updating (or calibrating) the spacecraft oscillator frequency on ground command indicated that an appropriate objective to result in this source having very little effect upon the range rate measurement error is a maximum of .005 meters per second. To achieve this goal, stability requirements of one part in  $10^9$  for the spacecraft translation oscillator and five parts in  $10^{10}$  for the ground station translation oscillator were established. (The errors introduced by the ground translation oscillator and the vehicle translation oscillator should add in an rms manner as they are uncorrelated.) It is anticipated that the ground station stabilities will be achieved by monitoring VLF transmissions. These stabilities are reflected in the values in Table 4.

The very short term oscillator drifts should produce only negligible errors. Establishing an objective of a maximum drift of .02 cps or one part in  $10^{11}$  for the maximum transit time (50 milliseconds) ensures a maximum range rate error of less than .0015 meters per second.

Utilizing Equation 8 to estimate the error due to the coherence time of the received carrier, and assuming the conservative value of  $10^8$  seconds

for the coherence time of the basic 5 Mc source, the range rate error due to thermal noiselike instability is found to be less than  $3 \times 10^{-3}$  meters per second for all points. In this case the effects of the 2005 Mc chain do not enter the calculation, and the equivalent coherence time is therefore approximately twice the value found earlier, or  $2 \times 10^2$  seconds.

(If the previously discussed, highly conservative estimate for the 5 Mc oscillator coherence time,  $8 \times 10^5$  seconds, is used, the resulting error is still less than .02 meters per second at the representative point).

#### (2) Timing and Controls

The 6 nanosecond requirement indicated earlier is also applicable to the range rate measurement and results in the error of less than .0005 meters per second shown in Table 4, for the minimum cycle counting time of 0.1 seconds.

#### 2.5.3.3 Quantization Errors

The quantization errors established as objectives for the range and range rate readings are 0.29 meters and .0075 meters per second, respectively. The range error requires a quantization "box" of 1 meter and was selected to be sufficiently small to have almost no effect on the total range measurement error at the representative point. The range rate error was chosen as a compromise between a desire to avoid a counter operating at more than 10 Mc in the spacecraft and a desire to make this error insignificant.

#### 2.5.3.4 Multipath Errors

The carrier frequency and the antenna approach for the ground station were selected to make multipath errors negligible for large portions of the AROD operating envelope. In the analysis of multipath effects in Section 4.2.4 it is shown that this objective can be achieved except at very low elevation angles. Even at these low angles it is only under extreme conditions that the errors indicated in Table 4 will be encountered.

#### 2.5.4 Total Errors

The errors indicated in Table 4 will probably have probability distributions and subtle correlations that make difficult their combining to obtain a total error. To obtain a first approximation, however, the total error (standard deviation) was estimated to be the square root of the sum of the squares of the individual contributions.

#### 2.6 Summary

In summary, Section 2 has established reasonable equipment performance objectives for a "design point." To indicate how the families of tradeoff curves that were one of the principal outputs of the AROD Feasibility Study were obtained, it is still necessary to present the procedure for selecting the spacecraft equipment penalty, computing the required ground station capability, and extrapolating from the design point. This information is discussed in Sections 3 and 4.

## Section 3

### SYSTEM DESIGN

#### 3.1 Introduction

The system design presented in this section was undertaken to demonstrate that the AROD concept is feasible and to define the penalty factors associated with the performance objectives established in the system analysis portion of this report (Section 2). This design was optimized only to the extent permitted by the scope of the Feasibility Study and should be regarded as representative. The degree of optimization that was carried out, however, went well beyond what is normally required to resolve the question of feasibility. Further optimization of the system design must await the Design Study Phase (Phase B) of the AROD Program. At that time the mission, environment, and reliability requirements of the operational equipment will be better defined and a re-evaluation of all the design approaches can be made as well as a re-examination of the equipment performance objectives. Detailed designs of the critical circuits should also be accomplished during the Phase B Study, supported by experimental investigations of selected circuits and components.

The governing philosophy for the system design in the Feasibility Study was to achieve the performance objectives with minimum penalty to the spacecraft, while simultaneously achieving a ground station design capable of unattended operation for prolonged periods in remote areas. Although no quantitative reliability objective was established for the Feasibility Study, reliability factors strongly influenced the choices of the recommended design approaches for the system. A noteworthy example of the influence of these factors is the provision of circuits in the spacecraft for receiving and processing signals from four ground stations simultaneously.

In this manner, during critical periods of the flight profile of the vehicle, where four stations are in view, sufficient AROD tracking data will be available to the guidance system to permit a real time orbit determination in spite of an inoperative condition in one of the ground stations or in one of the signal processing circuits of the spacecraft.

In the representative design, the largest sources of equipment errors (notably thermal noise) are maintained in economic balance with the other two major sources of measurement error not attributable to the equipment, namely the uncertainty in  $c$  and the residual propagation errors. To attempt to improve the absolute accuracy of the system by means of a large reduction in thermal noise errors would seem imprudent unless the accuracy to which  $c$  is known and our ability to characterize the atmosphere are greatly improved. With the present knowledge, however, reduction of thermal noise errors at a high cost in vehicle equipment weight and power would only be justified if the ensuing improvements in incremental accuracy were of interest to the user of the AROD system.

With the exception of thermal noise and multipath errors, all errors introduced by the AROD equipment have been allocated at either insignificant or negligible levels since the penalties incurred thereby are justifiably small. The errors caused by multipath effects at elevation angles near the horizon have not been made negligible because of the cost required to do this. A large component of the total range rate measurement error at the  $5^\circ$  minimum elevation angle (See Section 2.5) may be introduced by multipath effects. However, this error decreases rapidly with elevation angle, contributing less than 1 per cent of the total range rate error at elevation angles greater than  $15^\circ$ .

It must be noted that the economic balance of errors discussed above applies only when the absolute values of the range and range rate errors are considered. Where incremental measurements are useful to the guidance system, an order of magnitude improvement in accuracy may be achievable. Biased measurement errors such as the entire error due to the uncertainty of  $c$  and a major portion of the propagation error can be

eliminated. Non-biased errors which are subject to short term smoothing of which thermal noise errors are the most important, can also be significantly reduced for incremental measurements.

The remainder of this section includes:

1. A tabulation of equipment parameters for the representative AROD system.
2. A functional description of the recommended AROD system including the operating principles and the bases for choosing the recommended design approaches and critical components.
3. An analysis of the system parameters and the procedure employed in the study for choosing them.
4. A comparison of the recommended design approach for the unattended ground transponder with competing design approaches.
5. A trade-off analysis relating system measurement accuracy to system penalty factors. The basis for choosing the representative system over cheaper and more costly systems (in terms of system penalty factors) is given.

It is appropriate at this point to summarize the "ground rules" that governed the system design. The performance objectives for the equipment have been assumed to be those established in the error "budget" in Section 2.5. In accordance with discussions with the Contracting Officer's Representative, modulation techniques that were considered for the system design were restricted to the type termed "sidetone ranging" schemes. In these systems all the spectral components of the transmissions are continuous waves. Multiple ranging tones are employed for system timing, the highest frequency tone being used for fine range determination, the lower frequency tones being employed for resolving range ambiguities in successively larger range quanta.

It was assumed that the vehicle trajectories to be considered would lie between altitudes of 90 and 2000 nautical miles. Although it is desirable for the ground transponders to track the vehicle from horizon to horizon, it became apparent early in the program that three factors militated against this. Propagation errors and multipath errors increase very

rapidly at angles approaching the horizon, and a finite portion of the vehicle pass must be allocated for acquisition of the tracking filters employed in the vehicle and transponder. A minimum elevation angle of  $5^{\circ}$  was chosen by examining the system complexity required to prevent multipath and propagation errors from becoming dominant, and to acquire the tracking filters rapidly.

The remaining "ground rule" that required definition for the system design to proceed was the selection of a reasonable as well as representative weight and power input penalty incurred by the spacecraft equipment. Informal discussions with the Contracting Officer's Representative led to selections in the region of 25 pounds and 100 watts.

The most significant operating parameters and penalty factors for the representative system are tabulated in Table 5.

### 3.2 Principle of Operation

A functional description of the representative AROD system design which evolved from the Feasibility Study is given in the following paragraphs. For a more detailed discussion of important implementation problems introduced by the representative system design, refer to Section 4, Equipment Implementation.

#### 3.2.1 Spacecraft Equipment

A functional block diagram of the vehicle equipment design is shown in Figure 14. The design shown employs only solid state components that are presently available. The diagram shows the elements for processing signals from a single ground station. Signals from the three other ground stations are processed in an identical manner by additional tracking filters and measurement circuits following the multiplex filter.

The four ground stations responding simultaneously are isolated from each other by means of a unique translation frequency employed in each ground station within view of the spacecraft. The command transmitter issues turn-on signals and selects the translation frequencies for the four activated stations. A simple coding scheme will be employed to prevent unauthorized or unintentional turn-on of the ground stations.

Table 5

## Parameters of the Representative AROD System

## VEHICLE EQUIPMENT

Center Frequency (Nominal)	2000 Mc
Antenna Gain (Minimum)	Unity
Antenna Coverage (Minimum)	Horizon to Horizon
Transmitter Power Output (Minimum)	12.5 watts
Receiver Effective Noise Temperature (Maximum)	900° K
Receiver Tracking Bandwidth (Carrier Loops)	200 cps ( $h_v^* > 500$ nautical miles) 1000 cps ( $h_v < 500$ nautical miles)
Acquisition Interval (99% probability)	$E^{**} \leq 5^\circ$ (Vehicle Ascending)
Data Sampling Rate (Maximum)	10 samples/second
Equipment Weight (Estimated)	27 pounds
Equipment Power Input (Estimated)	114 watts
Equipment Volume (Estimated)	800 cubic inches

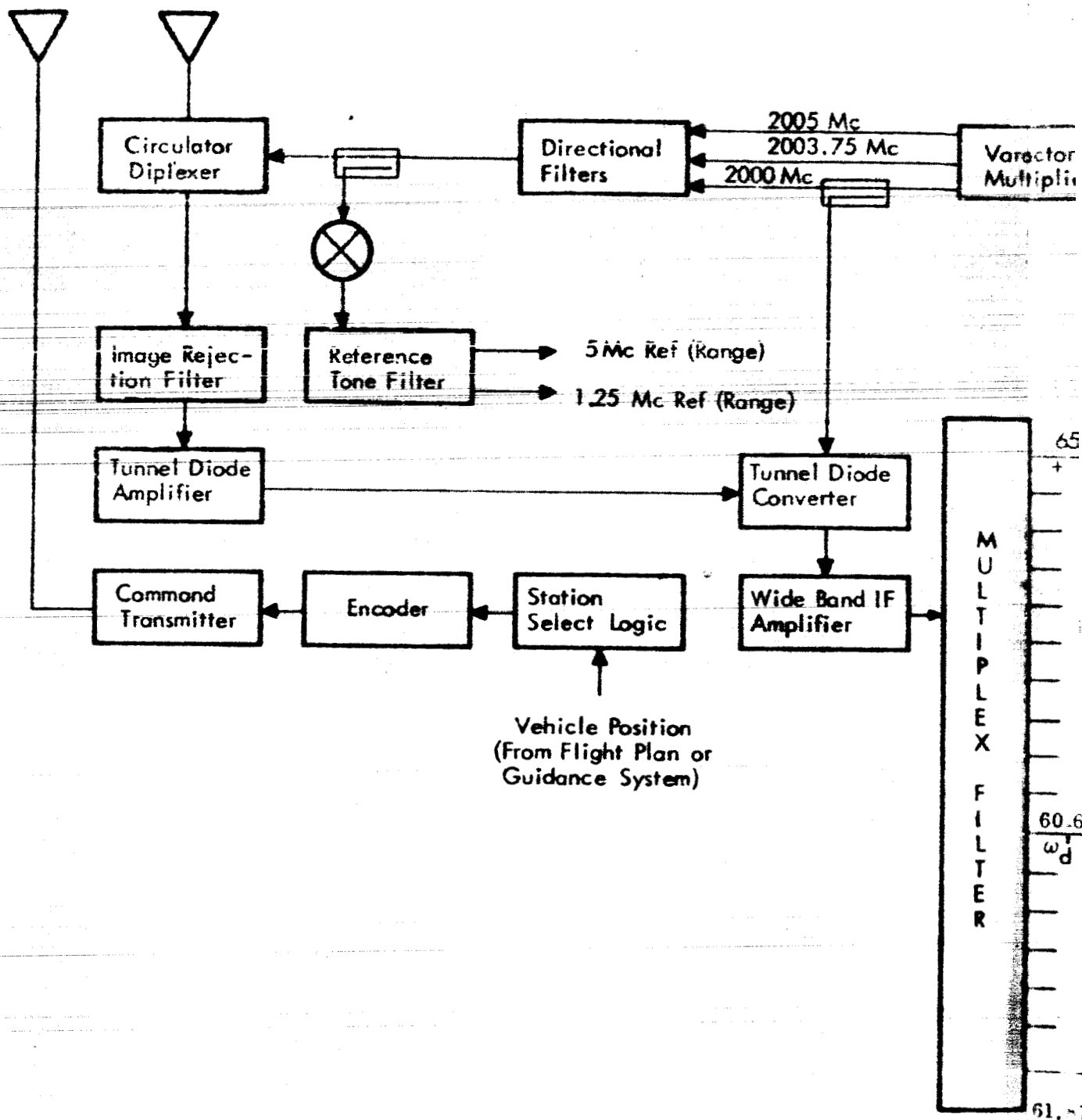
## GROUND TRANSPONDER

Translation Frequency (Nominal)	60 Mc
Antenna Gain (Minimum)	13 db ( $E = 5^\circ$ ) 7 db ( $E = 90^\circ$ )
Number of Beams	13
Antenna Coverage	Omnidirectional in Azimuth for $E > 5^\circ$ .
Transmitter Power Output (Minimum)	20 watts
Receiver Effective Noise Temperature (Maximum)	600° K
Receiver Noise Bandwidth (Maximum)	1 Kc (for principal spectral components)
Acquisition Interval (99% probability)	$E \leq 4^\circ$

## SYSTEM DESIGN MARGIN

10 db

\* $h_v$  = Vehicle Altitude\*\* $E$  = Vehicle Elevation Angle to Ground Transponder



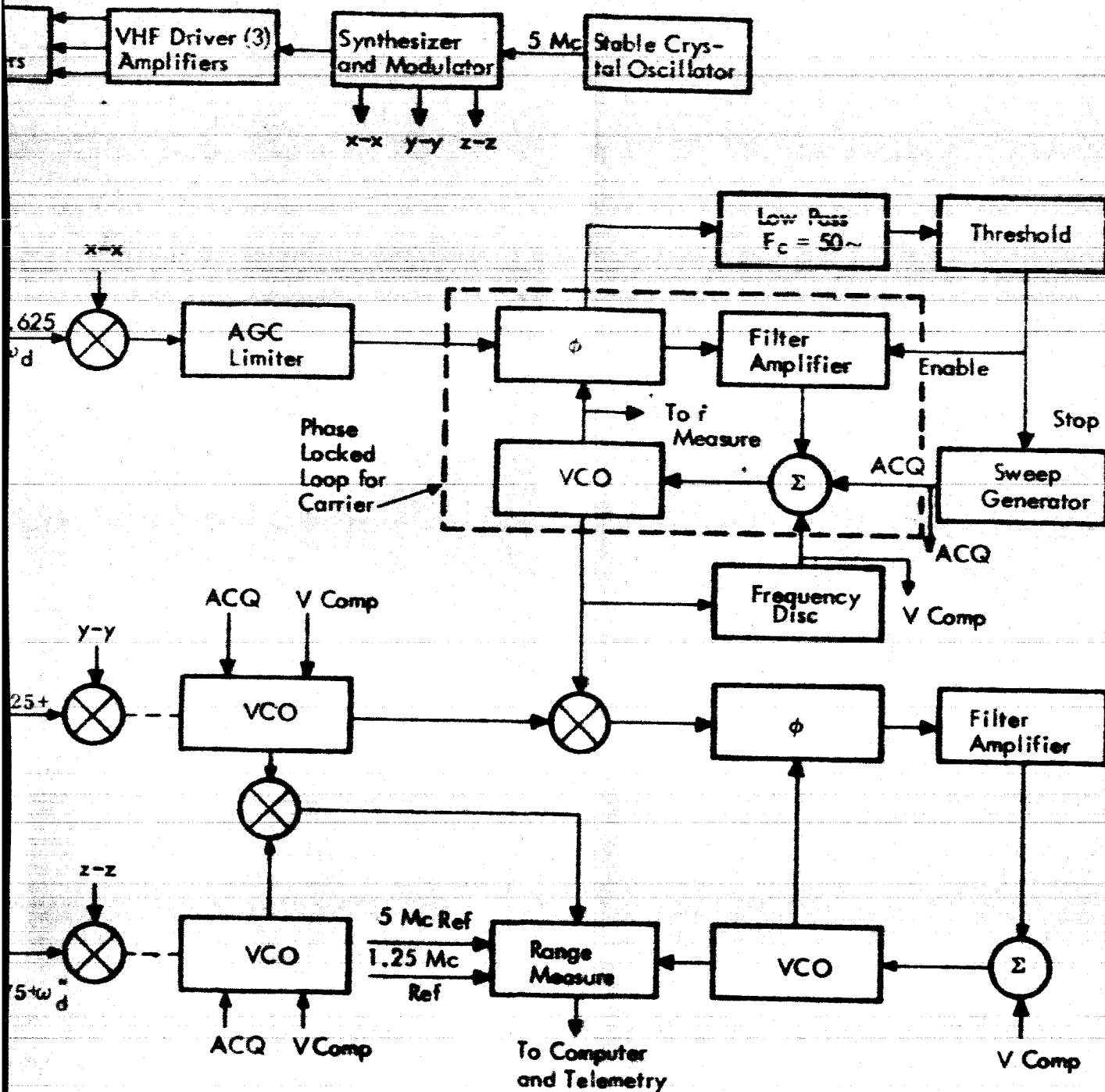


Figure 14. Vehicle Equipment Functional Block Diagram

The most important subsection of the vehicle equipment is the transmitter chain because it weighs more and requires more input power than any other portion of the equipment. Moreover, achieving a given level of reliability is almost always more difficult for transmitting components than it is for the receiving and data processing components which constitute the balance of the vehicle equipment. Several approaches toward the achievement of r-f power outputs in the range of 2.5 to 30 watts of cw power at 2000 megacycles\* which could be suitably modulated for the sidetone ranging scheme and capable of the frequency stabilities dictated by the performance objectives of the system, were assessed during the study. The factors viewed in making the comparison between the various approaches were efficiency, reliability, ruggedness, flexibility, ease of modulation, weight and size. Among the components evaluated were klystrons, crossed field devices including amplitrons and voltage tuned magnetron oscillators, traveling wave tubes, thermionic amplifiers and oscillators, and varactor harmonic generators.

The varactor harmonic generators were selected as the recommended r-f power source over the other approaches by a rather clear margin. They are outstanding from the point of view of reliability and ruggedness, especially since, unlike the other approaches, they are low voltage devices with far less critical power supply requirements than the competing components. Varactors available today are capable of a 2.5 watt output at S-band. With present day transistors, driving the varactor chain somewhat below 100 Mc is optimum. An overall efficiency, that is the ratio of r-f power output to dc power input to the transistor driver, of 15 per cent is estimated for the recommended approach where the varactor chain is driven at approximately 60 Mc and a multiplication of 32 is afforded by the varactor chain. This efficiency may appear grossly inferior when viewed against the extremely high efficiencies, 50 per cent or higher, that are quoted for some of the other components, notably the amplatron.

---

\*The reasons for selecting these parameters are discussed in Section 3.3.

However, the efficiencies quoted for these devices refer to the plate circuit efficiency. When one takes into account the power losses in the high voltage converter, the regulating circuit (a constant current source for the amplatron), the filament circuit, and the driver circuit, it is doubtful that more than 25 per cent overall efficiency can be achieved while maintaining the phase stability requirements of the AROD system. Another important factor favoring the transistor driver-varactor multiplier approach over the competing components is the anticipated extension of capabilities of these components in the near future. Since their introduction for microwave applications, varactors have shown a continuing improvement in power output and efficiency at higher and higher frequencies. In addition, high frequency transistors have shown continuing improvement in these respects, although at a somewhat slower pace.

The total r-f power output of the vehicle transmitter of 12.5 watts is developed by means of 5 harmonic generator chains, each with a 2.5 watt output. Five watts of cw power are generated at nominal frequencies of 2000 and 2005 Mc to provide the 5 Mc fine ranging tone. The remaining 2.5 watts are developed at a carrier frequency of 2003.75 Mc which is phase modulated by range ambiguity resolving tones of approximately 156 kc, 9.8 kc, 610 cycles and 19 cycles. All the carrier frequencies and sidetone frequencies are derived from a common stable crystal oscillator operating at 5 Mc.

The circuits required for receiving and tracking the retransmitted and translated signals from the ground station will now be discussed.

Three types of low noise r-f preamplifiers were considered for this application: traveling wave tubes, parametric amplifiers, and tunnel diodes. Although the tunnel diodes are at a slight disadvantage with respect to the other approaches in terms of sensitivity, they were chosen on the basis of their reliability, ruggedness and simplicity of the r-f circuit. Traveling wave tubes were rejected because of the excessive weight and power input penalties associated with them, as well as the need for a high voltage power supply. For the AROD applications, the higher instantaneous bandwidths that can be achieved with the Esaki diode circuits are an important advantage

in minimizing the uncompensatable differential phase errors between the spectral components of the signal. Parametric amplifiers are relatively narrow band and require a more complex r-f circuit when pumping requirements are considered. Moreover, it appears reasonable to assume that the improvements in sensitivity performance of the Esaki diodes will continue in the near future.

Each of the three carrier signals will be tracked by a phase locked loop (for each of the four ground transponders). The voltage controlled oscillator (VCO) output of the phase locked loop tracking the translated and down converted 2000 Mc carrier will be applied to a digital range rate measuring circuit. The Doppler offset frequency will be measured by means of a digital frequency comparator using a reference frequency derived from the 5 Mc stable oscillator. For the signal tracking circuits shown in Figure 14, the frequencies denoted at the output of the multiplex filter in the receiver arise from a downward translation of 65.625 Mc at the ground transponder. Using a sample of the 2000 Mc carrier output of the spacecraft transmitter as the local oscillator, intermediate frequencies of 65.625 Mc, 60.625 Mc and 61.875 Mc represent the 2000 Mc, 2005 Mc and 2003.75 Mc carrier signals, respectively, for a zero Doppler offset condition. The outputs of the voltage controlled oscillators tracking the translated and down converted 2000 and 2005 Mc carriers are applied to a product detector whose difference frequency output is tracked by a fourth phase locked loop. The output of this VCO is compared in phase to the 5 Mc reference tone in a digital range measuring circuit for the determination of fine range.

The first ambiguity resolving signal is developed by product detection of the outputs of the VCO's tracking the 2005 and the 2003.75 Mc carriers. No additional phase locked loops are required for tracking the lower frequency ambiguity resolving signals. These signals are tracked by dividing the frequency of the output from the VCO tracking the fine ranging tone by the appropriate ratio and using individual phase tracking filters as shown in the block diagram, Figure 15. The frequency divided versions of the VCO output are in essence, the equivalent of a VCO in a conventional

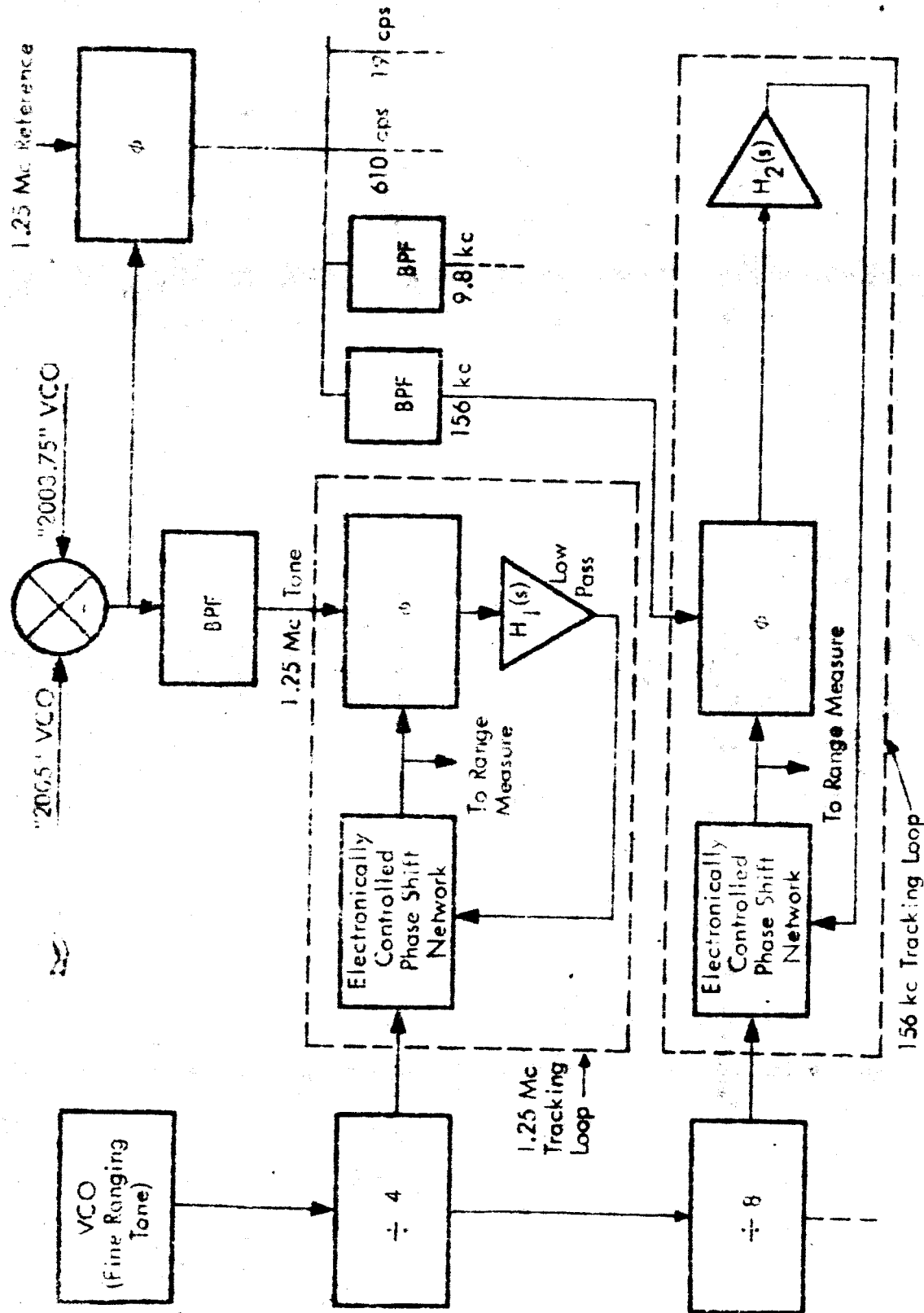


Figure 15. Block Diagram of Range Ambiguity Resolving Tones Tracking Circuits

phase locked loop. In a phase tracking filter, the divided VCO output is adjusted in phase to coincide with the phase of the noisy ambiguity resolving tones extracted by phase demodulating the first ambiguity resolving tone signal using the 1.25 Mc reference tone as the phase reference. The phase adjustment is accomplished by a voltage variable phase shift network employing electronically controlled reactances (saturable reactors or varactors); the network is controlled by a loop filter with a proportional term and an integration term.

For the spectrum chosen in the representative system, the 2.5 watts allocated to the ambiguity resolving tones is sufficient to maintain the probability of resolving a range ambiguity erroneously in any of the tones to less than 0.1 per cent. The method of synthesizing the transmitted spectrum permitted by the modular varactor harmonic generator transmitter scheme affords a great deal of flexibility in the system design. For certain missions and trajectories it may be desirable to allocate a greater portion of the total vehicle transmitter power to the carrier on which the Doppler frequency is being measured. The derivation of the reference range tones after all the spectral components have been combined in the multiplex filter is recommended for the reason that the system will be immune to differential phase distortions and perturbations introduced by the transmitter chain or multiplex filters that occur over a period greater than the two way propagation delay.

### 3.2.2 Ground Station Equipment

The overriding design objective of the unattended ground station is to provide sufficient signal-to-noise-ratio at the vehicle to meet the performance objectives and to achieve a high order of reliability within reasonable equipment costs. It is reasonable to assume that an operational AROD system would be expected to achieve a useful life of many years. By obviating the need for frequent logistics support, the system designer can achieve a saving in operating costs which could easily exceed the cost of establishing the AROD ground network.

A functional block diagram of the representative ground transponder suitable for unattended operation in remote areas is shown in Figure 16. The major design problem for the ground transponder is to meet simultaneous requirements for continuous tracking of the spacecraft within an almost hemispherical volume and a minimum power gain requirement ranging between 13 db at a  $5^{\circ}$  elevation angle and 7 db at the zenith. The ground station design approach that was selected during the Feasibility Study features a multi-beam antenna with stacked beams in elevation. Two beams with semi-annular coverage in azimuth are provided for each elevation quantum. A total of 13 beams are required, the lowest of which has a beamwidth of  $5^{\circ}$  centered at an elevation angle of  $5^{\circ}$ . Beam cross-over points in elevation are 1.5 db down from the maximum. The beamwidths of the higher elevation beams are tapered in accordance with the inverse of the slant range squared for the 2000 miles maximum altitude. Around the zenith, a conical beam whose half angle is  $35^{\circ}$  is provided.

A superheterodyne receiver employing a parametric amplifier front end is provided for each of the 13 ports of the antenna. Because of the limited vehicle transmitter power dictated by vehicle penalty considerations, the signal-to-noise ratio available over the one-way Doppler band of  $\pm 50$  kc is much less than unity (refer to subsequent paragraphs for details). For this reason, the noiseband must be limited to much less than the Doppler bandwidth prior to retransmission; otherwise, at high vehicle altitudes, gross inefficiency would result in the ground station retransmission, in that the signal power output would be only a small part of the total power output.

For each of the 13 receivers in the representative design approach, following IF amplification of the received signal spectrum by means of three amplifiers whose bandwidth is much larger than the Doppler band, the IF output for the 2000 Mc received carrier is applied to an automatic frequency control circuit. This circuit will acquire the minimum received signal within an offset of 400 cycles per second, within one third of a second, with a probability of .9.<sup>11</sup> The probability of acquisition



increases to .999 for a one second interval. After acquisition, the tunable VHF oscillator will track the signal to an accuracy of 100 cycles per second. An active condition in any one of the thirteen receivers will be sensed by individual threshold circuits which will enable a gate associated with each receiver. The purpose of the gates is to prevent thermal noise from inactive receivers (or beams) from entering the transmitter circuits. Following summation of all the gate outputs (only one active), the entire spectrum is multiplexed through seven crystal filters. Each crystal filter has a bandwidth of less than one kc and matched phase delay characteristics. This technique will introduce uncompensatable phase errors well within the error allocated in Section 2.5. Active circuits in the entire signal processing chain of the transponder are always much wider in bandwidth than the band limiting, passive components. Following demultiplexing of the signal components, the IF signals are heterodyned up to S-band by means of the same local oscillator signal that was used for down conversion in the front end translated to a lower frequency by the ultra-stable translation oscillator selected in the command link. This output, on the order of a milliwatt, is applied to a single transmitter chain employing coaxial UHF triodes. The transmitter output is nominally 25 watts and is applied to a ferrite switching matrix which is controlled by the threshold detectors in the frequency tracking loops. The ferrite switching matrix directs the transmitter output to the active beam for retransmission to the spacecraft.

### 3.3 Parametric Analysis

#### 3.3.1 Signal Parameters

The operating envelope of the AROD system is bounded by the minimum vehicle altitude of 90 nautical miles, the maximum altitude of 2000 nautical miles, and a minimum elevation angle at which the ground transponders will operate within the performance given in Section 2.5. The minimum elevation angle is dictated by multipath and propagation error considerations.

Both these sources of error increase rapidly as the radiation path approaches the horizon. A lower limit of  $5^\circ$  has been chosen as the point where propagation effects do not contribute dominant measurement errors. In addition, only a moderate degree of complexity need be introduced in the ground station antenna design to achieve a sufficiently low sidelobe level at the horizon to also prevent multipath errors from being dominant.

The significant signal parameters that result from a carrier frequency of 2 Gc are tabulated for circular overhead passes in Table 6.

Table 6

AROD Signal Parameters

Vehicle Altitude (naut.mi.)	Elevation Angle (degrees)	Range (naut. mi.)	Doppler Freq. (cps)	Doppler Rate (cps/sec.)	Acquisition Time (sec.)	Space Loss (db)
90	5	600	$10^5$	68	10	159
90	90	90	0	$5 \times 10^3$	—	143
2000	5	3940	$5.3 \times 10^4$	1.7	25	176
2000	90	2000	0	91	—	170

The overhead pass imposes the most severe requirements on the equipment with respect to maximum Doppler shift and maximum Doppler rate. The acquisition time requirement shown in the table is the interval during which the ascending vehicle occupies the elevation angle increment of  $4-5^\circ$ . This interval will be minimum for the overhead pass, hence, the equipment requirement is again most severe for this case. Path losses shown for the boundary conditions in the table are dependent only on the vehicle altitude and elevation angle and will be the same for overhead and non-overhead passes. It can be concluded therefore, that the system performance objectives can be met for all vehicle trajectories if they are met for the overhead pass.

### 3.3.2 Choice of Operating Frequency

Among the AROD system parameters, the operating frequency has the strongest influence upon system performance and penalty factors. A nominal operating frequency of 2 Gc for the AROD system was established during the study from the results of the propagation error investigation and the equipment design considerations given below. The propagation error results are summarized in paragraph 2.2.2 and are treated in detail in Appendix B. Propagation errors contribute to the AROD measurement errors as do equipment errors and the errors due to the uncertainty of the vacuum velocity of light. By examining the basic design constraints of the AROD system where:

- Vehicle antenna gain is restricted to unity by the need for horizon to horizon coverage;
- Ground transponder antenna gain is restricted to low orders from considerations of complexity (hence, cost and reliability) and the need for nearly hemispherical coverage; and
- Increasing the vehicle transmitter power output introduces severe weight and power input penalties to the spacecraft,

it became clear that the operating frequency should be the lowest at which the system measurement accuracy objective could be achieved. This follows from the consideration that, for the same signal to noise ratios and with all other system parameters remaining fixed, the product of vehicle power output and ground station antenna power gain is related inversely to the square of the frequency. However, this trend is opposed by the fact that propagation and multipath errors increase rapidly as the operating frequency is lowered.

At 2 Gc, the range and range rate errors introduced by the uncertainties of the propagating medium are in reasonably good balance with the errors due to the uncertainty of  $c$ . The range propagation errors estimated during the study were more strongly considered in choosing the operating frequency than the range rate errors for several reasons, the most important of which was the higher confidence level in the range error estimates.

This was necessitated by the paucity of published data useful to the estimation of range rate errors for AROD.\*

The range error due to the uncertainty of the propagation velocity of light in a vacuum is only range dependent and ranges from less than 0.2 meters to more than 7 meters over the extremities of the operating envelope of the AROD ground station.

At 2 Gc, the residual range errors due to the uncertainty of the characteristics of the propagating medium (after corrections are made for a standard atmosphere, vehicle altitude, and elevation angle) are in general less than or equal to the error due to the uncertainty of  $c$ . At 1 Gc, the residual propagation errors in range would be approximately three times greater. For this reason, the performance objective for total range measurement error could not be attained. An increase of operating frequency, say to 4 Gc, would at best reduce propagation errors by a factor of two. For the same vehicle penalties and ground station investment the total range and range rate measurement errors increase by about 50 per cent with the 4 Gc system compared to the 2 Gc system.

Higher operating frequencies might become attractive for missions requiring operation at ranges of tens of thousands of miles and beyond where wide field of view antennas are no longer required. In these applications directive antennas can be used to great advantage at the vehicle. Choice of a higher operating frequency is particularly attractive for these applications where the antenna aperture and weight are constrained by vehicle limitations.

### 3.3.3 Range Equation Parameters

The fundamental limitation of the AROD equipment accuracies for both range and range rate are the errors due to thermal noise. The finite

---

\*For missions where range rate errors affect system performance more strongly than range errors, the conclusions on the optimum operating frequency may have to be re-evaluated. It appears that more useful data for estimating range rate errors introduced by the propagating medium will be available in the near future.

signal-to-noise ratios that can be achieved in the tracking filters in the vehicle receivers are determined by the available signal power, the spectral density of the noise surrounding the signal, and the bandwidth of the receiver tracking filters. The bandwidth of the tracking filters must be sufficiently wide to track the dynamics of the input signals. The dynamic characteristics of the signals are introduced by the velocity and acceleration of the spacecraft with respect to the ground stations. These cause the Doppler frequency shift and the rate of change of Doppler frequency.

It will be shown in Section 3.3.4 that, with a signal power-to-noise power density factor  $(S/N_o)$  of  $2 \times 10^3$  cycles per second or greater available at the vehicle receivers for the two principal spectral components of the AROD transmission, the objectives for noise errors established in Section 2.5 can be realized. The  $(S/N_o)$  ratio at the vehicle is also crucial from the point of view of establishing the acquisition time of the tracking filters. The  $(S/N_o)$  ratio at the spacecraft receiver can be expressed by the following:

$$\left[ \frac{S}{N_o} \right]_{RV} = \frac{P_{RG} A_G G_{TG} L_S^{-1} M_U^{-1} L_U^{-1}}{N_{oV} + N_{oG} A_G G_{TG} L_S^{-1} L_U^{-1}} \quad (9)$$

where:

- $\left[ \frac{S}{N_o} \right]_{RV}$  - is the signal power-to-noise power density ratio at the vehicle receiver.
- $P_{RG}$  - is the signal power received by the ground transponder.
- $A_G$  - is the net electronic amplification of the transponder.
- $G_{TG}$  - is the transmitting antenna power gain of the transponder.
- $L_S$  - is the space loss.
- $M_U$  - is the system design margin for the up link.
- $L_U$  - is the transmitting loss at the transponder.
- $N_{oV}$  - is the power density of the self noise of the vehicle receiver.
- $N_{oG}$  - is the power density of the self noise of the ground receiver.

The vehicle antenna gain is assumed to be 0 db for receive and transmit by virtue of the horizon-to-horizon coverage that is needed. It can be seen from Equation 9 that  $[S/N_O]_{RV}$  will always be smaller than the  $S/N_O$  ratio at the ground transponder receiver by a factor greater than  $M_U$  because of the degradation introduced by the self noise of the vehicle receiver,  $N_{OV}$ . It is important to note that increasing  $A_G$  indefinitely does not obtain a significant improvement in  $[S/N_O]_{RV}$  at levels where the retransmitted noise from the ground station swamps out the receiver self noise at the vehicle.

Since primary power is far more expensive at the vehicle than at the ground station, even for remote sites with only occasional maintenance, it is appropriate that the component of noise at the input to the vehicle receiver due to the amplified noise of the transponder be greater than the self noise of the vehicle receiver. If we make:

$$N_{OG} A_G G_{TG} L_S^{-1} L_U^{-1} = 3 N_{OV} \quad (10)$$

the degradation of  $[S/N_O]_{RV}$  due to  $N_{OV}$  is 1.2 db compared with a 3 db degradation if both components are equal. A further increase of the transmitted noise component by a factor of 3 will reduce the  $N_{OV}$  degradation by only an additional 0.7 db and appears to be uneconomical. The technique of swamping out the vehicle receiver self-noise provides a second important advantage by reducing the effect of vehicle receiver sensitivity degradation on overall system performance, and thus effectively increasing the system design margin. For the operational AROD system the apparently uneconomical extension of this technique may be warranted by the reduction in vulnerability to interference that the technique affords. This is particularly applicable at ground stations where commercial power is available and frequent servicing is possible. Although the ground stations are vulnerable to interference, both hostile and unintentional, they do not pose as serious a problem in this respect when compared to the vehicle equipment, inasmuch as the system degrades gradually as ground stations become inoperative by responding to interfering signals.

In addition, greater sidelobe reduction at and near the horizon can be employed at the ground station, thereby restricting the volume from which interference could enter the ground receiver or alternatively, increasing the intensity of the interference required to degrade transponder performance. The susceptibility to interference of the system is fundamental to the modest signal power that is developed at the spacecraft and ground terminals, and serves to emphasize the importance of carefully choosing the operating frequencies for the system as well as the siting of the ground stations.

From Equation 10, the product of net electronic gain and transmitting antenna power gain ( $A_G G_{TG}$ ) for the ground transponder can be determined for the maximum range of 3940 nautical miles.

$$\left[ A_G G_{TG} \right]_{\max} = \frac{3T_{eV}}{T_{eG}} L_S \max L_U \quad (11)$$

where:  $T_{eV}$  - is the effective noise temperature of the vehicle receiver.

$T_{eG}$  - is the effective noise temperature of the ground receiver.

Conservative estimates for effective noise temperatures are  $900^\circ$  Kelvin for the tunnel diode r-f preamplifier in the spacecraft and  $600^\circ$  Kelvin for an uncooled parametric amplifier at the transponder. A 1 db transmitting loss is assumed for the up link. At 3940 nautical miles, the space loss is 176 db and the maximum value of  $A_G G_{TG}$  is therefore,  $2.5 \times 10^{18}$  or 184 db.

The minimum value of the  $(S/N_o)$  ratio at the ground transponder can now be calculated:

$$\left[ \frac{S}{N_o} \right]_{RG \min} = \frac{4}{3} \left[ \frac{S}{N_o} \right]_{RV \min} M_U \quad (12)$$

The system design margin for the transponder to spacecraft link,  $M_U$ , is taken as 5 db to allow for component degradation. An additional 5 db is assumed for the down link. Equation 12 results in a minimum value for  $\left[ \frac{S}{N_o} \right]_{RG}$  of  $8.3 \times 10^3$  cycles per second where the noise power

density is given in terms of power per cycle per second. The minimum power for the received signal at the ground station can be established from this ratio. For the all solid state transmitter that has been selected for the representative system with a total power output of 12.5 watts, 5 watts is allocated to each of the principal spectral components at 2000 and 2005 megacycles with the remaining 2.5 watts allocated to the phase modulated secondary carrier at 2003.75 megacycles. The minimum received signal power required for each of the major spectral components at the ground station is given by:

$$P_{RG \min} = 8.3 \times 10^3 k T_{eG} = -162 \text{ dbw} \quad (13)$$

where:  $k$  - is Boltzman's constant

The receiving antenna power gain that is required at the ground station at  $5^\circ$  elevation angle can be calculated from:

$$G_{GR}(5^\circ) = \frac{P_{RG} L_{S \max} M_D L_D}{P_{oV}} = 13 \text{ db} \quad (14)$$

where:  $M_D$  - is the system design margin for the down link.  
 $L_D$  - is the transmitter losses at the vehicle.  
 $P_{oV}$  - is the vehicle transmitter power output for each principal spectral component.

As with the up link,  $M_D$  is taken as 5 db. The transmitting losses at the vehicle total 1 db; 0.5 db for the multiplex filter network which combines the varactor output into the antenna line, 0.3 db for the circulator employed in the diplexer and 0.2 db transmission line losses.

The receiving antenna gain required at higher elevation angles can be tapered downward with the square of the slant range for the 2000 nautical miles orbit to a minimum of 7 db at the zenith while maintaining the required  $(S/N)_{oRG}$  of  $8.3 \times 10^3$  cycles per second.

The power output of the AROD ground transmitter will be maintained constant by means of a simple AGC loop. The gain control for the AGC loop will be provided at the intermediate frequencies where the required gain swing of less than 40 db can be provided easily. The total power

output of the ground station, which includes the amplified receiver noise, is given by:

$$P_{TG} = 2.5 \left[ P_{RG \min} A_{G \max} + N_{oG} B_G A_{G \max} \right] \quad (15)$$

where:  $B_G$  - is the noise bandwidth of the ground transponder about each of the principal spectral components.

$A_G$  can be established from Equation 11 where the maximum value required for the product  $A_G G_{TG}$  was determined to be 184 db. The 13 db antenna required on reception can be utilized on transmit to reduce the power output requirements of the ground transmitter. The maximum net electronic amplification required of the transponder,  $A_{G \max}$ , is therefore, 171 db. The noise component of the ground transmitter output would exceed the signal power by about 12 db if no provision were made in the transponder to narrow the noise bandwidth to less than the double Doppler band of 100 kilocycles. An automatic frequency tracking circuit similar to those employed in conventional radar front ends can be employed to reduce the noise bandwidth about each spectral component to less than one kilocycle, thereby insuring that the noise spectrum power surrounding the principal spectral component will be at least 8 db down from the signal power under all conditions. It follows that the total power output required from the ground transmitter is 18.75 watts by (exact) solution of the range equations. An output of 25 watts has been assumed as the nominal requirement for the system design.

### 3.3.4 Signal Tracking Parameters

The tracking filters employed in the spacecraft receiver can be considered to be narrow band filters which reject the noise energy arriving at the input terminal lying outside the effective bandwidth of the filter. This is accomplished by synchronizing and tracking a voltage controlled oscillator to the noisy signal by means of a cross correlation. This process essentially enhances the signal to noise power ratio at the output by a factor equal to the ratio of input noise bandwidth to the loop noise bandwidth, assuming uniform noise spectral density at the input.

The tracking and acquisition performance of phase locked loops as a function of signal parameters and loop parameters are discussed in detail in Section 4.1.3. Considering the minimum value of signal power to noise density ratio  $[S/N_o]_{RV}$  of  $2 \times 10^3$  cycles per second available at the spacecraft receiver and the two way Doppler band of  $\pm 100$  kilocycles, the signal to noise ratio at the input can be as low as - 20 db at the maximum range within the coverage envelope.

Initially, the loop oscillator will be operating at a different frequency than the input signal, and if no external aiding is provided, it will lock in a time which is a function of frequency offset, loop gain and loop bandwidth. Viterbi<sup>12</sup> has estimated the pull-in time for second order phase locked loops for noiseless signals as:

$$t_{PI} = \frac{\lambda_{eff}^2}{2\zeta\omega_n^3} \quad (16)$$

where:

- $t_{PI}$  - is the pull in time.
- $\lambda_{eff}$  - is the frequency difference between the VCO and signal at the beginning of pull-in.
- $\zeta$  - is the loop damping factor.
- $\omega_n$  - is the natural frequency of the loop.

Experimental data at the Jet Propulsion Laboratory (JPL) have shown good agreement with Equation 16 for signal to noise ratios of 10 db and lower. A minimum output S/N of 10 db will be assumed under all conditions for the loops in the AROD system in order to avoid thresholding effects. Experiments reported by Frazier and Page<sup>13</sup> have shown that near optimum acquisition performance is obtained with the loop damping factor,  $\zeta$ , set from 0.5 to 0.85. Since minimum loop noise bandwidth is obtained at a damping factor of 0.5, this value has been chosen for all the tracking filters in the vehicle. It can be seen from the foregoing considerations and the relationship of loop noise bandwidth to  $\omega_n$  derived in Section 4.2.3, that the maximum value for  $\omega_n$  in the carrier tracking loop that satisfies the 10 db signal to noise requirement, is 200 radians/second and from Equation 16, the pull-in time for an unaided loop is greater than

$10^4$  seconds. It is necessary, therefore, to provide an external means of presetting the VCO in order to bring the acquisition time within requirements. By sweeping the VCO linearly at a rate of  $10^4$  cycles/seconds<sup>2</sup> and using a 100 cycle filter followed by a threshold detector as the sensor, the positive half of the Doppler band (vehicle approaching the ground station) of 100 kilocycles will be swept in 10 seconds. For the case of minimum received  $S/N_0$  at the vehicle at 3940 nautical mile range, a 13 db signal to noise ratio will be present at the output of the 100 cycle filter when the VCO intercepts the signal. When the threshold is exceeded at the output of the 100 cps filter, the sweep will be stopped and the phase locked loop will be enabled for final pull-in. At this point, the VCO will be preset within 100 cycles of the signal. From Equation 16, the time required for final pull-in will be less than 0.1 seconds where the loop undamped natural frequency,  $\omega_n$ , is equal to 200 radians/second. The threshold detector will be set at a value corresponding to a false alarm rate of  $10^{-6}$  so that for a 13 db signal to noise ratio, the probability of detection will be 90 per cent.<sup>11</sup> Under these conditions, the cumulative false alarm probability for the entire sweep will be  $10^{-3}$ . Referring back to Table 6, 25 seconds are available for acquisition at the maximum vehicle altitude. The probability of detection within this period is greater than 99 per cent. In the event of a false alarm in the acquisition circuit, an "in lock" sensing circuit will re-initiate the acquisition sweep if an "in lock" indication does not occur within approximately one second of the time that the phase locked loop was enabled. For the 90 nautical mile orbit, where acquisition within 10 seconds is required, the signal to noise ratio at the output of the 100 cps filter is 30 db and the probability of detection on the first ten-second sweep is increased to greater than 99.99 per cent.

In the tracking mode, the output of the VCO locked to the translated and down converted 2000 Mc carrier will be used to measure the range rate. The effective loop noise bandwidth will be 200 cps at vehicle altitudes greater than 500 nautical miles. The 200 cps noise bandwidth is

the maximum bandwidth that satisfies the requirement for S/N at the output of the tracking filter to be equal to or greater than 10 db. The unsmoothed range rate error due to thermal noise in this tracking filter will be less than 0.04 meters/second at the maximum range. At lower vehicle altitudes, the increased Doppler rate due to higher vehicle accelerations introduce larger steady-state tracking errors in the phase locked loops due to lag (see Section 4.1.3). Although these errors have a negligible effect on range rate measurement accuracy as long as the loops remain in lock, they tend to drive the loop towards the non-linear and unstable operating region. Two methods of reducing the steady-state tracking errors will be employed which are extremely simple to implement. By sensing the Doppler offset in the carrier tracking loop by means of a simple frequency discriminator, velocity bias compensation can be introduced as an open loop correction. This reduces the static error in the tracking loop by the fractional accuracy to which the correction is made. Compensation to one part in one hundred is easily obtained with available discriminators. This technique is described further in Section 4.1.3.

The second method of reducing dynamic errors is to capitalize on the greater signal power that is available at the lower altitudes at which the signal dynamics are most severe, by increasing the loop bandwidth as a function of altitude. By the simple expedient of changing the loop bandwidth from 200 cycles to 1000 cycles at altitudes below 500 nautical miles, the steady-state error due to Doppler rate will be reduced by a factor of 25, while the thermal noise error will not exceed 0.038 meters/second. Control of the loop bandwidth can be accomplished by changing the loop gain or the time constant of the loop integrator.

Two additional phase locked loops with the same parameters as the one described above will be included in the vehicle receiver for tracking the translated carriers that are transmitted at the vehicle at frequencies of 2005 and 2003.75 megacycles. Velocity compensation for these loops will be provided from the discriminator in the 2000 megacycle tracking filter.

The 5 megacycle fine range tone signal will be developed by product detection of the 2000 and 2005 megacycle carriers. A 3 db degradation of  $S/N_0$  will be encountered in the detection process (see Appendix D) so that the minimum input  $S/N_0$  to this loop will be  $10^3$  cycles per second. The maximum Doppler shift and Doppler rate will be reduced by a factor of approximately 400 for this loop, due to the frequency ratio of the carrier to the fine range tone. Velocity compensation will be provided to this loop from the 2000 megacycle tracking filter to reduce the steady-state tracking errors. Unlike the range rate measurements, steady-state phase errors in the tracking filter are added to the thermal noise in the range measurement. Steady-state errors in the 2000 and 2005 megacycle loops are essentially equal, depending on how well the parameters of the two loops are matched, and will cancel each other in the product detector. However, the total thermal noise errors are summed in an rms fashion. The optimum value for  $\omega_n$  of the 5 megacycle loop is approximately 30 cycles per second and will result in a total tracking error of 1.6 meters at the maximum range of 3940 nautical miles.

#### 3.4 Comparison of the Transponder Design Approach to Other Approaches

The requirement for unattended operation in remote areas was the overriding consideration governing the selection of the ground station design approach. For these unattended stations, the paramount design objective should be simplicity of the transponder design, employing a minimum number of critical circuits and components. With the vehicle transmitter power output established by vehicle penalty considerations and the error budget, operating frequency, receiver antenna gain, and effective noise temperature of the transponder receiver are the parameters which most strongly affect ground station complexity.

The design factors affecting the choice of the 2000 Mc nominal carrier frequency are treated in Section 3.3.2. These factors affect all competing design approaches to the ground station in a similar manner.

Conceptually, use of a Maser receiver in conjunction with a carefully shaped single beam antenna covering the AROD operating envelope and with extremely low sidelobes at the horizon, is ideal. However, at this writing, no Maser is known to exist which has been proven feasible for unattended operation. If such a device were to be developed in the near future, it is doubtful that the cost could be competitive with the recommended design approach. Moreover, such a design is inherently extremely vulnerable to interference and would probably necessitate the use of complex, anti-interference techniques.

The two design approaches described in IBM Proposal "Airborne Ranging and Orbit Determination System (AROD)" dated 20 April 1962, submitted to MSFC, were considered during the study. The recommended design approach is generically related to the approach termed "Active Ground Station" in the proposal. The "semi-passive" approach<sup>20</sup> was rejected for two principal reasons. First, for the highly directive case, where hundreds or more elements are employed, the cost of providing a high gain amplifier for each element is prohibitive. If a 1000 element retroreflective antenna is taken as an example, approximately 140 db of net electronic amplification would be required for the 4000 mile maximum slant range. In addition, the problems of maintaining differential phase delays at the carrier frequencies within limits prescribed by keeping defocussing effects within reasonable limits, are difficult for amplifiers of this order of gain. Contrastingly, in the preferred design, absolute carrier frequency phase shifts in the single signal processing channel are of little concern. Only the uncompensatable differential phase delays between spectral components introduce measurement errors in the recommended approach. The use of a single wideband multiplexed amplifier, in lieu of the individual amplifier channels, does not appear feasible with a practical design, insofar as the performance objectives established on the study are concerned, by virtue of unavoidable intermodulation effects. The second major reason for the rejection of the semi-passive approach is the fact that its antenna gain, as a function of direction, is not compatible with the operational envelope of the AROD system. If planar arrays are

employed, at low elevation angles where maximum antenna gain is required, the gain of the planar array would be a minimum. No economical design approach was conceived during the study to circumvent this incompatibility. Use of the self-focussing semi-passive approach and designing for more modest antenna gain would ameliorate only the economic shortcomings of the approach because of the large reduction of the number of elements needed. However, all the other disadvantages would still apply.

For the recommended approach, annular beams stacked in elevation, where the gain for each beam can be individually controlled, are ideal for the AROD application. This served as the major reason for selecting the recommended antenna design in favor of the Luneberg lens that was described in the IBM Proposal. The beam geometry of the selected antenna is also ideal from the point of view of minimizing system performance degradation due to multipath transmissions, inasmuch as the maximum directivity is afforded in the elevation plane. This permits control of the fractional transmitted power illuminating the surrounding sea or ground clutter. For the recommended antenna, sidelobe level at the horizon will be maintained below -20 db with respect to the peak of any of the beams. This will obviate any significant fading and will maintain multipath errors within the budget.

Utilization of the recommended antenna in a system employing only one scanning receiver channel introduces the complexities of implementing a track-while-scan capability. Although more complex than the recommended approach for the unattended ground station, the single receiving channel approach would afford a considerable saving in equipment costs. This follows from the fact that the cost of the additional r-f switch matrix in the receiver and the track-while-scan logic will be more than offset by the elimination of 12 receiving channels, each containing a parametric amplifier. On the other extreme, the most reliable utilization of the multi-beam antenna would be to provide individual transmitter chains for each beam. This is the equivalent of 13 independent transponders operating with a common antenna structure. In this manner, failure of any one of the transponders would result only in introducing a gap in the coverage envelope of the ground station.

It is obvious that the system designer should tend towards the redundant approach where the unattended station with minimal logistic support is concerned. In terms of acquisition time, where a single receiver scans the 13 antenna ports, the acquisition time would be increased by a factor of 13. This may be only marginally acceptable. Recalling that noise band limiting is essential in the ground transponder, by virtue of the limited spacecraft power output which results in a signal-to-noise ratio of less than -10 db at the maximum range, a frequency tracking scheme must be included. Once available, the frequency tracking circuit affords a simple means of determining an active beam condition and permits the use of one-to-one logic in controlling the ferrite switching matrix at the output of the transmitter. For these reasons, use of multiple receivers rather than multiple transmitters is justifiable on the grounds that transponder performance is improved thereby, as well as reliability. The recommended system design can be regarded, therefore, as a hybrid where the best compromise is sought between reliability and equipment cost. Ultimate decision as to the final configuration for the unattended stations must await the evaluation of the reliability factors and the logistics costs incurred by component failures. It is appropriate that this be performed on the design study phase of the AROD program.

It is interesting to note, that for the representative system design chosen for this report, ground stations located where logistic support is readily available, by tending towards the more complex track-while-scan configuration, would result in lower equipment cost than the redundant configurations. An additional large investment in the key parameters of the ground station, namely antenna gain or effective noise temperature, would effect only a modicum of system performance enhancement and is, therefore, not economical. An alternate approach for selecting the active beam of the multi-beam antenna which appears promising for the manned ground station is to employ an interferometer at the command link frequency for controlling receiver and transmitter switching matrices in the S-band transponder. This approach may be competitive in cost and reliability to the track-while-scan system and is worthy of further study. At the

contemplated command link frequency (in the region of 136 megacycles), ray bending due to refraction of the atmosphere would not introduce any significant problems in the interferometer. The maximum gross angular error at a  $5^{\circ}$  elevation angle would be approximately  $0.5^{\circ}$ ; however, by introducing a correction function in the read-out of the interferometer, this error could be reduced to less than  $0.2^{\circ}$ .<sup>14</sup> The interferometer, is not recommended for the unmanned station for the same reason as the track-while-scan approach, namely complexity.

### 3.5 Trade-off Analysis

As indicated earlier, the performance objectives for the representative system design were established from an analysis of all error sources, and the system penalties were derived from estimates of the weight and input power tolerable on the spacecraft. Next will be analyzed the variations in system performance that result from changes in system parameters to indicate the trade-offs that are to be considered in the selection of the operational AROD system.

In Table 7, the representative system design is compared with other possible system configurations on the basis of the total measurement error. Several assumptions were necessary to facilitate the comparison; the more important of these assumptions are:

- The operating frequency is fixed at 2000 Mc, hence the propagation-induced errors are the same for all systems.
- All systems employ a varactor harmonic generator as the r-f source in the vehicle.
- The same ground station design approach, i.e., multi-beam antenna and multiple receivers, is employed in the ground stations for all systems being compared.

To obtain the trade-off data shown in Table 7, estimates were made of the weight and input power requirements for two spacecraft systems other than the representative system (see Section 4.1.6) and the antenna gain and relative cost of two other ground stations. The relative equipment costs shown in the table apply to unattended stations. For stations

Table 7  
Trade-Off Table

System No.	Vehicle Equipment			Ground Station Equipment			Measurement Errors at h=500 mi, R=1000 mi.	
	Weight (lbs.)	Input Power (watts)	Power Output (watts)	Max. Antenna Gain (db)	No. of Beams	Relative Equip. Cost	$\sigma_r$ (meters)	$\sigma_p$ (meters/sec.)
1	21	55	2.5	19	~ 50	2.5	3.2	.037
2	21	55	2.5	13	13	1.0	4.0	.069
3 (low cost)	21	55	2.5	7	5	.7	6.1	.13
4	27	114	12.5	19	~ 50	2.5	3.0	.022
5 (representative)	27	114	12.5	13	13	1.0	3.2	.034
6	27	114	12.5	7	5	.7	3.8	.062
7 (high cost)	40	250	25	19	~ 50	2.5	3.0	.019
8	40	250	25	13	13	1.0	3.1	.027
9	40	250	25	7	5	.7	3.4	.045

- with better logistics support, a smaller variation in relative costs between the three systems would result from the tendency to employ less redundancy. The total measurement errors for the nine systems resulting from all combinations of the three vehicle systems and the three ground stations were then calculated from the data in Section 2.5.

Several trends and conclusions are apparent from Table 7. The economy of keeping the various error sources "in balance" can be seen by comparing system 7 (highest cost), system 5 (representative system), and system 3 (lowest cost). The data for these systems indicate that performance degrades rapidly as equipment capability is decreased, while substantial increases in equipment capability result in only minor improvements in performance. Thus, an objective of 3.2 to 3.4 meters for the range measurement error seems reasonable. With respect to the range rate measurement error, approximately 0.03 meters per second seems to be a reasonable.

objective, although the balancing of this error was not a primary goal of the Feasibility Study.

The data contained in the Trade-Off Table will provide useful guidelines for the design of the operational AROD system and for the division of system penalty factors between spacecraft and ground station. For example, System 1 might be preferable to the representative system if the number of ground stations were sufficiently small, or if the vehicle penalty reductions could justify the increased investment in the ground stations. Alternatively, System 9 might be a superior choice to the recommended system if the additional vehicle penalty were tolerable or if the number of ground stations were sufficiently large. The ultimate choice must await the design phase of the AROD program when missions and requirements are further defined and the system can be optimized. The use of a representative system design was appropriate for the Feasibility Study because the ultimate choice does not reflect significantly on the question of feasibility.

## Section 4

### EQUIPMENT IMPLEMENTATION

#### 4.1 Spacecraft Equipment

The discussion of the important implementation considerations affecting the design of the representative AROD system will begin with the spacecraft equipment. In this subsection, emphasis is placed upon the transmitter, wideband receiver, phase-locked loops, and measurement circuits. An estimate of the weight, power and volume required for the spacecraft equipment is included.

##### 4.1.1 Spacecraft Transmitter

The vehicle transmitter requires more power, weighs more, and occupies more volume than any other portion of the AROD spacecraft equipment. Considerable attention was devoted, therefore, to the selection of the design approach used in the representative system.

##### 4.1.1.1 R-F Sources

At the outset of the AROD Feasibility Study, an investigation was initiated to determine which r-f sources could be considered suitable for use in the AROD spacecraft transmitter. In consideration of the anticipated maximum operating range of 3940 nautical miles and the desired AROD measurement accuracies, power sources between 2.5 and 30 watts at frequencies between 1.0 and 2.5 Gc were considered. Both amplifier and oscillator devices were investigated and a comparison was made, based on reliability, efficiency, weight, packaging factors, modulation flexibility, phase stability, power supply requirements and ruggedness.

The following components were investigated for suitability as the transmitter output stage:

- Klystrons
- Crossed field devices including cw amplitrons and voltage tuned magnetron oscillators.
- Traveling wave tube amplifiers.
- Supported Drift Tube Klystrons.
- Thermionic triode-cavity oscillators, amplifiers and multipliers.
- Thermionic tetrode-cavity amplifiers.
- Varactor harmonic generators (selected approach).

#### Stability Requirements

Regardless of whether the spacecraft transmitter output stage were an oscillator, amplifier, or harmonic generator, a high degree of frequency and/or phase stability would be required in order to satisfy the measurement accuracy objectives established in Section 2.5. If a high stability crystal oscillator employing proportional type temperature control and having a basic output frequency in the region of 5 Mc is considered as representative of a state-of-the-art frequency standard for spaceborne application, a short-term stability (1 to 10 seconds) of  $\pm 2 \times 10^{-10}$  could be achieved with a reasonable expenditure of temperature control power. If it is assumed that the frequency varies linearly during the one second interval, a drift of  $1 \times 10^{-11}$  will be encountered in the maximum propagation time (50 milliseconds) for the AROD system. Long term stability of the same unit after warm-up would be less than  $1 \times 10^{-9}$  per day. These stabilities meet the performance objectives established in Section 2.5.

Indications are that frequency standards suitable for use in a space environment and having short term stability of 5 parts in  $10^{11}$  per second will soon be available. Small transistorized portable laboratory type units of the above stability are now available off-the-shelf.

If the output stage of the spacecraft microwave transmitter is self-excited, the same degree of stability as that of a crystal standard would be desirable. If an amplifier is employed at the transmitter output, the

r-f oscillator stability must be preserved throughout any multiplier and driver stages, as well as in the amplifier stage. The requirements for a harmonic generator output stage are essentially similar to those of the multiplier-driver, except for the higher power handling capability.

### Klystrons

The investigation of the Klystron oscillator showed that a high degree of frequency stability can be achieved in ground-based equipment by either passive stabilization or by phase-lock to a quartz crystal reference. Several state-of-the-art phase-lock systems are capable of one part in  $10^8$  per second short term stability and one part in  $10^6$  per week over  $\pm 5^\circ \text{C}$  temperature range, but the efficiency and the ruggedness of such equipment is not well suited for space application. In consideration of the phase stability requirements of an amplifier stage at the output of the transmitter, the Klystron amplifier is quite inefficient due to the requirement for a high degree of power supply regulation in addition to the basic amplifier inefficiency.

### Crossed Field Devices

Of the crossed field devices, the Amplitron has been found to be the most efficient. The Raytheon QKS997 is capable of producing a minimum power output of 25 watts at 2200 Mc with a plate circuit efficiency in excess of 50 per cent. The driving power at this output level would be approximately 250 milliwatts. This could be easily supplied by a crystal oscillator and a varactor multiplier chain. Although the Amplitron presents a number of advantages, power supply regulation becomes a considerable problem when a curve such as that shown in Figure 17 is considered. The extreme slope of the V-I characteristic makes the maintenance of phase stability very difficult for any constant current supply suitable for spacecraft installation. At the moment, this appears to be the principal problem associated with the use of the low power cw Amplitron in the ARQD spaceborne transmitter.

The problem of maintaining the low power cw Amplitron at the critical operating point has been studied for some time by the manufacturer. Since

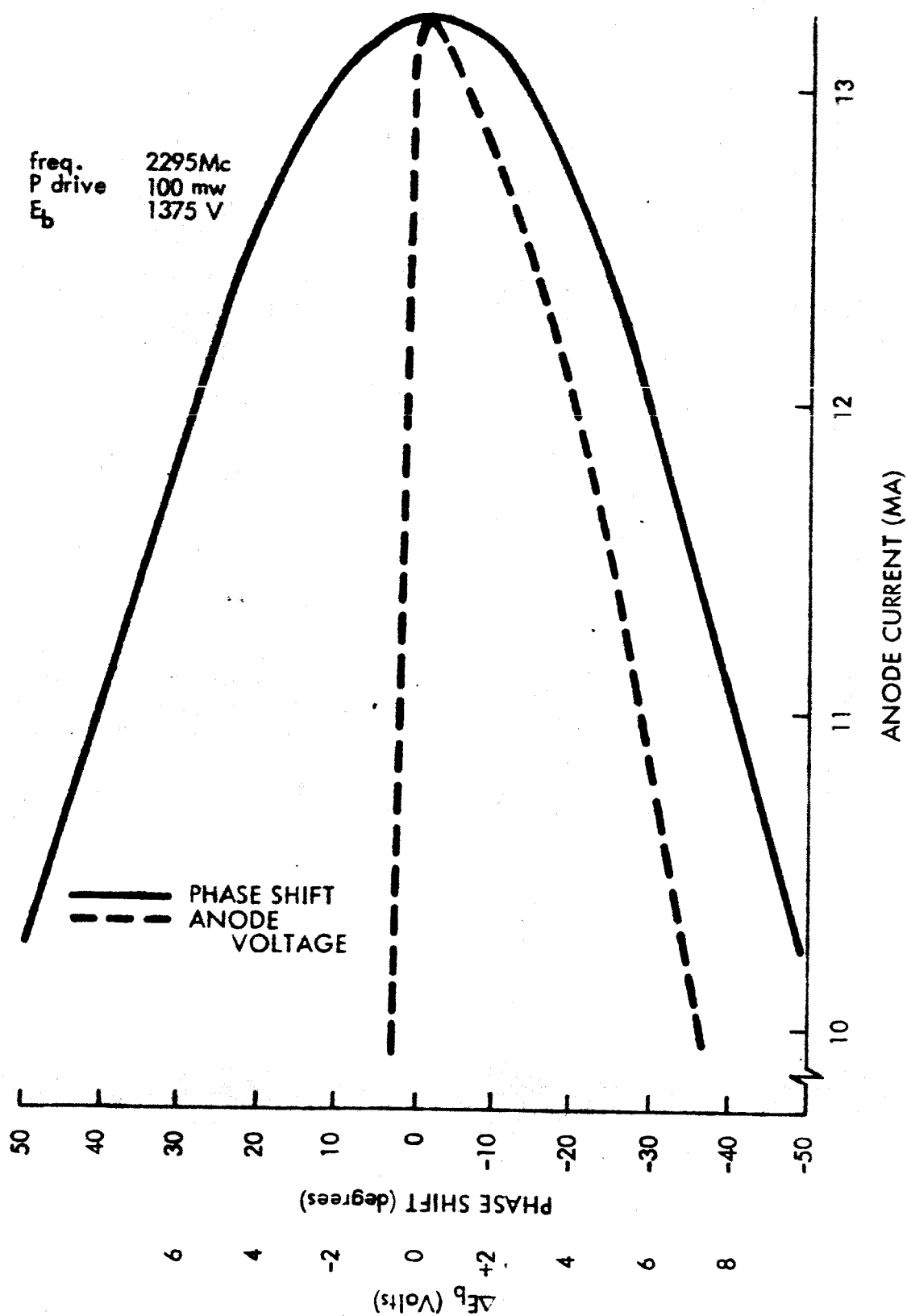


Figure 17. Amplitron Phase Pushing Measurements

little anode current can be drawn, except at the correct voltage for interaction at the frequency of the drive signal applied, the key to successful operation is that the Amplitron must be maintained at a constant current level.<sup>15</sup> It is therefore convenient to set the voltage with a power supply that utilizes a feedback circuit for current regulation. A suitable current supply has been designed and developed by the Amplitron manufacturer, but considerable additional work is needed to prove that performance is satisfactory for AROD mainly with regard to efficiency.

Problems associated with the permanent magnet that is part of the Amplitron structure must also be considered. Figure 18 illustrates temperature characteristics of a Raytheon QKS997 Amplitron.

An interesting characteristic of the Amplitron is its ability to serve as a passive transmission line when the high voltage is removed. With a low forward insertion loss of 0.2 to 1.0 db, an additional element of reliability is added to the system if the driver power level is suitable for use as an output signal in an emergency. Furthermore, this point may be an important factor if the higher power capability of the Amplitron were to be employed only for long range operation and at other times, the transmitter power were reduced to conserve spacecraft primary power. Further improvements in the cw Amplitron may make it suitable for AROD application, especially where higher r-f power levels are desirable; however its suitability from the reliability standpoint remains to be proven.

Since the Voltage Tunable Magnetron (VTM) can be frequency controlled, frequency or phase modulated, and can withstand the vibration and shock associated with operation in a spaceborne environment, it was considered for use as the output stage of the AROD spacecraft transmitter. VTM's are available in frequencies ranging from 0.5 to 10.5 Gc with outputs from 0.5 watts to 50 watts. Typical plate efficiency is about 40 per cent. The VTM is essentially a wide-band device that can be linearly tuned at rates in excess of  $10^{12}$  cycles per second squared. To adapt it to a narrow-band application involves utilizing special techniques in high voltage regulation and AFC to hold the center frequency within the specified tolerance. To provide a high degree of frequency stability, a feedback circuit is required. Circuits that are applicable include:

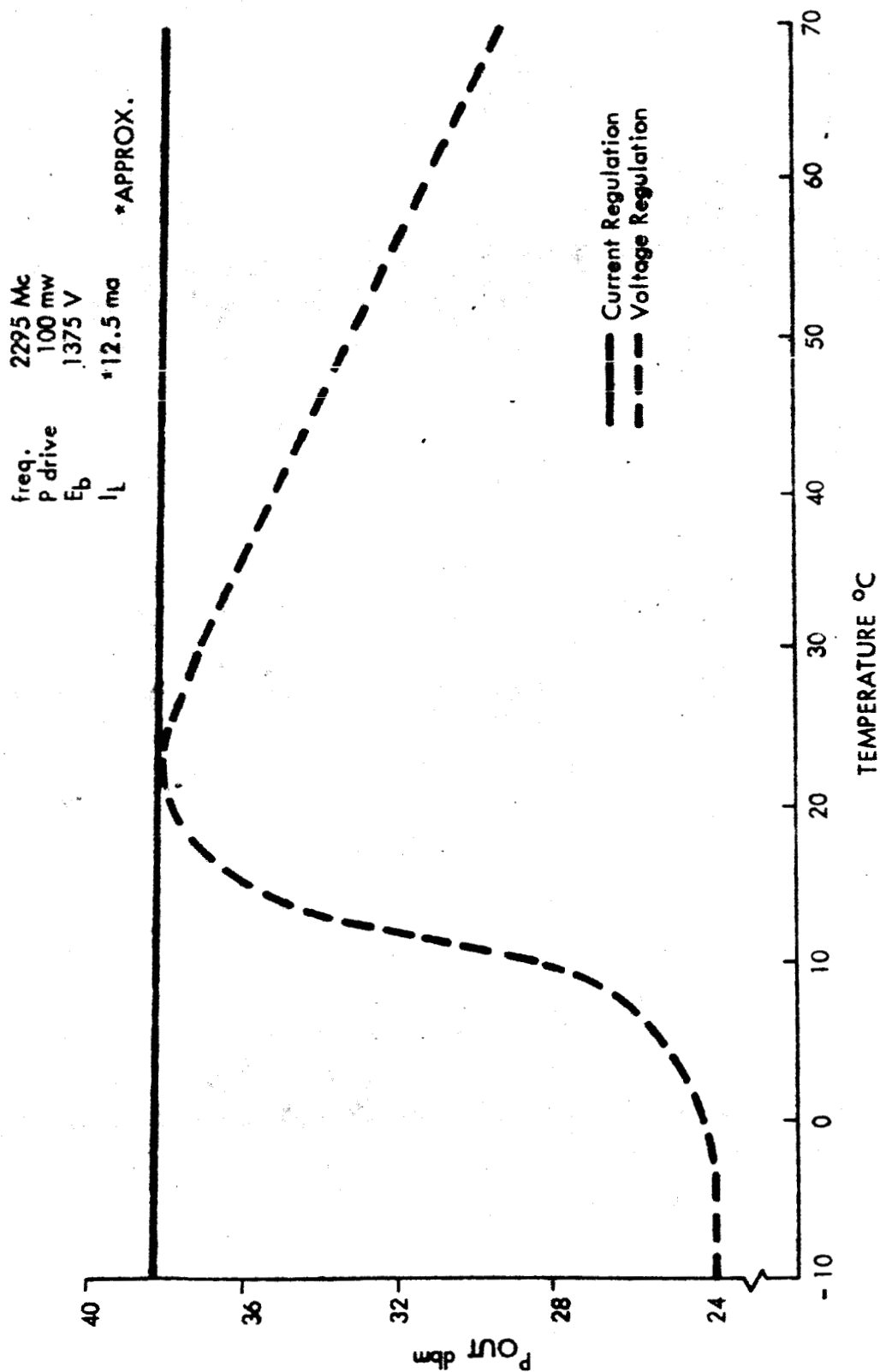


Figure 18. Amplitron Thermal Stability Measurements (QKS997)

- Frequency comparison
- Phase comparison
- Injection locking
- Load mismatch

Of these, injection locking appears to be the most suitable for AROD use since it provides continuous control of the output frequency and does not present problems associated with the comparison rate of the frequency comparison and the phase comparison circuits. Control by load mismatch is not applicable to AROD needs, since frequency error would be no less than about 0.1 per cent. With injection locking, power supply regulation problems are similar to those associated with the Amplitron, except for the peculiarity that exists in the Amplitron control locus. No known similarity exists for the VTM. An additional problem of concern is permanent magnet flux density variations caused by changes in magnet temperature. During the manufacturing process, the tube's permanent magnet is stabilized and temperature cycled to minimize these variations, but even with special design the measured temperature/frequency variation is presently  $1.8 \times 10^{-3}$  percent per degree C. Fundamentally, the applicability of the VTM to AROD compares to that of the Amplitron. The overall efficiency would undoubtedly be somewhat less due to the lower efficiency of the tube.

#### Traveling Wave Tube Amplifiers

The investigation of the Traveling Wave Tube (TWT) has indicated that there are a number of units available for spaceborne application in the S-band frequency region. The state-of-the-art for these units is well advanced and several S-band units including solid-state power supply are available off-the-shelf. These units have been primarily designed for satellite telemetry-communication wideband microwave amplification. The efficiency for the tube (including heater power) is approximately 30 per cent at midband. For a 12 watt r-f output package, including an all solid-state power supply, the nominal overall efficiency is approximately 15 per cent. In an AROD application, the point of concern for the TWT would be the phase instabilities which are generally functions of power

supply variations and changes in environmental conditions. At the time of the investigation, no exact data was available on this point, but it was generally agreed among manufacturers that a "rule of thumb" to follow would be that 0.01 per cent changes in helix voltage will cause a 1 degree change in phase. The anode and grid sensitivities are approximately 10 per cent of the helix sensitivity.

#### Supported Drift Tube Klystrons

The Eimac Supported Drift Tube Klystron (SDTK) has been considered during the spacecraft transmitter component investigation, since it appears to offer simplicity, ruggedness, and high degree of stability without some of the disadvantages of other tube devices. Mainly, since the SDTK does not employ a magnetic field, the problems associated with the use of a permanent magnet are eliminated. Significant features of the Eimac X-1005 are 10 watts output in the region 2200 to 2300 megacycles with .005 per cent frequency stability when operating as a power oscillator. It appears that it would be difficult to achieve a frequency stability better than one part in  $10^7$  even by phase locking to a crystal oscillator-multiplier chain. The efficiency (including heater power) is estimated as being greater than 30 per cent.

The major problem associated with this device is that of modulating the output signal. Presently, the modulation bandwidth is specified as being  $\pm 200$  kc although it is estimated that an electronic bandwidth of  $\pm 1$  Mc can be achieved through the use of a varactor modulator that is coupled to the oscillator cavity. Further investigation would be required to determine if the SDTK could fulfill the AROD frequency stability requirements via phase-lock to a crystal controlled frequency generator and at the same time provide the desired modulation bandwidth. Considering that the AROD modulation index is small, the SDTK may be useful if power supply regulation requirements do not present unusual problems. This device is not known to have unusual voltage or current characteristics.

### Thermionic Devices

A number of cavity thermionic devices were investigated including the following:

- Cavity oscillators
- Cavity amplifiers
- Cavity multipliers

Of these, the cavity amplifier is most suitable for use in the design of an AROD transmitter, although its use includes the usual problems associated with regulation of the high voltage supply.

Several cavity triode amplifier units are available off-the-shelf for spaceborne operation at S-band. Models are available with r-f output power up to 25 watts. Plate circuit efficiency for these units is approximately 35 percent.

Until recently, the triode and the cavity for all of these units were built separately and a suitable combination was chosen by the designer and manufacturer of the unit assembly. An advancement in the state-of-the-art that is said to provide increased stability is a cavity-triode assembly manufactured as a single unit. The cavity of this unit is evacuated during the manufacturing process. An additional feature of this device is a second filament that provides quick warm-up for intermittent operation. If employed in the AROD transmitter, this feature would be a desirable one, since it may provide a considerable power saving.

Among the disadvantages associated with the use of the cavity triode amplifier in the AROD transmitter design is the low gain which is approximately 10 db for the higher power units. Although a cavity tetrode could possibly provide increased gain, no suitable unit was found for operation at S-band.

### Varactor Harmonic Generators

As is the case for most spaceborne electronic equipment, the high degree of reliability to be realized from the use of solid-state components is extremely desirable in the spaceborne transmitter of the AROD system.

Through the use of the varactor Harmonic Generator (HG), it may be possible to generate r-f energy at S-band having the same degree of stability as that of its lower frequency driving source which can be a transistorized temperature controlled crystal oscillator. With this design, the requirements for extremely well regulated high voltage supplies and regulated filament supplies are eliminated. However, a well regulated low voltage source will be required for generating sufficient VHF energy to drive a varactor multiplier chain to the desired output level at S-band. Present state-of-the-art capability for the varactor harmonic generator at 2 Gc is approximately 2.5 watts r-f output power and the efficiency will be dependent upon the order of multiplication. Typical efficiencies for the HG when driven in the 100 megacycle region are: 70-80 per cent doubling, 50-70 per cent tripling, and 40-50 per cent quadrupling. Presently, efficiencies at S-band are somewhat less, but considering the rapid advance of the device technology, both the efficiency and the power handling capability should soon approach the present performance at VHF. Typical conversion efficiencies for various types of harmonic generator circuits at S-band have been shown to range from 35 per cent for a quadrupler to 60 per cent for a doubler when using a micro-etch germanium varactor diode.

In addition to the epitaxial and gallium arsenide varactor diodes that have cut-off frequencies above 100 Gc and are suitable for efficient harmonic generation at S-band, the diffused-junction silicon varactor diode such as the Raytheon CK 303 is of interest, since it can deliver approximately 100 watts of r-f power at 100 megacycles with an efficiency of 85 per cent as a doubler.

For the varactor HG to be useful in the AROD spacecraft transmitter it may be necessary for the r-f energy at the output stage to contain the range tone modulation. It has been shown<sup>16</sup> that the varactor frequency multiplier can be amplitude, frequency or phase modulated in that it can reproduce the driver modulation at the output of the multiplier. Amplitude modulation is not of interest in the design of the AROD transmitter. Therefore, it will not be considered. In both FM and PM, since the total power remains constant throughout the sequence of modulation, the HG chain can

be optimized at only one power level with no concern for input-output power linearity. Since a typical doubler can provide approximately 10 per cent bandwidth, no difficulty should be experienced in passing the significant sidebands that contain the AROD range tone modulation if a low modulation index is employed. Parameters for the AROD system indicate that only a low index is required. Since several cascade multipliers will be required to generate the S-band energy, the half power bandwidth of the multiplier chain must be considered. Again, no problem is foreseen, since a large number of significant sidebands at the transmitter output is neither required nor desirable and the modulation bandwidth will be relatively small.

Among the problems associated with the use of the cascade HG is the degradation of performance with changes in average varactor capacitance, circuit inductance changes, etc., caused by various environmental conditions. Obviously, if the number of components can be kept small, the complications will be minimized. Therefore, an important qualitative consideration in the design of a multiplier chain is the harmonic number, since it will directly influence the number of components. It has been pointed out that the key to obtaining good efficiencies in high order multipliers is the use of "idler" circuits.<sup>17,18</sup> Since this will entail the use of additional components, high order harmonic generation in a single stage must be compared against the use of doubler stages on more than just the basis of efficiency. When the output frequency is as much as one-tenth of the varactor cut-off frequency, the doubler has been found to be decidedly more efficient than higher order multipliers. On this basis, a doubler appears to be the best choice for the final stage of the varactor HG AROD spacecraft transmitter.

#### 4.1.1.2 Solid State Transmitter Design

This section treats the design of the spacecraft transmitter for the representative AROD system based on the choice of the varactor HG as the most suitable design approach.

In order to employ the varactor Harmonic Generator in the design of an S-band AROD spacecraft transmitter, some means must be found to generate the r-f spectrum energy in excess of the state-of-the-art capability of a single varactor output stage. Since the AROD spectrum will be made up of both modulated and unmodulated fixed frequency microwave signals, it becomes possible to generate the signals individually in separate HG chains. The energy can then be summed and fed to a single antenna for transmission. This approach is employed in the design description that follows.

The microwave r-f spectrum to be transmitted is illustrated in Figure 19. To satisfy AROD performance requirements as discussed in Section 3.2, frequencies  $f_1$  and  $f_3$  are each generated at a level of approximately 5 watts. To accomplish this, the output energies of two 2.5 watt HG chains are summed. Since modulation is not employed on either of these signals, the problem of maintaining correct phase relationship is not a serious one. When properly designed to compensate for environmental changes such as temperature variations, each channel can be pre-adjusted for optimum performance. Since the two branches of a single channel are driven from a common source, only phase stability is of concern.

Frequency  $f_2$  is phase modulated by the four lowest frequency range ambiguity resolving tones. These are harmonically related signals and all are generated in the frequency synthesizer. In the design of the r-f spectrum, the range tones were selected so that the power level at frequency  $f_3$  (including the sideband power) need not be greater than 2.5 watts. This permits the use of a single HG chain for generating carrier frequency  $f_3$  and the associated modulation spectrum.

Power summing will be one of the problem areas associated with the design of a transmitter where the r-f energy from three separate sources, each having a different frequency, is to be summed into a single antenna. As explained earlier, the individual branches of a channel having a common frequency, for instance the 2.000 Gc channel, should cause no serious problems, since phase and amplitude can be adjusted so that a hybrid ring can be employed to sum the power. Very little loss should occur at the difference port of the ring if phase and amplitude stability is assured. This arrangement is illustrated in Figure 20 for frequencies  $f_1$  and  $f_3$ .

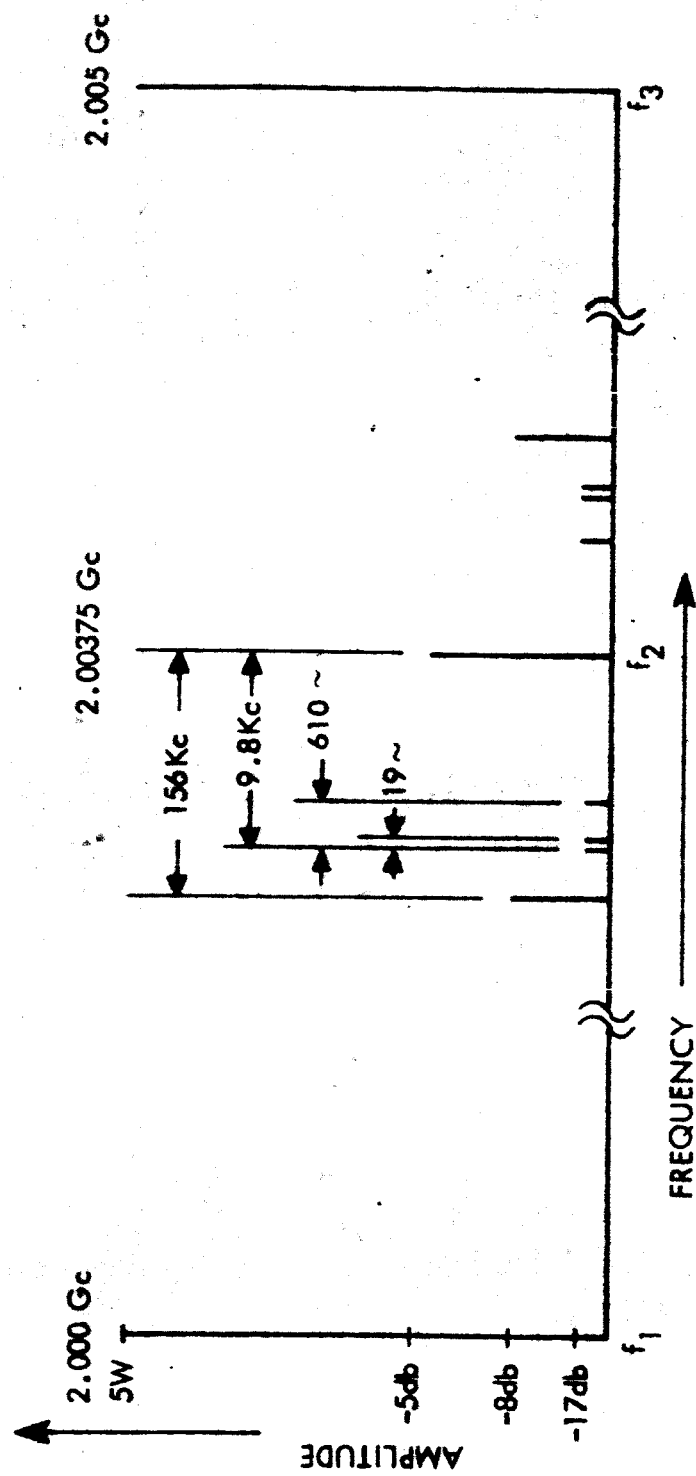


Figure 19. AROD Spacecraft Transmitter R-F Spectrum

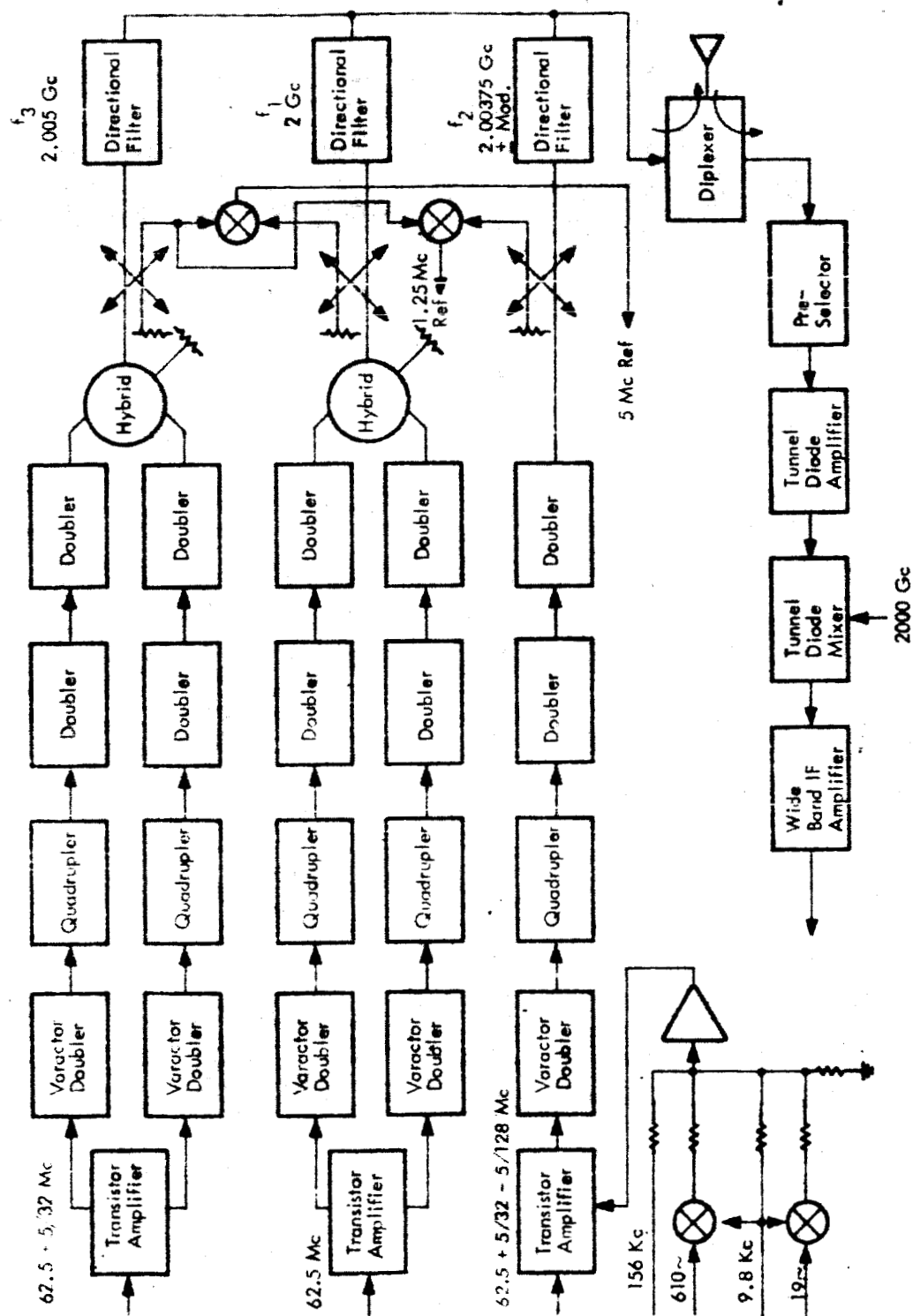


Figure 20. Block Diagram, AROD Vehicle Transmitter-Receiver R-F Section

To sum frequencies  $f_1$ ,  $f_2$ , and  $f_3$  into the common antenna, directional filters are employed. Since the separations between frequencies are relatively small, high-Q cavity type filters will be required. Strip-line configuration is ruled out at this point since the unloaded Q of typical dielectric material indicates insufficient isolation would result.<sup>19</sup>

Although directional filters and a common antenna are suggested, and are illustrated in the block diagram of the transmitter, the use of separate antennas for each of the radiated frequencies offers another possibility. The important point here would be to achieve a common phase center in the design of the antenna. A design such as a turnstile could satisfy this condition. In addition, the cross polarization would provide good isolation between channels due to the low mutual coupling. Three elements would be required for the three frequency AROD spectrum. Any single element could be used for reception, since circular polarization is suggested as most desirable for the ground station antennas.

A basic block diagram of the r-f section of an all solid-state AROD transmitter design approach is shown in Figure 20. This illustration also includes the input section of the spacecraft receiver which will be discussed later. Five varactor HG chains are employed in this design and each is supplied with sufficient r-f energy in the region of 60 megacycles to produce the desired output level at microwave frequencies. Highly stabilized input signals are supplied from the spacecraft frequency synthesizer, and transistor amplifiers are used to generate the required drive level. Since a 5 watt power level is desired at 2.000 Gc and 2.005 Gc, two HG chains are used at each frequency and the power is summed to produce the 5 watt level. In this case, the transistor amplifiers must provide sufficient power to drive the parallel branches.

Since only 2.5 watts of power, including the sideband power, is required at 2.00375 Gc, a single HG chain is used. The transistor amplifier for driving this multiplier chain provides approximately one-half the r-f power level of those for driving the parallel HG chains.

#### 4.1.1.3 Modulator

Referring to the illustration of the transmitter r-f spectrum, (Figure 19) microwave frequency  $f_2$  is shown phase modulated by ambiguity resolving tones of the following frequencies:

$$5/32 \text{ Mc} \approx 156 \text{ kc}$$

$$5/512 \text{ Mc} \approx 9.8 \text{ kc}$$

$$*5/8192 \text{ Mc} \approx 610 \sim$$

$$*5/262,144 \text{ Mc} \approx 19 \sim$$

\*To assure reliable performance of the spacecraft receiver phase-locked loop whose purpose will be to track the carrier frequency  $f_2$ , the 610  $\sim$  and the 19  $\sim$  range tones are complemented with the 9.8 kc tone.

This removes modulation tones from the vicinity of the carrier. The mixing process to accomplish this is shown in Figure 20 along with the linear mixing of all ambiguity resolving tones to provide the composite input signal to the modulator.

Since the modulation index of the range tones will be kept small in order to limit the significant sidebands to only a first order set per range tone, multiplication of the modulation index need not be resorted to in order to produce the desired results. Therefore, there are a number of points along the chain of transistor amplifier and varactor harmonic generator stages of the  $f_2$  microwave channel at which modulation could be accomplished. For simplicity, this point is shown at the transistor amplifier in Figure 20.

Indications are that a varactor frequency multiplier may be made to serve the dual purpose of harmonic generator and phase modulator.<sup>8</sup> Particularly, since the modulation bandwidth requirement is small, it may be desirable to modulate in a later stage of the carrier generator chain. The quadrupler or first microwave doubler may prove to be a desirable point for injecting modulation.

Given a power capability of approximately 2.5 watts, it is desirable to distribute this power as follows:

Carrier	-	1.5 watts
156 kc	-	0.8 watts (total first order sidebands)
9.8 kc	-	0.1 watts (total first order sidebands)
600 ~	-	0.1 watts (total first order sidebands)
19 ~	-	0.1 watts (total first order sidebands)

The modulation index for the 156 kc tone would be approximately 0.8 radian. For the remaining tones, an index of approximately 0.3 radian would be required.

#### 4.1.1.4 Frequency Synthesizer

Repeating the figures that have been given earlier in the report regarding frequency stability of the AROD transmitted signal, it is within the state-of-the-art to achieve a short term stability of approximately 5 parts in  $10^{11}$  per second. Indications are that stability per day would be better than 1 part in  $10^9$ . This degree of frequency stability requires proportional temperature control matched precisely to the turning point temperature of the crystal. Quartz crystals operating in the frequency region of 2.5 to 5 megacycles seem most suitable. In selecting the basic frequency for the AROD frequency synthesizer, 5 Mc seems a logical choice, since direct calibration against frequency standards, for example WWV, is easily achieved.

From this one frequency standard carried aboard the spacecraft, all radio frequency, intermediate frequency, and range tone signals will be generated. Figure 21 is the basic block diagram of the synthesizer. In this illustration, only the range tones, the Doppler bias frequency, and the transmitter driving signals are synthesized. In addition, twelve intermediate frequency local oscillator signals will be required for the spacecraft receiver.

For simplicity, circuitry for generating the local oscillator signals has been omitted from the diagram, since the generation process is identical with that shown for other signals.

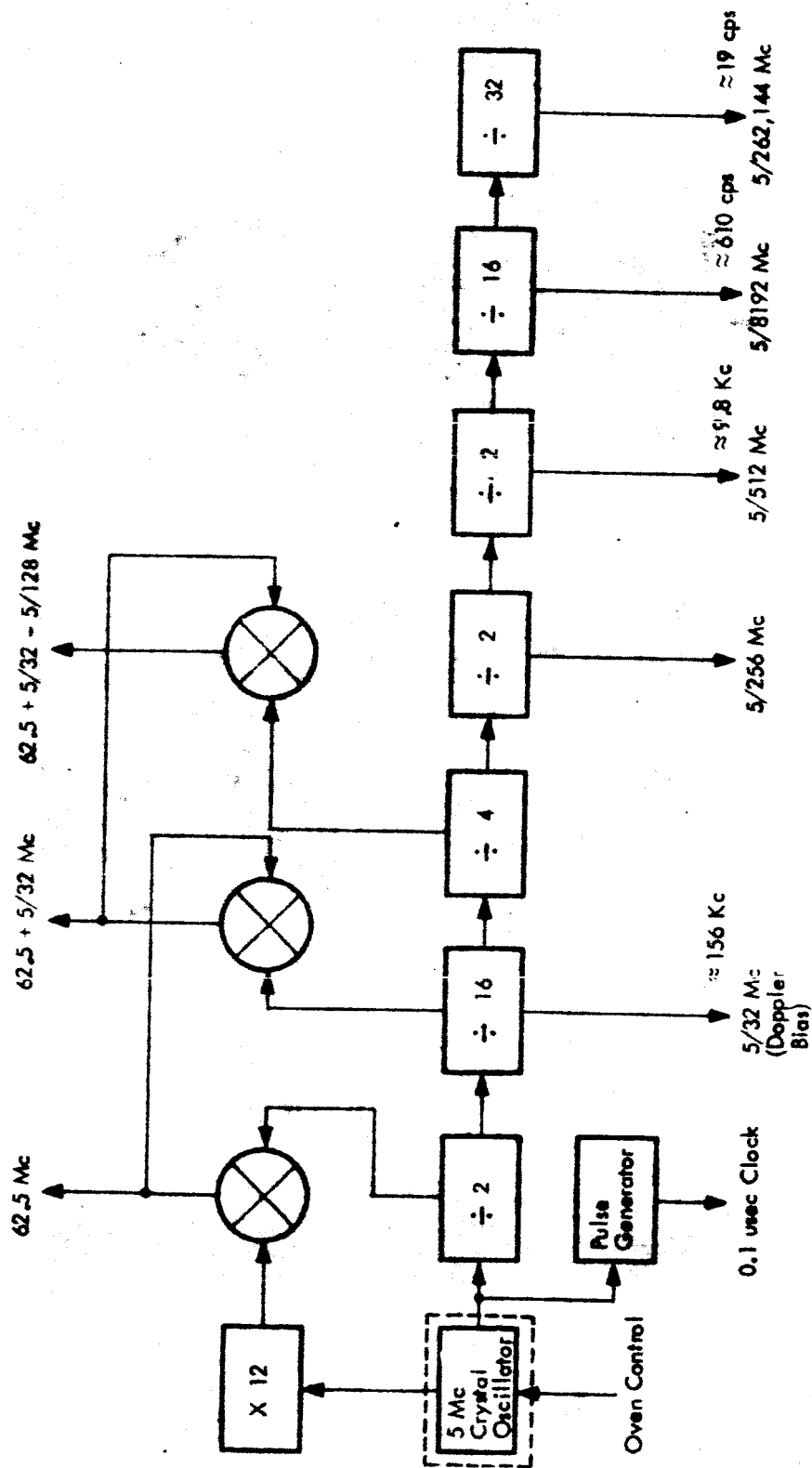


Figure 21. Block Diagram AROD Radio Frequency and Range Tone Synthesizer

A time-base will be required for making Doppler and range measurements. This signal will be derived from the 5 Mc frequency standard. The exact circuitry of the timing pulse generator illustrated in the block diagram, Figure 21, will be dictated by measurement requirements and computer interface parameters.

#### 4.1.2 Wideband Receiver

The spacecraft receiver will sense the retransmitted spectrum from up to four command selected ground stations. For any single ground station, the spectrum at the receiver will be similar to that sent to the ground by the transmitter (see Figure 19) except that it will be shifted by the ground station translation frequency plus the two-way Doppler. It is important to minimize overall receiver bandwidth and to assure minimum cross-talk between the four sets of signals. The four-station spectrum illustrated in Figure 22 has been chosen as representative for this study. Four ground stations so arranged would occupy a maximum bandwidth of 11.250 Mc plus two times the two way Doppler, or approximately 12 megacycles.

##### 4.1.2.1 R-F Amplifier

Referring to the illustration of the vehicle AROD transmitter-receiver r-f section, Figure 20, the 12 megacycle spectrum received by the spacecraft transmit-receive antenna is presented to the input of the receiver r-f amplifier through a diplexer and a pre-selector filter. A tunnel diode amplifier will be used to amplify the incoming spectrum before down converting to the intermediate frequency (i-f). Off-the-shelf tunnel diode microwave amplifiers are presently available having a noise figure of less than 4 db, and a gain of approximately 20 db. These amplifiers are capable of bandwidths in excess of 100 Mc. Therefore, no problem is foreseen in obtaining uniform response within the 12 Mc passband required for the AROD receiving spectrum.

1945.625 Mc

1934.375 Mc

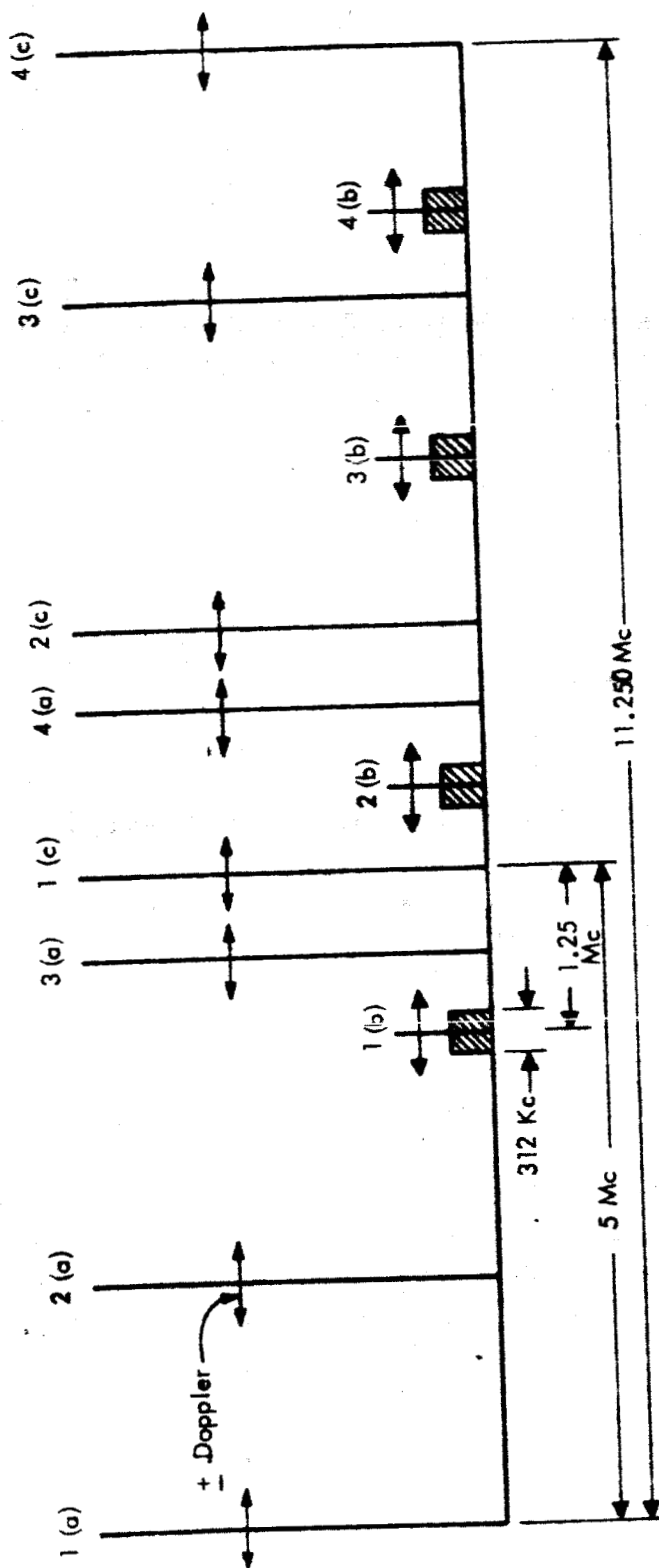


Figure 22. Four Station AROD Spectrum—as Seen by Vehicle Receiver (Zero Doppler Assumed)

#### 4.1.2.2 Mixer

A tunnel diode mixer will be used to down convert the amplified microwave signal spectrum to the i-f spectrum of approximately 54 to 66 megacycles. Since this converter requires only  $10^{-6}$  watts of local oscillator power, a small sample of the 2,000 Gc signal from the transmitter output can be employed as the receiver microwave local oscillator. Deriving the local oscillator signal in this manner will permit preservation of the transmit-receive signal relationships which are essential to the performance of accurate AROD measurements.

Isolation will be a point of concern in the design and development of the r-f section of the receiver. For the assumed system parameters, the center of the microwave spectrum received from the four ground stations will be about 60 megacycles lower in frequency than the 2,000 Gc transmitted signal. Therefore, the minimum separation between transmitted and received signals at the space vehicle will be approximately 54 megacycles. Although it would be considerably less difficult to achieve the desired receiver-transmitter isolation if a greater frequency separation were employed, AROD measurement accuracy requirements dictate that the frequency translation at the ground stations be made as small as possible in order to reduce the effects of translation oscillator drift. A mean translation frequency of 60 megacycles appears to be a reasonable choice whereby receiver-transmitter isolation requirements can be satisfied. Miniaturized coaxial circulators and multi-section pre-selectors are applicable for achieving the isolation. Sub-miniature circulators are now available for operation at S-band having a nominal isolation of 20 db and an insertion loss of less than 0.3 db. With optimum antenna match, isolation could be increased to approximately 30 db. The unit weight is less than 3 ounces and size is approximately 3 cubic inches.

To achieve an isolation of approximately 70 db between transmitter and receiver, a 4 section interdigital bandpass filter can be added between the circulator receiver port and the receiver. For a rejection of approximately 40 db of the transmitted microwave spectrum at the receiver input and a

passband of 15 megacycles, the filter insertion loss would be approximately 0.5 db. Size of the unit would be approximately 10 cubic inches and weight is estimated at 0.5 pounds.

Another device that may find application in the design of the AROD transmitter-receiver microwave r-f section is the ferrite limiter. Several models are available using a garnet sphere in a dielectric-filled strip-line configuration whereby the integration of the limiter with other circuit components into a single strip-line subassembly is facilitated. In the frequency region of 2 Gc, it has been estimated that the limiting threshold of such a unit could be made as low as a few microwatts if the bandwidth were small. Although the insertion loss is high when compared with other microwave components in the receiver input section, the acceptance of the 2 db loss could prevent overload in a later receiver section, for instance the tunnel diode amplifier.

Since the minimum power requirement for the receiver local oscillator is approximately 67 db below the power level of the 2.000 Gc transmitted signal, sufficient isolation must be provided in the diplexer and the receiver pre-selector to prevent receiver overloading. Even more important regarding the isolation problem will be the elimination of receiver interference from the 2.00375 Gc and the 2.005 Gc transmitted signals. To aid in accomplishing this, the transmitter and receiver spectrums have been so arranged that the transmitter interference signals are furthest from the receiving spectrum.

#### 4.1.2.3 Wideband I-F Amplifier

Before separating the twelve major signals contained in the down converted microwave spectrum, a wideband intermediate frequency amplifier will be employed to increase the signal amplitude. An i-f center frequency of 60 Mc has been chosen since it is compatible with both bandwidth and gain requirements. Up to 100 db of gain can be achieved in off-the-shelf equipment that includes tunnel diode microwave amplifier, tunnel diode mixer, and transistorized i-f amplifier.

#### 4.1.2.4 Post I-F Receiver Circuits

In order to provide similar characteristics for detecting each of the twelve major signals of the received spectrum, wherever possible identical circuitry is employed in each channel of the post i-f section of the receiver. Figure 23 is a simplified block diagram of this receiver section. It illustrates the equipment associated with the reception of one ground station. Referring to the AROD frequency allocation table, the microwave frequencies transmitted from ground station number 1 would be 1934.375 Mc, 1938.125 Mc  $\pm$  modulation tones, and 1939.375 Mc. These frequencies are based on a translation at the particular ground station of 65.625 Mc. Zero Doppler is assumed for this example.

After down conversion in the r-f section of the receiver, the microwave signals transmitted from ground station number 1 appear at 65.625 Mc, 61.875 Mc (plus sidebands) and 60.625 Mc respectively.

Identical 5 Mc passband amplifiers are employed to feed each of these signals to a phase-lock tracking filter. Each amplifier will have a passband somewhat in excess of two times the maximum Doppler bandwidth for the signal returned from the ground station. This will be approximately 500 kc. Each incoming signal is converted to a mean frequency of 5 Mc by mixing with a signal that is derived by combining an r-f signal from the frequency synthesizer.

To prevent cross coupling of the intermediate frequency local oscillator signals, isolation amplifiers are employed to couple the output of the 60 Mc wideband amplifier to the individual mixer circuits that drive the phase-lock loops. Isolation is important here, since some local oscillator signals may be identical in frequency to that of a down converted received signal in another channel.

Automatic Gain Control (AGC) should be provided to the wideband amplifier to prevent possible overloading, but since the signal levels from the individual ground stations may differ, separate AGC signals are generated in each channel of the receiver. In the final design, it may be possible to simplify circuitry somewhat by generating only one AGC signal for controlling all receiving circuitry associated with a single ground station.

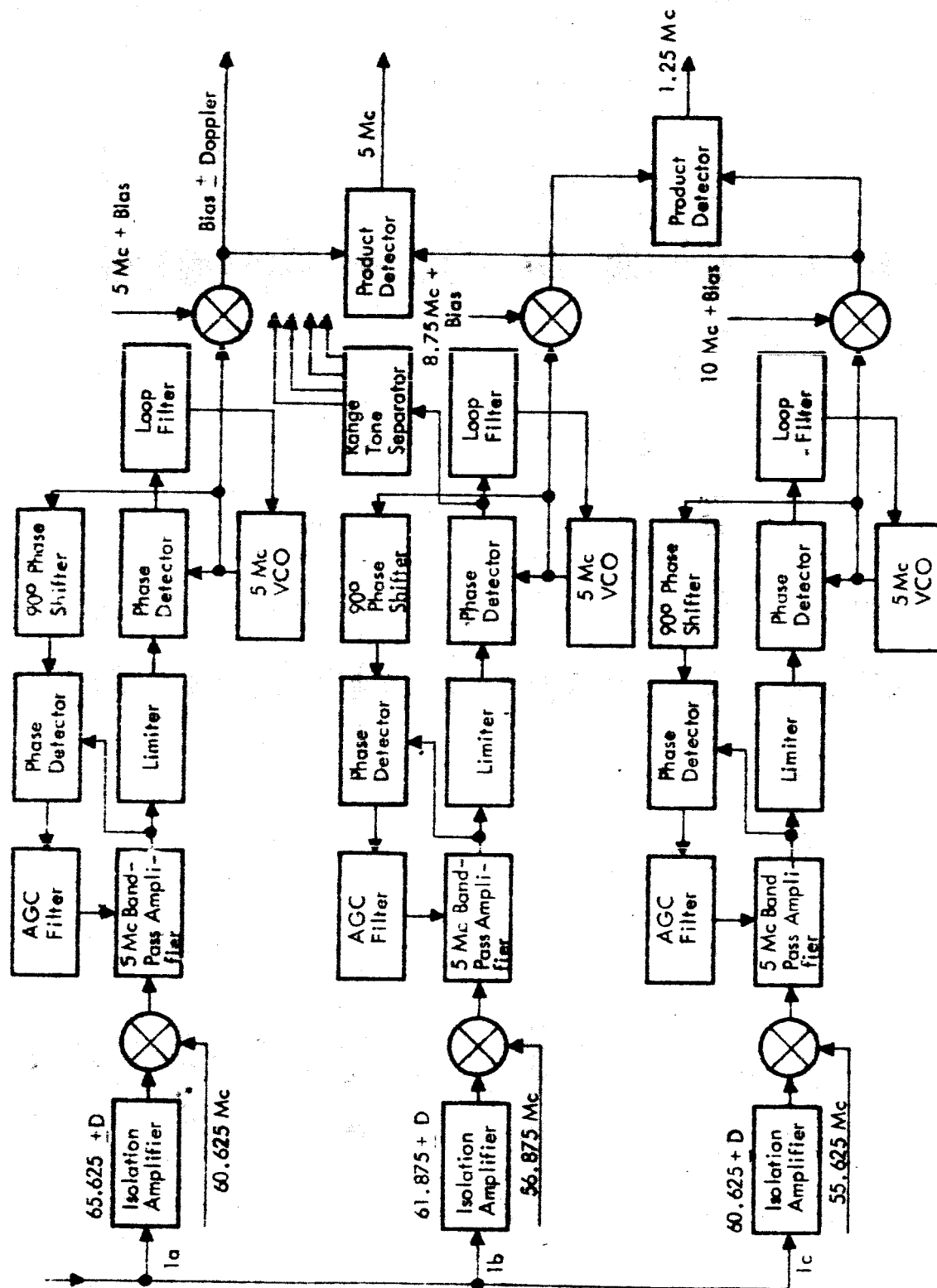


Figure 23. Block Diagram AROD Vehicle Receiver, IF and Phase-Lock Section

To generate an AGC signal that controls the gain of the 5 Mc bandpass amplifier, the output signal is mixed with the 5 Mc VCO output that has been shifted by 90 degrees. A filter is used to remove variations such as might be caused by modulation, etc., and to provide the desired AGC time constant. The output of the filter is used to control the gain of the bandpass amplifier.

The output signal of the 5 Mc amplifier is passed through a limiter circuit before being applied to the phase detector where the signal phase is related to the phase of the 5 Mc VCO signal. After phase-lock is accomplished in each of the three channels, Doppler information is extracted from the channel associated with the 2.000 Gc transmitted signal. Product detectors are employed to extract the 1.25 and 5 Mc signals, and the 156 kc, 9.8 kc, 610 cps and 19 cps ambiguity resolving tones are extracted from the receiver channel (1b) associated with the 2.00375 Gc transmitted signal. Since these signals have been mixed during transmission to produce complement tones, a reverse process will be required at the receiver to regenerate the 19 cps and 610 cps range tones. The preservation of phase information contained in the lower frequency ambiguity resolving tones is equally important to that for the 1.25 and 5 Mc tones. This is to be considered in the design of the de-complementing circuitry. This point is also of concern in separating the range tones.

#### 4.1.3 Phase Locked Loops

This subsection contains a discussion of the design of phase locked loops which are required as a part of the AROD spacecraft equipment. The first part illustrates the type of loops required and some operations on the signals which simplify the task required of the phase locked loops. This is followed by a brief discussion of the operating principles of phase locked loops during both acquisition and tracking.

Phase locked loops are used in the spacecraft receiver as narrow band filters. This results in an improvement in signal-to-noise ratio (S/N) which is equal to the ratio of the bandwidth of the noise at the input to the loop to the noise bandwidth of the loop. The required input noise bandwidth is

principally determined by the range of Doppler frequencies which must be tracked, and the noise bandwidth of the loop is essentially determined by the rate of change of Doppler frequency. An improvement of the order of 100 to 1 is typical for the loops considered in this report. However, before the increase in signal-to-noise ratio can be obtained, the input frequency must be determined. In addition, the loop must be capable of changing the center of its passband rapidly enough to track the signal as its frequency changes. Hence, it is imperative that we investigate both the acquisition and tracking properties of the loop.

The spectrum described in Section 4.1.1.2 requires phase locked loops which operate on frequencies of 5, 2000, and 2005 megacycles. Phase locked loops are not required for the range ambiguity tones (Section 3.2). Since the frequency difference between 2000 and 2005 megacycles is small compared to 2000 megacycles, the loops which are locked to these frequencies will contain similar components.

#### 4.1.3.1 The Range Rate Loop

The carrier frequency (2000 megacycles) is the first signal component acquired by the AROD system. The three important goals for the AROD system which make the frequency acquisition problem a difficult one are the following:

1. It is required that the signal be acquired within ten seconds for the 90 nautical mile trajectory. (Section 3.4)
2. In order for the AROD system to be able to acquire at any point in a vehicle's trajectory, it must be capable of acquiring over the complete Doppler range of 100 kc: (Section 3.4)
3. The signal-power-to-noise-power ratio at the output of the Voltage Controlled Oscillator (VCO) (Figure 24) must be greater than 10 to avoid threshold effects.<sup>21</sup>

The simultaneous realization of these goals is difficult to achieve because, as will be shown later, a short acquisition time requires a large natural loop frequency (Equation 41), as does a large acquisition range (Equations 37 and 40) while a large signal-to-noise ratio requires a small natural loop

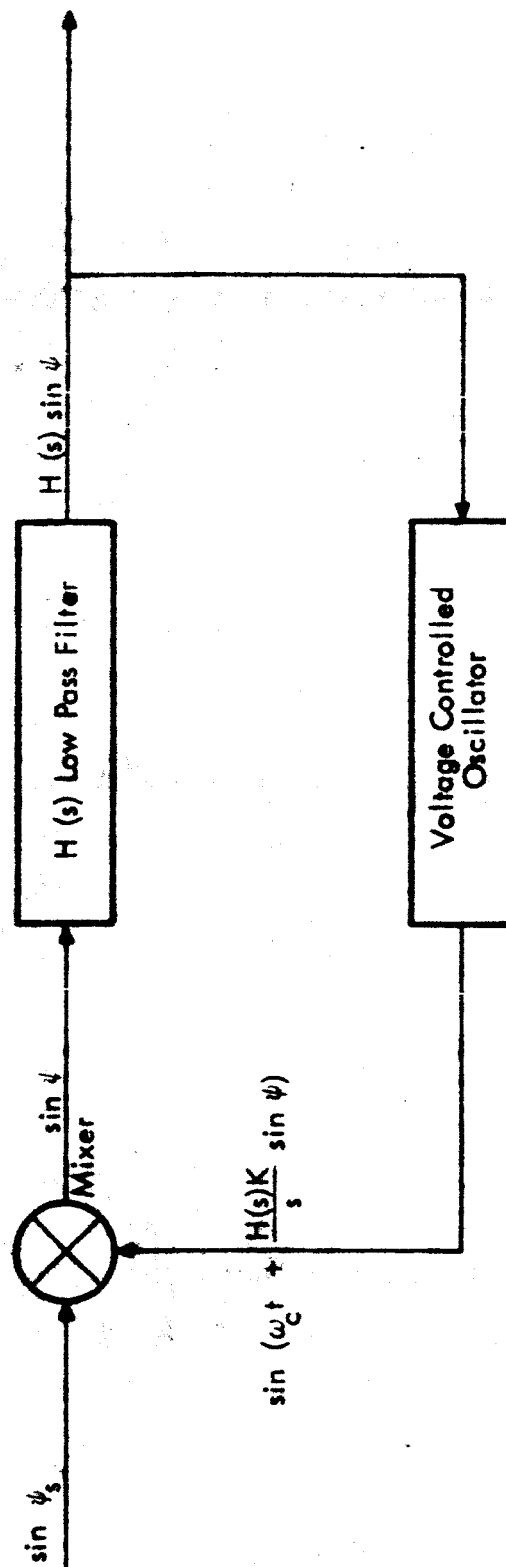


Figure 24. Basic Phase Locked Loop

frequency (Equation 18). In order to achieve our objectives it is necessary to add an external acquisition scheme to the basic phase locked loop shown in Figure 24.

During the early part of the AROD Feasibility Study the most promising external acquisition scheme for the tracking receivers was believed to be a Chirp matched filter.<sup>22</sup> However, as the signal dynamics requirements became better established (see Appendix D), it was found that a simpler technique would suffice. In essence, this technique requires an external sweep circuit which sweeps the entire range of possible Doppler frequencies as is shown in Figure 25. The operation of this circuit can be described as follows:

1. Initially, the problem is the acquisition of a signal of known carrier frequency perturbed by an unknown Doppler which may vary over the range of + 100 kc to 0. In order to accomplish this, gate 2 is open and gates 1 and 3 are closed, so that the VCO (voltage controlled oscillator) is being swept at a rate of  $10^4$  cps per second. Hence, it takes 10 seconds to sweep the complete 100 kc range. The resultant output from the mixer is passed through a filter with a passband from 0 to 100 cps. The output of the filter peaks when the frequency of the input signal coincides with the frequency of the sweep generator. For the signal-power-to-noise-power ratios obtained by the AROD system, the threshold can be set so that the probability of detection will exceed .9 in a single pass and the false alarm probability will be less than  $10^{-6}$ . (Section 3)

2. After a signal has been detected, gate 2 is closed and gates 1 and 3 are opened. The phase locked loop takes over the remainder of the acquisition function and then tracks the signal. The time required to complete acquisition of this signal is much less than one second because the Doppler uncertainty has been reduced to 100 cycles per second. (Equation 41)

The discriminator shown in Figure 25 assists the basic phase locked loop during tracking by feeding back a voltage which is proportional to the Doppler frequency portion of the VCO output. The advantage accruing to the loop from the use of this feedback can be explained best by considering

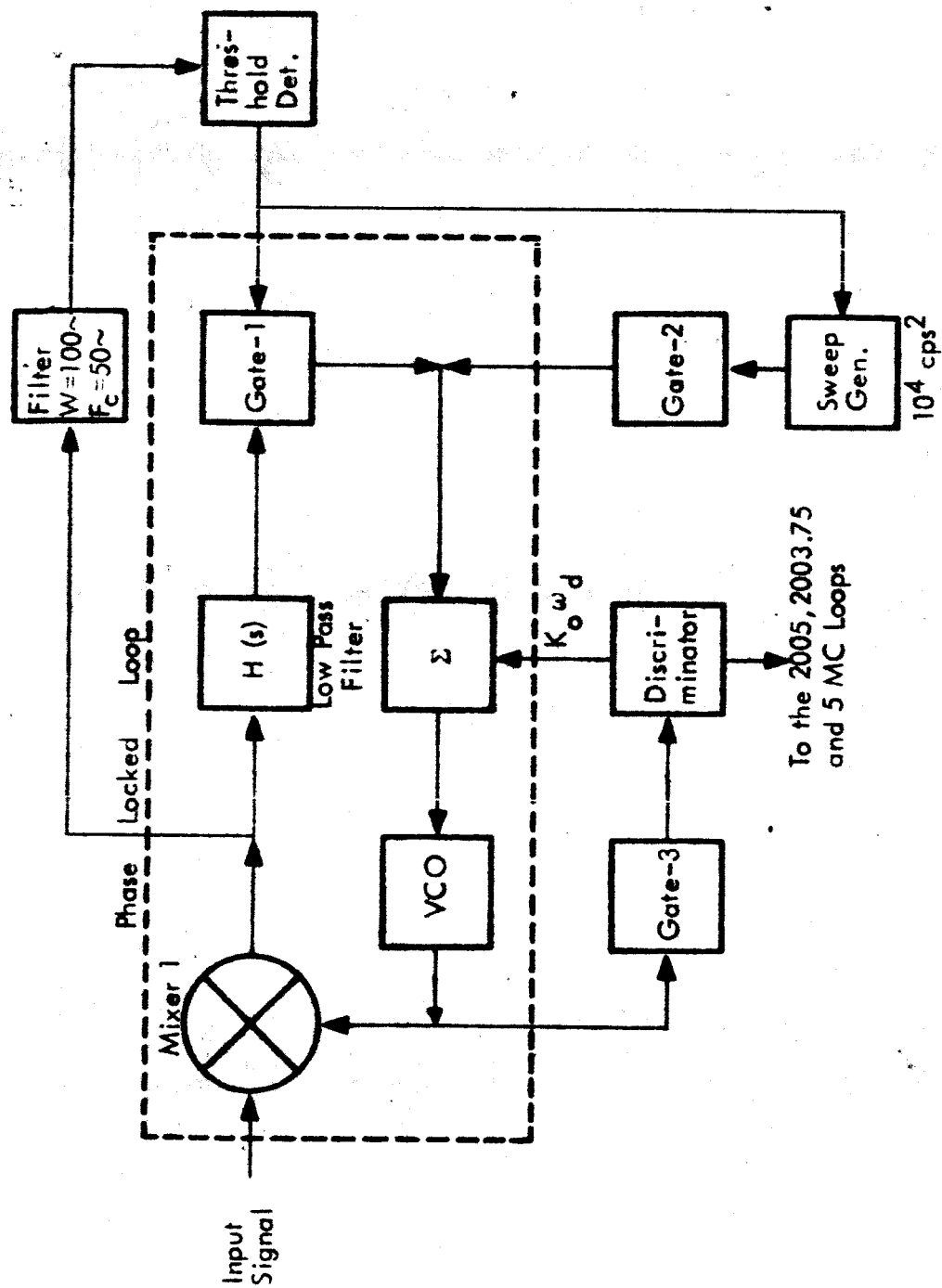


Figure 25. Carrier Acquisition and Tracking Loop

the tracking performance of the phase locked loop both with and without feedback. The essential difference can be appreciated for an input signal of constant frequency  $\omega_c + A$ , where  $\omega_c$  is the frequency of the input signal for zero Doppler frequency and  $A$  is the Doppler frequency. It is convenient to design the VCO so that its output frequency is  $\omega_c$  when its input is zero volts.

It will be shown in Section 4.1.3.2 that the steady state tracking error (i.e., the phase difference between the input signal and the VCO output) is proportional to  $A$  in the absence of feedback. The effect of the feedback is to continuously bias the VCO so that in the absence of an error signal from the low pass filter, after a time  $t_0$ , the frequency of the VCO output continues at the value it had attained at  $t_0$ ; in the absence of feedback the VCO output frequency would tend towards  $\omega_c$  after time  $t_0$ . This heuristic argument is an indication of how the discriminator continuously biases the VCO, and hence, makes the effective value of  $A$  proportional to how well the response curves of the VCO and the discriminator are matched. (It is easy to match these curves to one part in a hundred). With this circuit, the tracking error due to the Doppler offset and the rate of change of Doppler frequency are balanced. Naturally, the linear range of the VCO is independent of whether or not feedback is used and must be greater than the total Doppler frequency. The output of the discriminator is also used as a bias compensator for the VCO in the 5 Mc fine range phase locked loop.

In addition, it has been found that the loop performance can be significantly improved by varying parameters as a function of vehicle altitude. At high altitudes, the signal-power-to-noise-power density ratio is small, and hence, the loop bandwidth must also be relatively small so that the signal-power-to-noise-power ratio is acceptable. Fortunately, the frequency of the signal being tracked does not change rapidly so that the tracking error given by Equation 20 is not excessive and the small loop bandwidth is acceptable. At lower altitudes, higher Doppler rates are expected, and hence, larger loop bandwidths are necessary to avoid large tracking errors; the signal-power-to-noise-power density ratio also increases so that the loop bandwidth can be increased without exceeding the noise error

requirements. The improvement obtained by using one set of parameters at altitudes above 500 nautical miles and another set below 500 miles is indicated under "Computation of Loop Performance."

#### 4.1.3.2 Fine Ranging Tone Phase Locked Loop

The design objectives for the fine ranging tone and range rate phase locked loops differ greatly. The requirements for the fine ranging tone loop and the reasons they differ from the requirements of the carrier loop are the following:

1. The fine ranging tone must be acquired in less than one second. This is consistent with the overall system requirement to begin tracking after approximately ten seconds for the 90 mile orbit since acquisition of the 5 Mc tone cannot begin until after the carrier signal has been acquired. The acquisition of the carrier and fine range tone must be performed sequentially because the fine range tone is derived by mixing the 2000 and 2005 Mc loop VCO outputs.

2. This loop must be capable of acquiring over a Doppler range of 250 cycles per second. This is much less than the Doppler range of the carrier signal because Doppler frequency is proportional to the frequency of the tone.

These conditions are easy to meet because the carrier loop is locked to the correct frequency. Hence, the output of the discriminator on the range rate loop (Figure 25) can be used to bias compensate the fine range tone loop (Figure 26) as well as the range rate loop. This means the loop needs to acquire a signal which differs in frequency by a small amount from the biased center frequency of the VCO. In addition, the bias compensation which has been added to the loop will help reduce the tracking errors to significantly smaller values than would be otherwise obtained. The performance of the loops are shown in the next section.

#### 4.1.3.3 Computation of Loop Performance

The acquisition and tracking performance of the carrier phase locked loop circuit is described in summary form in Tables 8 and 9. Table 8

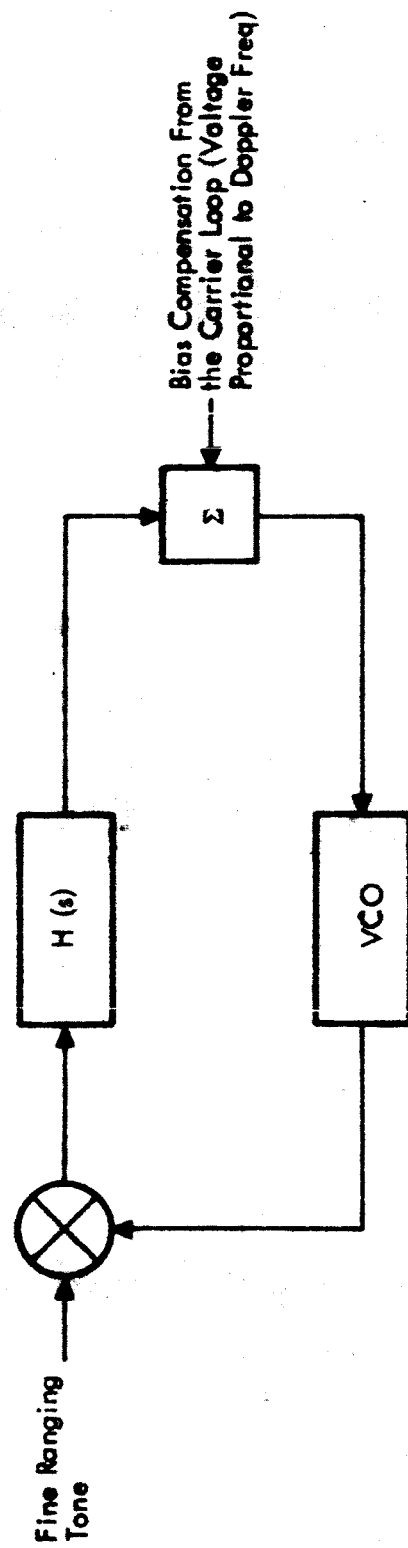


Figure 26. Fine Ranging Tone Phase-Locked Loop

illustrates the performance of a carrier loop for one set of loop circuit parameters; Table 9 shows the improved characteristics when the loop parameters are a function of vehicle altitude. For the case illustrated in Table 9, one set of parameters is used for altitudes which are above 500 nautical miles and another set is used below 500 nautical miles. (Optimization of the loop parameters and switching altitude was not a primary goal of the Feasibility Study but is an appropriate subject for study in subsequent phases of the AROD program.)

Implementation of a circuit which utilizes the two sets of parameters is simple since it only requires two low-pass filters and a switch to activate the appropriate filter into the loop. A further improvement in the operation of the loop can be obtained by making the loop parameters a continuous function of altitude. This may be done by simply using a potentiometer in place of the resistor  $R_1$  shown in Figure 27 and is worthy of further study.

Table 10 illustrates the performance of a loop which is designed for tracking the 5 Mc fine ranging tone.

A short discussion of these tables follows: (A more complete discussion and derivations of all formulas used are contained in Sections 4.1.3.2 and 4.1.3.3.):

1. The parameters  $K$ ,  $\tau$ , and  $\tau'$  are the circuit parameters of the loop. The loop gain in radians per second per radian is  $K$ , and  $\tau$  and  $\tau'$  are the time constants of the low pass filter (Figure 27).<sup>23</sup>

2. The performance of the phase locked loops is shown for altitudes ( $h$ ) from 90 to 2000 nautical miles and elevation angles ( $E$ ) from  $5^\circ$  to  $90^\circ$ . The effective offset frequency,  $A_{\text{eff}}$  is obtained from Equation 21 and Appendix D; the rate of change of Doppler frequency ( $\dot{A}$ ) is taken from Appendix D.

3. The effect of noise during tracking is described by the standard deviation of the phase error due to noise ( $\sigma_n$ ). For large signal-to-noise ratios

$$\sigma_n = \left[ \frac{B}{2 S/N_o} \right]^{1/2} \text{ (radians)} \quad (17)$$

Table 8

## Constant Parameter Carrier Loop

Altitude $h$ (Naut. Mi.)	Elevation Angle $E$ (Degrees)	Effective Doppler $A_{eff}$ (Rad/Sec)	Doppler Rate $\dot{A}$ (Rad/Sec <sup>2</sup> )	Loop Natural Frequency $\omega_n$ (Rad/Sec)	$S/N_0$ (cps)	S/N	Noise Error $\sigma_n$ (Rad.)	Tracking Error $\phi_e$ (Rad.)	Acquisition Time $t_{P.I.}$ (Sec.)	Pull-In Range $\Omega$ (Rad/Sec)
90	5	$2000\pi$	430	200	$8.6 \times 10^4$	430	.03	.07	.05	$6 \times 10^3$
90	90	0	$3 \times 10^4$	200	$9.6 \times 10^5$	$4.8 \times 10^3$	.01	.85	.05	$6 \times 10^3$
500	5	$1700\pi$	$28\pi$	200	$1.12 \times 10^4$	56	.09	.05	.05	$6 \times 10^3$
500	23	$1600\pi$	510	200	$1.56 \times 10^4$	78	.08	.06	.05	$6 \times 10^3$
500	90	0	$1400\pi$	200	$3.12 \times 10^4$	156	.06	.11	.05	$6 \times 10^3$
2000	5	$1000\pi$	$3.4\pi$	200	$2 \times 10^3$	10	.2	.03	.05	$6 \times 10^3$
2000	90	0	570	200	$2 \times 10^3$	10	.2	.01	.05	$6 \times 10^3$

Frequency  $2 \times 10^9$  cps,  $K = 10^5$  Rad. per sec. per rad.,  $r' = 2.5$ -sec.,  $r = .005$  sec.

Table 9

## Variable Parameter Carrier Loop

Altitude $h$ (Naut. Mi.)	Elevation Angle $E$ (Degrees)	Effective Doppler $A_{eff}$ (Rad/Sec)	Doppler Rate $A$ (Rad/Sec <sup>2</sup> )	Loop Natural Frequency $\omega_n$ (Rad/Sec)	S/N <sub>0</sub> (cps)	S/N	Noise Error $\sigma_n$ (Rad.)	Tracking Error $\phi_e$ (Rad.)	Acquisition Time $t_{p.l.}$ (Sec.)	Pull-in Range $\Omega$ (Rad/Sec)
90	5	$2000\pi$	430	$10^3$	$8.6 \times 10^4$	86	.08	.06	$< 10^{-3}$	$10^4$
90	90	0	$3 \times 10^4$	$10^3$	$9.6 \times 10^5$	960	.02	.03	$< 10^{-3}$	$10^4$
500	5	$1700\pi$	$28\pi$	$10^3$	$1.12 \times 10^4$	11.2	.2	.05	$< 10^{-3}$	$10^4$
500	23	$1600\pi$	510	$10^3$	$1.56 \times 10^4$	15.6	.2	.05	$< 10^{-3}$	$10^4$
500	90	0	$1400\pi$	$10^3$	$3.12 \times 10^4$	31.2	.1	.004	$< 10^{-3}$	$10^4$
500	5	$1700\pi$	$28\pi$	200	$1.12 \times 10^4$	56	.09	.05	.05	$6 \times 10^3$
500	23	$1600\pi$	510	200	$1.56 \times 10^4$	78	.08	.06	.05	$6 \times 10^3$
500	90	0	$1400\pi$	200	$3.12 \times 10^4$	156	.06	.11	.05	$6 \times 10^3$
2000	5	$1000\pi$	$3.4\pi$	200	$2 \times 10^3$	10	.2	.03	.05	$6 \times 10^3$
2000	90	0	570	200	$2 \times 10^3$	10	.2	.01	.05	$6 \times 10^3$

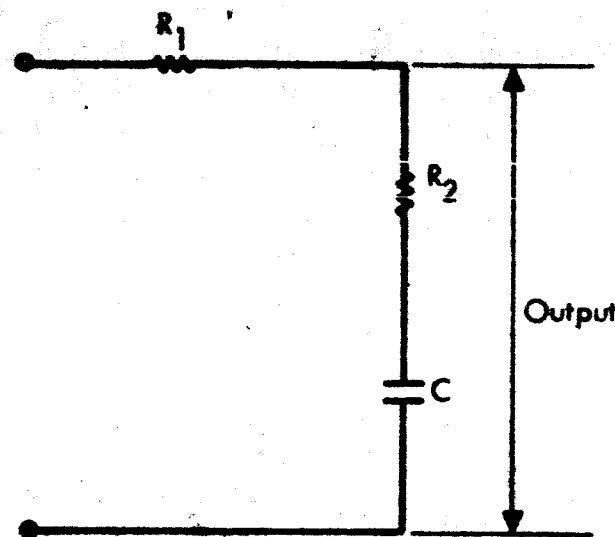
Frequency  $2 \times 10^9$  cps,  $K = 10^5$  Rad. per sec. per rad.,  $\tau = .001$  secs.

Table 10

## Fine Ranging Tone Loop

Altitude $h$ (Naut. Mi.)	Elevation Angle $E$ (Degrees)	Effective Doppler $A_{eff}$ (Rad/Sec)	Doppler Rate $A$ (Rad/Sec <sup>2</sup> )	Loop Natural Frequency $\omega_0$ (Rad/Sec)	$S/N_0$ (cps)	S/N	Noise Error $\sigma_n$ (Rad.)	Tracking Error $\phi_e$ (Rad.)	Acquisition Time $t_{p.l.}$ (Sec.)	Pull-in Range $\Omega$ (Rad/Sec)
90	5	$5\pi$	1	30	$4.3 \times 10^4$	1430	.02	.01	< .01	$2 \times 10^2$
90	90	0	75	30	$4.8 \times 10^5$	$16 \times 10^3$	.006	.08	< .001	$2 \times 10^2$
500	5	$4.2\pi$	.9	30	$5.6 \times 10^3$	187	.05	.01	< .01	$2 \times 10^2$
500	23	$4\pi$	1.3	30	$7.8 \times 10^3$	260	.04	.01	< .01	$2 \times 10^2$
500	90	0	11	30	$1.56 \times 10^4$	521	.03	.01	< .001	$2 \times 10^2$
2000	5	$2.5\pi$	.025	30	$10^3$	33	.1	.008	< .01	$2 \times 10^2$
2000	90	0	1.4	30	$10^3$	33	.1	.002	< .001	$2 \times 10^2$

Frequency  $5 \times 10^6$  cps,  $K = 10^3$  Rad. per sec. per rad.,  $\tau' = 1.1$  sec.,  $\tau = .033$  sec.



$$\tau = R_2 C$$

$$\tau' = [R_1 + R_2] C$$

$$R_1 \gg R_2$$

$$H(s) = \frac{1 + s\tau}{1 + s\tau'}$$

**Figure 27. Low Pass Filter**

The signal-power-to-noise-power density ratio ( $S/N_0$ ) is calculated from Equation 9 in Section 3, with the antenna gain assumed to be 13 db, 10 db, and 7 db for elevation angles of  $5^\circ$ ,  $23^\circ$ , and  $90^\circ$ , respectively, based upon the beam crossover points indicated in Figure 33. B in cycles per second is defined as the loop noise bandwidth and equals  $\omega_n$  in radians per second. In order to avoid threshold effects during both the tracking and acquisition modes, the system is designed so that:

$$\frac{S}{N_0 B} \geq 10 \quad (18)$$

for all points in the AROD operating envelope.<sup>21</sup> Therefore, the minimum value of  $S/N_0$  determines the largest acceptable B or  $\omega_n$  and:

$$(\omega_n)_{\max} = .1 (S/N_0)_{\min} \text{ (radians)} \quad (19)$$

4. The tracking error was calculated from<sup>12</sup>:

$$\sin \phi_e = \frac{\dot{A}}{\omega_n^2} + \frac{A_{\text{eff}}(t)}{K} \quad (20)$$

where  $\dot{A}$  represents the rate of change of Doppler frequency and  $A_{\text{eff}}(t)$  represents the Doppler frequency offset from the biased center frequency of the VCO. The discriminator in Figure 25 reduces  $A_{\text{eff}}$  to:

$$A_{\text{eff}} \approx .01A \quad (21)$$

for all loops during tracking.

5. It is important to check the acquisition properties of the loops. The use of the external sweep circuit to obtain an initial estimate of the carrier Doppler frequency and bias discrimination on both the carrier and fine range tone loops greatly assist the carrier loop acquisition. The frequency pull-in range ( $\Omega$ ) within which a loop can acquire a signal of constant frequency is:

$$\Omega \leq 2 \omega_n \sqrt{\frac{1}{2} \omega_n \tau' + 1} \quad (22)$$

Since  $\Omega$  is greater than  $A_{\text{eff}}$  the loop is capable of acquiring the signal. The assumption of constant frequency during acquisition is reasonable because the loop acquires very quickly. The acquisition time is

$$t_{\text{PI}} = \frac{\tilde{A}_{\text{eff}}^2}{2\zeta\omega_n^3} \quad (23)$$

The sweep circuit reduces  $\tilde{A}_{\text{eff}}$  to approximately 100 cps. Substituting this value into Equation 23 shows that the total acquisition time for the carrier loop is essentially equal to the 10 seconds which are required by the external sweep circuit. For the fine ranging tone loop,  $\tilde{A}_{\text{eff}} = A_{\text{eff}} \approx .01A$  due to bias compensation.

#### 4.1.3.4 Frequency Acquisition

An understanding of the acquisition properties of phase locked loops is basic to all of the acquisition schemes which have been considered for the AROD system. The basic parameter of interest in the discussion of acquisition properties is the "uncertainty" of the signals to be acquired. For example, if an estimate of the Doppler shift is obtained, then the phase locked loop needs to acquire the signal only over the region of uncertainty. This will be discussed more fully in subsequent paragraphs.

A block diagram for the basic phase locked loop is shown in Figure 24. The input signal to the loop may be represented as:

$$V_1(t) = S(t) \exp i [\omega_c t + A_0 t + 1/2 \dot{A} t^2 + \psi_0] + n(t). \quad (24)$$

Here  $\omega_c$  is the radian frequency of the transmitted signal. In the AROD system, loops will be considered for carrier frequencies of 2 Gc and 5 Mc. The  $A_0$  term represents the two way Doppler shift due to the radial velocity (at  $t = 0$ ) and  $\dot{A}$  represents the rate of change of frequency due to the radial acceleration of the satellite. Higher order derivatives of  $A$  are neglected since  $\dot{A}$  is reasonably constant during the short time of acquisition.  $\psi_0$  is a phase shift which contains the information in the range loop. Unfortunately, much remains to be learned about the effects of noise on the acquisition

properties of a phase locked loop circuit. However, in the AROD system the signal-to-noise ratio will never be less than 10, and hence, the effect of noise on the acquisition will be of second order. In the absence of noise, the instantaneous phase ( $\psi_s$ ) and radian frequency ( $\omega_s$ ) of the input signal are:

$$\psi_s = (\omega_c + A_o) t + \frac{1}{2} \dot{A} t^2 + \psi_o \quad (25)$$

$$\omega_s = \frac{d\psi_s}{dt} = \omega_c + A_o + \dot{A} t \quad (26)$$

The frequency of the output of the voltage controlled oscillator (VCO) is a constant  $\omega_c$ , plus a time varying term which is proportional to the voltage at the input of the VCO. The low pass filter only passes the difference frequency term. Hence, from Figure 24:

$$\sin \psi = \sin [\psi_s - \omega_c t - K \frac{H(s)}{s} \sin \psi] \quad (27)$$

Here,  $\psi$  is the instantaneous phase of the output of the mixer and K is the loop gain expressed in units of radians per second per radian; H(s) is the transfer function of the low pass filter. Differentiation of Equation 27 yields the general equation for the instantaneous phase error in a phase locked loop:

$$\dot{\psi} + KH(s) \sin \psi = \dot{\psi}_s - \omega_c \quad (28)$$

During acquisition,  $\psi$  takes on a wide range of values, and hence, it is not possible to linearize Equation 28. The solution of this equation has been studied in detail by A. J. Viterbi<sup>12</sup> for several different low pass filters and both a constant reference signal ( $\dot{A} = 0$ ) and a linearly varying input signal frequency.

In the AROD system, the simple RC low pass filter shown in Figure 27 is sufficient. The transfer function of this filter is:

$$H(s) = \frac{1+s\tau}{1+sT}, = \frac{\tau}{T} \left( \frac{s+1/\tau}{s+1/T} \right) \quad (29)$$

The DC gain of this filter is unity and the three db points can be shown to be:

$$\omega = \pm [\tau'^2 - 2\tau^2]^{-1/2} \quad (30)$$

Substitution of Equations 26 and 29 into Equation 28 yields:

$$\frac{d^2\psi}{dt^2} + (2\zeta\omega_n \cos\psi + \frac{1}{\tau'})\dot{\psi} + \omega_n^2 \sin\psi = \dot{A} + \frac{A_0}{\tau'} + \frac{\dot{A}t}{\tau'} \quad (31)$$

with  $\omega_n^2 \equiv \frac{K}{\tau'}$  and  $2\zeta\omega_n = K\frac{\tau}{\tau'}$ . The quantity  $\omega_n$  is known as the natural frequency of the loop and  $\zeta$  is the damping coefficient.<sup>23</sup> Since this is a second order differential equation, the loop is known as a second order loop. In general, this non-linear equation cannot be solved in closed form.

Valuable information about the acquisition properties of the loop can be obtained by substituting  $y = \frac{d\psi}{dt}$  and  $x = \psi$  into Equation 31. This yields:

$$\frac{dy}{dx} = \frac{dy/dt}{dx/dt} = (-2\zeta\omega_n \cos x + \frac{1}{\tau'}) + \frac{\dot{A} + \frac{A_0}{\tau'} + \frac{\dot{A}t}{\tau'} - \omega_n^2 \sin x}{y} \quad (32)$$

A graph of  $y = \dot{\psi}$  vs.  $x = \psi$  is known as the phase portrait in the phase plane method. From this graph, it is possible to determine the behavior of  $\dot{\psi}$  and  $\psi$  with time. It should be noted that Equation 32 is periodic in  $x$  with a period of  $2\pi$ . Hence, it is necessary to plot the phase plane trajectories only in the region from  $-\pi$  to  $\pi$ . This procedure is quite tedious to perform by hand computation, but can readily be simulated on an analog computer.

Fortunately, the equilibrium points of the loop can be obtained without actually solving Equation 32. For example, in phase plane analysis it is well known that the system can achieve equilibrium only at points for which  $\frac{dy}{dx}$  is indeterminate.<sup>24</sup> Hence, the points of equilibrium are:

$$y = 0, x = \sin^{-1} \frac{\dot{A} + \frac{A_0}{\tau'} + \frac{\dot{A}t}{\tau'}}{\omega_n^2} \pm 2N\pi \quad (33)$$

$$y = 0, x = \sin^{-1} \frac{\dot{A} + \frac{A_0}{\tau'} + \frac{\dot{A}t}{\tau'}}{\omega_n^2} \pm (2N+1)\pi \quad (34)$$

where  $N$  is an integer.

Case I A = 0

If the phase locked loop is attempting to acquire a signal with a constant input frequency, then Equations 33 and 34 imply that the stable point of the system is described by:

$$\sin x = \frac{A_o}{\omega_n^2 \tau'} \quad (35)$$

Hence, the system cannot be stable and cannot achieve lock or stay in lock if

$$A_o > \omega_n^2 \tau' \quad (36)$$

Unfortunately it cannot be assumed that the system will lock on if Equation 36 is not satisfied.

In addition to the requirement that Equation 36 does not hold, one of the following criteria must be met:<sup>12</sup>

1. A second order phase locked loop will always lock in to a constant frequency signal as long as the frequency of the signal being acquired lies between the center frequency of the VCO and the initial frequency of the VCO.

2. If the signal frequency does not satisfy condition 1, lock will still occur if:

$$A_{\text{eff}} < \Omega = 2\omega_n \sqrt{\frac{1}{2} \tau' \omega_n + 1} \text{ (rad/sec).} \quad (37)$$

Here,  $\Omega$  is the pull-in range or the amount by which the signal frequency can differ from the VCO center or biased frequency. In the AROD system, Equation 37 is satisfied with a great deal to spare because of the use of acquisition aiding on the carrier and bias compensation on the other tones. For the loop shown in Table 8, the pull-in range is approximately 6000 radians/second, while the acquisition aiding reduces the uncertainty on the input signal to 100 cps or 200  $\pi$  radians/second.

### Case II Linearly Varying Reference Frequency

The ability of a phase locked loop to acquire a ramp in frequency can be determined by two simple considerations. First, we note from Equations 33 and 34 that singular points will exist if and only if:

$$\omega_n^2 > \dot{A} + \frac{A_o + \dot{A}t}{\tau'} = \dot{A} + \frac{A(t)}{\tau'} \quad (38)$$

If this inequality is not satisfied the loop will not be able to acquire the signal and, in addition, a loop which is initially in lock will not remain in lock. For the parameters shown in Tables 8, 9 and 10:

$$\frac{\dot{A} + \frac{A_{\text{eff}}(t)}{\tau'}}{\omega_n^2} < .5 \quad (39)$$

Since this inequality is satisfied, we may estimate the pull-in range as:

$$\Omega \approx \frac{\zeta \omega_n^3}{A} \text{ rad/sec } \zeta = \frac{1}{2} \quad (40)$$

The effective Doppler offset is less than the pull-in range for all cases (when the acquisition aiding is considered).

### Acquisition Pull-In Time

A formula for estimating acquisition time which has been derived by Viterbi<sup>12</sup> is:

$$t_{PI} = \frac{\tilde{A}_{\text{eff}}^2}{2 \zeta \omega_n^3} \quad (41)$$

In the following section, it will be shown that for a given  $\omega_n$  the effects of noise are minimized by choosing  $\zeta = 1/2$ . In this case, Equation 41 becomes:

$$t_{PI} \approx \frac{\tilde{A}_{\text{eff}}^2}{\omega_n^3} \quad (42)$$

This formula can be derived under the assumption that the filter ( $H(s)$ ) which is used in the phased locked loop has a long time constant or equivalently a narrow low pass bandwidth. In addition, it is assumed that the frequency of the input signal does not change by a large amount during the pull-in time.

It is obvious from Equation 42 that the pull-in time is minimized by simultaneously maximizing the natural frequency of the loop ( $\omega_n$ ) and minimizing  $\tilde{A}_{eff}$ . The maximum value of  $\omega_n$  is determined from the signal-to-noise ratio and is given in Equation 19. The value of  $\tilde{A}_{eff}$  is determined by the acquisition aiding system.

#### 4.1.2.5 Tracking

After the carrier and ranging tones have been acquired in frequency, it is necessary to "lock on" and track in phase. Fortunately, the non-linear equation which describes the phase lock loop during acquisition can be linearized when the loop is phase-locked since the phase of the error signal out of the mixer is small and hence,  $\sin \psi \approx \psi$  and  $\cos \psi \approx 1$ . It follows that Equation 31 reduces to:

$$\frac{d^2\psi}{dt^2} + (2\zeta\omega_n + \frac{1}{\tau'}) \frac{d\psi}{dt} + \omega_n^2 \psi = \dot{A} + \frac{\dot{A}_o}{\tau'} + \frac{\dot{A}_t}{\tau'} \quad (43)$$

This is a linear differential equation and hence, in the tracking mode the phase locked loop may be analyzed by standard linear techniques. The linear circuit which is shown in block diagram form in Figure 28 represents a phase transfer model for a linearized phase locked loop.

We are interested in the ability of a loop to track the phase of an input signal which has been distorted by noise. The phase error,  $\psi_e$ , is defined as:

$$\psi_e \equiv \psi_s - \psi_{osc} = \psi_s (1 - \frac{\psi_{osc}}{\psi_s}) \quad (44)$$

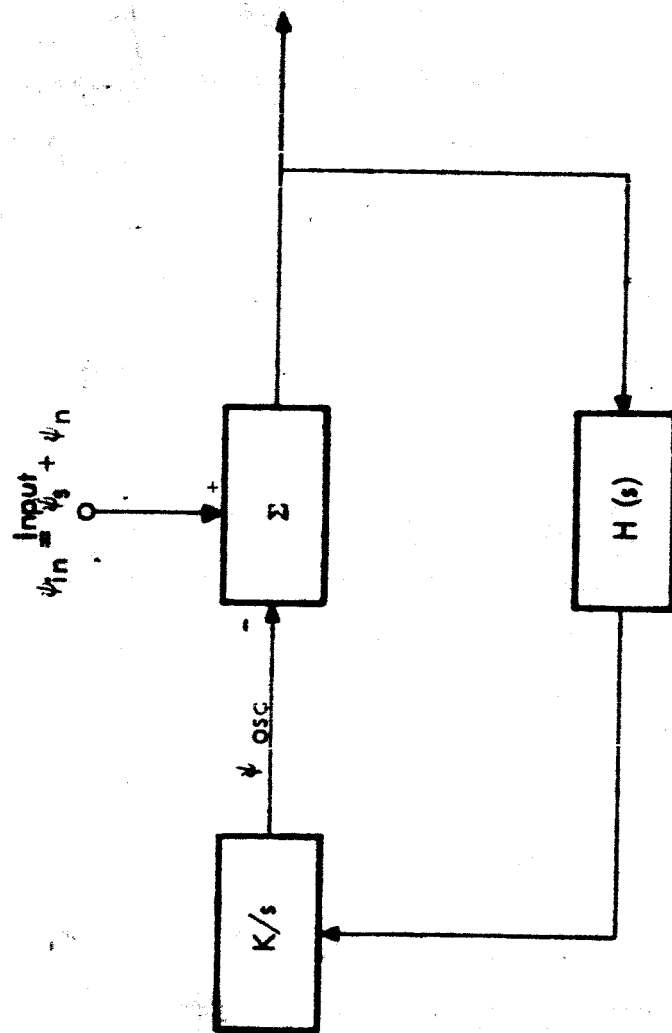


Figure 28. Linearized Phase Transfer Model

However, the loop operates on the noisy input signal which has a phase that differs from the phase of the pure signal. Hence, it is convenient to describe the loop in terms of the closed loop transfer function:

$$H_L(s) = \frac{\psi_{osc}(s)}{\psi_{in}(s)} \quad (45)$$

In order to develop a relationship which describes the phase error of the loop in terms of the closed loop transfer function the input and signal phases must be related. This may be done by considering narrow-band signal and additive noise so that:

$$V_{in} \cos \psi_{in}(t) = V_s \cos (\omega_o t + \phi_s) + V_n \cos (\omega_o t + \phi_s + \phi_n). \quad (46)$$

$V_{in} \cos \psi_{in}(t)$  — represents the input to the loop;

$V_s \cos (\omega_o t + \phi_s)$  — represents the signal;

$V_n \cos (\omega_o t + \phi_s + \phi_n)$  represents the noise.

Equation 46 may be rewritten in the form:

$$V_{in} \cos \psi_{in}(t) = V_s \left\{ \cos (\omega_o t + \phi_s) + \frac{V_n}{V_s} \cos (\omega_o t + \phi_s + \phi_n) \right\}$$

or

$$V_{in} \cos \psi_{in}(t) = V_s \left\{ \left( 1 + \frac{V_n}{V_s} \cos \phi_n \right) \cos (\omega_o t + \phi_s) - \frac{V_n}{V_s} \sin \phi_n \sin (\omega_o t + \phi_s) \right\} \quad (47)$$

For large signal-to-noise ratios  $V_n/V_s \ll 1$ , use of the approximations:

$$\cos \left[ \frac{V_n}{V_s} \sin \phi_n \right] \approx 1 \text{ and } \sin \left[ \frac{V_n}{V_s} \sin \phi_n \right] = \frac{V_n}{V_s} \sin \phi_n \quad (48)$$

yields:

$$V_{in} \cos \psi_{in}(t) = V_s \left\{ \cos \left[ \omega_0 t + \phi_s + \frac{V_n}{V_s} \sin \phi_n \right] + \frac{V_n}{V_s} \cos \phi_n \cos \left[ \left( \omega_0 t + \phi_s + \frac{V_n}{V_s} \sin \phi_n \right) - \frac{V_n}{V_s} \sin \phi_n \right] \right\} \quad (49)$$

Expanding the second term of Equation 49 and discarding all terms of higher than first order in  $(V_n/V_s)$  yields:

$$V_{in} \cos \psi_{in}(t) = V_s \left( 1 + \frac{V_n}{V_s} \cos \phi_n \right) \cos \left[ \omega_0 t + \phi_s + \frac{V_n}{V_s} \sin \phi_n \right] \quad (50)$$

Hence, 
$$V_{in} = V_s \left( 1 + \frac{V_n}{V_s} \cos \phi_n \right) \quad (51)$$

and 
$$\psi_{in} = \omega_0 t + \phi_s + \frac{V_n}{V_s} \sin \phi_n \quad (52)$$

The fluctuations in  $V_{in}$  are eliminated by the use of a limiter prior to the mixer in the phase locked loop. The instantaneous phase can be written as the sum of a phase due to the input signal ( $\psi_s$ ) and a phase shift due to noise ( $\psi_n$ ). In other words:

$$\psi_{in} = \psi_s + \psi_n \quad (53)$$

where: 
$$\psi_s = \omega_0 t + \phi_s, \text{ and } \psi_n = \frac{V_n}{V_s} \sin \phi_n. \quad (54)$$

Since  $V_n/V_s \ll 1$ , it follows that

$$\frac{\psi_n}{\psi_s} \ll 1 \text{ and } \frac{\psi_{in}}{\psi_s} \approx 1 \quad (55)$$

From Equations 44, 45, and 52 to 55, it follows that:

$$\psi_e = [1 - H_L(s)] \psi_s + H_L(s) \psi_n \quad (56)$$

We note that one component of the phase error is due to noise ( $H_L \psi_n$ ) and another component, which exists even in the absence of noise, is a tracking error.

The steady state tracking error of the loop  $[(\psi_e)_{ss}]$  when it is attempting to follow an excitation in phase can be obtained by use of the final value theorem:

$$\begin{aligned} (\psi_e)_{ss} &= \lim_{s \rightarrow 0} s \psi_e \\ (\psi_e)_{ss} &= \lim_{s \rightarrow 0} s [1 - H_L(s)] \psi_s \end{aligned} \quad (57)$$

The phase variation due to noise is naturally a random variable. From Equation 54 it follows that for white noise of zero mean value:

$$E \{ \phi_n \} = 0 \quad (58)$$

and

$$\sigma_n^2 = E \{ \psi_n^2 \} = E \left\{ \frac{V_n^2}{V_s^2} \sin^2 \phi_n \right\} \quad (59)$$

Here,  $\sigma_n$  is the standard deviation of the phase due to noise. ( $\sigma_n$  is in units of radians.) For white Gaussian noise  $V_n$  and  $\phi_n$  are independent of each other. Hence:

$$\sigma_n^2 = E \left\{ \frac{V_n^2}{V_s^2} \right\} E \{ \sin^2 \phi_n \} = \frac{1}{2} \frac{N}{S} = \frac{1}{2} \frac{N_0 B}{S} \quad (60)$$

Here,  $B$  is the effective noise bandwidth of the phase locked loop. Since the loop is a linear system in the tracking mode, it follows that:<sup>25</sup>

$$B = \frac{\int_{-\infty}^{\infty} |H(j\omega)|^2 d\omega}{|H_{\max}|^2} \quad (61)$$

The loop noise bandwidth has been related to the natural frequency of the loop by Develet.<sup>5</sup> He has shown that for a loop with a large gain K that

$$B = \omega_n \left[ \frac{1 + 4\zeta^2}{4\zeta} \right] \quad (62)$$

where B is in cycles per second and  $\omega_n$  is in radians per second. It follows immediately that for a given  $\omega_n$ , the minimum value of B occurs when,  $\zeta = 1/2$ . In the remainder of this report, it will be assumed that  $\zeta = 1/2$ , so that B in cycles per second will be equal to  $\omega_n$  in radians per second. Hence,

$$\sigma_n^2 = \frac{N_o \omega_n}{2S} \quad (63)$$

The steady state error for a phased locked loop in a tracking mode is calculated from Equation 57. The closed loop transfer is obtainable from Figure 28 and is:

$$H_L(s) = \frac{KH(s)}{s + KH(s)} \quad (64)$$

If the instantaneous frequency is a ramp as is shown in Figure 29, then:

$$\frac{d\phi}{dt} = f(t) = A_o + \dot{A} \{tu(t) - (t - T)u(t - T)\} \quad (65)$$

where  $u(t)$  is a unit step function.

Hence,

$$s\psi(s) = \frac{A_o}{s} + \frac{\dot{A}}{s^2} (1 - e^{-sT}) \quad (66)$$

where,  $\psi(s)$  is the Laplace Transform of the instantaneous phase. The steady state error becomes:

$$(\psi_e)_{ss} = \lim_{s \rightarrow 0} \frac{s}{s + KH(s)} \left\{ \frac{A_o}{s} + \frac{\dot{A}}{s^2} (1 - e^{-sT}) \right\} \quad (67)$$

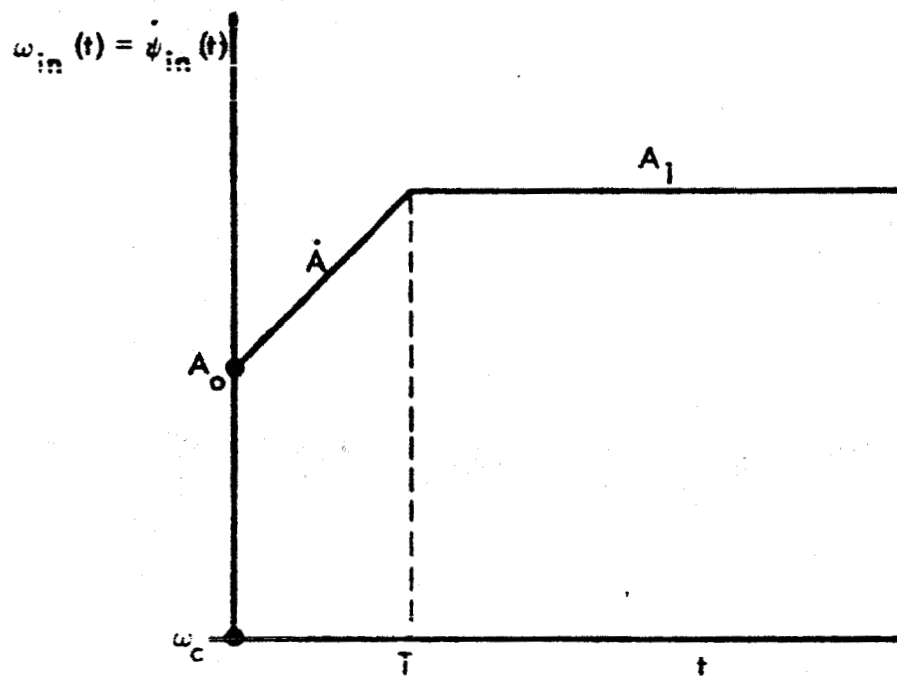


*Figure 29. Frequency Ramp*

For the filter used in the AROD system Equation 29,  $\lim_{s \rightarrow 0} H(s) = 1$ . By expanding  $e^{-st}$  in a Taylor series and performing the limiting process Equation 67 becomes:

$$(\psi_e)_{ss} = \frac{1}{K} \{A_0 + A_1 T\} = \frac{A_1}{K} = \frac{A_1}{\tau \omega_n^2} \quad (68)$$

This result is valid as long as the steady state error does not exceed about .5 radians. If the steady state error exceeds this value the non-linear model for a phase locked loop must be considered since the linear analysis is no longer valid.

#### 4.1.4 Range Rate Measurement

In this section, we will discuss simple methods for measuring the Doppler frequency ( $f_d$ ) to the .1 cps (rms) accuracy established as an objective in Section 2.5. This is equivalent to a range rate quantization error of:

$$\Delta \dot{r} = \frac{c}{2} \frac{\Delta f_d}{f_t} = \frac{3 \times 10^8}{2} \left( \frac{.1}{2 \times 10^9} \right) = .0075 \text{ meters/sec.}$$

It will also be assumed that counters operating at a rate in excess of 10 Mc are to be avoided in the spacecraft, if possible.

The two-way Doppler frequency tone can be obtained in the satellite by mixing the received signal with the transmitted signal. However, if this were done in the satellite, it would be necessary to distinguish between positive and negative Doppler frequencies. This difficulty may be avoided by biasing the Doppler frequency by an amount  $f_b$  so that  $f_b + f_d$  is always greater than zero. This biased Doppler frequency is generated by mixing the received signal with a signal which has a frequency equal to the transmitted frequency minus  $f_b$ . For convenience,  $f_b$  is chosen as 156.25 kc because this is the frequency of the nearest ambiguity resolving tone and hence, this bias is easy to generate. This frequency will be known to 1 part in  $10^9$  (Section 4.1.1.1) so that we will be able to neglect errors in the bias frequency in the formulation in the next paragraph.

The biased Doppler frequency is measured by calculating:

$$(f_d + f_b)_m = \frac{\phi}{T} \quad (69)$$

where  $\phi$  is the phase change of the biased Doppler signal in the measurement time  $T$ . Then, if  $\phi = \phi_o + \Delta\phi$  and  $T = T_o + \Delta T$  where  $\phi_o$  and  $T_o$  are the actual phase change and measurement time respectively and  $\Delta\phi$  and  $\Delta T$  are the errors in phase and time, we can obtain the Doppler frequency error  $\Delta f_d$  from Equation 69:

$$f_d + f_b + \Delta f_d = \frac{\phi_o + \Delta\phi}{T_o + \Delta T} = \frac{\phi_o}{T_o} \frac{1 + \frac{\Delta\phi}{\phi_o}}{1 + \frac{\Delta T}{T_o}} \quad (70)$$

$$\text{and: } f_d + f_b = \frac{\phi_o}{T_o} \quad (71)$$

where  $\Delta f_b$  is neglected for the reason given in the previous paragraph. If the relative errors  $\Delta\phi/\phi_o$  and  $\Delta T/T_o$  are small compared to one (as is certainly the case), we obtain:

$$\Delta f_d = (f_d + f_b) \left[ \frac{\Delta\phi}{\phi_o} - \frac{\Delta T}{T_o} \right] \quad (72)$$

This implies that for fixed relative errors the Doppler frequency error is largest when  $f_d$  takes on its maximum value of 100 kc. Since the error in  $f_d$  should not exceed .1 cps the requirement placed on the measuring circuit is

$$\left| \frac{\Delta\phi}{\phi_o} \right| + \left| \frac{\Delta T}{T_o} \right| \leq \frac{\Delta f_d}{f_d + f_b} = 4 \times 10^{-7} \quad (73)$$

Accuracy of this order of magnitude can be achieved only through the use of digital techniques. One method which can satisfy this requirement is the following:

1. A high accuracy clock is used to initiate the measurement. This clock is capable of a standard deviation which does not exceed 6 nanoseconds in the .1 seconds used to obtain a Doppler measurement (Section 2.5).

2. A digital counter is used to determine the time,  $t_1$ , to the first positive going zero crossing. The error in measuring  $t_1$  is determined essentially by the frequency ( $f_c$ ) of the counter which determines the quantization interval of the digital circuit. The standard deviation of  $t_1$  due to quantization is:

$$\sigma_{t_1} = \frac{1}{f_c \sqrt{12}} \text{ seconds.} \quad (74)$$

A reasonable counter frequency might be  $f_c = 10 \text{ Mc.}$

3. Another counter is used to determine the number ( $N_o$ ) of complete cycles during the .1 second measurement time (Section 2.5).

4. A third counter is reset to zero at each positive going zero crossing. This counter is stopped at the end of the .1 second measurement time and contains a measure of the time ( $t_2$ ) since the last zero crossing. The standard deviation of  $t_2$  is given by Equation 74.

From this procedure it is evident that the measured Doppler frequency is:

$$f_d = \frac{N_o}{.1 - t_1 - t_2} - f_b \quad (75)$$

In this method:

$$T_o = .1 - t_1 - t_2 \quad (76)$$

The errors in measuring the .1 second interval and  $t_1$  and  $t_2$  can be considered as uncorrelated. Hence, we obtain the standard deviation of  $T_o$  by summing errors in an rms fashion to obtain:

$$\sigma_{t_o} = \Delta T = \sqrt{(6 \times 10^{-9})^2 + \frac{2}{12} (10^{-7})^2} = 4 \times 10^{-8} \text{ seconds} \quad (77)$$

Since phase is not measured in this scheme,  $\Delta\phi = 0$ . (78)

We conclude from substitution of Equations 77 and 78 into Equation 73 that the Doppler method described in this section satisfies the AROD requirements.

#### 4.1.5 Range Measurement Circuit

To estimate equipment penalties and the concomitant accuracies, the range measurement circuit that has been assumed in the AROD Feasibility Study is similar to units used elsewhere.<sup>4</sup> In the system under consideration a clock is started when all of the ranging tones of the transmitted signal simultaneously cross zero in the same direction. In essence, the clock is stopped when the tones of the received signal simultaneously cross zero. The time measured by the clock is naturally an analogue of range. However, for the one meter range quantization objective established in Section 2.5, it is necessary to measure the phase of the 5 Mc fine ranging tone to  $12^\circ$ . This requires a clock which is capable of operating at a frequency of 150 Mc. This requirement may be eliminated by the reasonably simple heterodyne scheme which is shown in Figure 30. The received 5 Mc fine ranging tone is tracked by a phase locked loop and the clean output from the VCO is mixed down to a frequency of 15 kc; the reference 5 Mc tone is also mixed down to 15 kc. The outputs of the mixers retain the phase information on the 5 Mc tone as long as the mixers are well matched to avoid differential phase shifts. The mixing process makes it possible to reduce the counting speed by the ratio of 5 megacycles to 15 kc so that a one megacycle counter will be sufficient.

The mixers will be well matched if the diodes used in the mixers are also well matched. This can be accomplished by adding the precision resistors  $r_1$  and  $r_2$  to the diodes as is shown in Figure 31. The effective forward and back resistances  $R'_f$  and  $R'_b$  become:

$$R'_f = \frac{(R_f + r_1) r_2}{R_f + r_1 + r_2} \quad (79)$$

$$R'_b = \frac{(R_b + r_1) r_2}{R_b + r_1 + r_2} \quad (80)$$

where,  $R_f$  and  $R_b$  are the forward and back resistances of the diode by itself. Now, if the precision resistors are chosen so that:

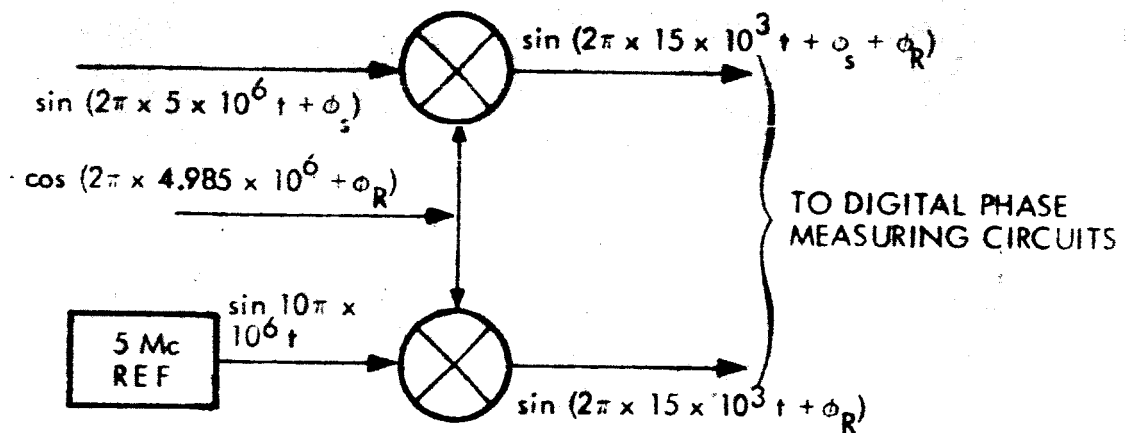


Figure 30. Fine Ranging Tone Down Converter

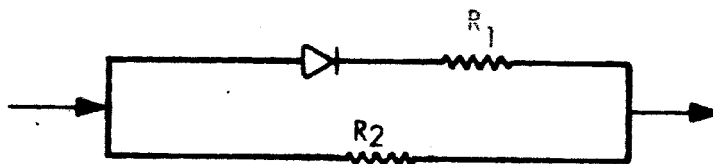


Figure 31. Diode Matcher

$$R_b \gg r_2 \gg r_1 \gg R_f \quad (81)$$

the effective resistances become:

$$R_f' = r_1 \quad (82)$$

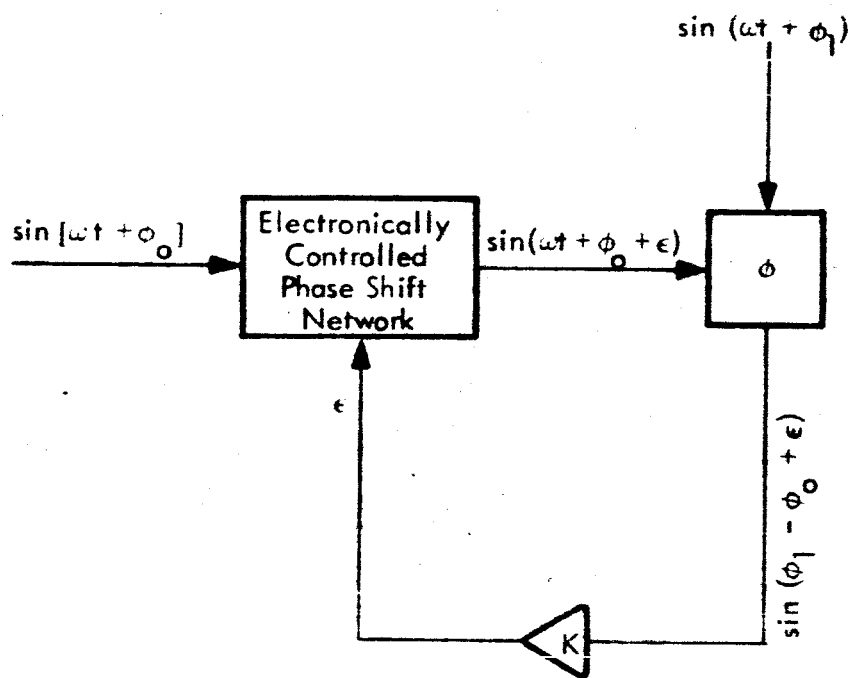
$$R_b' = r_2 \quad (83)$$

#### 4.1.5.1 Tracking the Ambiguity Resolving Range Tones

Tracking filters can be furnished for the ambiguity resolving range tones which are generated as side tones in the AROD spectrum. These tones are synthesized as sub-harmonics of the 5.0 Mc fine range tone, the highest of which is transmitted as a carrier displaced 1.25 Mc below the 2005 Mc carrier. All successively coarser ambiguity resolving tones are introduced into the spectrum as phase modulation of the carrier at 2003.75 Mc.

The suggested method for tracking the range ambiguity resolving tones is shown in block diagram form in Figure 15. The output of the VCO (voltage controlled oscillator) is divided down in frequency by the appropriate amount to yield a signal at each ambiguity resolving tone frequency. Since the output of the VCO has a large signal-to-noise ratio (Section 4.1.3.3, Table 10) and contains the Doppler shift, the output of the frequency divider is a clean signal with the appropriately scaled down Doppler shift. The other input to the tracking loop is the demodulated ambiguity resolving tone which we wish to track. The 1.25 Mc signal is obtained by mixing the 2005 Mc and 2003.75 Mc components; the other ambiguity resolving tones are obtained by phase detection of the modulated 1.25 Mc signal with a reference 1.25 Mc signal and filtering the result through a wide bandpass filter to minimize phase distortion.

The operation of the tracking loop can be understood most easily by considering the phase transfer model shown in Figure 32. The electronically controlled phase shift network adjusts the phase of the frequency divided output from the fine range tone VCO to the phase of the appropriate ambiguity resolving tone. The phase detector output is proportional to the sine of the phase difference between its two inputs and is fed back to the phase shift



$$\epsilon = K \sin(\phi_1 - \phi_0 - \frac{\pi}{2})$$

Figure 32. Phase Transfer Model

network through a low pass filter. It is interesting to note that once the input is acquired, the signal fed back to the electronically controlled phase shift network is constant because the phase difference between the two inputs remains constant. Hence, after acquisition, an extremely narrow band low pass filter is desired. This makes it possible to obtain the same  $S/N_0$  at the output of the range ambiguity resolving tone tracking loops as at the output of the voltage controlled oscillator in the fine range tone phase locked loop. This circuit should be analyzed in more detail during the next phase of the AROD program.

#### 4.1.6. Weight and Power Estimates

##### 4.1.6.1 Transmitter

In reviewing the spacecraft electronic equipment requirements for the AROD system, it is seen that the transmitter will consume the most power, contribute most to the package weight, and be the largest in size of any single unit that makes up the spacecraft AROD package. (See Table 11.)

In order to make an estimate of the transmitter size and weight, environmental and operational requirements have been studied and state-of-the-art capabilities for solid state harmonic generators and associated transistorized driving circuitry have been projected to bring them in line with the AROD time frame. The estimates to be given for the transmitter include harmonic generator circuitry and microwave power summing and diplexing components, and driving circuitry other than the frequency synthesizer.

For a design such as has been shown in Figure 20, the transmitter efficiency is estimated at 15 percent. For a total of 12.5 watts of r-f power into the vehicle antenna, the input power would be 83 watts. To provide for heat dissipation under these operating conditions, sufficient mass must be included in the unit housing to permit adequate heat sinking.

It is estimated that a single 2.5 watt channel of a design such as shown in Figure 20 would occupy 65 cubic inches of space and would weigh approximately two pounds. For five channels arranged as shown to produce 12.5 watts of microwave energy, the unit size would be approximately 350 cubic inches and the weight would be about 12 pounds, including power summing components.

In addition to the transmitter; VHF, UHF, and microwave circuitry; the modulation circuitry; and the receiver microwave pre-selector could also be included in a unit of this estimated size and weight.

TABLE 11

## Spacecraft ARCD Equipment Estimates

	POWER (watts)	SIZE (cubic inch)	WEIGHT (pounds)
Transmitter	83.0	350	12.0
Receiver RF Section	0.3	20	0.8
I.F. and Phase-Lock Loop (4 units)	8.0	240	7.0
Frequency Synthesizer	6.0	100	2.5
Power Regulator	8.0 (loss)	25	3.0
Range Rate Measurement Circuits	2.7	25	0.6
Range Measurement Circuits	3.2	10	0.3
Power Supplies for Range and Range Rate	3.0 (loss)	20	1.0
Totals	114.2 watts	790 cubic inches	27.2 pounds

#### 4.1.6.2 Receiver

The AROD receiving equipment to be carried aboard the spacecraft will include a microwave r-f section, a wide band i-f amplifier and four units such as the one shown in the block diagram, Figure 23. From a study of off-the-shelf tunnel diode microwave equipment, it is estimated that the microwave and wideband i-f amplifier section of the receiver can be contained in a single unit of less than 20 cubic inches having a weight of approximately 0.8 pound. Power for this assembly would be about 0.3 watts. The size and weight estimate is made assuming that the receiver pre-selector or interdigital bandpass filter will be included in the microwave assembly of the transmitter unit.

Each of the bandpass amplifiers and phase locked loop units of the receiver would require about 60 cubic inches. For a unit containing four single loop circuits as shown in the block diagram, the power per unit is estimated to be 2 watts.

The total receiver power estimate is then 8.3 watts and size is estimated at 260 cubic inches. Weight would be approximately 7.8 pounds.

#### 4.1.6.3 Frequency Synthesizer

The frequency synthesizer for the spaceborne AROD system will contain circuitry for generating highly stabilized signals ranging from low frequency audio through VHF. Each of these signals will be synthesized from the temperature controlled 5 megacycle crystal oscillator contained in the unit.

The power level of each output signal will be low, since a significant amount of driving power is required only at the input of the transmitter varactor harmonic generator chain and this energy is generated in the transistor amplifier section of the transmitter unit.

The most significant power requirement for the frequency synthesizer is that for temperature stabilization. Manufacturer's estimates are that this would be from 2 to 4 watts after warm-up. Total operational power requirements for the unit is estimated at 6 watts and the unit size and weight would be approximately 100 cubic inches and 2.5 pounds.

#### 4.1.6.4 Power Conversion and Regulation

Considering the frequency and phase stability requirements of the AROD system, it can be assumed that any primary spacecraft power available for operating the AROD equipment will require some degree of regulation. For regulation of the transmitter power, a DC/DC converter will most likely be required. In this case, an efficiency of approximately 85 to 90 percent will result from the conversion and regulation process. Considering the estimated transmitter input power of 83 watts, the power supply size and weight is estimated to be 25 cubic inches, and 3 pounds, assuming proper mounting for heat sinking to some member of the vehicle.

A small amount of power could also be supplied to other AROD units where required. Most of the lower power requirements could be satisfied directly by solid state diode regulators.

#### 4.1.6.5 Range and Range Rate Measuring Circuits.

The circuits necessary to measure range and range rate in the space vehicle are discussed in Sections 4.1.4 and 4.1.5. The analog sections in both arrangements consist basically of a mixer followed by a low pass filter. The power necessary to drive this portion will be supplied from outside circuits and therefore, will be neglected at this point. The remaining circuits are digital in nature and consist basically of transistor flip-flops or diode logic. All counter stages operating at or below 500 kc can be built using IBM-COMPASS circuit techniques which need about 30 mw per flip-flop and associated gating circuits, and have a packing density of about 20 flip-flops per cubic inch. The high frequency counter stages will be built using conventional low voltage transistor circuits which will need more space but not more power. Since every measuring circuit will be needed, four times the final estimates will be obtained by multiplying the individual requirements by four.

#### 4.1.7 Equipment Interfaces

Although it was not a primary goal of the feasibility study, an analysis of the equipment interfaces for the AROD system was necessary to uncover any potential problem areas and to provide guidelines for future phases of the AROD program. Three interfaces were considered to be of sufficient importance to deserve some analysis in the feasibility study: the interface with the vehicle computer, the interface with the telemetry system, and the interface with the command link.

##### 4.1.7.1 Computer Interface\*

The analysis of the interface between the AROD equipment and the vehicle computer emphasized the definition of the tasks which the computer may have to perform. In addition, the most recent estimate of the computational capability available for AROD was obtained and is included in this discussion.

The first and primary AROD task to be performed in the vehicle computer is the conversion of the range and range rate information obtained from the AROD ground stations to the parameters of interest to the vehicle's guidance system. In the Feasibility Study, it was assumed that these parameters were the spacecraft's position and velocity; however, it may be desirable to compute instead the orbital parameters for the vehicle or the vehicle's position at some future time. To convert the AROD data, it will probably be desirable to make the transformations from time to meters and from cycles (plus time) to meters per second in the vehicle computer. For the range transformation, it will be necessary to interpolate readings to determine the vehicle's "average position" during the propagation time. For the range rate transformation, the velocity of the ground station due to the Earth's rotation must be considered, and the exact formula  $f_d (c - \dot{r}) = 2 f_t \dot{r}$  must be used

---

\* By request of NASA's Contracting Officer's Representative, this interface was de-emphasized because of the likelihood that the early AROD test flights would be on vehicles on which the computer would not be used for AROD computations.

(Section 2.2.3.2). The computer may also be called upon to update its stored value of transmitted frequency, on ground command, to improve the accuracy of the AROD measurements. Additional conversion functions which may have to be performed are the conversion from the initial parameters to a coordinate system which is moving with the vehicle and the extrapolation of the initial locations of the ground stations to their locations at the present time, in the reference coordinate system of interest.

The second task which the computer may likely be called upon to perform is the computation of propagation corrections to the measured range and range rate from each station based upon a standard atmosphere (see Appendix B). This standard correction will be stored in the vehicle computer, either as a table or as a set of equations, in both cases with the correction varying with the vehicle's altitude and elevation angle (or, alternatively, altitude and range). The computer requirements for this table or set of equations cannot be specifically defined at this time because of the lack of knowledge of the required accuracy and the range of altitudes that must be stored. However, it appears that a negligible "quantization" error would be introduced if the "brute-force" approach of storing a table of 100 to 300 six-bit entries were followed. If formulas are stored instead, the storage requirement will be markedly reduced, but the computational requirements will be increased.

As mentioned in Section 3.2.1, the computer may be called upon to select the appropriate ground stations for use in the AROD measurements.

Another function which the computer might perform is the precomputation of the anticipated Doppler from a particular ground station. This information could be put to several uses. It could possibly be used for aiding initial signal acquisition in the spacecraft by biasing the voltage controlled oscillator in the range rate phase-locked loop (for this ground station) to the anticipated frequency. It might also be used to aid the ground station in acquiring the spacecraft's transmissions by an encoded command to inform the ground station of the approximate Doppler that it will be encountering. An additional use for this information might be the computation

of the velocity- and acceleration-induced phase tracking error encountered in the 5 Mc tracking loop, and the compensation for, and removal of, this error.

Another task which the vehicle computer might usefully perform is the resolution of range ambiguities. In the system design discussed earlier, a sufficient number of ambiguity resolving tones is included to completely resolve all ambiguities for a 4000 nautical mile range. The position information that may be available in the vehicle computer could prove very useful for reducing the number of ambiguity resolving tones required.

A final task to be considered for the vehicle computer is the smoothing of the data which are gathered from the various ground stations. The advantages of performing this task in the computer depend to a great extent upon the permissible time for the smoothing and the probability distributions of the measured data.

Information concerning the capabilities of the Saturn ASC-15 computer to perform the AROD tasks was obtained in conversations with personnel working on the computer. The computer currently planned for the Saturn C-1 will probably have the following capabilities:

- a. 6000 operations per second
- b. 500 multiplies per second
- c. Perhaps 50 programmed divides per second
- d. Perhaps 50 square root operations per second
- e. 6000(23-bit) words of storage on the magnetic drum

Current estimates for the computer indicate that the guidance operations will require at most a 50% to 75% duty cycle.

Changes to these capabilities and requirements are expected in the near future. It is also anticipated that an advanced version of the ASC-15 computer will be available for the C-1B and later versions of the Saturn vehicles. Among other changes, the new computer will have 16,000 words of storage.

#### 4.1.7.2 Telemetry Interface

In the early AROD flight tests, it will be necessary to telemeter the range and range rate measurements to the ground via the Saturn telemetry system. These data will be used for post-flight evaluation of the performance of the AROD system. In addition, in the operational AROD systems, it may also be necessary to telemeter the range and range rate information at various points in the mission to verify satisfactory operation of the AROD equipment. For these reasons, a brief analysis of the telemetry interface was conducted in the AROD Feasibility Study.

In discussions with NASA personnel in the Telemetry Branch of the Marshall Space Flight Center, a satisfactory picture of the telemetry interface was obtained. From this information, it can be concluded that there appear to be no major problems involved in interfacing with the telemetry system.

Saturn data are currently organized into data "boxes" of 100-bit capacity. In these boxes ten groups (or words) of 10 bits each are temporarily stored and read into a word-formatting device at a rate of 8 milliseconds per word. The output of the word formatting device is 60 words per frame.

At 4000 miles, a one meter range quantization (Section 4.1.5) requires 23 bits; at the maximum Doppler point, a range rate quantization of .026 meters per second (Section 4.1.4) requires 19 bits. If the AROD data consist of four range and range rate readings and four station identifications (at six bits per identification), the total requirement for one reading would be 192 bits. In addition, a time indication would be required. To satisfy these requirements two data boxes (giving 200 times 12 or 2400 bps) would be satisfactory. A buffer capable of holding about 200 bits of AROD data would be sufficient to interface with the data boxes. This buffer would be supplied by the AROD equipment design group.

Readout from the buffers is at present non-synchronous. However, sync information could be provided to the AROD buffer to prevent readout while the AROD information is changing. At present, this situation is "avoided" by a bit which indicates "bad" data to the telemetry interpretation equipment on the ground, if the data in the buffer is being changed during readout.

#### 4 1.7.3 Command Link Interface

At any one time, the four selected ground stations have to transmit at different translation frequencies to allow for signal separation and identification at the spaceborne receiver. Station selection and control will require a command link from the space vehicle to the ground stations. Via this link, the space vehicle will be able to select the optimum four ground stations for the range and range rate measurements. Possible bit requirements are indicated below.

Function	Bits per Selection
Select station	6
Select frequency	2
On-off	1
Doppler information	10
Error-detection-correction	5
Total per 1 selection	24 bits

For early flight tests of short duration, these commands could be pre-programmed in the vehicle on the basis of the anticipated flight plan by means of a clock which is initiated at launch and which feeds a simple pre-programmed logic unit. In future flights of long duration, a completely pre-programmed command procedure may be unsatisfactory unless provision is made for updating the program periodically. For these flights, it is likely that the computer will be operating on the vehicle so that updating may be a minor problem. If the computer is on board for prolonged flights, it is quite possible that the best solution to the command problem would be a stored table as part of the computer memory. This table could be arranged according to discrete volumes of vehicle position, each having a unique combination of four ground stations associated with it. This method is, of course, predicated on the assumption that the vehicle position will be known to the guidance system at all times. In any event, the accuracy to which the vehicle position need be known for the purpose of selecting the ground stations to be activated at any time is

rather nominal. This can be verified by examining the overall system performance curves, Figures 4 and 5, where it is seen that overall system accuracy varies gradually as distance to a station changes during a single pass. For this reason, it is unlikely that the station selection provision in the vehicle will introduce an important penalty factor.

One further application of the command link may be to aid the ground-based receiver. If the spacecraft knows its approximate velocity to a particular ground station, it can make an estimate of the Doppler shift on the signal. At 2 Gc a maximum Doppler shift of  $\pm 50$  kc will be encountered; reducing this uncertainty from 100 cps would require an additional 10 bits in the command word.

The choice of a digital command code makes it very convenient to change codes for security reasons, since additional bits could, for instance, be used to specify for the ground station, the coding to be used in the subsequent transmissions. It is also possible to use some bits for simple error detection or error correction procedures at the ground.

## 4.2 Ground Station Equipment

### 4.2.1 Antenna

In order to meet the AROD system performance objectives with the vehicle output power limited to 12.5 watts, it is necessary that the ground antenna have appreciable gain. Because of the ground station coverage requirements, however, it is necessary that the ground antenna have virtually hemispherical coverage. The severe reliability demands of unattended operation indicate that the most advantageous approach would employ a multi-beam antenna with stationary beams. Utilization of an independent receiver for each antenna beam and a single transmitter which is switched to the active antenna beam by the receivers is recommended, based on the considerations discussed in Section 3.4.

From the analysis in Section 3.3, it is known that omni-azimuth coverage is required and that at least 13 db antenna gain is needed at an elevation angle of  $5^\circ$ , and 7 db at the zenith. In addition, it is essential from multipath considerations to achieve maximum sidelobe suppression at low elevation angles, in particular below  $5^\circ$ .

In arriving at a suitable ground antenna, several systems were considered, including Luneberg lenses and planar arrays with multiple beam forming networks. The approach selected for the representative system consists of 13 independent antennas (arrays) giving the fixed beam lobes shown in Figure 33. The lowest antenna beam is centered around a  $5^\circ$  elevation angle and gives omni-directional coverage in the azimuth plane. Actually, this antenna beam is formed from two independent antennas each covering two diametrically opposite quadrants in azimuth. Five similar annular antenna beams and one solid-angle beam cover the higher elevation angles up to the zenith. The gain decreases from 15 db at  $5^\circ$  elevation angle to 10 db at the zenith, and similarly the elevation beamwidth increases from  $5^\circ$  at  $5^\circ$  elevation to  $70^\circ$  around the zenith. The beams overlap at their 1.5 db points and hence, give essentially continuous coverage over the portion of the hemisphere above  $5^\circ$ . The beamwidth of the various beams is given by  $2/G = \cos \theta_1 - \cos \theta_2$ , where  $\theta_1$  and  $\theta_2$  are angles measured from array normal and define the beam limits ( $\theta_2 > \theta_1$ ), and G is the desired gain. This relationship follows from:

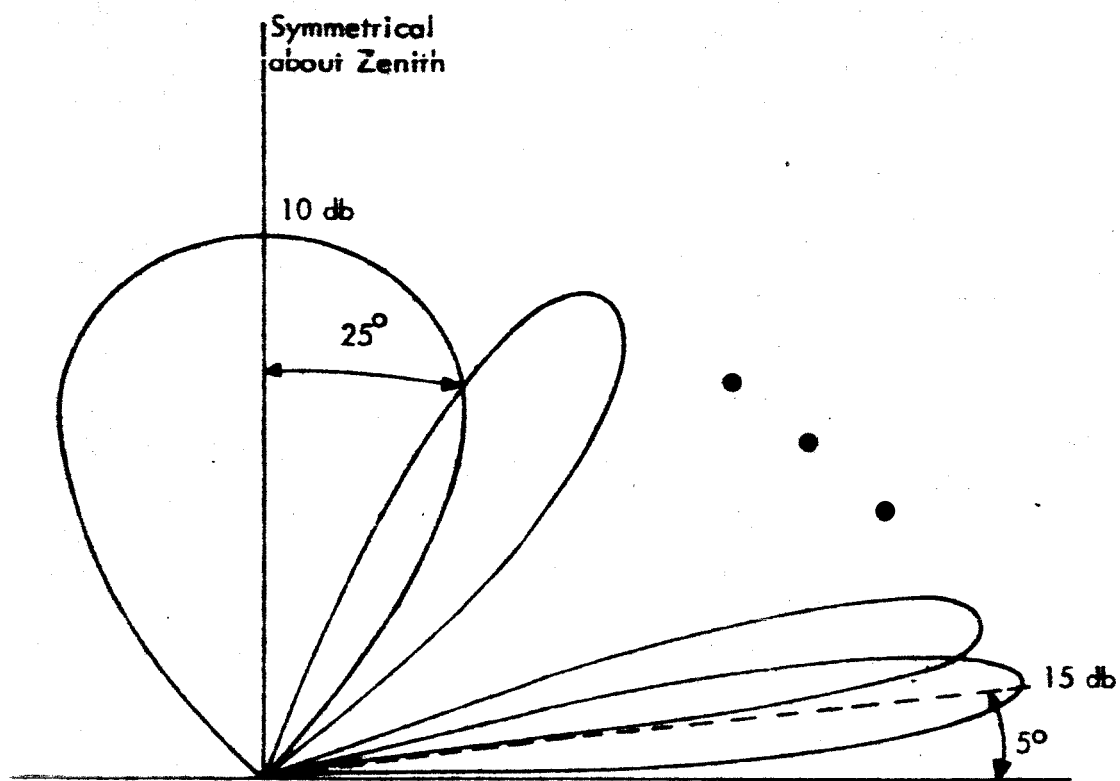


*Figure 33. Ground Antenna Beam Pattern*

$$G = \frac{4\pi}{\Omega} \quad (84)$$

and:

$$\Omega = 2\pi \int_{\theta_1}^{\theta_2} \sin \theta \, d\theta \quad (85)$$

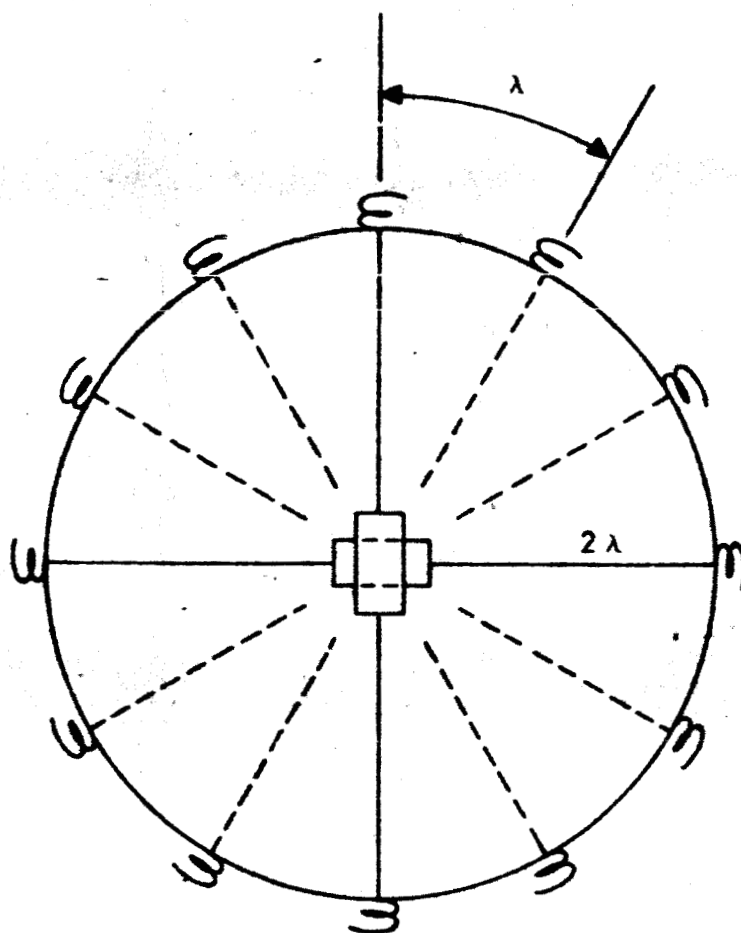
where  $\Omega$  is the beam solid angle.

Each of the annular antenna beams is formed from a set of four vertical linear arrays spaced  $\pi/2$  apart around a vertical cylindrical surface. Diametrically opposite pairs of the four arrays are connected to a common feed point from which they are fed in phase to give two-quadrant azimuth coverage. In the vertical plane, the array elements are phased to give the desired elevation angle, or angle off-broadside of the array.

A fortunate natural property of a linear array is that it produces a fan beam following a conical surface when phased to produce an off-broadside beam. The conical surface lies at a constant angle from the array normal, the angle being equal to the desired elevation angle in this case.

The vertical arrays covering the lower elevation angles would require about 20 uniformly illuminated elements at  $1/2$  wavelength spacing to produce the  $5^\circ$  beamwidth. Such an array would produce its first sidelobe maximum in the direction  $2.5^\circ$  below the local horizon, and this lobe would have gain of 18 db below the main lobe. If the number of array elements is increased, to say 40, then by appropriate phase and amplitude distribution, the sidelobe level can be reduced to -20 to -30 db below the main lobe, and the required beamwidth of the main lobe can be maintained.

At 2000 Mc, a 40 element array would be about 3 meters long. Even though the lower gain, higher angle beams require less elements, the total height of all the arrays stacked end to end would be rather large. Consequently, the circumference of the cylindrical surface on which the vertical arrays are mounted is made sufficiently large to interleave three sets of vertical arrays within the same height. This arrangement is shown in cross section in Figure 34. A total of 12 vertical arrays connected together in pairs are spaced around the cylindrical surface.



3 sets of antennas in same cylinder height. Each set consists of 4 linear arrays spaced at  $\pi/2$  around the cylinder. Diametrically opposite arrays are connected together and to a common receiver.

*Figure 34. Cross Section of the Recommended Antenna*

In order to minimize the coupling between arrays, a minimum spacing of a wavelength,  $\lambda$ , between arrays is maintained. This requires a cylinder radius of approximately  $2\lambda$ . If the cylinder radius could have been maintained at about  $\lambda/2$ , then four vertical arrays could have been connected together to give complete omni-azimuth coverage. Under the circumstance of a larger radius, destructive interferences would occur at various directions between the elements to give pattern nulls. However, with only two diametrically opposite elements connected, the radiated beam intensity from one vertical array is essentially zero in the region where the other is appreciable.

Since full coverage requires a total of 7 stacked beams, a second tier of 3 sets of vertical arrays will be located around the same cylinder directly above the lower set, and in addition, a single antenna will be located at the top of the cylinder aimed directly toward the zenith.

In the zenith region, annular coverage degenerates into solid angle coverage, and the antenna located at the top of the structure will cover the zenithal  $\pm 35^\circ$  giving a gain of 10 db. A schematic representation of the total ground antenna layout is shown in Figure 35.

For obvious reasons, it is necessary that the ground antenna transmit and receive circular polarization. In the vertical arrays, flat spiral elements are proposed rather than quadrature-fed crossed dipoles because of the limited vertical coverage of the dipole element. The pattern of a vertical dipole would have its 3 db point at an elevation angle of about  $35^\circ$ ; whereas coverage is needed up to an elevation angle of about  $60^\circ$ , at which point, the vertically pointed antenna takes over. The usual Archimedean spiral element has a half beamwidth of about  $65^\circ$ .

For the zenith-pointing antenna, a slightly flared circular horn or an axial mode helical antenna is contemplated.

Compared to various other antenna schemes for realizing a satisfactory ground station, the foregoing system offers several advantages: First, compared to a Luneberg lens, it eliminates the dielectric losses in the lens itself, and in addition, it eliminates the problem of transmitting elements radiating directly across the lens into receiving elements.

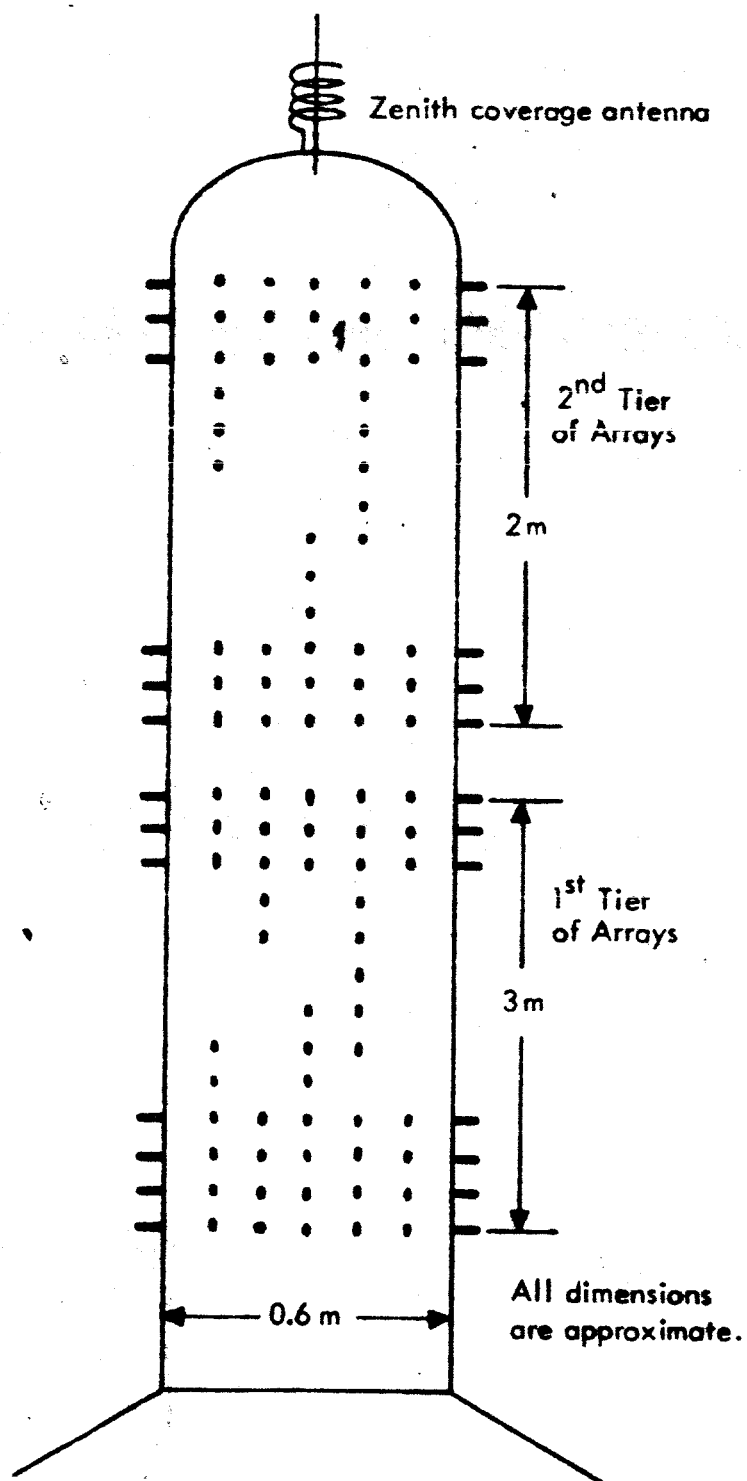


*Figure 35. Antenna Layout*

Second, compared to a planar array with a multiple beam forming network, the annular beam approach gives much more efficient low elevation angle coverage with much better side lobe control. It is conceivable that one set of vertical arrays with a multiple beam forming network could be used with the annular approach to produce 12 of the required 13 beams. However, since the tight coupling that would be required for efficiency is difficult to realize simultaneously with good sidelobe control, independent arrays afford the more promising solution.

Third, compared to multiple horn or helix antennas covering conical spatial sections, the annular beam approach offers much narrower vertical beams at low elevation angles with the resulting reduction in multipath errors.

One minor disadvantage of the annular antenna for this application is that its radiation phase center moves; this will introduce an error into the range measurements. The nature of this error is illustrated in Figures 36 and 37. In the cross sectional view (azimuthal plane) of the cylindrical antenna, ray #1 coming in normal to one of the vertical arrays travels a distance  $R$  from the antenna element to point  $o$  at the center of the cylinder, which will be taken as the antenna feed. On the other hand, ray #2 which enters the vertical array at an angle to the normal travels a longer path in getting to point  $o$ . The maximum error occurs at a  $45^\circ$  angle of incidence. From the geometry shown in Figure 36, the error in this case is  $.29R$ . For the representative AROD system, where  $\lambda = 15$  cm and  $R = 2\lambda$ , this error is 9 cm.

In the vertical plane, the radiation center errors are about the same as for the azimuthal plane. However, in this plane, due to the vertical separation of some of the arrays from the others, a fixed path difference also exists. This fixed difference, which is compensatable, is the distance  $E$  shown in Figure 37. The minimum value of  $\theta$  is about  $35^\circ$  and the maximum antenna separation is 3 meters for the proposed antenna, making  $E$  have a maximum value of 2.5 meters. On the other hand, the maximum value of  $\phi$  is about  $7^\circ$ , and thus, the maximum uncompensatable difference,  $F$ , is about 12 cm.

In both the vertical and azimuthal cases, the uncompensated error amounts to a longer path for both plus and minus directions around the central direction. Hence, it could be compensated to  $\pm 4.5$  cm for the azimuth plane and  $\pm 6$  cm for the vertical plane. Due to much larger sources of measurement errors in the representative system design, an error of this magnitude is not significant.

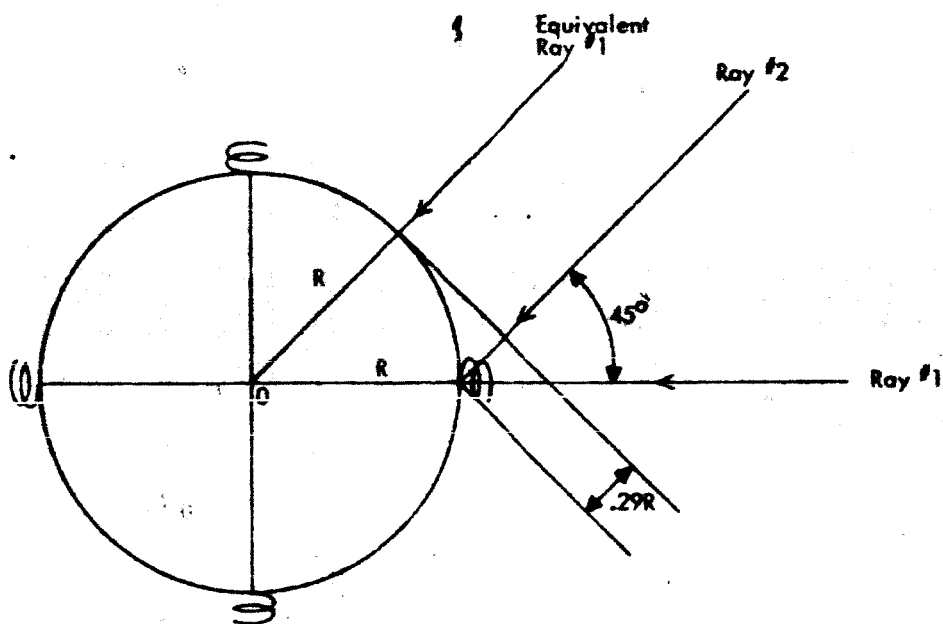


Figure 36. Radiation Center Errors in Azimuth Plane

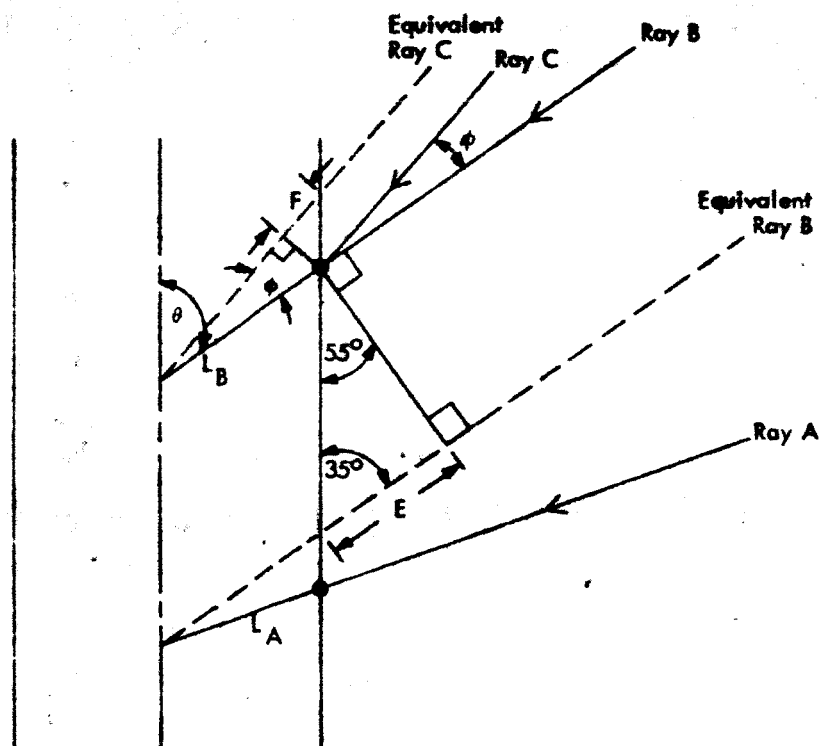


Figure 37. Radiation Center Errors in Vertical Plane

For the ground antenna beam network described, a total of 13 receivers, one for each independent beam is desirable. All the receivers are operating simultaneously to give the system full time reception over the entire operating envelope. In addition, each independent antenna beam feed must be capable of duplex operation when the transmitter is switched into it. For getting the energy to and from the antennas, rigid coaxial transmission lines to the principal antenna terminals and stripline corporate feeds to the array elements, all inside the cylinder, are contemplated.

#### 4.2.2 Ground Transmitter

In view of the fact that the AROD ground stations will most likely be controlled by command from the space vehicle, the requirements for this type of operation must be considered when selecting the component to be used for the ground station transmitter output stage. Referring to the AROD Frequency Allocation Table, Table 12, a ground station will be commanded by the space vehicle to employ one of four possible translation frequencies when transmission from that station to the spacecraft is desired. Under these conditions, the microwave frequency spectrum transmitted from the spacecraft is translated in frequency at the ground station and the resulting spectrum is amplified and transmitted to the spacecraft. For the channel assignments that have been chosen, the lowest frequency that need be considered for transmission by the ground station would be 1934.375 Mc minus a maximum one-way Doppler of approximately 50 kc. The highest frequency to be considered would be 1945.625 Mc plus 50 kc. The resulting frequency spread is approximately 11.5 Mc.

In selecting the component for the ground station transmitter output stage, a bandwidth several times larger than 11.5 Mc frequency spread must be considered in order to prevent the differential phase shift between the frequencies of the transmitted AROD spectrum from exceeding approximately  $\pm 3$  degrees.\* A half-power bandwidth of 50 Mc is considered satisfactory for the output stage and any intermediate driver stages, if required.

\* Three degrees has been allocated to this error source from the  $6^\circ$  objective established for the ground station in Section 2.5.

Table 12. AROD Frequency Allocation Table

Ground Station Number and Channel	Microwave Frequency From Ground Station (Mc)	I-F at Vehicle Receiver (Mc)	L.O. Signal From Vehicle Frequency Synthesizer (Mc)	Translation Frequency at Ground Station (Mc)	Vehicle Transmitted Frequency (Mc)
1(a)	1934.375	65.625	60.625	65.625	2000.000
2(a)	1936.250	63.750	58.750	63.750	2000.000
1(b)	1938.125	61.875	56.875	65.625	2003.750
3(a)	1938.750	61.250	56.250	61.250	2000.000
1(c)	1939.375	60.625	55.625	65.625	2005.000
2(b)	1940.000	60.000	55.000	63.750	2003.750
4(a)	1940.625	59.375	54.375	59.375	2000.000
2(c)	1941.250	58.750	53.750	63.750	2005.000
3(b)	1942.500	57.500	52.500	61.250	2003.750
3(c)	1943.750	56.250	51.250	61.250	2005.000
4(b)	1944.375	55.625	50.625	59.375	2003.750
4(c)	1945.625	54.375	49.375	59.375	2005.000

\* All frequencies shown are for zero Doppler condition

Disregarding, for the moment, the noise power density at the output of the amplifier which will be a function of the signal-to-noise ratio at the output of the ground receiver, the total r-f output power requirement of the amplifier will be 18.75 watts. This energy will be distributed as follows:

Frequency a	(unmodulated cw)	7.5 watts
Frequency b	(phase modulated)	3.75 watts
Frequency c	(unmodulated cw)	<u>7.5 watts</u>
		18.75 watts

Assuming that the individual signals which make up the AROD spectrum have been properly processed by preceding stages of the ground station transmitter-receiver so that only the noise power within passband of the narrow band filters (less than 1 kc) need be considered, a maximum r-f power capability of 25 watts is deemed adequate for the transmitter output stage.

The following microwave components have characteristics that may permit their use as the microwave power amplifier for the AROD ground station:

- Traveling Wave Tube Amplifier
- Klystron Amplifier
- Planar Triode Amplifier (Recommended Approach)

Regardless of which component is selected, the power supply regulation requirements will be similar, although the planar triode could offer some advantages in that the voltage level may be less than that required for the traveling wave tube or the klystron amplifier. In any case, bulky and perhaps inefficient equipment can be tolerated to satisfy the regulation and reliability requirements since size, weight and efficiency are not of major importance for the ground station.

Once the stability requirement has been satisfied, differential phase shift throughout the passband of the amplifier must be considered. The objective for this parameter is the phase deviation for two frequencies separated by as much as 5 Mc shall not vary by more than  $\pm 3$  degrees throughout a 12 Mc bandwidth. If this condition is satisfied, any bias differential phase shift throughout the amplifier bandwidth between the input signals and the output signals can be canceled by compensating networks.

The specification for maximum permissible differential phase shift may eliminate the use of the traveling wave tube. It has been found that the phase variations in this tube are quite periodic and analysis shows that this behavior is due to internal reflections which cause standing waves on the helix in the tube. The standing waves cause phase variation as a function of frequency. If these reflections can be eliminated, most of the differential phase variation will disappear, but considering that the tube is in the order of 20,000° long, holding the deviation below  $\pm 3$  degrees is likely to be quite difficult. Figure 38 illustrates a typical differential phase measurement made between two TWT's of the same type. Using this method, differential phase shift can be accurately measured within about 0.1 degrees.

Multi-cavity klystron amplifiers that can satisfy the output power requirement of the AROD ground station are available off-the-shelf, but manufacturers who were contacted were unable to supply data relating to differential phase stability. However, it has been indicated that with extremely well regulated power supplies, the phase stability measurements that have been taken for a single frequency indicate that it may be possible to satisfy the AROD objective for maximum permissible differential phase shift. The advantage of using the klystron when compared with a planar triode would be the high gain that could be obtained in a single stage. With proper tuning of the individual cavities, the gain could be made approximately equal to that of the TWT. It would be necessary to compromise tuning for maximum gain against minimum differential phase shift within the 12 Mc AROD bandwidth in order to produce optimum operating conditions.

Considering the fact that the ground station transmitter bandwidth must be of the order of 50 Mc, the power gain of a single planar triode amplifier stage would be less than 10 db. Therefore, several such stages would be required to bring the final amplifier output level to a value suitable for AROD use. Even so, a multi-stage planar triode r-f amplifier appears to be a good choice for the ground station transmitter design, since phase jitter due to power supply noise and tube noise for a single amplifier stage has been shown to be below .003° rms for a  $\Delta f$  of 0.1 Mc.<sup>26</sup>

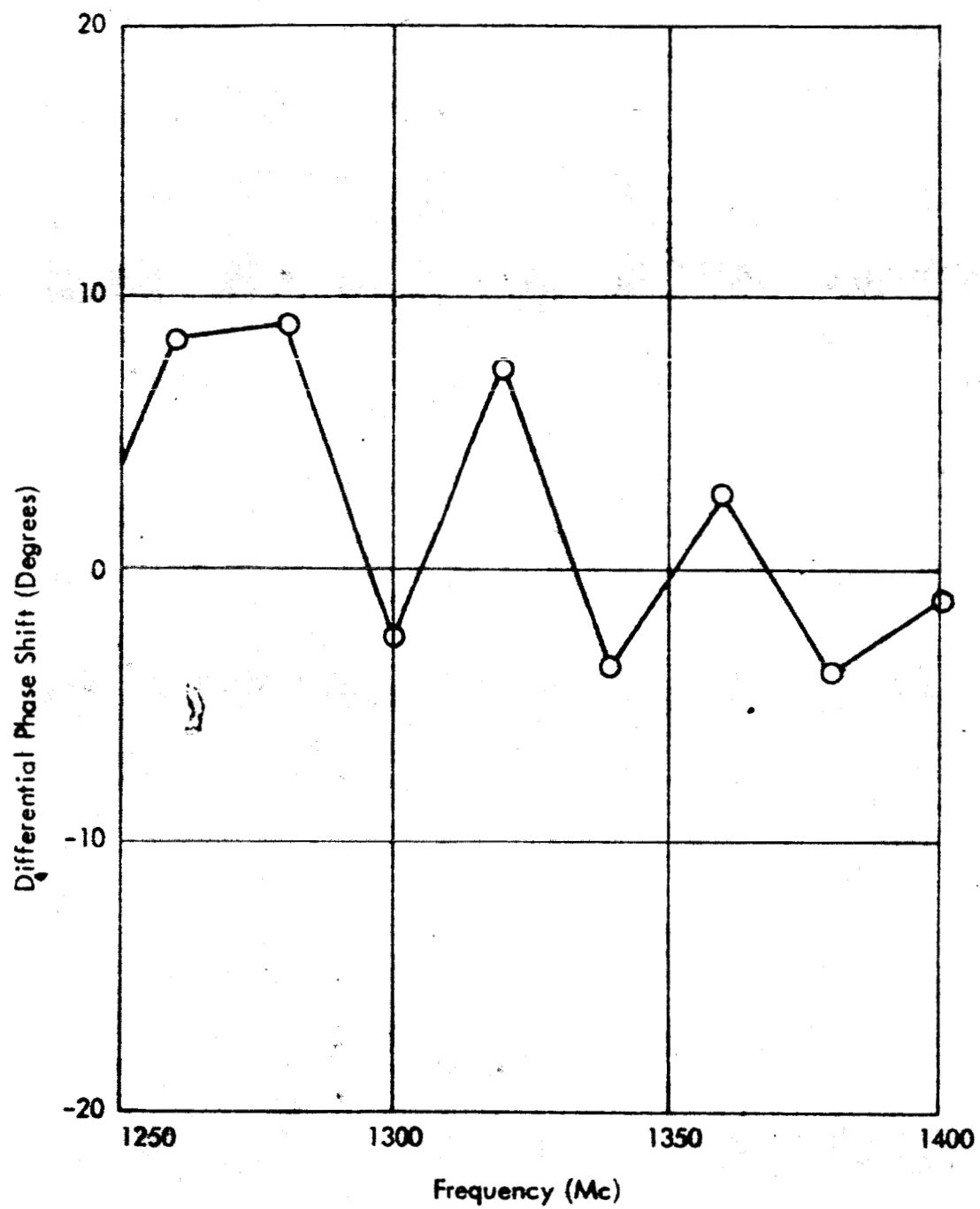


*Figure 38. Differential Phase Shift Between Two Traveling Wave Tubes*

#### 4.2.3 Ground Station Signal Processing

Nonlinear characteristics in any active circuit in the ground transponder will degrade the incoming signal. It can be assumed that the input stages of the ground transponder, where the incoming signals are very small, will have more linear characteristics over their operating range than the later stages. Therefore, in the representative system design, the bandwidth will be widest at the input circuitry and will be reduced in every following stage.

In addition to the contribution of white noise, feedthrough of the relatively high level output of the transponder transmitter into the receiver introduces noise components of high spectral density and extremely small bandwidth.

Basically, the design of the ground station requires high selectivity of the individual circuits to reduce any noise contribution. At the same time, great care must be taken to minimize differential phase distortions between the individual components of the received spectrum while they are being amplified and translated in frequency. In the representative system design the high selectivity is obtained in passive devices, while the active circuits are made wideband. In all circuits, the bandwidth is made sufficiently wide so that the received frequency bands are passed in a region of constant time delay; in addition, the region of constant time delay is made wide enough to encompass the maximal Doppler frequency shifts.

##### 4.2.3.1 R-F Receiver Components

The r-f input circuitry for each beam of the antenna must suppress the interference from the transponder's transmitter. The transmitter frequency band is lower in frequency than the received frequency band; the minimum separation is 54 Mc. The difference in power between the received and retransmitted signals, for operation close to the horizon, can be as large as 171 db. Therefore, a number of stages are required to suppress the interfering frequency band sufficiently.

The circulator of the antenna, having a bandwidth of no more than 100 Mc and being tuned to the received frequency band, will provide a 30 db

reduction in the transmitter feed through. This isolation, which can be obtained in the non-reciprocal device, can be maintained only when the voltage reflection coefficient of the antenna input is less than 0.03.

Further reduction of the transmitter interference will be accomplished in a bandpass filter circuit. Great care must be taken in the design of the frequency selective circuit that phase distortions of the received frequency band are minimized. In the sidetone ranging system a range error will be introduced by uncompensated differential phase shifts between spectral components of the signal. A nominal phase difference between the reference signals can be compensated for in the spacecraft equipment. However, this phase difference must remain constant under operational conditions; this means that it should not vary when the received frequency band is translated by the Doppler frequency shift or when the geometry, and with it the center frequencies of the filtering circuit, changes under severe environmental conditions. The requirement for constant time delay,  $\frac{d\theta}{d\omega}$ , over the range of possible displacements of received frequency band can be met only when the signal bandwidth including its displacement in frequency is small in comparison to the filter bandwidth.

In the representative AROD system, three reference signals and sidebands are received; the bandwidth of this spectrum is 5 Mc and the interfering frequency band from the transmitter (which has to be rejected in the filter circuit) is only 54 Mc below the lowest spectrum line of the received signal. In order to obtain a rejection of at least 80 db of the interfering signals in one filter and to make the filter passband much wider than the received signal bandwidth, a large number of resonant circuits would be required for this filter. The losses within the passband of the filter would become high.

If the system specifications for phase error, rejection of the interfering transmitter, and low losses in the r-f input circuitry cannot be met for the given design parameters, then alternatives are available. Either the translation frequency, which separates the transmitter frequency band from the received frequency band, can be increased substantially or three separate bandpass filters to pass the three carrier signals and their modulation sidebands can be used. For this latter design, it may be necessary to change the modulated carrier frequency

from 2003.75 Mc to 2011.25 Mc. This issue, along with other design factors related to the choice of transmitted spectrum, should be investigated during the subsequent phase of the AROD program.

An example of a three branch multiplex filter, capable of accommodating a signal spectrum utilizing a 2011.25 Mc carrier, is shown schematically in Figure 39. The three carrier signals, including the modulation sidebands for the 2011.25 Mc carrier, are passed through individual filters and subsequently recombined. The three filters are of identical design; in the filters the center frequencies are identical to the frequencies of the signals which are transmitted from the spacecraft. Thus, the reference signals are placed at the center of the filter passband where the time delay can be assumed to be constant. Deviation of the signal frequencies from the transmitter output frequencies because of Doppler shifts or a change of filter geometry will still maintain signals in a region close to the center frequency of the filter passbands where the time delay is constant. The phase characteristics of these filters, which are of identical design, will track each other to a large degree.

For branching and recombination of the three reference signals, advantage is taken of the fact that the image impedance of a filter is resistive for its passband frequencies and reactive outside the passband. For high Q filters whose passbands are smaller than their separation, the filters can be spaced relative to each in the three-branch junction in such a manner that each signal passes through its filter while the two other branches represent very large susceptances at the junction.

In addition to the circulator and suitable bandpass filter system, band-rejection filters formed by YIG spheres are used to suppress the interfering transmitter another 30 db with very small effects on the phase characteristics of the received frequency band. Thus, the overall reduction of the interfering transmitter in the r-f input circuitry of the beam forming antenna which can be achieved is approximately 140 db.

Following the isolation circuits, the received signals are applied to a parametric amplifier. With commercially available parametric amplifiers operating at S-band, the following characteristics can be obtained: amplifier gain, 17 db; bandwidth, 40 Mc; noise figure, less than 3.5 db.

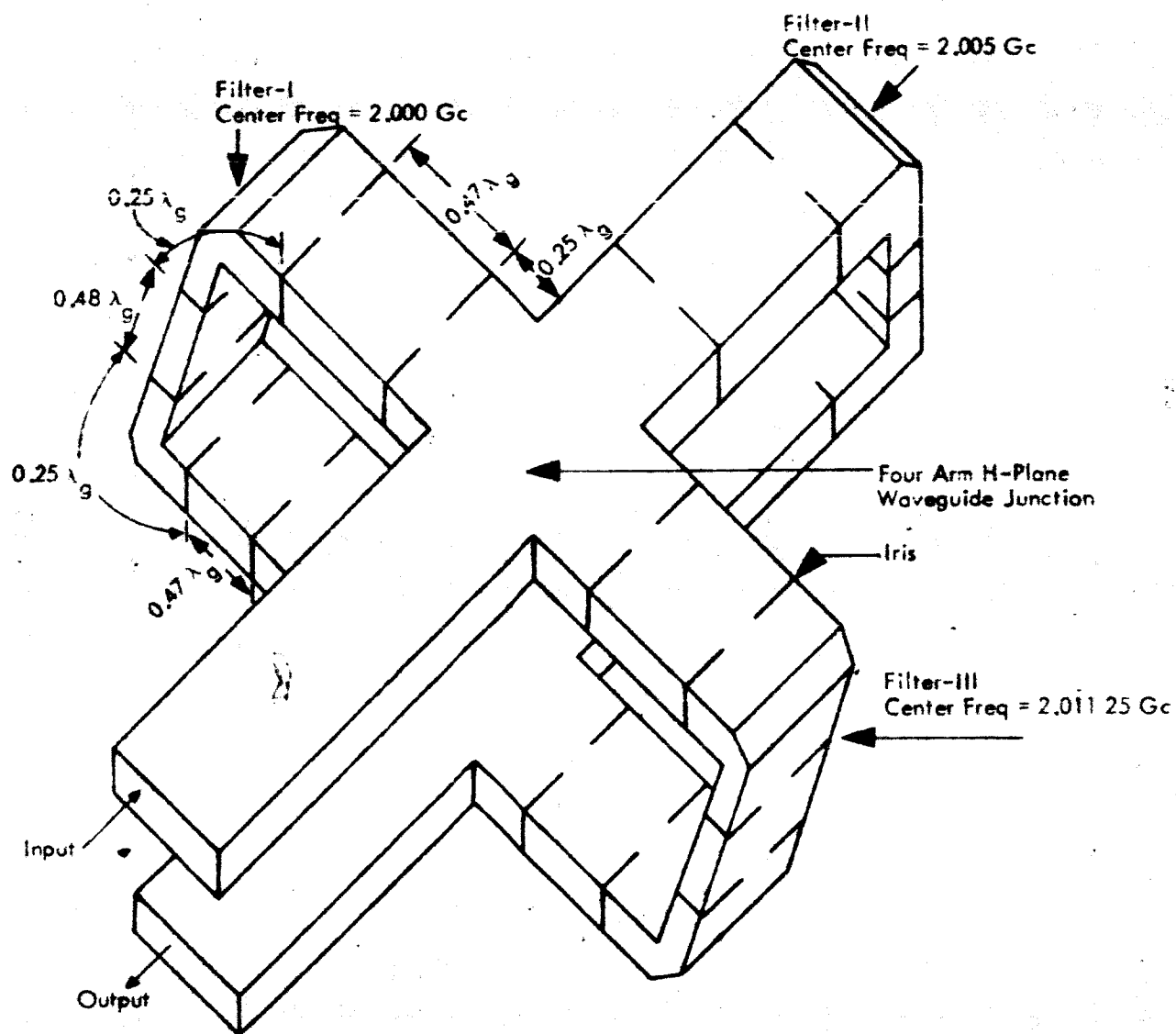


Figure 39. Three Filter RF Multiplexer

The interfering transmitter, which will be no more than 30 db above the minimum signal received in the parametric amplifier, will be outside the passband of the amplifier. The presence of the larger interfering signal, which is outside the passband, will cause only a small change in the gain of the amplifier. Intermodulation products between the received signal and the interfering transmitter will fall outside the i-f passband.

#### 4.2.3.2 Down and Up Conversion

In the ground transponder, care must be taken that none of the frequency components of the retransmitted spectrum or of the modulation spectrum of the up-converter are identical in frequency with the spectrum lines of the received signal. This is important since a feed-through signal of the same frequency as one of the received signals will be superimposed on it and the phase of the resultant vector will be different from the phase of the received signal.

In the representative design for the ground transponder, an S-band stable oscillator generates a reference voltage; its frequency is  $f_r$ . The local oscillator frequency of the down-converter is the difference between the frequency of the reference voltage and the frequency of a VHF oscillator  $f_v$ .

$$f_{L.O.} = f_r - f_v \quad (86)$$

The VHF oscillator is voltage tunable over a frequency range greater than the double-sided Doppler band. The frequency of the local oscillator will be adjusted by an automatic frequency control loop to remain 18 Mc below the frequency of the lowest spectrum line in the received frequency band. The resultant i-f frequency band of the down-converter is given by:

$$f_{if} = f_R + \Delta f_R - (f_r - f_v) \quad (87)$$

The i-f frequency band is amplified and applied to an up-converter. The modulation frequency of the up-converter is derived from the local oscillator voltage of the down-converter; its frequency is the difference

between the local oscillator frequency and the frequency  $f_t$  of an ultra-stable oscillator whose frequency identifies the ground station. The up-converted frequency band is the upper modulation sideband generated in a single band modulator; its frequency is given by:

$$\begin{aligned} f_{TR} &= f_r - f_v - f_t + f_R \pm \Delta f_R - (f_r - f_v) \\ &= f_R \pm \Delta f_R - f_t \end{aligned} \quad (88)$$

The retransmitted frequency band is translated by the highly stable frequency  $f_t$ ; the local oscillator frequency is not contained in the retransmitted spectrum. The phase relation between the spectrum lines is preserved.

It can be assumed that in a conventional single sideband modulator spectrum, the first-order lower modulation sideband is 20 db below the upper sideband. However, in the proposed system it is especially important that the higher-order upper sidebands be greatly suppressed. The reason is that the second, third, and fourth order upper sidebands are in the frequency interval between transmitted frequency band and received frequency band and partly overlap with the received frequency band. The local oscillator frequency can be chosen such that none of the spectrum lines generated in the SSM (Single Sideband Modulator) are identical with the spectrum lines in the received frequency band. The suppression of the lower modulation sidebands of the SSM is of less importance, since their frequencies are below the transmitted frequency band.

#### Down-Converter

The down-converter in the ground transponder will be a conventional balanced crystal mixer with a bandwidth of approximately 40 Mc and a conversion loss of 6 db. The balanced design has the function of suppressing the noise accompanying the local oscillator. To accomplish this, the admittances of the diodes at their operating point have to be very well matched. To keep the noise in the down-converter to a minimum, an additional requirement is that the noise sidebands on the local

oscillator, over a bandwidth of twice the i-f frequency, be at least 80 db below the main signal. This requirement can be met by most microwave oscillators, since their noise sidebands generally result from power supply variation or statistical variations which are much lower in frequency than the i-f frequency.

The image frequency in the down-converter which is given by

$$f_{im} = 2(f_r - f_v) - (f_R \pm \Delta f_R) \quad (89)$$

is below the received frequency band and outside the passband of the parametric amplifier. The impedance of the parametric amplifier outside its passband becomes reactive, consequently, the image frequency termination becomes reactive. The transfer admittance of the down-converter (given by the ratio of the current of the incoming signal to the voltage of the i-f signal) is dependent on the image frequency admittance. The phase characteristic of the transfer admittance in the down-converter is related in a rather complex function to the image admittance. There are regions of very small delay distortions and of comparatively large ones, depending on the image admittance. It will be important to adjust the image admittance by choosing the distance between the parametric amplifier and down-converter such that the down-converter will operate in a region of small delay distortions.

#### I-F Amplifier

The down converted frequency band is divided and each of the reference signals and their modulation sidebands are passed through individual i-f preamplifiers. The bandwidth of the preamplifiers is 1 Mc. At the input to the i-f preamplifier, the power level of each of the major spectral components at maximum slant range is approximately  $10^{-15}$  watts, the noise power in the amplifiers is approximately  $10^{-13}$  watts. In the preamplifiers, the amplitude of the signals and of the noise spectral density is sufficiently small to assume that the preamplifier characteristics are linear.

The gain of the i-f preamplifiers will be made 40 db to bring the power in the three reference signals to  $10^{-11}$  watts. The three preamplifiers will be of identical design and great care will be taken to match the time delay in the three amplifiers.

To compensate for the Doppler frequency shift  $\pm f_d$  of the received frequency, the frequency  $f_v$  of the tunable VHF oscillator has to be corrected in order to bring the i-f frequencies to the center of their respective crystal filters in the narrow band post i-f circuitry. The bandwidth of the post i-f crystal filters will be less than 1 kc so that the minimum signal-to-noise ratio of the recombined signal will always be greater than 8 db.

The filters and the amplifiers which operate in parallel must be of identical design and very carefully calibrated so that the time delay for all the spectrum lines which are amplified will be the same.

The gain of the main i-f amplifier is made 90 db to bring the signal level to approximately 10 mw.

#### Up-Converter

The up-converter in the ground transponder will be a single sideband modulator. The SSM which is proposed has comparatively wide bandwidth and, in addition, sufficient isolation is provided to minimize the effect of possible internal reflections which could introduce phase errors. The SSM is shown schematically in Figure 40. In the SSM, the carrier at a frequency of  $f_r - f_v - f_t$  is divided in a 3 db hybrid junction and directed to the two balanced modulators. In the scattering matrix of the hybrid, the voltage transmission coefficients,  $S_{23}$  and  $S_{32}$  are zero. This indicates that waves which might be reflected at one of the balanced modulators will not be coupled in the other balanced modulator. The balanced modulators are hybrid junctions with nonlinear-resistance mixer diodes placed in the symmetrical arms. Modulation is obtained by taking advantage of the nonlinear d-c characteristic of the diodes. The diodes function as AM modulators and the balanced modulator characteristic is obtained by suppression of the carrier in the AM spectrum by correct phasing of two modulated signals.

The output signals of the balanced modulators are combined in the output hybrid junction, and the upper sideband is used.

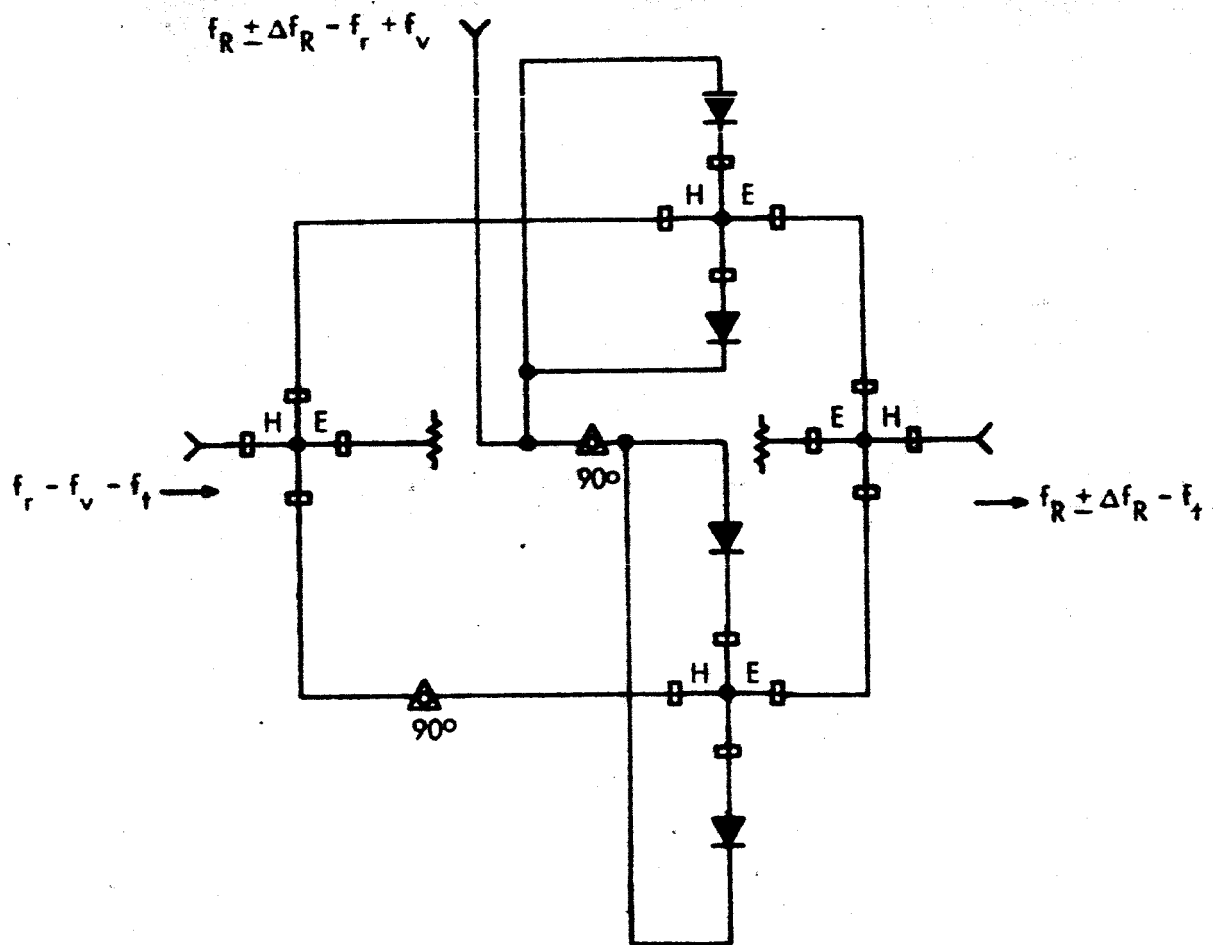


Figure 40. Single Sideband Up-Converter

For an input power of 10 milliwatts to the SSM, the power output at the carrier of the frequency  $f_r - f_v - f_t$  will now be about 1 milliwatt. This is sufficient to drive the transmitter chain to the nominal output level of 25 watts.

#### 4.2.4 Multipath Effects

Signal propagation to and from the ground based antennas suffers from interference effects due to intermediate reflection of part of the AROD signal from the earth's surface. This interference is a possible source of measurement error and must be considered in the system design.

The effects of intermediate reflections, or multipath signals, can be greatly reduced by judiciously locating the ground antenna and by tailoring its design to produce sharp lobe extinction beyond the needed coverage. However, there are natural limits in both the surrounding environment and in the antenna design beyond which it is virtually impossible to go. For example, the reflection coefficient of ground or water near grazing incidence takes on rather "universal" properties independent of the surface properties. This follows since, except for very dry ground,  $|\epsilon_c| \gg 1$ , where  $\epsilon_c$  is the complex dielectric constant of the ground or water. With this approximation:

$$\Gamma_v = \rho_v e^{-i\phi_v} \approx \frac{\sqrt{\epsilon_c} \sin \psi - 1}{\sqrt{\epsilon_c} \sin \psi + 1} \quad (90)$$

and

$$\Gamma_h = \rho_h e^{-i\phi_h} \approx \frac{\sin \psi - \sqrt{\epsilon_c}}{\sin \psi + \sqrt{\epsilon_c}}, \quad (90A)$$

where: the v and h are subscripts indicating vertical and horizontal polarization;  $\Gamma$  is the complex reflection coefficient of magnitude  $\rho$  and phase  $\phi$ ; and  $\psi$  is the grazing angle.<sup>27</sup> It can be seen from Equations 90 and 90A that for  $\psi = 0$  and  $\epsilon_c$  finite  $\Gamma_v = \Gamma_h = -1$ . If  $\epsilon_c$  approaches  $\infty$ ,  $\Gamma_h$  approaches -1 for all values of  $\psi$ . However,  $\Gamma_v$  approaches +1 for all values of  $\psi$ .

except  $\psi = 0$ . For intermediate values of  $\epsilon_c$ ,  $\Gamma_v$  is a considerably more complex function of  $\psi$  than is  $\Gamma_h$ . Specifically, when  $\epsilon_c$  is real,  $\rho_v$  approaches 0 when  $\sin \psi = 1/\sqrt{\epsilon_c}$ . (This value of  $\psi$  is the complement of Brewster's polarizing angle). When  $\psi$  is less than this critical value,  $\phi_v = \pi$ , but at the critical angle it decreases abruptly to zero, where it remains for larger values of  $\psi$ . When  $\epsilon_c$  is complex  $\rho_v$  can decrease only to a minimum value greater than zero, reaching the minimum value at an angle smaller than  $\sin^{-1}(1/\sqrt{\epsilon_c})$ . At the same time  $\phi_v$  is no longer discontinuous at this angle, but it decreases rapidly from somewhat less than  $\pi$  to a small value and decreases slowly thereafter. As  $\epsilon_c$  approaches  $\infty$ , the critical angle approaches 0 and  $\Gamma_v$  approaches +1 for all values of  $\psi$ .

Usually only small values of  $\psi$  are of interest in the microwave region since relatively narrow beamwidths are generally used and illumination entering at large depression angles is much reduced relative to that close to beam center. Also, the effects of surface roughness will significantly reduce the effectiveness of specular reflection at high depression angles. A divergence factor due to the earth's curvature will further reduce the intensity of specular reflection.

Rather than make an exhaustive analysis of various combinations of antenna designs and site locations at this time, only the ground antenna design which we consider most suitable for the AROD system will be examined. Further, only the worst environment for multipath interference, namely, surrounding sea water, will be considered. Although this environment is a worst assumption, it is a very real possibility for an AROD ground station location. Local obstacles will not be considered since the difficulty they present can usually be overcome by careful siting.

- The AROD system requires coverage down to  $5^\circ$  above the horizon, and at this angle, an antenna gain of 13 db is required to give the desired signal strength. The proposed antenna is composed of a stack of 13 independent antennas, each having semi-annular coverage, while the vertical coverages differ. The antenna covering the  $5^\circ$  elevation angle, has a vertical beamwidth of about  $5^\circ$ . Such an antenna has a sidelobe minimum along the local horizon, and since a vertical array with some illumination

control is contemplated. -20 db sidelobe peaks should be readily obtainable. The radiation center of this antenna is assumed to be located approximately 10 meters above the sea. The earth's curvature limitation on the horizontal line-of-sight distance corresponding to this height is about 7 miles. Reflection from areas of the sea beyond this distance therefore are of no consequence since they would never reach the antenna. With the  $5^\circ$  minimum elevation angle restriction and under specular reflection conditions the sea area contributing the multipath signal is located about 115 meters from the antenna. This condition is shown in Figure 41, and the path difference between the direct ray and the reflected ray is:

$$\frac{115}{\cos 5^\circ} (1 - \cos 10^\circ) = 1.74 \text{ meters}$$

In order to calculate the error introduced into the range measurement, the tone method of measuring range in the AROD system must be considered. The range measurement is made by measuring the phase of the 5 Mc tone derived by product detection of the two principal components of the transmitted spectrum. The transmitted signal is composed of two equal amplitude components of angular frequency  $\omega_0$  and  $\omega_0 + \omega_m$  (where  $\omega_m/2\pi = 5 \text{ Mc}$ ). Thus, the direct signal voltage to the ground terminal is:

$$e_d = A \cos \omega_0 t + A \cos (\omega_0 + \omega_m) t, \quad (91)$$

where  $A$  is the peak amplitude of the components. The indirect signal is correspondingly:

$$e_R = B \cos \omega_0 (t + \Delta t) + B \cos (\omega_0 + \omega_m) (t + \Delta t), \quad (92)$$

where  $B$  is the peak amplitude of the components,  $\Delta t = l/c$ ,  $l$  is the additional path length, and  $c$  the velocity of light. After retransmission, both signals enter the spacecraft receiver and the output at  $\omega_m$  is recovered. This is given by:

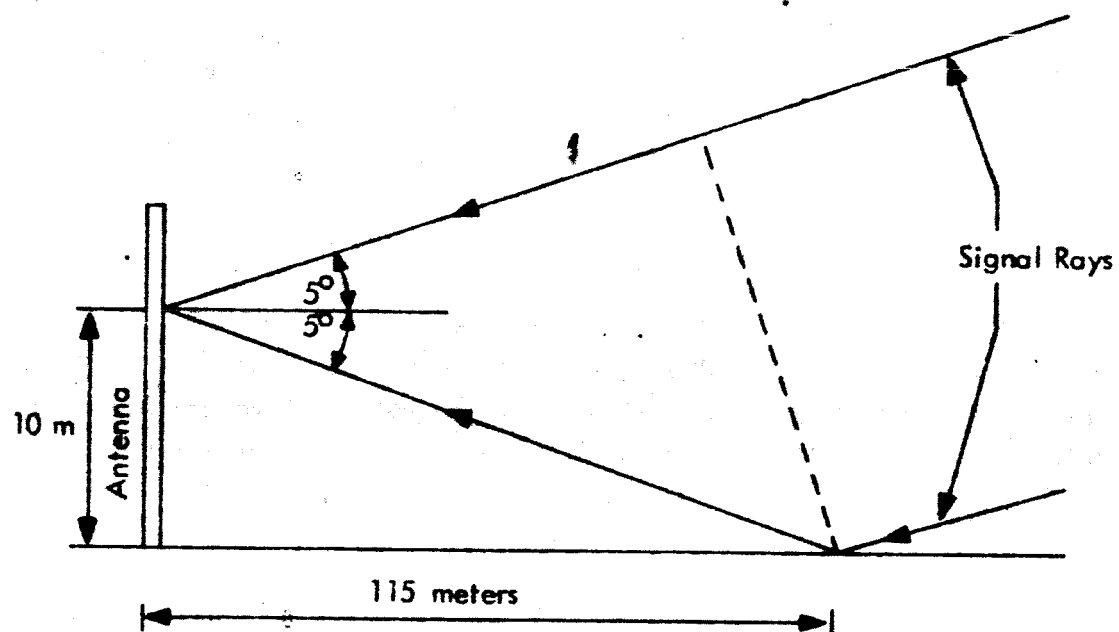


*Figure 41. Multipath Interference at Ground Antenna*

$$\begin{aligned}
e_m = & A^2 \cos \omega_m t + B^2 \cos (\omega_m t + \omega_m \Delta t) \\
& + AB \cos (\omega_m t - \omega_0 \Delta t) \\
& + AB \cos (\omega_m t + \omega_m \Delta t + \omega_0 \Delta t)
\end{aligned} \tag{93}$$

This expression contains two phase shift terms due to the time delay, namely,  $\omega_0 \Delta t$  on the carrier and  $\omega_m \Delta t$  on the beat frequency. Since the reflected signal will enter the antenna on a sidelobe,  $B < A$ , and terms in  $B^2$  will be neglected. The remaining components are shown on a vector diagram in Figure 42.

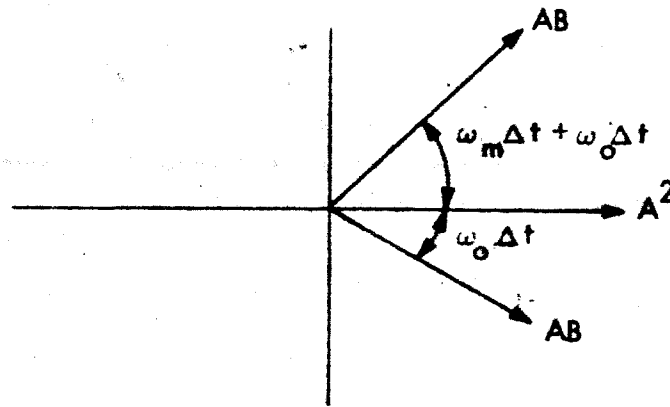


Figure 42. Vector Diagram of Multipath Signals

The phase error,  $\delta$ , introduced into the resulting signal,  $e_m$ , is given by:

$$\delta = \tan^{-1} \frac{AB [\sin (\omega_m \Delta t + \omega_0 \Delta t) - \sin \omega_0 \Delta t]}{A^2 + AB [\cos (\omega_m \Delta t + \omega_0 \Delta t) + \cos \omega_0 \Delta t]} \tag{94}$$

Since the AROD system is only of interest if we can control the multipath error to a small fraction of the period of the  $\omega_m$  signal,  $\omega_m \Delta t$  will always be a small value and Equation 94 can be approximated by:

$$\delta = \tan^{-1} \frac{AB \omega_m \Delta t \cos \omega_0 \Delta t}{A^2 + AB \left[ 2 \cos \omega_0 \Delta t - \omega_m \Delta t \sin \omega_0 \Delta t \right]} \quad (95)$$

or further if  $B \ll A$ ,

$$\delta = \frac{B \omega_m \Delta t \cos \omega_0 \Delta t}{A} \quad (96)$$

and the range error is:

$$\Delta R = \frac{B}{A} l \cos \frac{2\pi l}{\lambda_0} \quad (97)$$

where  $\lambda_0$  is the wavelength corresponding to  $\omega_0$ .

Equations 96 and 97 describe the case of interest here. They indicate that the phase error in the  $\omega_m$  signal, which in turn determines the range error, depends directly on the time delay, or path difference, and is a sinusoidal function of the microwave phase delay. The magnitude of the error is of the order of  $B/A$ .

In the case illustrated in Figure 41, where  $l = 1.74$  meters,  $B/A = \frac{1}{10}$  (20 db sidelobes), and  $2\pi l/\lambda_0 = n\pi$ , the range error from Equation 97 is 0.174 meters.

In addition to the range error given by Equation 97, a Doppler error also results from the interference of multipath signals. Since accurate Doppler measurements will be made on the carrier frequency, only a single carrier frequency,  $\omega_0$ , need be examined for this effect. By analogous relations to the modulated case above, the carrier phase error is:

$$\delta_c = \tan^{-1} \frac{B}{A} \sin \omega_0 \Delta t, \quad (98)$$

and the resultant amplitude function is:

$$R = A \left[ 1 + \frac{B}{A} \cos \omega_0 \Delta t \right], \quad (99)$$

where A and B are the direct and indirect signal amplitudes, respectively, and  $B < A$ . Small carrier amplitude modulation can be eliminated in a limiter before the Doppler measurement is made, and hence, only the phase modulation term is significant.

In order to estimate this error, consider the case illustrated in Figure 41 except this time with an elevation angle of  $10^\circ$  rather than  $5^\circ$ . For  $10^\circ$ , the point of specular reflection moves in to 56.5 meters, and the path difference between the direct and indirect ray becomes 3.60 meters. Thus, the path difference increases by 1.86 meters for an angle change of  $5^\circ$ . At 15 cm wavelength, this distance corresponds to 12 wavelengths. Since the error phase,  $\psi_c$ , varies from maximum positive to maximum negative for a wavelength change in  $\lambda$ , a phase modulation will be introduced on the carrier signal. For the 90 mile orbit the vehicle takes about 40 seconds to change its elevation angle from  $5^\circ$  to  $10^\circ$ ; the modulation rate is about 1/4 cps for one way transmission or double this rate for the round trip. The maximum phase excursion of the resultant carrier is  $B/A$  radians. For the case of -20 db sidelobes,  $\Delta w_{\max} = 0.1$ , and thus, the sideband amplitudes are about 5 per cent of the carrier.

This same phase modulation term appears in Equation 97, and thus, the range error is a function of time. However, the angular velocity of the vehicle with respect to the ground station is so slow that little smoothing can be done to reduce the error.

Multipath errors due to signals incident at larger elevation angles will be considerably less than the low grazing angle case considered above for two reasons:

1. The scattering from the sea surface becomes diffuse and much weaker than the specular case, and
2. The radiation enters the ground antenna on weaker sidelobes further from the main beam.

Indirect signals generated by backscattering from the sea are much weaker than the forward scattered signals except near normal incidence to the surface; in this case, the scattered radiation can only enter by a weak backlobe of the antenna, and consequently, is of little importance.

## Section 5

### CONCLUSIONS AND RECOMMENDATIONS

#### 5.1 Conclusions

The primary conclusion of the AROD Feasibility Study is that the AROD System is feasible. No technological breakthroughs are required to implement this highly accurate, self-contained, real-time orbit determination system. In fact, a representative state-of-the-art system has been designed and is discussed in some detail in this report.

However, rather than restrict the study to the technological feasibility of a particular design, the more general approach of determining the economic factors, or equipment penalties, associated with achieving various accuracies was followed. Two families of curves (Figures 1 and 2) were generated to indicate the measurement accuracy that can be achieved as a function of spacecraft equipment penalty and ground station complexity. From these curves, a potential user of the system can determine whether the equipment penalties associated with achieving the accuracy he requires are tolerable, and whether the AROD system "cost" is lower than those of competing approaches.

Using the representative system as an example, the range and range rate measurement errors (rms) at an altitude of 500 miles and a range of 1000 miles are approximately 3.2 meters and .034 meters per second, respectively, when all error sources are considered. Thus, with a spacecraft equipment weight of approximately 27 pounds, an input power requirement of less than 115 watts, and reasonably modest ground stations capable of unattended operation for long periods of time, a precise orbit determination system can be achieved that capitalizes on the basic advantages of the AROD approach:

- Good "geometry," that is, a high degree of accuracy in a large volume surrounding the ground stations.
- Real time orbit determination.
- No requirement for intercommunications between ground stations.
- Simple, reliable, unattended ground stations.
- Efficient utilization of spacecraft power.

## 5.2 Recommendations for Phase B AROD Study

A design study of six months' duration is contemplated for the Phase B AROD Study. This effort would yield four major results:

1. A System Performance Specification, which will include the overall system accuracy, the measurement accuracy, and the equipment accuracy. (See definitions established in Section 2 of this report.) In addition, sub-system reliability requirements should be established for the operational system.
2. A System Design of an optimized system including the specification of system parameters, definition of the transfer functions of each functional block in the system, and circuit designs for all critical circuits. These design efforts should be supported by experimental investigations and evaluations. The system design specifications should include the constraints on vehicle equipment, weight, volume and input power requirements.
3. A development plan for the prototype AROD equipment through flight test.
4. A comparative analysis of a tracking system employing wide-band modulation techniques versus the cw sidetone ranging system, to which the Phase A Feasibility Study was limited.

### 5.2.1 Study Plan

In order to achieve these results in a six month design study, it will be necessary to make major assumptions as to the mission requirements at

the outset of the program. Otherwise, optimization of the system design cannot proceed. Ground rules that must be established include:

1. The operational envelope of the system, which is defined by the variation of orbital parameters for the vehicles to be employed, and the minimum elevation angle at which the vehicles are tracked.
2. Definition of the vehicle environments including boost-launch phase, orbital phase, and vernier correction phase.
3. Reliability requirements for both the vehicle equipment and the ground stations.
4. System accuracy and performance requirements.
5. Vehicle equipment, weight, volume and power input limitations.
6. Specifications for the vehicle antenna.

Many of the ground rules developed in this report may be applicable to the design study. If the overall program schedule dictates the need for establishing all the ground rules within a short period, it would appear appropriate to initiate the design study on the same ground rules. Concurrent with the start of the program, an intensive effort would be required to up-date these ground rules and to establish the environmental and reliability requirements in a timely manner.

It is recommended that the program be conducted in the manner depicted in the study phasing chart shown in Figure 43. Major subdivisions of the Phase B study indicated on the chart are:

- System Analysis
- System Design
- Evaluation of wideband modulation techniques

#### 5.2.2 System Analysis

This portion of the study should be primarily concerned with the evaluation of the performance of the AROD prototype designed in the System Design task. Additional subtasks are the determination of the computational and storage requirements imposed upon the ASC-15 computer by the AROD calculations and the evaluation of the incremental accuracy of AROD.

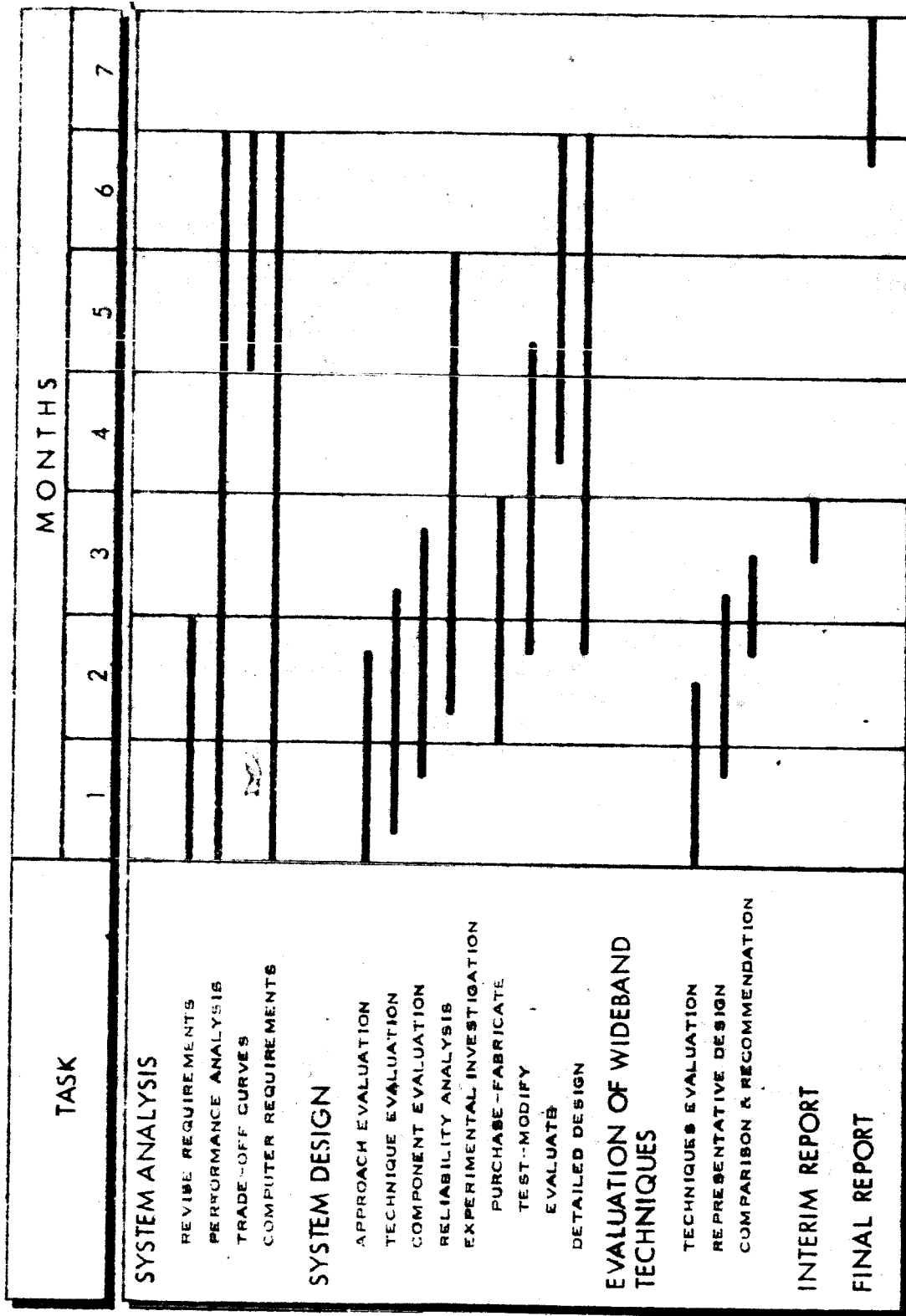


Figure 43. Design Study Phasing Chart

As indicated earlier, it may be necessary to assume that the mission requirements, performance objectives, and equipment penalties are essentially the same as those associated with the "representative" system design evolved in Phase A. However, it is recognized that revisions to these and other constraints will inevitably occur. Consequently, the first two months of the System Analysis task should be devoted to revision of the constraints, based upon close liaison with NASA. At the end of the first two months, a firm list of system and equipment requirements should be provided to the system designers.

General investigations into GDOP effects, errors in vehicle "track," and propagation errors should be conducted to improve system accuracy prediction capabilities. When these effects are combined with a reliability analysis they will permit an evaluation of the performance of the prototype design. Extrapolations from this "design point" will result in improved trade-off curves enabling a potential user to estimate the equipment penalties (spacecraft and ground) associated with a specific measurement accuracy requirement.

Based upon a careful study of the computational and storage capability of the ASC-15 computer planned for the Saturn CIB and an evaluation of the various tasks it might perform for AROD, a set of requirements for the computer should be generated.

The final subtask should be an investigation of incremental errors. It has been estimated that the incremental errors in range, range rate, position, and velocity would be an order of magnitude lower than the absolute errors investigated in the Feasibility Study. This reduction would result from the automatic elimination of many biased errors and the reduction of others by smoothing. An investigation into incremental errors should be conducted in Phase B to determine: 1) the utility of incremental measurements to the vehicle guidance system; 2) system performance in terms of incremental errors in position and velocity; and 3) an estimate of the magnitude of the biased components of the range and range rate measurement errors.

The end results of the System Analysis task would be:

1. System performance specifications for the AROD prototype design.
2. Trade-off curves indicating equipment penalties versus measurement accuracy.
3. ASC-15 computer requirements for AROD calculations.
4. An evaluation of the incremental accuracy of AROD.

### 5.2.3 System Design

The system design described in Section 3 of this report was optimized only to the degree allowed by the scope of effort applied to the Phase A study. However, it adequately served the purpose of establishing the feasibility of the AROD concept. For the design study, it would be most appropriate to evaluate the design approaches, system parameters, and circuit parameters that were chosen for the Feasibility Study in the light of more accurately defined mission requirements for AROD. Some of the more important of these issues are:

1. The choice of the transmitter output component: The spectrum that can be generated in the transmission is dependent on the choice of this component because of limitations on the accuracy to which phase and amplitude may be controlled. Within the constraints imposed by the transmitter components, the transmitted spectrum should be optimized for best utilization of the r-f energy and minimization of the effects of non-linearities in signal processing elements. This could be accomplished by means of a computer program for which a mathematical model of representative signal processing elements is devised to permit analysis of the resulting intermodulation outputs. Also dependent on the choice of the transmitter output component and spectrum is the difficulty that will be encountered in combining the outputs of distributed transmitting elements (if they are required).

2. The extent to which wideband receiver front end components are employed in the vehicle: The best location for the multiplex filter in the receiving chain will be determined on the basis of minimizing the effects of intermodulation on signal tracking performance in the presence of transmitter leakage.
3. The degree of redundancy employed for the ground station receiving and transmitting elements: This issue is of major importance in the design of the unattended ground station inasmuch as it will strongly influence ground network establishment and operating costs.

The spacecraft transmitter and correlation receivers have by far the strongest influence on the penalty factors attributable to the AROD system. For this reason, major effort in the experimental portion of the system design effort should be assigned to these circuits.

For the transmitter chain, the all-important question of choosing the output element should be narrowed down to at most two choices early in the study. If, for illustrative purposes, it is assumed that the choice of the varactor harmonic generator chain is substantiated during this re-evaluation, a single 2.5 watt transmitter chain should be constructed. This transmitter should be capable of operation in either the unmodulated cw mode (where phase stability is the important design consideration for summing purposes) or the mode employing phase modulation by multiple sidetones (where control of the spectrum power distribution is most important). Major emphasis on this experimental effort would be devoted to the transistor driver-amplifier and the varactor-multiplier chain following it. The components required for the frequency standard and synthesizer-modulator are commercially available, and the design problems introduced by this portion of the chain are relatively routine. In the event that another design approach is selected for the transmitter chain, a similarly representative experimental circuit should be constructed for evaluation.

An experimental program should also be carried out for the phase-locked loops needed in the spacecraft. During the early portion of the program, a conventional phase-locked loop should be constructed employing

state-of-the-art components and a signal simulator capable of generating the maximum Doppler offsets and Doppler rates that would be encountered in the missions of interest. Acquisition and tracking behavior of the unaided loop should be evaluated for various Doppler offsets and Doppler rates as a function of the loop parameters. Using this loop as a "test bench," the major portion of the effort on the correlation receivers would be to evaluate techniques for providing acquisition and tracking aids by means of sensing elements external to the loops themselves. Methods for improving pull-in time, probability of lock-on and tracking accuracy will be evaluated.

It is recommended that a third experimental effort be conducted on the front end components for the spacecraft. The primary purpose of this investigation would be to verify the analytical results governing the choice of transmitted spectrum. The major concern with isolation circuits and low noise components is the effects of leakage and nonlinearities on signal tracking accuracies. Critical components for the diplexer should be investigated in order to determine realistic leakage levels. Leakage of the transmitter spectrum should be simulated experimentally for injection into the low noise receiver. Optimization of the transmitter spectrum, the ground station translation frequency, and the retransmitted spectra will result from this effort.

Other portions of the system design can be subdivided as follows: Spacecraft r-f components, range and range rate measuring circuits, telemetry and computer interface components, ground antenna, ground r-f components, ground receiver, and ground transmitter. It is anticipated that only limited experimental investigations will be conducted in these areas. These investigations will be limited to isolated circuits which are deemed critical. Paper designs to the circuit level should be accomplished for all but the routine subsections of the equipment.

#### 5.2.4 Investigation of Wide Band Modulation Techniques

The basic techniques for generating spread spectrum waveforms with very large time bandwidth products should be investigated from the point of

view of ease of modulation and economy of matched filter design. Phase reversal, frequency stepping and frequency swept, for both continuous and intermittent burst type of transmissions, should be evaluated. Major consideration should be given to the problems of establishing phase-lock within the acquisition intervals specified. The technique of overlapping the spectra of the retransmissions of all the ground stations should be thoroughly explored. This appears possible by employing unique codes for each of the ground station retransmissions.

It is expected that the spread spectrum techniques will introduce additional complexity to both the vehicle and ground equipment. This complexity should be assessed against the improvement in interference invulnerability that these techniques afford to provide the basis for the final recommendations.

Because of the major system design changes that may result from this investigation, it is recommended that this investigation be completed during the first three months of the Phase B Study.

## REFERENCES

1. K. D. Froome, Proc. Roy. Soc. (London) A223, 195-215 (1954).
2. "Reference Data for Radio Engineers," Fourth Edition, ITT Corp.
3. E. R. Cohen, et al., "Analysis of Variance of the 1952 Data on the Atomic Constants and a New Adjustment, 1955," Reviews of Modern Physics, Vol. 27, pp 363-380; October, 1955.
4. P. D. Engels and H. W. Shafer, "Extension of the Range and Range Rate System for Rendezvous Tracking," Goddard Space Flight Center Report No. X-520-62-135, August 5, 1962.
5. J. A. Develet, Jr., "Fundamental Accuracy Limitations in a Two-Way Coherent Doppler Measurement System," Trans. SET, September, 1961.
6. W. A. Edson, "Noise in Oscillators," Proc. IRE, August 1960.
7. "Final Report on Advanced Guidance Studies, Volume IV, Appendix I. Fundamental Sensitivity Limitations for Second-Order Phase-Lock Loops," Space Technology Laboratories, Inc., Report No. 7216-0003-PU-V01, 31 May 1961, Astia No. AD 260196.
8. R. Solem, et al., "Goddard Range and Range Rate System Design Evaluation Report," Motorola Report No. W2719-2-1, 16 March 1962.
9. "Space Communications Handbook," Philco Corp., Report No. WDL-TR 1162, 15 September 1959.
10. "Ultra-Precision Crystals," Reeves-Hoffman, Carlisle, Pa., No. 5GA9R32.
11. Busgang, et al., "A Unified Analysis of Range Performance of CW, Pulse and Pulse Doppler Radar" Proc. IRE, October, 1959.
12. A. J. Viterbi, "Acquisition and Tracking Behavior of Phase Locked Loops" JPL External Publication No. 673.

13. J. P. Frazier and J. Page, "Phase-Locked Loop Frequency Acquisition Study." Trans. PGSET, September, 1962.
14. V. A. Counter, "Calculations of Ground-Space Propagation Effects," Lockheed Aircraft Corp. Report No. LMSD-2461, 22 May 1958, Astia No. AD 162000.
15. Proposal for a 20-Watt CW S-Band Amplitron for Space Communication, Raytheon Company, Microwave Power Tube Division, Burlington, Massachusetts.
16. G. Luettgenu and J. Williams, TRW Electronics/Pacific Semiconductors, Inc., H. Miyahara, Space Technology Laboratories, Inc., "A Practical Approach to the Design of Parametric Frequency Multipliers."
17. Dr. A. Uhlir, Jr., "Similarity Considerations for Varactor Multipliers," The Microwave Journal, July 1962.
18. I. Kaufman and D. Douchette, "Harmonic Generation Using Idler Circuits," Proc. IRE, Vol. 48, pp 790-791, April 1960.
19. S. B. Cohn and F. S. Coale, "Directional Channel Separation Filters," Proc. of IRE, August 1956, pp 1018-1024.
20. C. M. Johnson and E. L. Gruenberg, "Semi Active Communication System for Satellite Telemetry," presented at the 1962 National Symposium on Space Electronics and Telemetry, Oct. 1962, Miami Beach, Florida.
21. E. J. Baghdady, "The Theory of FM Demodulation with Frequency-Compressive Feedback," IRE Transactions on Communications Systems, September 1962.
22. AROD Monthly Progress Report No. 2, July 30, 1962 to August 31, 1962.
23. W. J. Gruen, "Theory of AFC Synchronization," Proceedings of the IRE, August 1953.
24. W. J. Cunningham, "Introduction to Nonlinear Analysis," McGraw-Hill, 1958.
25. W. B. Davenport, Jr., and W. L. Root, "An Introduction to the Theory of Random Signals and Noise," p 201, McGraw-Hill, 1958.
26. G. W. Brauer, "Phase Jitter Technical Exhibit for Specification JPL No. 9912 Buffer Amplifier," Resdel Engineering Corporation, Pasadena, California.

27. Kerr, Fishback and Goldstein, "Propagation of Short Radio Waves,"  
Chapter 5, Vol. 13, MIT Radiation Laboratory Series, McGraw-Hill  
Book Co., New York, 1951.

N66-15816

Volume 2

**A  
R  
O  
D**

**IRBORNE**

**ANGING**

**and**

**RBIT**

**ETERMINATION**

**DESIGN FEASIBILITY REPORT**

**IBM**  
**FINAL REPORT**

# **AROD Design Feasibility Report**

March 20, 1963

Final Report for NASA Contract No. NAS 8-5098

PREPARED FOR

**GEORGE C. MARSHALL SPACE FLIGHT CENTER  
NASA  
HUNTSVILLE, ALABAMA**

**PROJECT MANAGER: A. VALAKOS**

**INTERNATIONAL BUSINESS MACHINES CORPORATION  
Federal Systems Division  
ROCKVILLE, MARYLAND**

## CONTENTS

### VOLUME 1

		Page
Section 1	INTRODUCTION AND SUMMARY	1
1.1	Introduction	1
1.2	Summary	2
Section 2	SYSTEM ANALYSIS	13
2.1	Introduction	13
2.2	Sources of System Errors	14
2.2.1	Uncertainty of the Vacuum Velocity of Light	14
2.2.2	Propagation Errors	15
2.2.3	Equipment Errors	16
2.2.4	Geodetic Errors	26
2.3	Geometrical Dilution of Precision	29
2.4	Smoothing	38
2.5	Equipment Performance Objectives (Error Budget)	40
2.5.1	Uncertainty of the Vacuum Velocity of Light	42
2.5.2	Propagation Errors	42
2.5.3	Equipment Errors	44
2.5.4	Total Errors	52
2.6	Summary	52
Section 3	SYSTEM DESIGN	53
3.1	Introduction	53
3.2	Principle of Operation	56
3.2.1	Spacecraft Equipment	56
3.2.2	Ground Station Equipment	65
3.3	Parametric Analysis	68
3.3.1	Signal Parameters	68
3.3.2	Choice of Operating Frequency	70
3.3.3	Range Equation Parameters	71
3.3.4	Signal Tracking Parameters	76
3.4	Comparison of the Transponder Design Approach to Other Approaches	80
3.5	Trade-off Analysis	84

		Page
Section 4	EQUIPMENT IMPLEMENTATION	87
4.1	Spacecraft Equipment	87
4.1.1	Spacecraft Transmitter	87
4.1.2	Wideband Receiver	105
4.1.3	Phase Locked Loops	111
4.1.4	Range Rate Measurements	137
4.1.5	Range Measurement Circuit	140
4.1.6	Weight and Power Estimates	145
4.1.7	Equipment Interfaces	149
4.2	Ground Station Equipment	155
4.2.1	Antenna	155
4.2.2	Ground Transmitter	163
4.2.3	Ground Station Signal Processing	168
4.2.4	Multipath Effects	177
Section 5	CONCLUSIONS AND RECOMMENDATIONS	185
5.1	Conclusions	185
5.2	Recommendations for Phase B AROD Study	186
5.2.1	Study Plan	186
5.2.2	System Analysis	187
5.2.3	System Design	190
5.2.4	Investigation of Wide Band Modulation Techniques	192
	References	195

## VOLUME 2

### Appendices

A	Geometrical Dilution of Precision	A-1
B	Errors Introduced by the Propagation Medium	B-1
C	Geodetic Aspects of AROD	C-1
D	Mathematical Derivations	D-1

# VOLUME 1

## ILLUSTRATIONS

Figure		Page
1	Range Measurement Performance as a Function of Spacecraft Penalty	4
2	Range Rate Measurement Performance as a Function of Spacecraft Penalty	5
3	Simplified Block Diagram	7
4	Typical AROD System Performance-Position	9
5	Typical AROD System Performance-Velocity	10
6	Propagation-Induced Range Errors at 2 Gc	17
7	Propagation-Induced Range Rate Errors at 2 Gc	18
8	Test Paths	32
9	System Performance at h = 90 Nautical Miles	34
10	System Performance at h = 500 Nautical Miles	35
11	System Performance at h = 2000 Nautical Miles with a 500 Nautical Mile Baseline	36
12	System Performance at h = 2000 Nautical Miles with a 1000 Nautical Mile Baseline	37
13	Influence of Range Measurement Errors and Station Coordinate Errors on Positional Accuracy	39
14	Vehicle Equipment Functional Block Diagram	59
15	Block Diagram of Range Ambiguity Resolving Tones Tracking Circuits	64
16	Ground Transponder Block Diagram	67
17	Amplitron Phase Pushing Measurements (QKS997)	90
18	Amplitron Thermal Stability Measurements (QKS997)	92
19	AROD Spacecraft Transmitter R-F Spectrum	99
20	Block Diagram, AROD Vehicle Transmitter-Receiver R-F Section	100
21	Block Diagram AROD Radio Frequency and Range Tone Synthesizer	104

Figure		Page
22	Four Station AROD Spectrum-as seen by Vehicle Receiver (Zero Doppler Assumed)	106
23	Block Diagram AROD Vehicle Receiver, IF and Phase-Lock Section	110
24	Basic Phase-Locked Loop	113
25	Carrier Acquisition and Tracking Loop	115
26	Fine Ranging Tone Phase-Locked Loop	118
27	Low Pass Filter	123
28	Linearized Phase Transfer Model	131
29	Frequency Ramp	136
30	Fine Ranging Tone Down Converter	141
31	Diode Matcher	141
32	Phase Transfer Model	143
33	Ground Antenna Beam Pattern	156
34	Cross Section of the Recommended Antenna	158
35	Antenna Layout	160
36	Radiation Center Errors in Azimuth Plane	162
37	Radiation Center Errors in Vertical Plane	162
38	Differential Phase Shift Between Two Traveling Wave Tubes	167
39	Three Filter R-F Multiplexer	171
40	Single Sideband Up-Converter	176
41	Multipath Interference at Ground Antenna	180
42	Vector Diagram of Multipath Signals	181
43	Design Study Phasing Chart	188

## VOLUME 1

### TABLES

Table		Page
1	Parameters of a Representative AROD System	6
2	Comparative Accuracies of Methods for the Determination of Geodetic Positions Over Extended Land Areas	28
3	Estimated Repeatability of Methods for the Determination of a Ship's Position	30
4	Measurement Error Summary for Various Points in the AROD System	43
5	Parameters of the Representative AROD System	57
6	AROD Signal Parameters	69
7	Trade-Off Table	85
8	Constant Parameter Carrier Loop	120
9	Variable Parameter Carrier Loop	121
10	Fine Ranging Tone Loop	122
11	Spacecraft AROD Equipment Estimates	146
12	AROD Frequency Allocation Table	164

## VOLUME 2

### ILLUSTRATIONS AND TABLES

Figure		Page
A-1	AROD System Geometry	A-2
A-2	AROD Error Evaluation Computer Program: Functional Block Diagram	A-4
A-3	Relation Between K and P for Covariance Error Analysis	A-6
A-4	Trajectory Program Coordinate Systems	A-10
A-5	Test Paths	A-26
A-6	System Accuracy for Fixed Value of Station Coordinate Standard Deviation ( $\sigma_{sc} = 3M$ ) and Various Combinations of Range, Range-Rate Standard Deviations (Runs 12, 7, 14)	A-30
A-7	System Accuracy for Fixed Value of $\sigma_{sc}$ (7M) and Various Combinations of $\sigma_r$ , $\sigma_f$ (Runs 1, 2, 3)	A-31
A-8	System Accuracy for Fixed Value of $\sigma_{sc}$ (15M) and Various Combinations of $\sigma_r$ , $\sigma_f$ (Runs 15, 8, 13)	A-32
A-9	System Accuracy for Fixed Values of $\sigma_r$ , $\sigma_f$ (3M, 0.5M/Second) and Various Values of $\sigma_{sc}$ (Runs 7, 8, 2, 16)	A-33
A-10	Influence of $\sigma_{sc}$ on $(\rho_p/K)_{min}$ , $(\rho_v/K)_{min}$ as Functions of $\sigma_r$ , $\sigma_f$	A-34
A-11	$(\rho_v/K)_{min}$ as Function of $\sigma_r$ for Fixed Value of $\sigma_{sc}$ and Several Values of $\sigma_f$	A-36

Figure		Page
A-12	Effects of Varying Orbital Altitude with Fixed Station Separation Distance (Runs 4, 5, 6)	A-37
A-13	Distance Covered on Earth Surface for Each Test Orbital Altitude	A-39
A-14	Effects of Varying Station Separation Distance for Fixed Orbital Altitude ( $h = 90$ nautical miles), (Runs 10, 4)	A-40
A-15	Effects of Varying Station Separation Distance for Fixed Orbital Altitude ( $h = 2000$ nautical miles), (Runs 11, 6)	A-41
A-16	Effect of Vehicle-to-Stations Relative Geometry (Runs 2, 5, 9)	A-42
B-1	Structure of the Atmosphere	B-2
B-2	Index of Refraction for Various Tropospheric Models	B-5
B-3	Electron Density in the Ionosphere (Chapman Distribution)	B-6
B-4	Index of Refraction in the Ionosphere for Various Frequencies	B-7
B-5	Estimated and Theoretical Electron Densities in the Ionosphere	B-8
B-6	Critical Frequency vs. Sunspot Number	B-10
B-7	Geometry for Ray Bending	B-12
B-8	Expected Range Deviation, $\overline{\Delta R}$	B-19
B-9	Standard Correction $\chi(\Delta R)$	B-19
B-10	Standard Error, $\sigma_s(\Delta R)$	B-20
B-11	Standard Error After Using $n_s, \sigma_m(\Delta R)$	B-20

Figure		Page
B-12	$\overline{\Delta R}$ , $\chi(\Delta R)$ , $\sigma_s(\Delta R)$ and $\sigma_m(\Delta R)$	B-21
B-13	Propagation-Induced Range Errors at 2 Gc	B-21
B-14	Tropospheric Bending	B-24
B-15	Tropospheric Error	B-25
B-16	Ionospheric Bending	B-26
B-17	Ionospheric Correction	B-27
B-18	Ionospheric Error	B-28
B-19	Propagation-Induced Range Rate Errors at 2 Gc	B-29
C-1	LORAN-C Coverage Diagram	C-14
C-2	Omega Coverage Diagram	C-16
D-1	Mixer Parameters	D-2
D-2	Mixer Output Spectra	D-4
D-3	Geometry for the Analysis of Signal Dynamics	D-9
Tables		
A-1	Summary of Test Run Conditions	A-28
B-1	U. S. Standard Atmosphere, 1962	B-4
B-2	Mean Critical Frequencies at Washington, D. C. 1959 (Noon)	B-9
B-3	Range Deviations Caused by the Ionosphere	B-16
C-1	Comparative Accuracies of Methods for Determination of Geodetic Positions Over Extended Areas	C-9

## Appendix A

### GEOMETRICAL DILUTION OF PRECISION

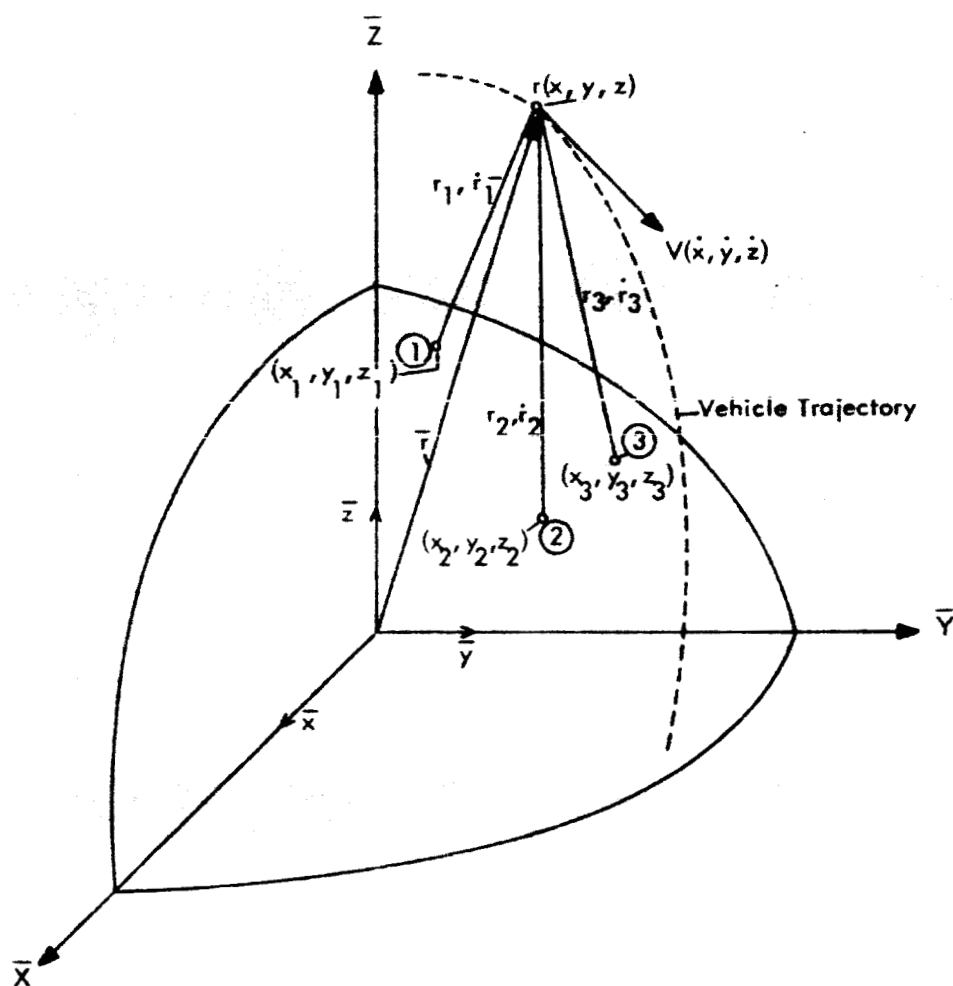
The errors in a spacecraft's position and velocity computed from imperfect measurements of range and range rate will vary with the spacecraft's position relative to a given ground station complex. It is the purpose of this appendix to discuss Geometrical Dilution of Precision (GDOP) and present the numerical results of some analyses of various spacecraft-ground station geometries.

The method for analyzing AROD GDOP has been a flexible computer program, the AROD Error Evaluation Computer Program. This appendix introduces the GDOP analysis performed as a part of the AROD Feasibility Study by describing this computer program. A discussion and derivations of the basic equations for the program are presented and the results of a series of test runs concludes the appendix.

#### 1.0 DESCRIPTION OF THE AROD ERROR EVALUATION COMPUTER PROGRAM

##### 1.1 Purpose and Scope

The purpose of the AROD Error Evaluation Computer Program is to provide a means for quantitatively evaluating the effects of vehicle-to-station relative geometry on the basic AROD measurement errors, over a wide range of mission trajectories. The AROD system is a range and range-rate orbital navigation system requiring three ground-based stations of known location, as indicated in Figure A-1. To provide the desired flexibility, station locations are supplied as program inputs which may be varied from run to run. Basic errors, which are supplied as program inputs,



$\bar{X}, \bar{Y}, \bar{Z}$  Arbitrarily Oriented Reference Frame (shown as geocentric-inertial)  
 $r_1, r_2, r_3$  Vehicle-to-Stations ①, ②, ③ Relative Range  
 $\dot{r}_1, \dot{r}_2, \dot{r}_3$  Vehicle-to-Stations ①, ②, ③ Relative Range-Rate  
 $x_i, y_i, z_i$  ( $i = 1, 2, 3$ ) Location Coordinates of Stations ①, ②, ③  
 $\bar{r} = x\bar{x} + y\bar{y} + z\bar{z}$  Vehicle Instantaneous Range Vector  
 $\bar{V} = \dot{x}\bar{x} + \dot{y}\bar{y} + \dot{z}\bar{z}$  Vehicle Instantaneous Velocity Vector

From Geometry, AROD Position Eqns are:

$$(x - x_i)^2 + (y - y_i)^2 + (z - z_i)^2 = r_i^2$$

From Which AROD Velocity Eqns are:

$$(x - x_i)\dot{x} + (y - y_i)\dot{y} + (z - z_i)\dot{z} = r_i\dot{r}_i$$

$i = 1, 2, 3$

Figure A-1. AROD System Geometry

include errors in the measurement of instantaneous range and range-rate, and errors in specification of the three position coordinates for each of the three ground-based stations comprising the system. To obtain a first estimate of the GDOP effects while remaining within the time and manpower limitations of the AROD Feasibility Study, all errors were assumed to be independent and normally distributed. Although only approximately true, this assumption gives realistic results while avoiding the cumbersome mathematical complexities of correlated error sources. In addition, provision is made in the program for inclusion of bias (i.e., non-zero mean) errors in the basic measurements and computation of their propagated effect on position and velocity determination.

As indicated in Figure A-2, vehicle trajectory data within the observation region of the three stations are supplied by an independent three-dimensional orbital computation program.\* This program is capable of generating both launch trajectories and orbital trajectories of arbitrary altitude, eccentricity, and inclination angle. Depending upon the degree of sophistication desired, the program can include the effects of earth oblateness (up to the sixth gravitational harmonic), atmospheric drag, rotation of the earth's atmosphere, thrusting schedules, and varying vehicle mass during thrusting periods. Specification of three values of initial position and three values of initial velocity are required for the orbital computation program.

The AROD Error Evaluation Computer Program generates the instantaneous values of the elements of the position and velocity error covariance matrices as overall measurements of geometrically-induced errors. These elements are then used to compute the magnitudes and spatial orientations of error ellipsoid semiaxes corresponding to the diagonalized forms of the position and velocity covariance matrices. In this way, a description of the error volumes within which vehicle position and velocity can be expected

---

\*Much of the orbital computation portion of the total program was developed as part of an earlier project. It is included here to describe the entire program used in the AROD GDOP analysis.

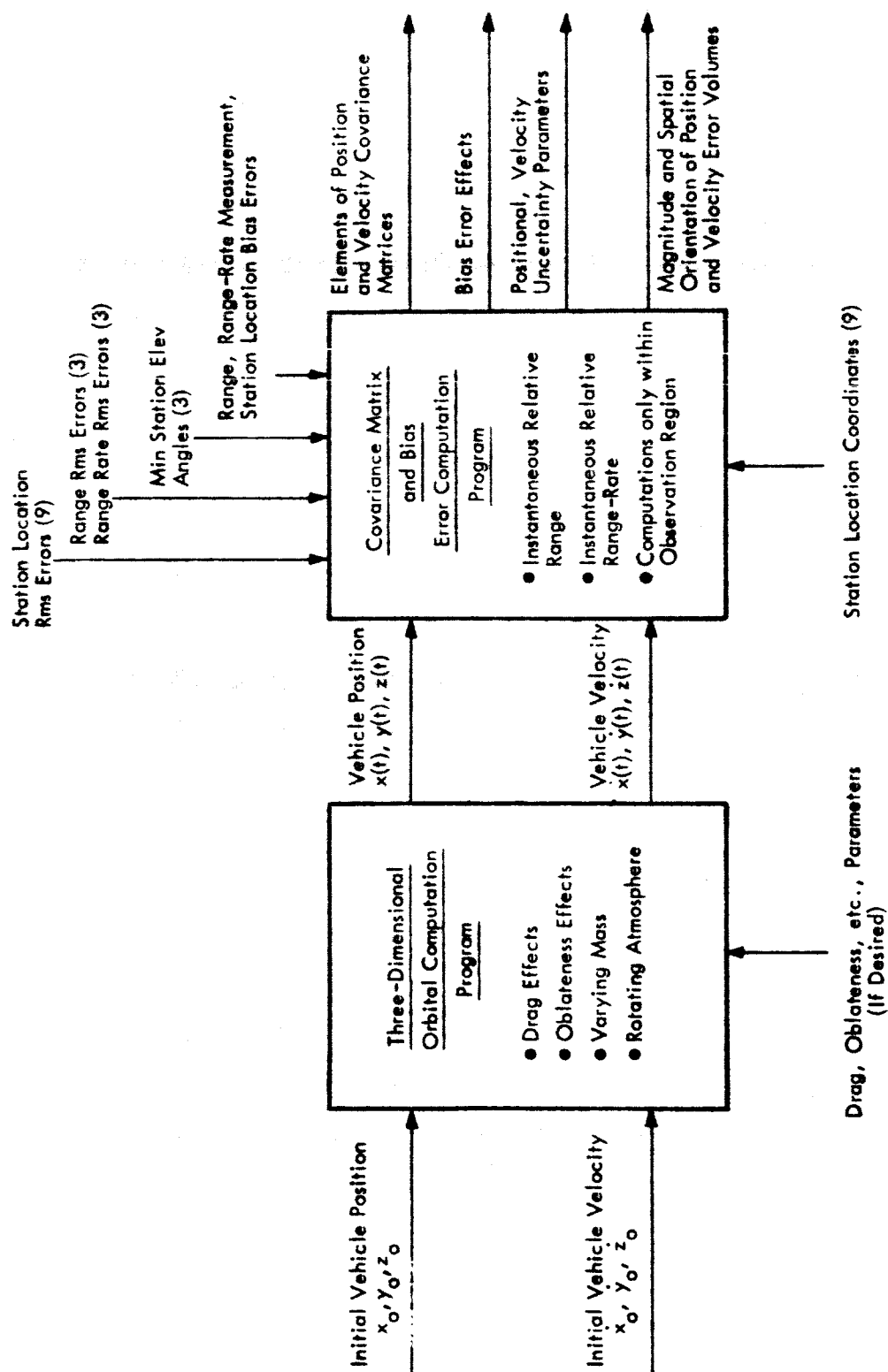


Figure A-2. AROD Error Evaluation Computer Program: Functional Block Diagram

to lie with a specified probability is obtained. These data are generated at specified increments of time within the observation region defined by the three ground-based stations. The relation between the covariance matrix and error volumes of specified probability levels is briefly discussed below.

## 1.2 Covariance Matrix Interpretation

The covariance matrix of position error is given by:

$$\Lambda_p = \begin{bmatrix} \sigma_{xx} & \sigma_{xy} & \sigma_{xz} \\ \sigma_{yx} & \sigma_{yy} & \sigma_{yz} \\ \sigma_{zx} & \sigma_{zy} & \sigma_{zz} \end{bmatrix}$$

where  $\sigma_{xx}$  = variance of x position error,  $\sigma_{xy} = \sigma_{yx}$  = covariance of x and y position errors, etc. This matrix contains all the information required to describe an error volume in space within which the vehicle lies with a specified probability. The computation procedure for extracting this information is as follows:

The matrix is first diagonalized by means of an orthogonal transformation C having the property that

$$C^{-1} \Lambda_p C = \begin{bmatrix} \sigma_{x'x'} & 0 & 0 \\ 0 & \sigma_{y'y'} & 0 \\ 0 & 0 & \sigma_{z'z'} \end{bmatrix} \equiv D_p, \text{ where } |C| = 1$$

The diagonal elements of  $D_p$  are error variances along a set of principal axes,  $x'$ ,  $y'$ ,  $z'$ , the spatial directions of which (relative to inertial axes) can be deduced from the elements of C. An error ellipsoid centered about the computed vehicle position, having semi-axes aligned with these principal axes and of lengths of  $K\sigma_{x'}$ ,  $K\sigma_{y'}$ ,  $K\sigma_{z'}$ , (where  $\sigma_{x'} = \sqrt{\sigma_{x'x'}}$ , etc.), can be expected to contain the actual vehicle position with a certain probability P. The probability level P is related to the proportionality factor K by a chi-square distribution function as shown in Figure A-3. For example, when  $K = 1$  the ellipsoid with semi-axes  $\sigma_{x'}$ ,  $\sigma_{y'}$ ,  $\sigma_{z'}$ , corresponds to a probability level of  $P = 0.2$  (20%); the 2-sigma ellipsoid ( $K = 2$ ) corresponds to a level about  $P = 0.75$ , etc.

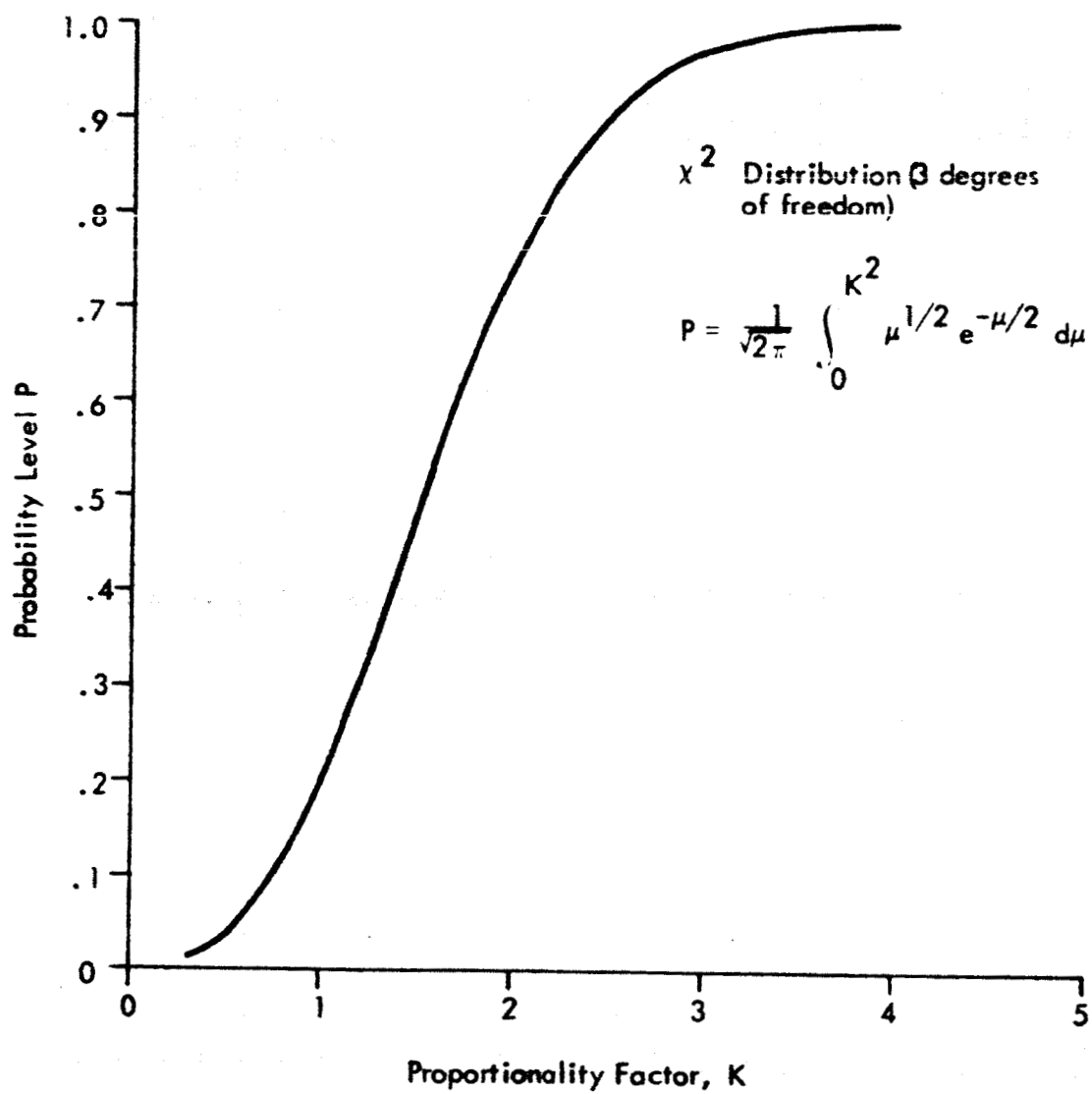


Figure A-3. Relation Between K and P for Covariance Error Analysis

As an approximate measure of position error, it is noted that the determinant  $|D_p|$  is related to the volume  $V_p$  of the K-sigma error ellipsoid by:

$$V_p = \frac{4}{3}\pi K\sigma_{x'} \cdot K\sigma_{y'} \cdot K\sigma_{z'} = \frac{4}{3}\pi K^3 \sqrt{|D_p|}$$

A sphere of equivalent volume thus has a radius  $\rho_p$  given by:

$$\rho_p = K|D_p|^{1/6}$$

or, since

$$|D_p| = |C^{-1}\Lambda_p C| = |C^{-1}| \cdot |\Lambda_p| \cdot |C| = |\Lambda_p|, |C| = 1$$

$$\rho_p = K|\Lambda_p|^{1/6}$$

Thus, the covariance matrix determinant prior to diagonalization can be used to obtain a radius  $\rho_p$ . In an approximate sense,  $\rho_p$  is an overall measure of positional uncertainty (with approximate probability level P related to the proportionality factor K as before), since the spherical volume of radius  $\rho_p$  as given above is equal to the K-sigma ellipsoid volume.

The error evaluation program computes both the value of  $\rho_p$  for  $K = 1$ , as well as the principal axes error variances  $\sigma_{x'x'}$ ,  $\sigma_{y'y'}$ ,  $\sigma_{z'z'}$ , and the spatial orientations of these axes. An entirely similar procedure is followed for the velocity error covariance matrix  $\Lambda_v$  to obtain velocity error volume data and uncertainty parameter  $\rho_v$ . The quantities  $(\rho_p/K)$ ,  $(\rho_v/K)$  are defined as the positional uncertainty parameter and velocity uncertainty parameter, respectively. These quantities are computed as functions of time within the observation region and are used as summary measures of position and velocity uncertainties.

### 1.3 Program Inputs

As summarized in the functional block diagram of Figure A-2, the required input quantities for the AROD Error Evaluation Computer Program are as follows:

- Three components of vehicle initial position  $(x_o, y_o, z_o)^*$
- Three components of vehicle initial velocity  $(\dot{x}_o, \dot{y}_o, \dot{z}_o)^*$
- Parameters to specify drag, oblateness, etc., effects, if these are to be included
- Nine station location coordinates  $(x_1, y_1, z_1, x_2, y_2, z_2, x_3, y_3, z_3)$
- Nine station location rms errors  $(\sigma_{x_1}, \sigma_{y_1}, \dots, \sigma_{z_3})$
- Three range and three range-rate measurement rms errors  $(\sigma_{r_1}, \sigma_{r_2}, \sigma_{r_3}; \sigma_{\dot{r}_1}, \sigma_{\dot{r}_2}, \sigma_{\dot{r}_3})$
- Range, range-rate measurement and station location bias errors
- Minimum allowable station elevation angles, one for each station

The minimum allowable station elevation angles account for station visibility limitations and thus ensure that only those relative ranges lying within the observation region for the three ground stations are employed in computing the desired covariance matrix data. All remaining input quantities may be varied at will, to cover all trajectories, relative geometries, and measurement rms values of interest.

#### 1.4 Program Outputs

The program outputs include (Figure A-2):

- Position and velocity covariance error matrices, together with matrix determinants and equivalent spherical volume radii (i.e., positional uncertainty parameters and velocity uncertainty parameters).
- Error ellipsoid principal axes directions and error variances along these axes.
- Position and velocity errors resulting from bias errors in range and range-rate measurements, and station location.

These outputs permit ready determination of position and velocity error volumes for any specified probability level, as a function of orbit geometry, station location, and vehicle position while the spacecraft is in the observation region defined by the three (elevation-angle-limited) ground-based stations.

---

\*In the orbital computation program, these quantities enter in terms of polar spherical coordinates  $(r_o, \lambda_o, \psi_o; \dot{r}_o, \dot{\lambda}_o, \dot{\psi}_o)$ ; see Section 2.1.

## 2.0 PROGRAM EQUATIONS

### 2.1 Trajectory Computations

#### 2.1.1 Coordinate Systems

The digital computer program employed to generate trajectory data for the AROD Error Evaluation Computer Program is based on a Runge-Kutta numerical integration of the differential equations of orbital motion in three dimensions. The orbital equations of motion are written in spherical polar coordinates relative to a geocentric inertial frame, as indicated in Figure A-4. The instantaneous position of the orbiting vehicle center of gravity, P, is defined by the spherical polar coordinates  $(r, \lambda, \psi)$  where:

- $r$  = radial distance of P from earth center.
- $\lambda$  = celestial longitude of P, measured (in the equatorial plane) from the positive  $\bar{X}$  inertial axis.
- $\psi$  = celestial latitude of P, measured (in the plane perpendicular to the equatorial plane and containing the earth polar axis  $\bar{Z}$ ) from the equatorial plane.

Associated with this coordinate system is an orthogonal set of unit vectors  $(\bar{i}_r, \bar{i}_\lambda, \bar{i}_\psi)$  which move with the vehicle, as illustrated in Figure A-4, and defined as follows:

- $\bar{i}_r$  is along the radius vector  $\bar{r}$  from O to P, positive outward
- $\bar{i}_\lambda$  is tangent to the circle of constant celestial latitude at P, positive to the east
- $\bar{i}_\psi$  is tangent to the meridian of celestial longitude through P, positive to the north

Components of vehicle linear velocity in this coordinate system are then:

- $V_r$  = radial velocity component, along  $\bar{i}_r = \dot{r}$
- $V_\psi$  = northward velocity component, along  $\bar{i}_\psi = r\dot{\psi}$
- $V_\lambda$  = eastward velocity component, along  $\bar{i}_\lambda$
- $V_\lambda = r\dot{\lambda} \cos \psi$ , relative to a non-rotating earth
- $V_\lambda = r(\dot{\lambda} - \Omega_e) \cos \psi$ , relative to a rotating earth

where, as indicated in Figure A-4,  $\Omega_e$  represents the magnitude of the earth angular velocity about the polar ( $\bar{Z}$ ) axis.

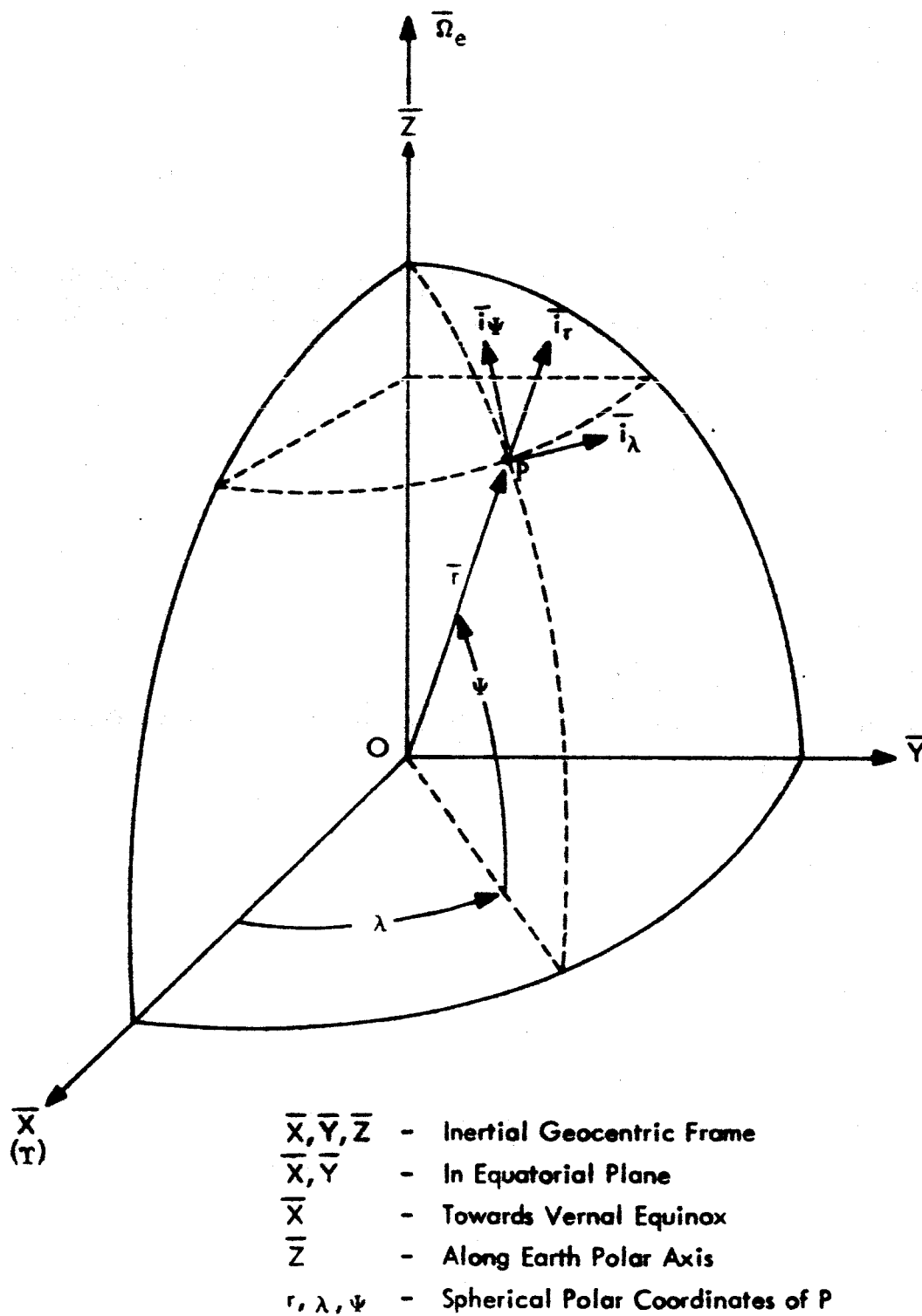


Figure A-4. Trajectory Program Coordinate Systems

As may be inferred from Figure A-4, the polar spherical coordinates  $(r, \lambda, \psi)$  of P are related to the geocentric inertial coordinates  $(X, Y, Z)$  of P, by the equations:

$$\begin{aligned} X &= r \cos \psi \cos \lambda \\ Y &= r \cos \psi \sin \lambda \\ Z &= r \sin \psi \end{aligned} \quad (A-1)$$

from which the inertial components of vehicle velocity are obtained as:

$$\begin{aligned} \dot{X} &= \dot{r} \cos \psi \cos \lambda - r \dot{\psi} \sin \psi \cos \lambda - r \dot{\lambda} \cos \psi \sin \lambda \\ \dot{Y} &= \dot{r} \cos \psi \sin \lambda - r \dot{\psi} \sin \psi \sin \lambda + r \dot{\lambda} \cos \psi \cos \lambda \\ \dot{Z} &= \dot{r} \sin \psi + r \dot{\psi} \cos \psi \end{aligned} \quad (A-2)$$

The geocentric inertial frame  $(\bar{X}, \bar{Y}, \bar{Z})$  is defined such that the  $\bar{X}$ ,  $\bar{Y}$ , axes lie in the equatorial plane; with  $\bar{X}$  directed in a convenient inertial direction (e.g., towards the vernal equinox); and  $\bar{Z}$  directed along the earth polar axis.

### 2.1.2 Equations of Motion

In terms of the spherical polar coordinates defined above, the equations of motion of point P about an oblate earth while under the influence of gravitational, drag, and thrust accelerations are

$$\begin{aligned} \ddot{r} - r\dot{\psi}^2 - r\dot{\lambda}^2 \cos^2 \psi &= \frac{G_r}{m} + \frac{F_r}{m} + \frac{D_r}{m} \\ r\ddot{\lambda} \cos \psi + 2r\dot{\lambda} \dot{\psi} \cos \psi - 2r\dot{\lambda} \dot{\psi} \sin \psi &= \frac{G_\lambda}{m} + \frac{F_\lambda}{m} + \frac{D_\lambda}{m} \\ r\ddot{\psi} + 2r\dot{\psi} \dot{\lambda} + r\dot{\lambda}^2 \sin \psi \cos \psi &= \frac{G_\psi}{m} + \frac{F_\psi}{m} + \frac{D_\psi}{m} \end{aligned} \quad (A-3)$$

In Equation A-3,  $m$  represents vehicle mass, and the  $G$ ,  $F$ , and  $D$  terms represent the indicated components of gravitational, thrust, and drag accelerations, respectively. Although the computer program, as currently written, includes the required expressions for  $F$  and  $D$  these quantities were neglected in the present AROD analysis (non-thrusting orbital motion in an essentially atmosphere-less environment was of primary interest).

To describe earth oblateness effects up to the sixth gravitational harmonic, the following expression for the earth's gravitational potential  $\phi$  is employed:

$$\begin{aligned} \phi = \frac{KM}{r} & \left[ 1 + \frac{J_2 R^2}{2r^2} (1 - 3 \sin^2 \psi) + \frac{J_3 R^3}{2r^3} (3 - 5 \sin^2 \psi) \sin \psi \right. \\ & - \frac{J_4 R^4}{8r^4} (3 - 30 \sin^2 \psi + 35 \sin^4 \psi) - \frac{J_5 R^5}{8r^5} (15 - 70 \sin^2 \psi + 63 \sin^4 \psi) \sin \psi \quad (A-4) \\ & \left. + \frac{J_6 R^6}{16r^6} (5 - 105 \sin^2 \psi + 315 \sin^4 \psi - 231 \sin^6 \psi) \dots \right] \end{aligned}$$

where

$KM$  = gravitational constant - mass product of earth =  $1.407654 \times 10^{16} \text{ ft}^3/\text{sec}^2$

$R$  = equatorial radius of earth =  $2.0926428 \times 10^7 \text{ ft}$

and  $J_2, \dots, J_6$  = coefficients of earth gravitational harmonics

The values employed in the computer program for the earth gravitational harmonic coefficients are those internationally adopted in 1961:

$$\begin{aligned} J_2 &= 1.08228 \times 10^{-3} \\ J_3 &= -2.3 \times 10^{-6} \\ J_4 &= -2.12 \times 10^{-6} \\ J_5 &= -0.2 \times 10^{-6} \\ J_6 &= 10^{-6} \end{aligned}$$

Components of higher-ordered oblate earth gravitational force per unit mass in the  $(r, \lambda, \psi)$  directions are the gradient components of the earth potential function  $\phi$  as given by Equation A-4.

$$\begin{aligned} \frac{Gr}{m} = \frac{\partial \phi}{\partial r} = \frac{KM}{r^2} & \left[ -\frac{1}{r} - \frac{3J_2 R^2}{2r^3} (1 - 3 \sin^2 \psi) - \frac{4J_3 R^3}{2r^4} (3 - 5 \sin^2 \psi) \sin \psi \right. \\ & \left. + \frac{5J_4 R^4}{8r^5} (3 - 30 \sin^2 \psi + 35 \sin^4 \psi) \right] \end{aligned}$$

$$\begin{aligned}
& + \frac{6J_5 R^5}{8r^6} (15 - 70 \sin^2 \psi + 63 \sin^4 \psi) \sin \psi \\
& - \frac{7J_6 R^6}{16r^7} (5 - 105 \sin^2 \psi + 315 \sin^4 \psi - 231 \sin^6 \psi) \dots \Big] \\
\frac{G_\lambda}{m} &= \frac{1}{r \cos \psi} \frac{\partial \phi}{\partial \lambda} = 0 \\
\frac{G_\psi}{m} &= \frac{1}{r} \frac{\partial \phi}{\partial \psi} = \frac{KM}{r^2} \left[ -\frac{3J_2 R^2}{r^2} \sin \psi \cos \psi + \frac{J_3 R^3}{2r^3} (3 - 15 \sin^2 \psi) \cos \psi \right. \\
& - \frac{J_4 R^4}{8r^4} (-60 \sin \psi + 140 \sin^3 \psi) \cos \psi \\
& - \frac{J_5 R^5}{8r^5} (15 - 210 \sin^2 \psi + 315 \sin^4 \psi) \cos \psi \\
& \left. + \frac{J_6 R^6}{16r^6} (-210 \sin \psi + 1260 \sin^3 \psi - 1386 \sin^5 \psi) \cos \psi \dots \right] \tag{A-5}
\end{aligned}$$

For purposes of the present AROD analysis, the coefficients  $J_2$  through  $J_6$  and the quantity  $\Omega_e$  were set equal to zero to consider only motion about a non-rotating spherical earth. Note, however, that earth oblateness effects are readily incorporated into the program by merely assigning the cited values to the  $J$  coefficients. Likewise, earth rotational effects are incorporated by assigning the appropriate value of earth angular velocity to  $\Omega_e$ .

Equations A-3 and A-5 represent the set of second order non-linear differential equations of motion which are numerically integrated, by means of standard Runge-Kutta procedures, to yield the desired AROD orbital data. Solution of these equations gives vehicle position and velocity in the polar spherical coordinates  $(r, \lambda, \psi)$ , which are readily converted to corresponding inertial coordinates by means of Equations A-1 and A-2. Specification of the components of vehicle initial position  $(r_o, \lambda_o, \psi_o)$  and velocity  $(\dot{r}_o, \dot{\lambda}_o, \dot{\psi}_o)$  are required in order to integrate Equations A-3 and A-5.

### 2.1.2 Relative Range and Range-Rate Computations

To compute the elements of the various matrices employed in the AROD Error Evaluation Program, instantaneous range and range-rate of the vehicle relative to each of the three ground stations are required. As indicated in Figure A-1, these quantities are given by:

$$\left. \begin{aligned} r_i &= \left[ (x - x_i)^2 + (y - y_i)^2 + (z - z_i)^2 \right]^{1/2} \\ \dot{r}_i &= \frac{1}{r_i} \left[ (x - x_i) \dot{x} + (y - y_i) \dot{y} + (z - z_i) \dot{z} \right] \end{aligned} \right\} i = 1, 2, 3. \quad (\text{A-6})$$

in which  $(x, y, z)$  and  $(\dot{x}, \dot{y}, \dot{z})$  are the instantaneous rectangular coordinates of vehicle position and velocity, respectively. These quantities are supplied by the trajectory program by means of Equations A-1 and A-2. In Equation A-6,  $x_i, y_i, z_i$  ( $i = 1, 2, 3$ ) are the rectangular coordinates of the three ground-based stations. These fixed quantities are computed in the program by means of the program inputs of radius ( $R_i$ ), longitude ( $\lambda_i$ ), and latitude ( $\psi_i$ ) of the three stations:

$$\begin{aligned} x_i &= R_i \cos \psi_i \cos \lambda_i \\ y_i &= R_i \cos \psi_i \sin \lambda_i \\ z_i &= R_i \sin \psi_i \end{aligned} \quad (\text{A-7})$$

Finally, to ensure that only data within the observation region defined by the three elevation-angle-limited stations are employed in the error computations, the instantaneous elevation angles  $\epsilon_i$  of each station to the vehicle are computed from:

$$\epsilon_i = \sin^{-1} \left[ \frac{r^2 - R_i^2 - r_i^2}{2R_i r_i} \right] \quad (\text{A-8})$$

$$i = 1, 2, 3; \left( -\frac{\pi}{2} \leq \epsilon_i \leq \frac{\pi}{2} \right)$$

At each time point, the error computations proceed if and only if the following three inequalities are all satisfied:

$$\epsilon_1 > \epsilon_{1m}$$

$$\epsilon_2 > \epsilon_{2m}$$

$$\epsilon_2 > \epsilon_{3m}$$

in which  $\epsilon_{1m}, \epsilon_{2m}, \epsilon_{3m}$  are program inputs specifying the minimum allowable elevation angle of each station.

## 2.2 Position Bias and Covariance Matrix Computations

From the basic AROD positional navigational equations (see Equation A-6), errors in vehicle position ( $\Delta x, \Delta y, \Delta z$ ) are related to errors in measurement of the three vehicle-to-station ranges ( $\Delta r_1, \Delta r_2, \Delta r_3$ ) and errors in the specification of the nine coordinates of station locations ( $\Delta x_1, \Delta x_2, \dots, \Delta z_3$ ) according to:

$$r_1 \Delta r_1 = (x - x_1)(\Delta x - \Delta x_1) + (y - y_1)(\Delta y - \Delta y_1) + (z - z_1)(\Delta z - \Delta z_1)$$

$$r_2 \Delta r_2 = (x - x_2)(\Delta x - \Delta x_2) + (y - y_2)(\Delta y - \Delta y_2) + (z - z_2)(\Delta z - \Delta z_2) \quad (A-9)$$

$$r_3 \Delta r_3 = (x - x_3)(\Delta x - \Delta x_3) + (y - y_3)(\Delta y - \Delta y_3) + (z - z_3)(\Delta z - \Delta z_3)$$

or

$$\Delta r_1 + a_{11}\Delta x_1 + a_{12}\Delta y_1 + a_{13}\Delta z_1 = a_{11}\Delta x + a_{12}\Delta y + a_{13}\Delta z$$

$$\Delta r_2 + a_{21}\Delta x_2 + a_{22}\Delta y_2 + a_{23}\Delta z_2 = a_{21}\Delta x + a_{22}\Delta y + a_{23}\Delta z \quad (A-10)$$

$$\Delta r_3 + a_{31}\Delta x_3 + a_{32}\Delta y_3 + a_{33}\Delta z_3 = a_{31}\Delta x + a_{32}\Delta y + a_{33}\Delta z$$

where the various a's are the elements of the 3 x 3 matrix M:

$$M = \begin{bmatrix} \frac{x - x_1}{r_1} & \frac{y - y_1}{r_1} & \frac{z - z_1}{r_1} \\ \frac{x - x_2}{r_2} & \frac{y - y_2}{r_2} & \frac{z - z_2}{r_2} \\ \frac{x - x_3}{r_3} & \frac{y - y_3}{r_3} & \frac{z - z_3}{r_3} \end{bmatrix} = \begin{bmatrix} a_{11} & a_{12} & a_{13} \\ a_{21} & a_{22} & a_{23} \\ a_{31} & a_{32} & a_{33} \end{bmatrix} \quad (A-11)$$

It is convenient to continue the development in matrix form. Rewrite

Equation A-10 as:

$$\begin{bmatrix} 1 & 0 & 0 \\ 0 & 1 & 0 \\ 0 & 0 & 1 \end{bmatrix} \underbrace{\begin{bmatrix} \Delta r_1 \\ \Delta r_2 \\ \Delta r_3 \end{bmatrix}}_{\Delta r} + \underbrace{\begin{bmatrix} a_{11} & a_{12} & a_{13} \\ 0 & 0 & 0 \\ 0 & 0 & 0 \end{bmatrix}}_{M_1} \underbrace{\begin{bmatrix} \Delta x_1 \\ \Delta y_1 \\ \Delta z_1 \end{bmatrix}}_{\Delta S_1} + \underbrace{\begin{bmatrix} 0 & 0 & 0 \\ a_{21} & a_{22} & a_{23} \\ 0 & 0 & 0 \end{bmatrix}}_{M_2} \underbrace{\begin{bmatrix} \Delta x_2 \\ \Delta y_2 \\ \Delta z_2 \end{bmatrix}}_{\Delta S_2} \\
 + \underbrace{\begin{bmatrix} 0 & 0 & 0 \\ 0 & 0 & 0 \\ a_{31} & a_{32} & a_{33} \end{bmatrix}}_{M_3} \underbrace{\begin{bmatrix} \Delta x_3 \\ \Delta y_3 \\ \Delta z_3 \end{bmatrix}}_{\Delta S_3} = \underbrace{\begin{bmatrix} \Delta x \\ \Delta y \\ \Delta z \end{bmatrix}}_{\Delta P} \quad (A-12)$$

Using the abbreviations indicated at the bottom of Equation A-12, the matrix  $\Delta P$  representing errors in vehicle position, may be written:

$$\Delta P \equiv \begin{bmatrix} \Delta x \\ \Delta y \\ \Delta z \end{bmatrix} = M^{-1} (\Delta r + M_1 \Delta S_1 + M_2 \Delta S_2 + M_3 \Delta S_3) \quad (A-13)$$

The covariance matrix representing random errors in vehicle position is obtained by right multiplying both sides of Equation A-13 by their respective transposes and statistically averaging both sides of the resulting matrix equation. Right multiplying both sides of Equation A-13 by their respective transposes, and utilizing the facts that  $(A+B)^T = A^T + B^T$ ,  $(AB)^T = B^T A^T$  yields:

$$\begin{bmatrix} \Delta x \\ \Delta y \\ \Delta z \end{bmatrix} \begin{bmatrix} \Delta x & \Delta y & \Delta z \end{bmatrix} = M^{-1} (\Delta r + M_1 \Delta S_1 + M_2 \Delta S_2 + M_3 \Delta S_3) \quad (A-14) \\
 (\Delta r^T + \Delta S_1^T M_1^T + \Delta S_2^T M_2^T + \Delta S_3^T M_3^T) M^{-1T}$$

After expanding and statistically averaging Equation A-14, matrix products such as  $\Delta r \Delta S_1^T$ ,  $\Delta S_1 \Delta S_2^T$ , etc., vanish by virtue of the assumption of independence in range measurement errors and station position errors.

For example:

$$\Delta r \Delta S_1^T = \begin{bmatrix} \Delta r_1 \\ \Delta r_2 \\ \Delta r_3 \end{bmatrix} \begin{bmatrix} \Delta x_1 & \Delta y_1 & \Delta z_1 \end{bmatrix} = \begin{bmatrix} \Delta r_1 \Delta x_1 & \Delta r_1 \Delta y_1 & \Delta r_1 \Delta z_1 \\ \Delta r_2 \Delta x_1 & \Delta r_2 \Delta y_1 & \Delta r_2 \Delta z_1 \\ \Delta r_3 \Delta x_1 & \Delta r_3 \Delta y_1 & \Delta r_3 \Delta z_1 \end{bmatrix} \quad (A-15)$$

When statistically averaged, all elements of the above matrix vanish, since  $\Delta r_1, \Delta r_2, \Delta r_3, \Delta x_1, \Delta y_1, \Delta z_1$  are all assumed independent. Thus, the only matrix products on the right of Equation A-14 which do not vanish when statistically averaged are those containing  $\Delta r \Delta r^T, \Delta S_1 \Delta S_1^T$ , etc., and these become diagonalized when averaged. The matrix on the left of Equation A-14 when statistically averaged, becomes the desired positional covariance matrix  $\Lambda_P$ \*. Hence,

$$\begin{bmatrix} \sigma_{xx} & \sigma_{xy} & \sigma_{xz} \\ \sigma_{yx} & \sigma_{yy} & \sigma_{yz} \\ \sigma_{zx} & \sigma_{zy} & \sigma_{zz} \end{bmatrix} = \Lambda_P = M^{-1} \left\{ \underbrace{\begin{bmatrix} \sigma_{r_1 r_1} & 0 & 0 \\ 0 & \sigma_{r_2 r_2} & 0 \\ 0 & 0 & \sigma_{r_3 r_3} \end{bmatrix}}_{\Lambda_r} + M_1 \underbrace{\begin{bmatrix} \sigma_{x_1 x_1} & 0 & 0 \\ 0 & \sigma_{y_1 y_1} & 0 \\ 0 & 0 & \sigma_{z_1 z_1} \end{bmatrix}}_{\Lambda_{S_1}} M_1^T + M_2 \underbrace{\begin{bmatrix} \sigma_{x_2 x_2} & 0 & 0 \\ 0 & \sigma_{y_2 y_2} & 0 \\ 0 & 0 & \sigma_{z_2 z_2} \end{bmatrix}}_{\Lambda_{S_2}} M_2^T + M_3 \underbrace{\begin{bmatrix} \sigma_{x_3 x_3} & 0 & 0 \\ 0 & \sigma_{y_3 y_3} & 0 \\ 0 & 0 & \sigma_{z_3 z_3} \end{bmatrix}}_{\Lambda_{S_3}} M_3^T \right\} M^{-1T} \quad (A-16)$$

\*Note that, although  $\Delta r_1, \Delta r_2, \dots, \Delta x_1, \dots, \Delta z_3$  are assumed independent, it is clear from Equation A-10 that  $\Delta x, \Delta y, \Delta z$  are not independent. It is thus necessary to consider the positional covariance matrix for a complete specification of positional errors.

Using the matrix abbreviations indicated at the bottom of Equation A-16. Equation A-16 is written in succinct matrix form as:

$$\Lambda_P = M^{-1} (\Lambda_r + M_1 \Lambda_{S_1} M_1^T + M_2 \Lambda_{S_2} M_2^T + M_3 \Lambda_{S_3} M_3^T) (M^{-1})^T \quad (A-17)$$

where the various matrix symbols are as defined in Equation A-12 and A-16. As written in Equation A-17, the positional covariance matrix  $\Lambda_P$  is readily programmed utilizing standard computer matrix sub-routines. Note also that Equation A-13 gives positional bias errors for specified range bias errors and station location bias errors.

Equations A-13 and A-17 are the matrix equations employed in the AROD Error Evaluation Computer Program to compute positional bias and positional covariance matrix data, respectively. Trajectory data supplied by the orbital computation program (described in Section 2.1) and program inputs are employed in computing the elements of the  $M$ ,  $M_1$ ,  $M_2$ , and  $M_3$  matrices. Program inputs are employed in computing the elements of the  $\Delta r$ ,  $\Delta S_1$ ,  $\Delta S_2$ ,  $\Delta S_3$ ,  $\Lambda_r$ ,  $\Lambda_{S_1}$ ,  $\Lambda_{S_2}$ , and  $\Lambda_{S_3}$  matrices.

### 2.3 Velocity Bias and Covariance Matrix Computations

The relationships between vehicle velocity errors ( $\Delta \dot{x}$ ,  $\Delta \dot{y}$ ,  $\Delta \dot{z}$ ), vehicle position errors ( $\Delta x$ ,  $\Delta y$ ,  $\Delta z$ ), range-rate measurement errors ( $\Delta \dot{r}_1$ ,  $\Delta \dot{r}_2$ ,  $\Delta \dot{r}_3$ ), range measurement errors ( $\Delta r_1$ ,  $\Delta r_2$ ,  $\Delta r_3$ ), and station location errors ( $\Delta x_1$ ,  $\Delta x_2$ , ...,  $\Delta y_2$ , ...,  $\Delta z_3$ ) are obtained from the basic AROD velocity navigation equations as:

$$\begin{aligned} r_1 \Delta \dot{r}_1 + \dot{r}_1 \Delta r_1 &= (x-x_1) \Delta \dot{x} + \dot{x}(\Delta x - \Delta x_1) + (y-y_1) \Delta \dot{y} + \dot{y}(\Delta y - \Delta y_1) \\ &\quad + (z-z_1) \Delta \dot{z} + \dot{z}(\Delta z - \Delta z_1) \\ r_2 \Delta \dot{r}_2 + \dot{r}_2 \Delta r_2 &= (x-x_2) \Delta \dot{x} + \dot{x}(\Delta x - \Delta x_2) + (y-y_2) \Delta \dot{y} + \dot{y}(\Delta y - \Delta y_2) \\ &\quad + (z-z_2) \Delta \dot{z} + \dot{z}(\Delta z - \Delta z_2) \\ r_3 \Delta \dot{r}_3 + \dot{r}_3 \Delta r_3 &= (x-x_3) \Delta \dot{x} + \dot{x}(\Delta x - \Delta x_3) + (y-y_3) \Delta \dot{y} + \dot{y}(\Delta y - \Delta y_3) \\ &\quad + (z-z_3) \Delta \dot{z} + \dot{z}(\Delta z - \Delta z_3) \end{aligned} \quad (A-18)$$

Proceedings as above, re-write Equation A-18 in matrix form:

$$\begin{bmatrix} \dot{r}_1 & 0 & 0 \\ 0 & \dot{r}_2 & 0 \\ 0 & 0 & \dot{r}_3 \end{bmatrix} \begin{bmatrix} \Delta r_1 \\ \Delta r_2 \\ \Delta r_3 \end{bmatrix} + \begin{bmatrix} r_1 & 0 & 0 \\ 0 & r_2 & 0 \\ 0 & 0 & r_3 \end{bmatrix} \begin{bmatrix} \Delta \dot{r}_1 \\ \Delta \dot{r}_2 \\ \Delta \dot{r}_3 \end{bmatrix} = \begin{bmatrix} x-x_1 & y-y_1 & z-z_1 \\ x-x_2 & y-y_2 & z-z_2 \\ x-x_3 & y-y_3 & z-z_3 \end{bmatrix} \begin{bmatrix} \Delta \dot{x} \\ \Delta \dot{y} \\ \Delta \dot{z} \end{bmatrix} \quad (A-19)$$

$$+ \begin{bmatrix} \dot{x} & \dot{y} & \dot{z} \\ \dot{x} & \dot{y} & \dot{z} \\ \dot{x} & \dot{y} & \dot{z} \end{bmatrix} \begin{bmatrix} \Delta x \\ \Delta y \\ \Delta z \end{bmatrix} - \begin{bmatrix} \dot{x} & \dot{y} & \dot{z} \\ 0 & 0 & 0 \\ 0 & 0 & 0 \end{bmatrix} \begin{bmatrix} \Delta x_1 \\ \Delta y_1 \\ \Delta z_1 \end{bmatrix} - \begin{bmatrix} 0 & 0 & 0 \\ \dot{x} & \dot{y} & \dot{z} \\ 0 & 0 & 0 \end{bmatrix} \begin{bmatrix} \Delta x_2 \\ \Delta y_2 \\ \Delta z_2 \end{bmatrix} - \begin{bmatrix} 0 & 0 & 0 \\ 0 & 0 & 0 \\ \dot{x} & \dot{y} & \dot{z} \end{bmatrix} \begin{bmatrix} \Delta x_3 \\ \Delta y_3 \\ \Delta z_3 \end{bmatrix}$$

It is desirable to utilize, in the velocity computations, as many of the matrices employed in the positional computations as possible. Thus, noting that:

$$\begin{bmatrix} \frac{1}{r_1} & 0 & 0 \\ 0 & \frac{1}{r_1} & 0 \\ 0 & 0 & \frac{1}{r_3} \end{bmatrix} \begin{bmatrix} x-x_1 & y-y_1 & z-z_1 \\ x-x_2 & y-y_2 & z-z_2 \\ x-x_3 & y-y_3 & z-z_3 \end{bmatrix} = M$$

and

$$\begin{bmatrix} \frac{1}{r_1} & 0 & 0 \\ 0 & \frac{1}{r_2} & 0 \\ 0 & 0 & \frac{1}{r_3} \end{bmatrix} \begin{bmatrix} r_1 & 0 & 0 \\ 0 & r_2 & 0 \\ 0 & 0 & r_3 \end{bmatrix} = \begin{bmatrix} 1 & 0 & 0 \\ 0 & 1 & 0 \\ 0 & 0 & 1 \end{bmatrix},$$

multiply both sides of Equation A-19 by the matrix

$$\begin{bmatrix} \frac{1}{r_1} & 0 & 0 \\ 0 & \frac{1}{r_2} & 0 \\ 0 & 0 & \frac{1}{r_3} \end{bmatrix}$$

to obtain:

$$\underbrace{\begin{bmatrix} \dot{r}_1 & 0 & 0 \\ \frac{\dot{r}_1}{r_1} & & \\ 0 & \dot{r}_2 & 0 \\ & \frac{\dot{r}_2}{r_2} & \\ 0 & 0 & \dot{r}_3 \\ & & \frac{\dot{r}_3}{r_3} \end{bmatrix}}_Q \underbrace{\begin{bmatrix} \Delta r_1 \\ \Delta r_2 \\ \Delta r_3 \end{bmatrix}}_{\Delta r} + \underbrace{\begin{bmatrix} \Delta \dot{r}_1 \\ \Delta \dot{r}_2 \\ \Delta \dot{r}_3 \end{bmatrix}}_{\Delta \dot{r}} = M \underbrace{\begin{bmatrix} \Delta \dot{x} \\ \Delta \dot{y} \\ \Delta \dot{z} \end{bmatrix}}_{\Delta V} + \underbrace{\begin{bmatrix} \frac{\dot{x}}{r_1} & \frac{\dot{y}}{r_1} & \frac{\dot{z}}{r_1} \\ \frac{\dot{x}}{r_2} & \frac{\dot{y}}{r_2} & \frac{\dot{z}}{r_2} \\ \frac{\dot{x}}{r_3} & \frac{\dot{y}}{r_3} & \frac{\dot{z}}{r_3} \end{bmatrix}}_N \underbrace{\begin{bmatrix} \Delta x \\ \Delta y \\ \Delta z \end{bmatrix}}_{\Delta P} \quad (A-20)$$

$$- \underbrace{\begin{bmatrix} \frac{\dot{x}}{r_1} & \frac{\dot{y}}{r_1} & \frac{\dot{z}}{r_1} \\ 0 & 0 & 0 \\ 0 & 0 & 0 \end{bmatrix}}_{N_1} \underbrace{\begin{bmatrix} \Delta x_1 \\ \Delta y_1 \\ \Delta z_1 \end{bmatrix}}_{\Delta S_1} - \underbrace{\begin{bmatrix} 0 & 0 & 0 \\ \frac{\dot{x}}{r_2} & \frac{\dot{y}}{r_2} & \frac{\dot{z}}{r_2} \\ 0 & 0 & 0 \end{bmatrix}}_{N_2} \underbrace{\begin{bmatrix} \Delta x_2 \\ \Delta y_2 \\ \Delta z_2 \end{bmatrix}}_{\Delta S_2} - \underbrace{\begin{bmatrix} 0 & 0 & 0 \\ 0 & 0 & 0 \\ \frac{\dot{x}}{r_3} & \frac{\dot{y}}{r_3} & \frac{\dot{z}}{r_3} \end{bmatrix}}_{N_3} \underbrace{\begin{bmatrix} \Delta x_3 \\ \Delta y_3 \\ \Delta z_3 \end{bmatrix}}_{\Delta S_3}$$

or, in abbreviated form:

$$Q \Delta r + \Delta \dot{r} = M \Delta V + N \Delta P - N_1 \Delta S_1 - N_2 \Delta S_2 - N_3 \Delta S_3 \quad (A-21)$$

The matrix symbols used in Equation A-21 are defined at the bottom of Equation A-20. Using Equation A-22 for  $\Delta P$ , Equation A-21 becomes:

$$M \Delta V = Q \Delta r + \Delta \dot{r} - N M^{-1} (\Delta r + M_1 \Delta S_1 + M_2 \Delta S_2 + M_3 \Delta S_3) \\ + N_1 \Delta S_1 + N_2 \Delta S_2 + N_3 \Delta S_3$$

$$\begin{aligned}
&= \Delta \dot{r} + (Q - NM^{-1}) \Delta r + (N_1 - NM^{-1}M_1) \Delta S_1 + (N_2 - NM^{-1}M_2) \Delta S_2 \\
&\quad + (N_3 - NM^{-1}M_3) \Delta S_3
\end{aligned} \tag{A-22}$$

Right multiply both sides of Equation A-22 by their respective transposes to obtain:

$$\begin{aligned}
M \begin{bmatrix} \Delta \dot{x} \\ \Delta \dot{y} \\ \Delta \dot{z} \end{bmatrix} \begin{bmatrix} \Delta \dot{x} \\ \Delta \dot{y} \\ \Delta \dot{z} \end{bmatrix}^T M^T &= \left[ \Delta \dot{r} + (Q - NM^{-1}) \Delta r + (N_1 - NM^{-1}M_1) \Delta S_1 + (N_2 - NM^{-1}M_2) \Delta S_2 \right. \\
&\quad \left. + (N_3 - NM^{-1}M_3) \Delta S_3 \right] \left[ \Delta \dot{r}^T + \Delta r^T (Q - NM^{-1})^T \right. \\
&\quad \left. + \Delta S_1^T (N_1 - NM^{-1}M_1)^T + \Delta S_2^T (N_2 - NM^{-1}M_2)^T \right. \\
&\quad \left. + \Delta S_3^T (N_3 - NM^{-1}M_3)^T \right]
\end{aligned} \tag{A-23}$$

Recognizing that all matrix products such as  $\Delta r \Delta S_1^T$  average to zero because of independence of error sources, Equation A-23 becomes, when expanded and averaged:

$$\begin{aligned}
M \Lambda_V M^T &= \Lambda_{\dot{r}} + (Q - NM^{-1}) \Lambda_r (Q - NM^{-1})^T + (N_1 - NM^{-1}M_1) \Lambda_{S_1} (N_1 - NM^{-1}M_1)^T \\
&\quad + (N_2 - NM^{-1}M_2) \Lambda_{S_2} (N_2 - NM^{-1}M_2)^T + (N_3 - NM^{-1}M_3) \Lambda_{S_3} (N_3 - NM^{-1}M_3)^T
\end{aligned}$$

or, finally:

$$\begin{aligned}
\Lambda_V &= M^{-1} \left[ \Lambda_{\dot{r}} + (Q - NM^{-1}) \Lambda_r (Q - NM^{-1})^T + (N_1 - NM^{-1}M_1) \Lambda_{S_1} (N_1 - NM^{-1}M_1)^T \right. \\
&\quad \left. + (N_2 - NM^{-1}M_2) \Lambda_{S_2} (N_2 - NM^{-1}M_2)^T + (N_3 - NM^{-1}M_3) \Lambda_{S_3} (N_3 - NM^{-1}M_3)^T \right] (M^{-1})^T
\end{aligned} \tag{A-24}$$

in which

$$\Lambda_V \equiv \text{Velocity Covariance Matrix} = \begin{bmatrix} \sigma_{\dot{x}\dot{x}} & \sigma_{\dot{x}\dot{y}} & \sigma_{\dot{x}\dot{z}} \\ \sigma_{\dot{y}\dot{x}} & \sigma_{\dot{y}\dot{y}} & \sigma_{\dot{y}\dot{z}} \\ \sigma_{\dot{z}\dot{x}} & \sigma_{\dot{z}\dot{y}} & \sigma_{\dot{z}\dot{z}} \end{bmatrix}$$

$$\Lambda_{\dot{\mathbf{r}}} \equiv \begin{bmatrix} \sigma_{\dot{\mathbf{r}}_1 \dot{\mathbf{r}}_1} & 0 & 0 \\ 0 & \sigma_{\dot{\mathbf{r}}_2 \dot{\mathbf{r}}_2} & 0 \\ 0 & 0 & \sigma_{\dot{\mathbf{r}}_3 \dot{\mathbf{r}}_3} \end{bmatrix} \quad (\text{A-25})$$

and all remaining matrix symbols are as previously defined.

From Equation A-22, the matrix equation giving velocity bias errors in terms of specified range-rate, range, and station location bias errors is:

$$\Delta \mathbf{V} \equiv \begin{bmatrix} \Delta \dot{x} \\ \Delta \dot{y} \\ \Delta \dot{z} \end{bmatrix} = \mathbf{M}^{-1} [\Delta \dot{\mathbf{r}} + (\mathbf{Q} - \mathbf{N}\mathbf{M}^{-1})\Delta \mathbf{r} + (\mathbf{N}_1 - \mathbf{N}\mathbf{M}^{-1}\mathbf{M}_1)\Delta \mathbf{S}_1 + (\mathbf{N}_2 - \mathbf{N}\mathbf{M}^{-1}\mathbf{M}_2)\Delta \mathbf{S}_2 + (\mathbf{N}_3 - \mathbf{N}\mathbf{M}^{-1}\mathbf{M}_3)\Delta \mathbf{S}_3] \quad (\text{A-26})$$

Equations A-21 and A-26 (written in forms that permit rapid programming by means of standard computer matrix sub-routines) are the matrix equations employed in the AROD Error Evaluation Computer Program to compute velocity covariance matrix and velocity bias data, respectively. Trajectory data are employed in computing the elements of the  $\mathbf{Q}$ ,  $\mathbf{N}$ ,  $\mathbf{N}_1$ ,  $\mathbf{N}_2$ , and  $\mathbf{N}_3$  matrices; the elements of the remaining matrices are computed in the manner indicated earlier.

#### 2.4 Covariance Matrix Diagonalization Computations

A complete geometrical interpretation of the covariance matrices  $\Lambda_{\mathbf{P}}$  and  $\Lambda_{\mathbf{V}}$  in terms of error volumes involves matrix diagonalization, i.e., a transformation to principal axes of error. Illustrating for position error, since  $\Lambda_{\mathbf{P}}$  is a symmetric matrix, there exists an orthogonal transformation:

$$\mathbf{C} = \begin{bmatrix} C_{11} & C_{12} & C_{13} \\ C_{21} & C_{22} & C_{23} \\ C_{31} & C_{32} & C_{33} \end{bmatrix} \quad \text{where } \mathbf{C}^{-1} = \mathbf{C}^T \text{ and } |\mathbf{C}| = 1$$

which diagonalizes  $\Lambda_P$  according to the relation:

$$C^T \Lambda_P C = \begin{bmatrix} \lambda_1 & 0 & 0 \\ 0 & \lambda_2 & 0 \\ 0 & 0 & \lambda_3 \end{bmatrix}$$

where the  $\lambda$ 's are the eigenvalues of  $\Lambda_P$ . The determination of the  $\lambda$ 's and the elements of  $C$  is accomplished in the program by a standard subroutine.

The transformation  $C$  has the following property: when applied to rotate the axis system  $\bar{X}, \bar{Y}, \bar{Z}$  (Section 2.1.1) to a new system  $\bar{X}', \bar{Y}', \bar{Z}'$  according to:

$$\begin{bmatrix} \bar{X}' \\ \bar{Y}' \\ \bar{Z}' \end{bmatrix} = C^T \begin{bmatrix} \bar{X} \\ \bar{Y} \\ \bar{Z} \end{bmatrix} \quad (A-27)$$

the trivariate normal distribution of position error becomes independent in the directions  $\bar{X}', \bar{Y}', \bar{Z}'$ . Further, the variances of error in these principal axes directions are the eigenvalues of  $\Lambda_P$ :

$$\begin{aligned} \sigma_{x'x'} &= \lambda_1 \\ \sigma_{y'y'} &= \lambda_2 \\ \sigma_{z'z'} &= \lambda_3 \end{aligned} \quad (A-28)$$

These variances and their corresponding standard deviations  $\sigma_{x'} (= \sqrt{\sigma_{x'x'}} = \sqrt{\lambda_1})$ ,  $\sigma_{y'}$ ,  $\sigma_{z'}$ , are available as part of the program printout.

The program also computes the spatial directions of  $\bar{X}', \bar{Y}', \bar{Z}'$  relative to  $\bar{X}, \bar{Y}, \bar{Z}$  by means of polar spherical azimuth and elevation angles based on the elements of  $C$ . For example, denoting  $A_x$  and  $E_x$  and the azimuth and elevation angles of  $\bar{X}'$ :

$$\bar{X}' = \cos E_x \cos A_x \bar{X} + \cos E_x \sin A_x \bar{Y} + \sin E_x \bar{Z} \quad (A-29)$$

But from A-27 and the definition of  $C$ :

$$\bar{X}' = C_{11} \bar{X} + C_{21} \bar{Y} + C_{31} \bar{Z} \quad (A-30)$$

Thus it follows by equating components in A-29 and A-30 that:

$$A_x = \tan^{-1} \frac{C_{21}}{C_{11}} \text{ and } E_x = \sin^{-1}(C_{31})$$

Similarly the direction angles of  $\bar{Y}'$  and  $\bar{Z}'$  are given by:

$$A_y = \tan^{-1} \left( \frac{C_{22}}{C_{12}} \right), E_y = \sin^{-1}(C_{32})$$

$$A_z = \tan^{-1} \left( \frac{C_{23}}{C_{13}} \right), E_z = \sin^{-1}(C_{33})$$

In the principal axes system, error volumes corresponding to different probability levels  $P$  are ellipsoids defined by equations of the form:

$$\frac{x'^2}{\sigma_{x'x'}^2} + \frac{y'^2}{\sigma_{y'y'}^2} + \frac{z'^2}{\sigma_{z'z'}^2} = K^2$$

where the semiaxes are  $K\sigma_{x'}$  ( $= K\sqrt{\sigma_{x'x'}}$ ),  $K\sigma_{y'}$ ,  $K\sigma_{z'}$ , in the  $\bar{X}'$ ,  $\bar{Y}'$ ,  $\bar{Z}'$  directions, respectively. The probability  $P$  of position error contained in an ellipsoid of size parameter  $K$ , is equivalent to the probability  $P$  that the chi-square variable (for 3 degrees of freedom) is defined by:

$$\chi^2 = \frac{x'^2}{\sigma_{x'x'}} + \frac{y'^2}{\sigma_{y'y'}} + \frac{z'^2}{\sigma_{z'z'}}$$

is less than the value  $K^2$ . The latter probability can be obtained from standard tables of the chi-square distribution; it was from such a table that the relation between  $K$  and  $P$  presented in Figure A-3 was obtained.

Although the initial program runs to be described below were primarily concerned with variations in the overall uncertainty parameters  $\left(\frac{\rho_P}{K}\right)$  and  $\left(\frac{\rho_V}{K}\right)$  (Section 1.2), the detailed geometric error volume data discussed above is available for more complete future analyses if desired.

### 3.0 PROGRAM RUNS AND RESULTS

#### 3.1 Description of Program Runs

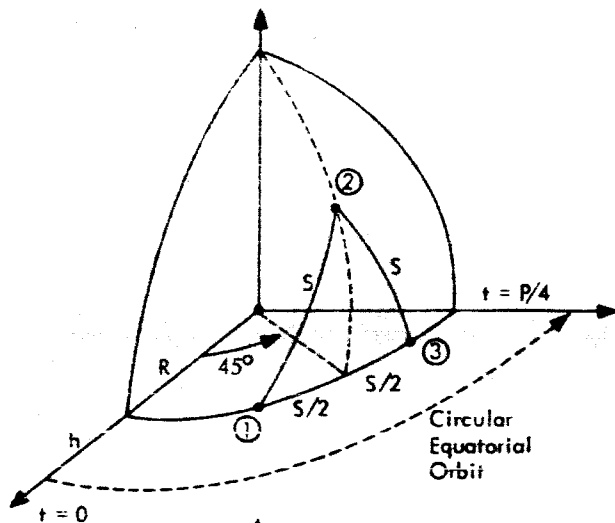
A set of program runs was generated to serve as first tests of overall AROD system performance and to aid in the system design. For purposes of these initial tests, a non-rotating drag-free spherical earth, equatorial circular orbits, and equilateral station arrays were assumed. In addition, standard deviations ( $\sigma_r$ ) in measurement of the three vehicle to station ranges were assumed equal, as were the three standard deviations ( $\sigma_{\dot{r}}$ ) in range-rate measurement, and the nine standard deviations ( $\sigma_{sc}$ ) in specification of station coordinates.

Combinations of three values of orbital altitude ( $h = 90, 500, 2000$  naut. mi.) and three values of (equal) great circle station separation distance ( $S = 300, 500, 1000$  naut. mi.) were incorporated in various runs. For several combinations of ( $h, S$ ), the station array was oriented relative to the vehicle orbital track so as to give three vehicle-to-station array paths. These three paths, and the corresponding station coordinate equations required to properly orient each station, are shown in Figure A-5. The paths illustrated in Figure A-5 were chosen as representative of the effects of vehicle-to-station array geometry, varying from "best" (Path 2) to "worst" (Path 3).

As indicated in Figure A-5, all orbital calculations commenced at  $t = 0$  which corresponds to an initial longitude displacement (from station 2) of  $45^\circ$ . Orbital calculations were performed for an orbit time of about one-quarter of orbital period (25 min for  $h = 90, 500$  naut. mi.; 50 min for  $h = 2000$  naut. mi.). During these time periods, the program utilized only those points within the three-station observation region (defined by  $\epsilon_M$ ) to perform error calculations.

For error source program inputs, several combinations of range-measurement standard deviation ( $\sigma_r$ ), range-rate measurement standard deviation ( $\sigma_{\dot{r}}$ ), and station coordinates standard deviations ( $\sigma_{sc}$ ) from the ranges:

$$\begin{aligned} 1.0 &\leq \sigma_r \leq 10.0 \text{ meters} \\ 0.02 &\leq \sigma_{\dot{r}} \leq 2.0 \text{ meters/sec} \\ 0 &\leq \sigma_{sc} \leq 15 \text{ meters} \end{aligned}$$

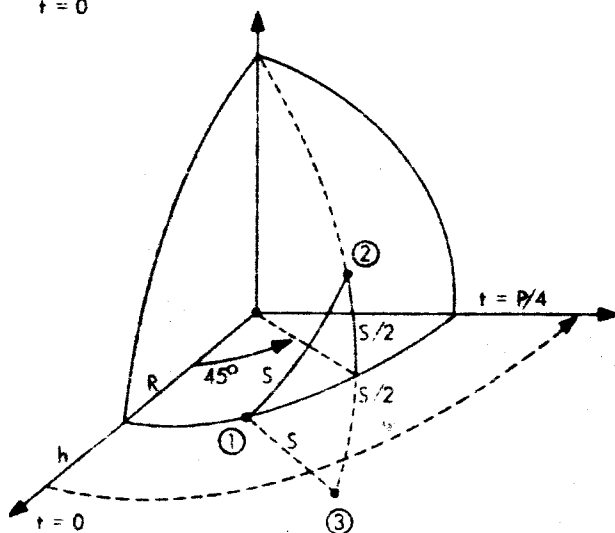


#### Path 1

$$R_1 = R_2 = R_3 = R$$

$$\psi_1 = \psi_3 = 0, \psi_2 = \cos^{-1}[\cos S / \cos(S/2)]$$

$$\lambda_1 = 45^\circ - S/2, \lambda_2 = 45^\circ, \lambda_3 = 45^\circ + S/2$$



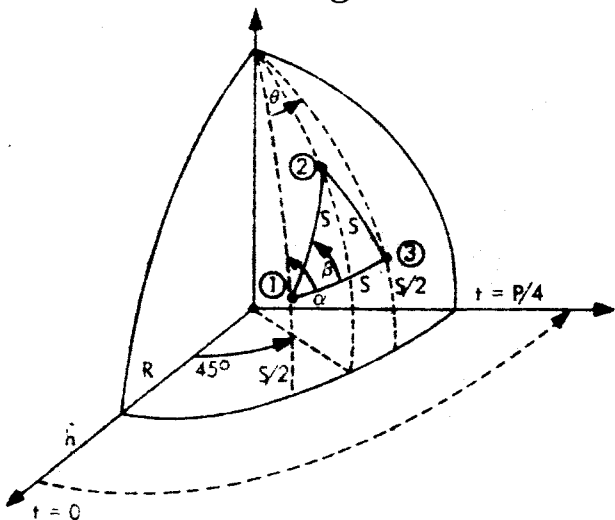
#### Path 2

$$R_1 = R_2 = R_3 = R$$

$$\psi_1 = 0, \psi_2 = S/2, \psi_3 = -S/2$$

$$\lambda_2 = \lambda_3 = 45^\circ$$

$$\lambda_1 = 45^\circ - \cos^{-1}[\cos S / \cos(S/2)]$$



#### Path 3

$$R_1 = R_2 = R_3 = R$$

$$\lambda_1 = 45^\circ - \theta/2, \lambda_2 = 45^\circ, \lambda_3 = 45^\circ + \theta/2$$

$$\psi_1 = \psi_3 = S/2,$$

$$\psi_2 = \cos^{-1}[\sin S \sin(\alpha - \beta) / \sin(\theta/2)]$$

$$\theta = \cos^{-1}\{[\cos S - \sin^2(S/2)] / \cos^2(S/2)\}$$

$$\alpha = \sin^{-1}[\sin \theta \cos(S/2) / \sin S]$$

$$\beta = \cos^{-1}[(\cos S - \cos^2 S) / \sin^2 S]$$

Figure A-5. Test Paths

were chosen. As mentioned earlier, the assumptions  $\sigma_{r1} = \sigma_{r2} = \sigma_{r3}$ ,  $\sigma_{\dot{r}1} = \sigma_{\dot{r}2} = \sigma_{\dot{r}3}$ , and  $\sigma_{sc1} = \sigma_{sc2} = \dots = \sigma_{sc9}$  were incorporated in these first test runs. Range, range-rate, and station location bias errors were assumed zero in all runs. Minimum elevation angles of  $5^\circ$  were assumed for each station.

In general, the above ranges of values for  $h$ ,  $S$ ,  $\sigma_r$ ,  $\sigma_{\dot{r}}$ ,  $\sigma_{sc}$ ,  $\epsilon_M$  were chosen to represent typical anticipated operating values for the AROD system. Table A-1 summarizes the values of orbital altitude, station separation distance, program input quantities, and paths assumed for each test run.

### 3.2 Discussion of Program Results

Some of the results obtained for the computer runs tabulated in Table A-1 have been discussed in Section 2.2 in the main body of this report. Other results obtained during the Feasibility Study are given in Figures A-6 to A-16. Note that in each figure the positional uncertainty parameter  $(\frac{\rho_P}{K})$  and the velocity uncertainty parameter  $(\frac{\rho_V}{K})$  are used as summary measures of system accuracy. In most of the figures, these parameters are plotted as functions of  $t$ , the time from the start of the orbit. The first and last points indicated on each time plot represent the first and last trajectory points lying within the elevation-angle-limited observation region; a direct measure of the total observation interval  $T$  is thus provided on each time plot.

The quantities  $(\frac{\rho_P}{K})$  and  $(\frac{\rho_V}{K})$  are related to position and velocity error volume radii for any probability level  $P$  via Figure A-3. To illustrate, the top curve of Figure A-6 shows a minimum value of 12.5 for  $(\frac{\rho_P}{K})$ . This means that, at this point, vehicle position can be approximated as being within a sphere centered at the true position and having a normalized radius  $\frac{\rho_P}{K} = 12.5$  with (approximate) probability level  $P$  given by Figure A-3 as a function of  $K$ . Thus for  $K = 1$ ,  $P = 0.2$ , and a sphere of radius 12.5 meters corresponds to a positional error probability of 20%, for  $K = 2$ ,  $P = 0.75$  and a sphere of radius  $12.5 \times 2 = 25$  meters corresponding to a 75% probability level, etc. These probability levels are actually associated with ellipsoids

TABLE A-1  
SUMMARY OF TEST RUN CONDITIONS

Run Number	Path	Orbital Altitude h, NM	Station Sep Distance S, NM	Station Location Stnd Dev. $\sigma_{sc}$ , M	Range Measurement Stnd Dev. $\sigma_r$ , M	Range-Rate measurement Stnd Dev., $\sigma_{\dot{r}}$ , M/sec.
1	2	500	500	1	1	0.2
2	↓	↓	↓	↓	3	0.5
3	↓	↓	↓	↓	10	2
4	1	90	↓	↓	3	0.5
5	↓	500	↓	↓	↓	↓
6	↓	2000	↓	↓	↓	↓
7	2	500	↓	3	↓	↓
8	↓	↓	↓	15	↓	↓
9	3	↓	↓	7	↓	↓
10	1	90	300	↓	↓	↓
11	↓	2000	1000	↓	↓	↓
12	2	500	500	3	1	0.2
13	↓	↓	↓	15	10	2
14	↓	↓	↓	3	↓	↓
15	↓	↓	↓	15	1	0.2
16	↓	↓	↓	0	3	0.5
17	1	↓	300	7	↓	↓
18	↓	↓	1000	↓	↓	↓
19	↓	90	↓	↓	↓	↓
20	2	500	500	7	3	0.2
21	↓	↓	↓	↓	10	0.5
22	↓	↓	↓	↓	1	↓
23	↓	↓	↓	↓	3	2
24	↓	↓	↓	0	1	0.2
25	↓	↓	↓	↓	10	2
26	↓	↓	↓	7	1	0.05
27	↓	↓	↓	↓	↓	0.02
28	↓	↓	↓	↓	3	0.05
29	1	↓	↓	↓	↓	↓
30	3	↓	↓	↓	↓	↓
31	1	90	↓	↓	↓	↓
32	2	↓	↓	↓	↓	↓
33	3	↓	↓	↓	↓	↓
34	1	2000	↓	↓	↓	↓
35	2	↓	↓	↓	↓	↓
36	3	↓	↓	↓	↓	↓
37	1	↓	1000	↓	↓	↓
38	2	↓	↓	↓	↓	↓

(see Section 2.4 of Appendix A) rather than with the "equivalent-volume" spheres of radii  $\rho_P$ . For preliminary system evaluation, however, the approximation is made that the same probability levels apply to the spheres.

The effects on system accuracy of varying range and range-rate measurement accuracies ( $\sigma_r$ ,  $\sigma_{\dot{r}}$ ) while preserving constant values of station coordinate standard deviations ( $\sigma_{sc}$ ) can be illustrated by the results shown in Figures A-6 through A-8. Data for these figures correspond to an orbital altitude of  $h = 500$  naut. mi., Path 2, and a station separation of  $S = 500$  naut. mi. (A total observation interval of  $T = 11$  min is noted to occur for these conditions). Range, range-rate standard deviation combinations of (10 m, 2 m/sec), (3 m, 0.5 m/sec), and (1 m, 0.2 m/sec) were used in generating the data given in Figures A-6 through A-8. For Figures A-6, A-7, and A-8, fixed values of  $\sigma_{sc} = 3$  m, 7 m, and 15 m, respectively, were selected.

It is noted from Figures A-6 to A-8 that the maximum, minimum, and average values of both  $(\frac{\rho_P}{K})$  and  $(\frac{\rho_V}{K})$  are reduced as  $\sigma_r$  and  $\sigma_{\dot{r}}$  are reduced. The degree of reduction of  $(\frac{\rho_P}{K})$ , however, is strongly dependent upon the relative magnitudes of  $\sigma_r$  and  $\sigma_{sc}$  as may be noted by comparing the spread of the  $(\frac{\rho_P}{K})$  curves in Figure A-6 with the spread in A-8. Comparison of the corresponding  $(\frac{\rho_V}{K})$  curves indicates that this quantity does not depend as strongly upon the magnitude of  $\sigma_{sc}$  for the range of parameters shown in Figures A-6 to A-8.

The relative insensitivity of  $(\frac{\rho_V}{K})$  to  $\sigma_{sc}$  (for this range of parameter values) is also indicated in Figure A-9, in which time plots of  $(\frac{\rho_P}{K})$  and  $(\frac{\rho_V}{K})$  are given for a fixed combination of  $\sigma_r, \sigma_{\dot{r}} = (3.0 \text{ m}, 0.5 \text{ m/sec})$  and four values of  $\sigma_{sc}$  (0, 3, 7, 15 m). For the  $(\frac{\rho_V}{K})$  scale in Figure A-9, differences in  $(\frac{\rho_V}{K})$  for  $\sigma_{sc} = 0$  and  $\sigma_{sc} = 3.0$  m are imperceptible.

A cross-plot of the data of Figures A-6 to A-9 is given in Figure A-10. Since the general shapes of each set of curves in Figures A-6 to A-9 is approximately preserved in varying  $\sigma_{sc}$ , the minimum values of  $(\frac{\rho_P}{K})$  and  $(\frac{\rho_V}{K})$  may be taken as approximate measures of system performance throughout the observation interval  $T$  for each run. These quantities are plotted as

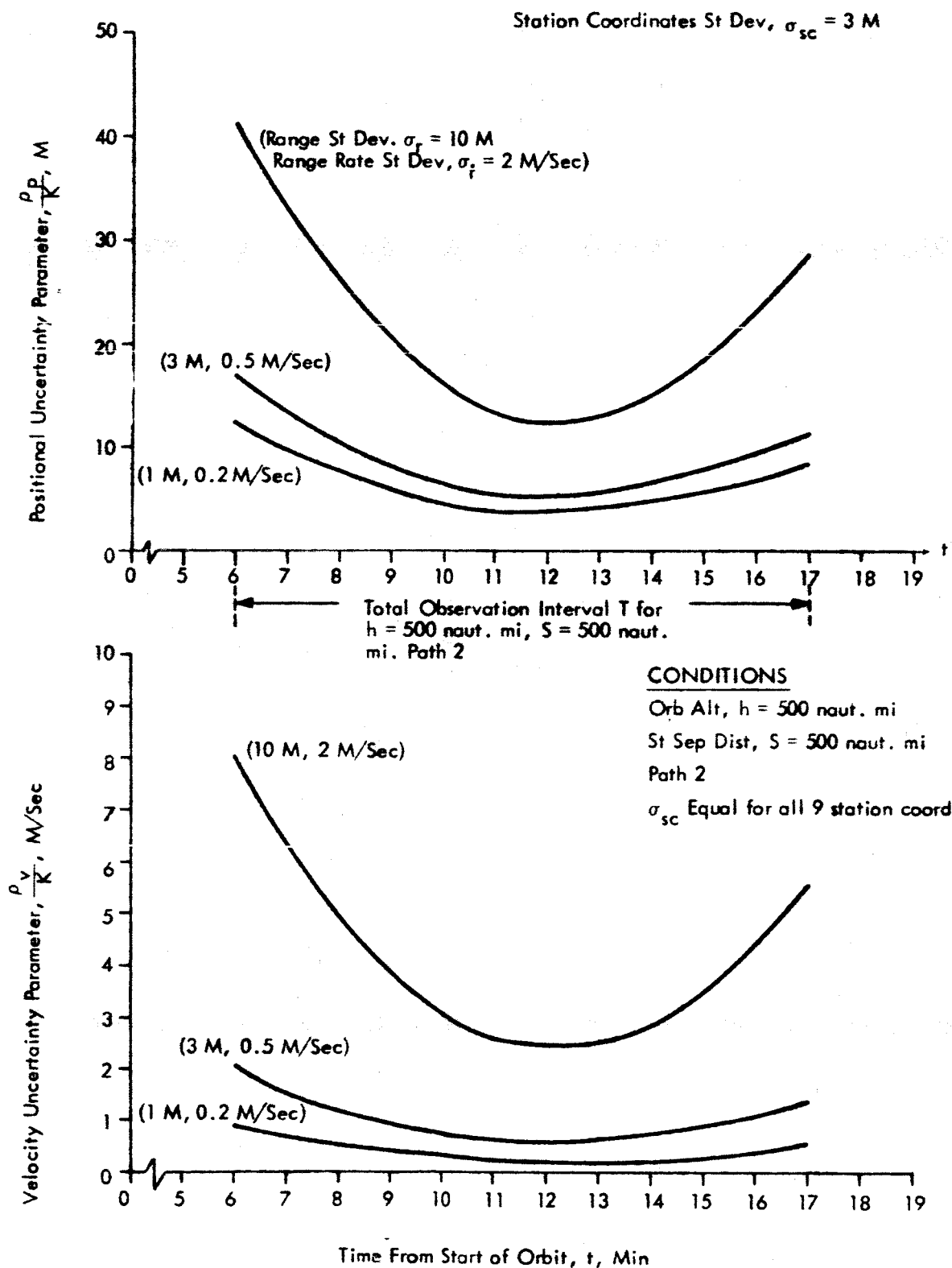


Figure A-6. System Accuracy for Fixed Value of Station Coordinate Standard Deviation ( $\sigma_{sc} = 3\text{M}$ ) and Various Combinations of Range, Range-Rate Standard Deviations (Runs 12, 7, 14)

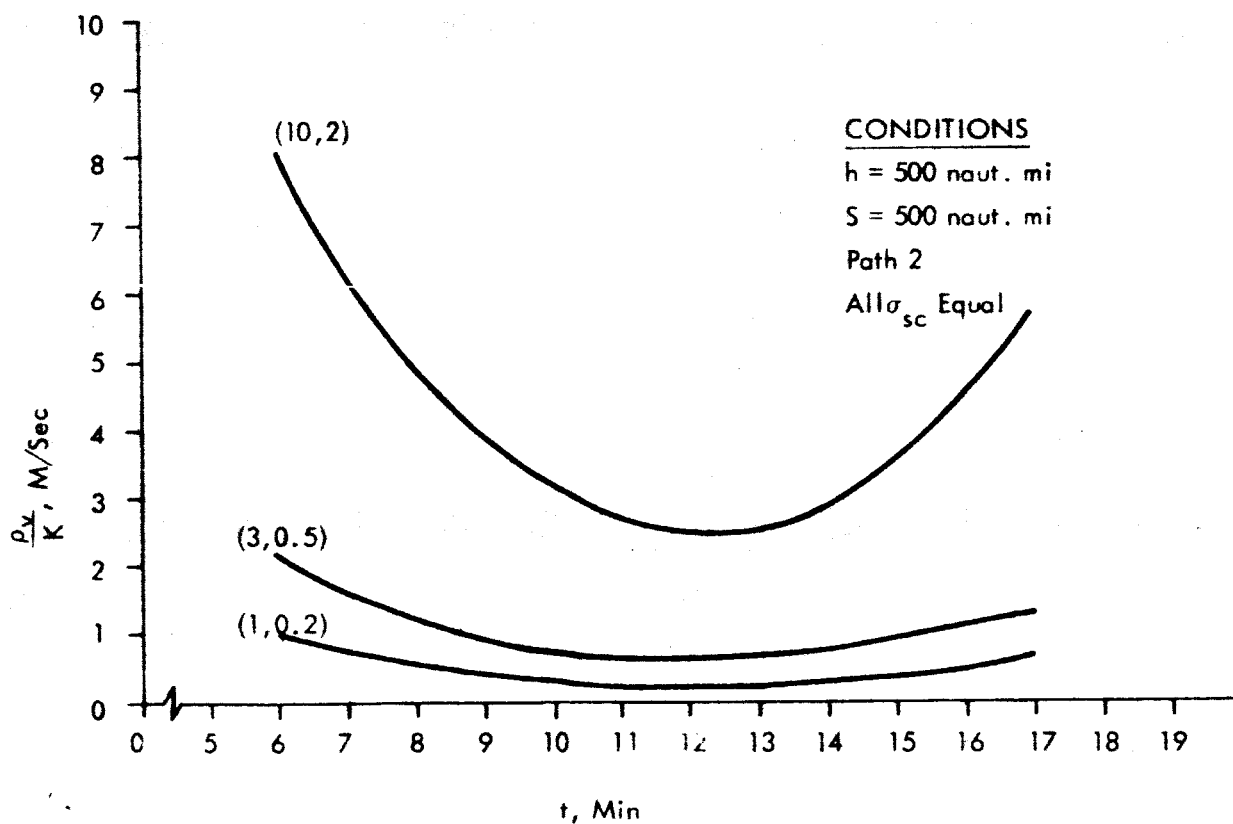
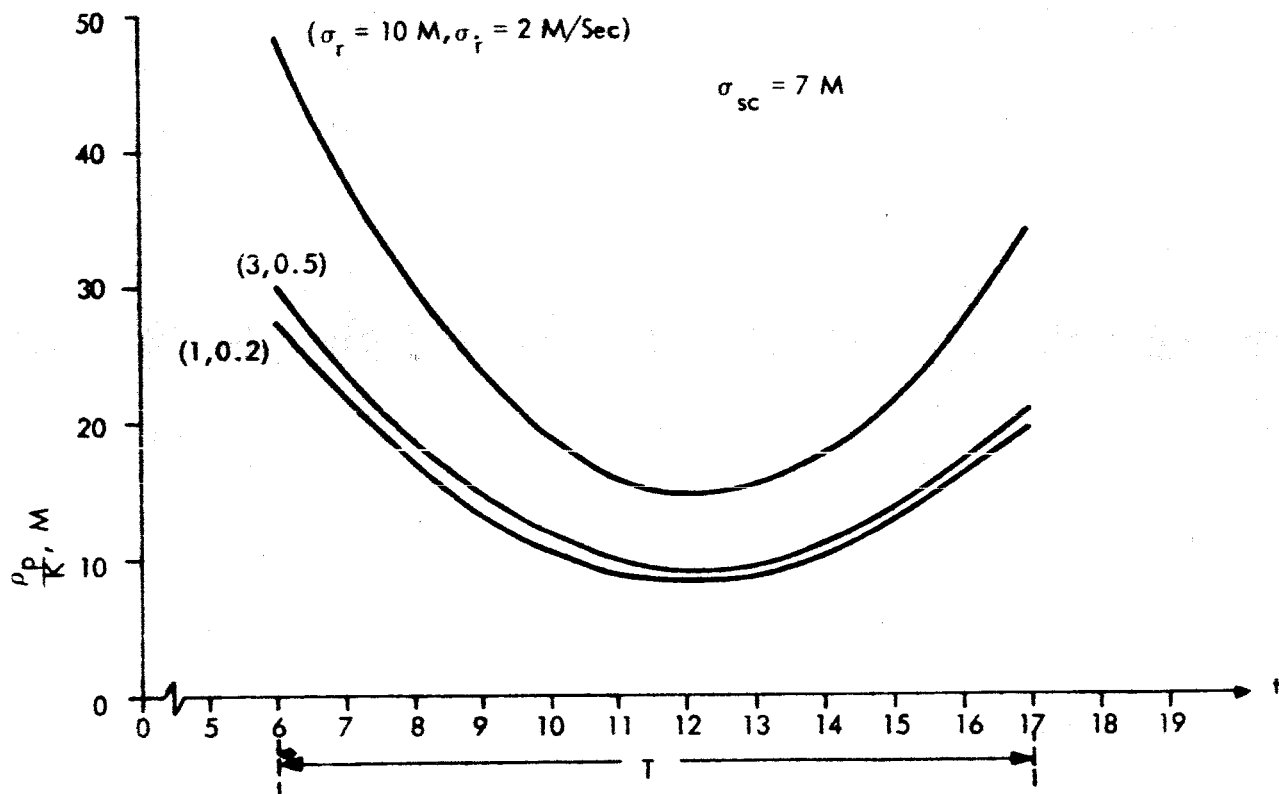


Figure A-7. System Accuracy for Fixed Value of  $\sigma_{sc}$  (7M) and Various Combinations of  $\sigma_r$ ,  $\sigma_{\dot{r}}$  (Runs 1, 2, 3)

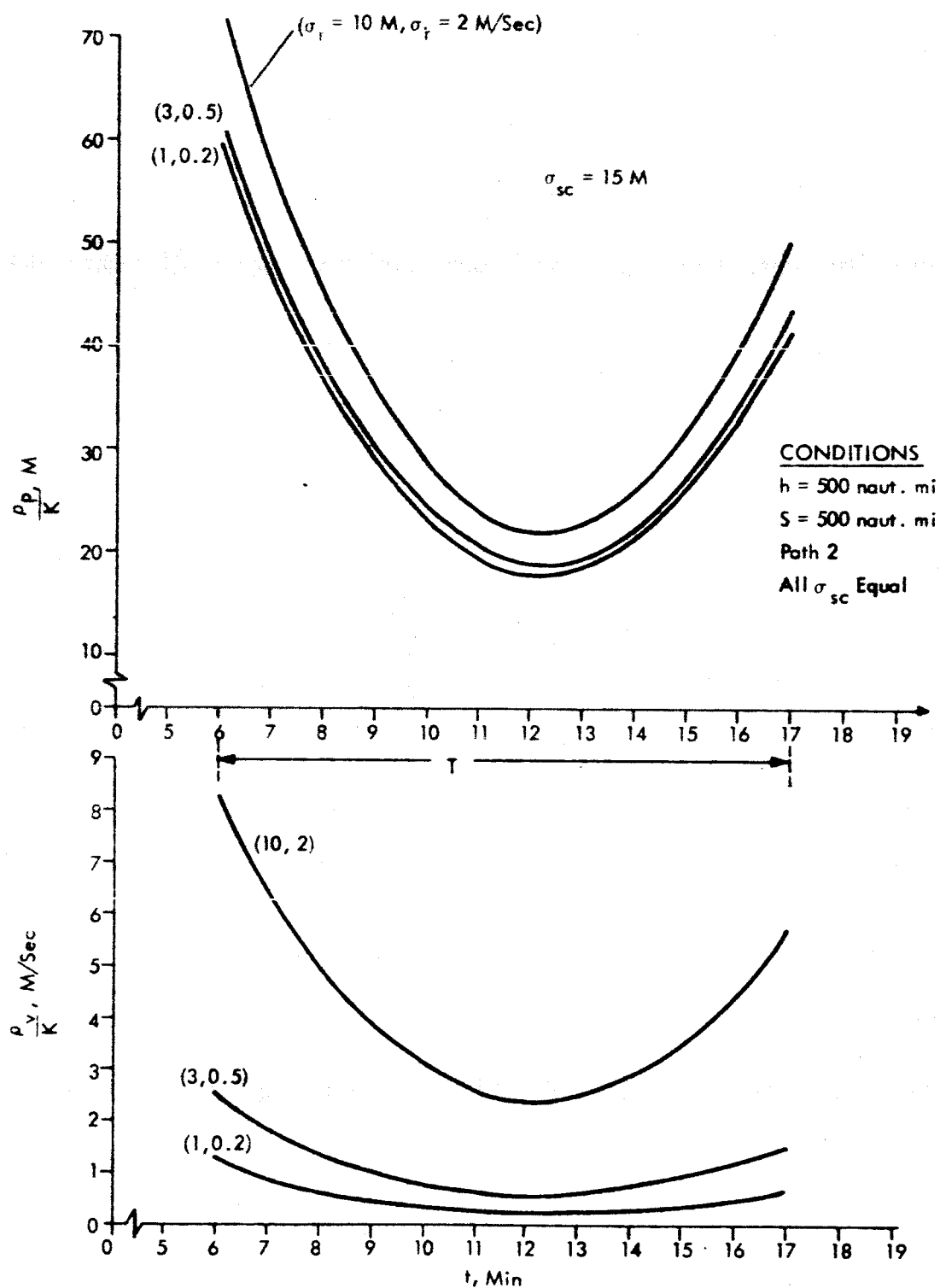


Figure A-8. System Accuracy for Fixed Value of  $\sigma_{sc}$  (15M) and Various Combinations of  $\sigma_{\gamma}$ ,  $\sigma_{\dot{\gamma}}$  (Runs 15, 8, 13)

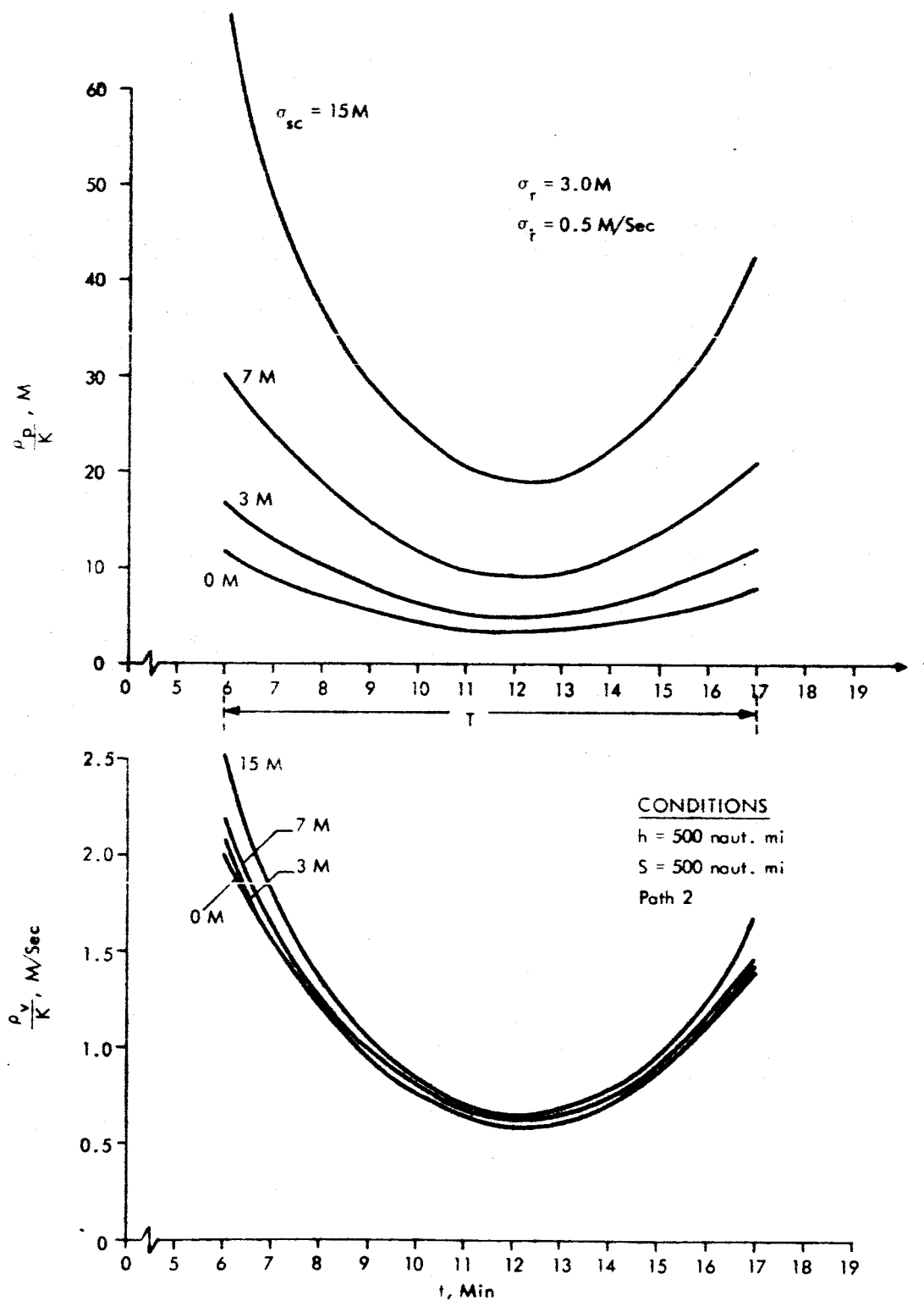


Figure A-9. System Accuracy for Fixed Values of  $\sigma_r$ ,  $\sigma_{\dot{r}}$  (3M, 0.5M/Second) and Various Values of  $\sigma_{sc}$  (Runs 7, 8, 2, 16)

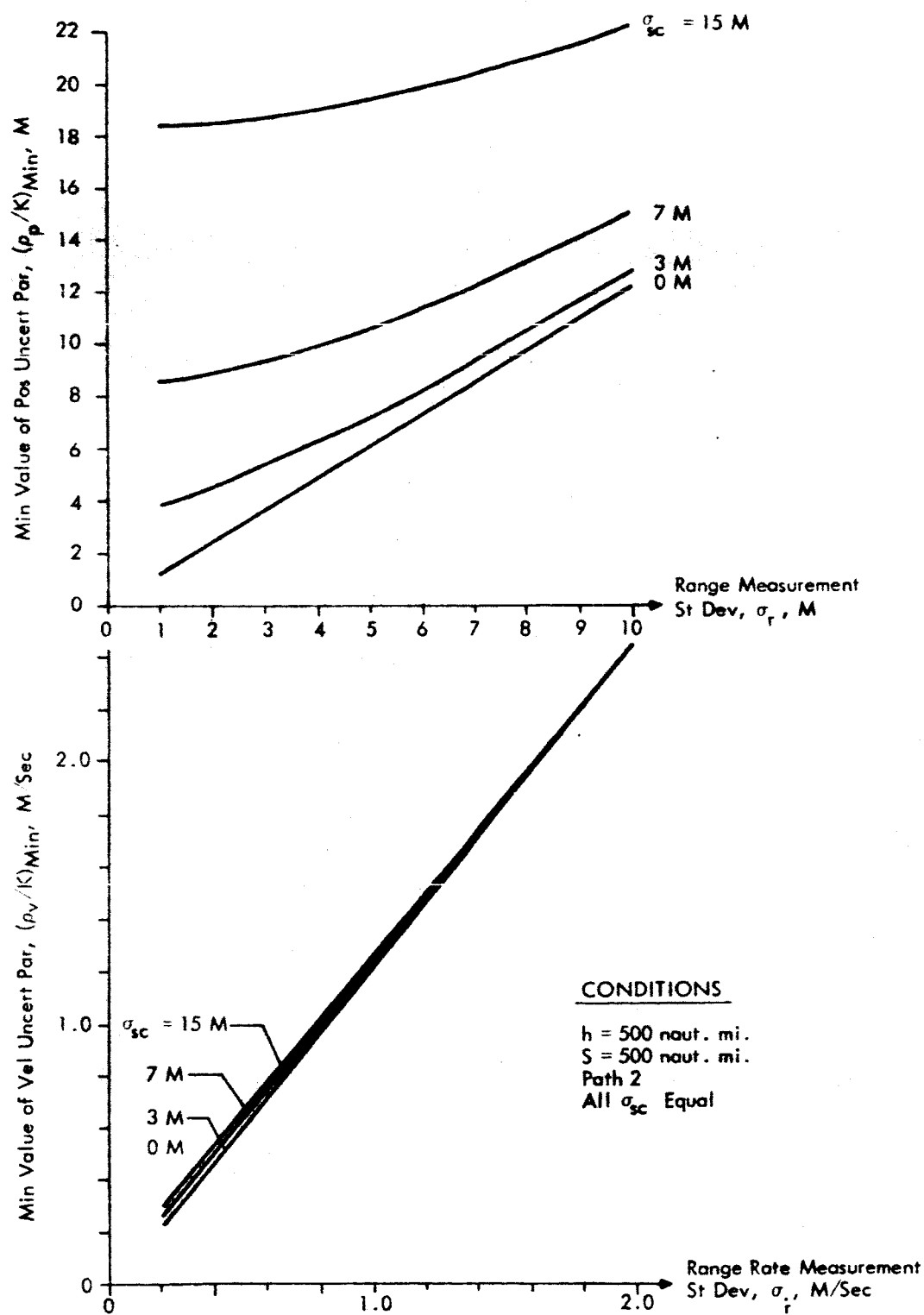


Figure A-10. Influence of  $\sigma_{sc}$  on  $(\rho_p/K)_{\min}$ ,  $(\rho_v/K)_{\min}$  as Functions of  $\sigma_r$ ,  $\sigma_{\dot{r}}$

functions of  $\sigma_r$  and  $\sigma_{sc}$ , respectively,\* for four values of  $\sigma_{sc}$  in Figure A-10. The insensitivity of  $(\frac{\rho V}{K})_{MIN}$  to variations in  $\sigma_{sc}$  is clearly displayed in Figure A-10;  $(\frac{\rho V}{K})_{MIN}$  varies linearly with  $\sigma_r$ , at essentially constant slope, for the values of  $\sigma_{sc}$  depicted. On the other hand, the slope of the quasi-linear variation of  $(\frac{\rho P}{K})_{MIN}$  with  $\sigma_r$  is reduced for large values of  $\sigma_{sc}$ . These preliminary results thus indicate that, for the combination of values of  $(\sigma_r, \sigma_{sc})$  assumed in Figures A-6 to A-9, only small improvements in system performance can be realized by a reduction of  $\sigma_r$  in the presence of relatively large values of  $\sigma_{sc}$ .

An additional cross plot of computer data for the  $h = 500$  naut. mi.,  $S = 500$  naut. mi., Path 2, runs is given in Figure A-11. In this figure, the minimum value of the velocity uncertainty parameter,  $(\frac{\rho V}{K})_{MIN}$ , is plotted as a function of  $\sigma_r$  for a fixed value of  $\sigma_{sc}$  (7.0 m) and several values of  $\sigma_{sc}$ . The data of Figure A-11 shows that, in the range  $1.0 \leq \sigma_r \leq 10$  m,  $(\frac{\rho V}{K})_{MIN}$  is essentially independent of  $\sigma_r$  for the parameter values indicated. Substantial reductions in the magnitude of  $(\frac{\rho V}{K})_{MIN}$ , however, are effected by reducing  $\sigma_r$ . For example, reducing  $\sigma_r$  by a factor of 10 (from 2 m/sec. to 0.2 m/sec.) reduces  $(\frac{\rho V}{K})_{MIN}$  by approximately the same factor (from 2.45 to 0.266 m/sec.).

In summary, the computer runs that have been conducted to analyze the effects of varying measurement errors and station coordinate errors on system performance have indicated that the AROD Error Evaluation Computer Program can be a powerful tool in selecting appropriate parameters for a system design. If the values for station coordinates errors and the mission profile are reasonably well known, intelligent goals for measurement errors can be set with the aid of this program.

An additional series of computer runs were conducted to investigate the influence of orbital altitude and station separation distance on system performance. Figure A-12 gives  $(\frac{\rho P}{K})$  and  $(\frac{\rho V}{K})$  data for a fixed value of  $S = 500$  naut. mi. and three values of  $h$  (90, 500, 2000 naut. mi.). Path 1 was selected to generate the data of Figure A-12 with  $\sigma_r = 3.0$  m,  $\sigma_{sc} = 0.5$  m/sec.

\*For the test runs under consideration in Figures A-6 to A-10, a given value of  $\sigma_r$  was always associated with a particular value of  $\sigma_{sc}$ .

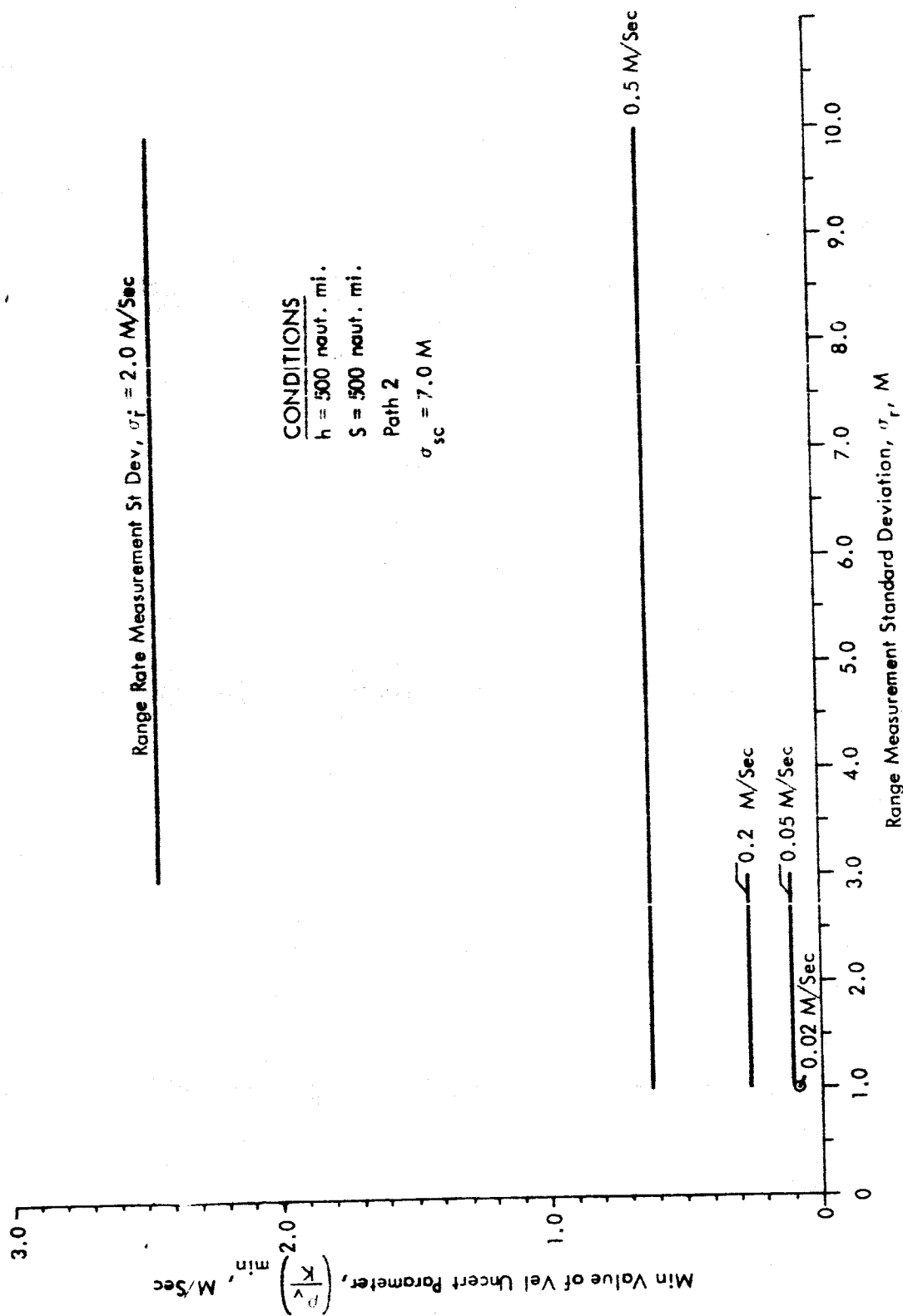


Figure A-11.  $(p_v/K)_{min}$  as Function of  $\sigma_r$  for Fixed Value of  $\sigma_{sc}$  and Several Values of  $\sigma_r$

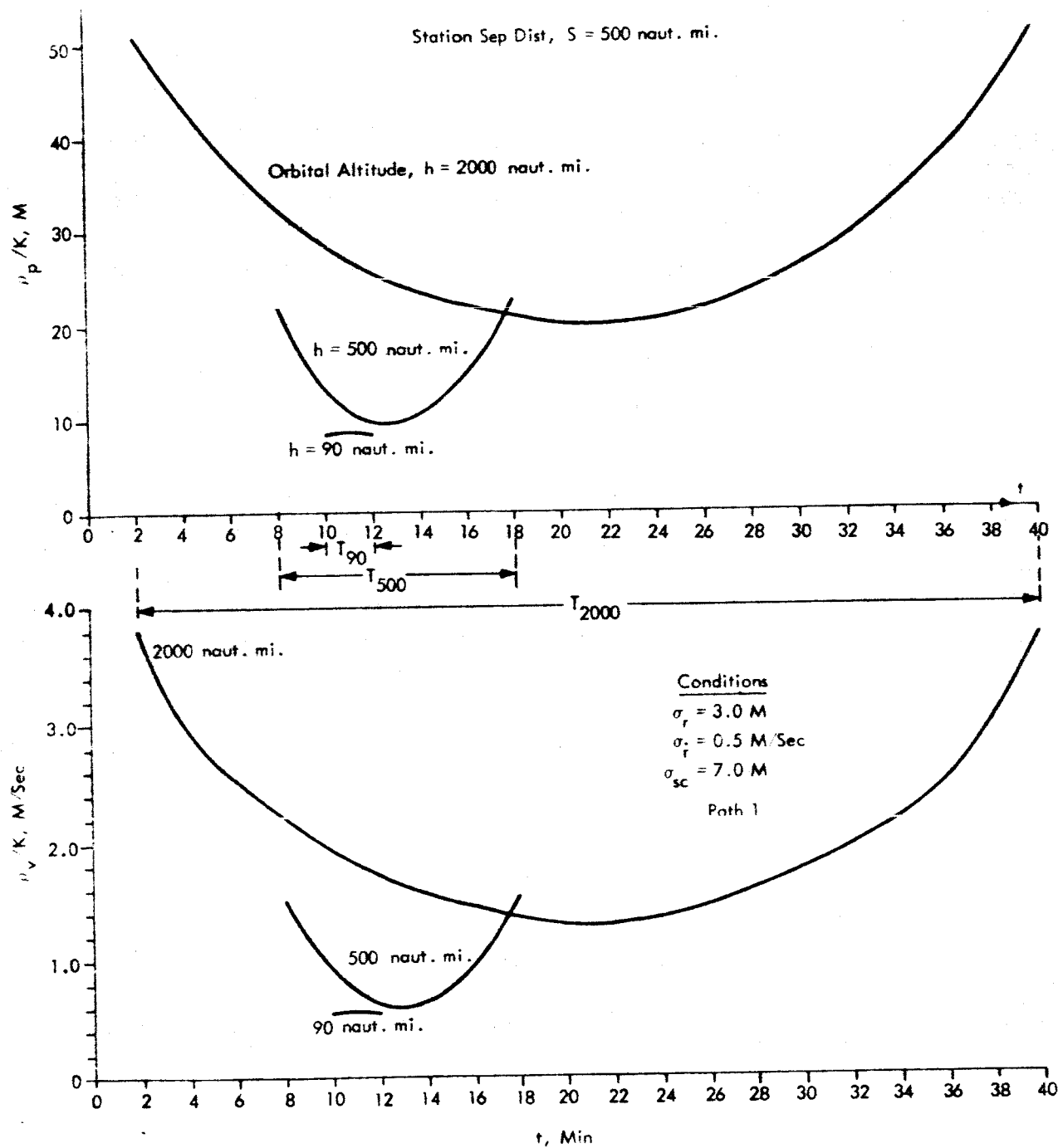


Figure A-12. Effects of Varying Orbital Altitude with Fixed Station Separation Distance (Runs 4, 5, 6)

and  $\sigma_{sc} = 7.0$  m. The shift of the mid-point time for each curve in Figure A-12 is a consequence of the change of orbital angular velocity with orbital altitude  $h$ . Figure A-13, which is a plot of earth distance covered by orbital motion at the three altitudes of Figure A-12, shows that the mid-point of each curve of Figure A-12 occurs at the same distance of approximately 2700 naut. mi.\*

Two effects of increasing  $h$  with  $S$  fixed are indicated in Figure A-12; system accuracy is decreased, and the total observation interval  $T$  is increased.

System performance effects of  $h$  and  $S$  are displayed in an alternative manner in Figures A-14 and A-15 where, for the same path and  $\sigma_r$ ,  $\sigma_{\dot{r}}$ ,  $\sigma_{sc}$  values used in Figure A-12,  $(\frac{\rho_P}{K})$  and  $(\frac{\rho_V}{K})$  are plotted for fixed orbital altitudes and varying station separation distance. In Figure A-14,  $h$  is fixed at 90 naut. mi. and  $S$  is assigned the values 300 naut. mi. and 500 naut. mi.; in Figure A-15,  $h$  is fixed at 2000 naut. mi. and  $S$  is assigned the values 500 naut. mi. and 1000 naut. mi. As  $S$  is increased for a fixed  $h$ , Figures A-14 and A-15 show that the system accuracy is increased at the edges of the coverage region and total observation time is decreased. These effects imply that an "optimum"  $S$  may exist for each  $h$ . However, the cross-over between the  $S = 300$  naut. mi. and  $S = 500$  naut. mi. curves of Figure A-14 indicate that the value selected for the "optimum"  $S$  strongly depends upon the criterion of optimality.

Although the computer runs employed in Figures A-12, A-14, and A-15 are not sufficient to precisely define an over-all optimum combination of  $h$  and  $S$ , the data serve to demonstrate the utility of the AROD Error Evaluation Computer Program in formulating basic system decisions. Following specific definition of the required altitude and operating region for the AROD system, additional computer runs can be performed to quantitatively establish optimum station separation distances.

Additional data obtained to show the effect of vehicle-to-station geometry on  $(\frac{\rho_P}{K})$  and  $(\frac{\rho_V}{K})$  are presented in Figure A-16 for  $h = 500$  naut. mi. and  $S = 500$  naut. mi. The data in Figure A-16 were obtained for the three orbital paths illustrated in Figure A-5, with  $\sigma_r = 3.0$  m,  $\sigma_{\dot{r}} = 0.5$  m/sec, and  $\sigma_{sc} = 7.0$  m.

Figure A-16 indicates that for the orbital paths and altitude chosen, the influence of geometry on system performance is not very strong. For the best

\*This distance is equivalent to an earth-subtended angle of  $45^\circ$ , which represents the mid-point of the baseline between stations 1 and 3 for Path 1 (see Figure A-5).

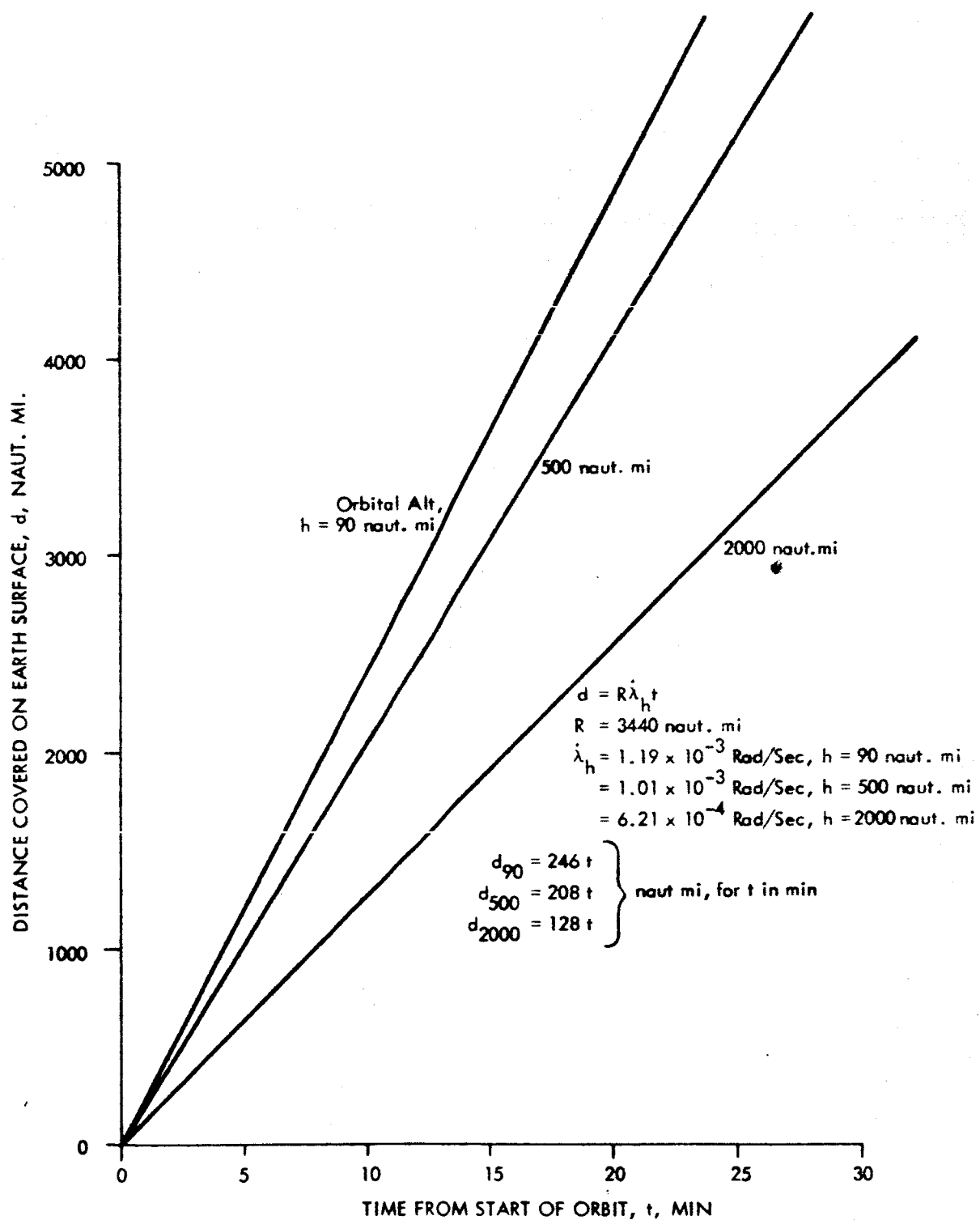


Figure A-13. Distance Covered on Earth Surface for Each Test Orbital Altitude

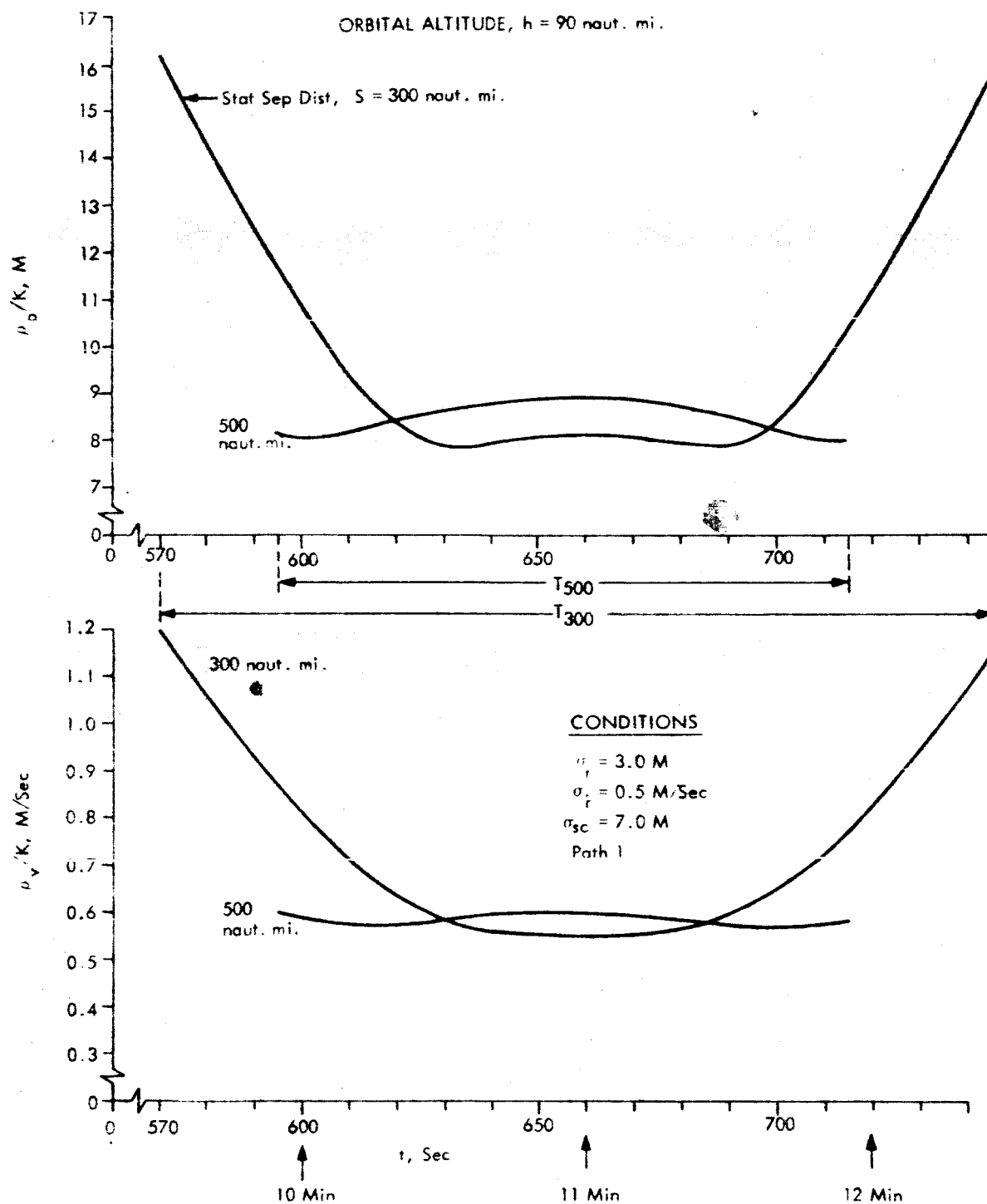


Figure A-14. Effects of Varying Station Separation Distance for Fixed Orbital Altitude ( $h = 90$  nautical miles) (Runs 10, 4)

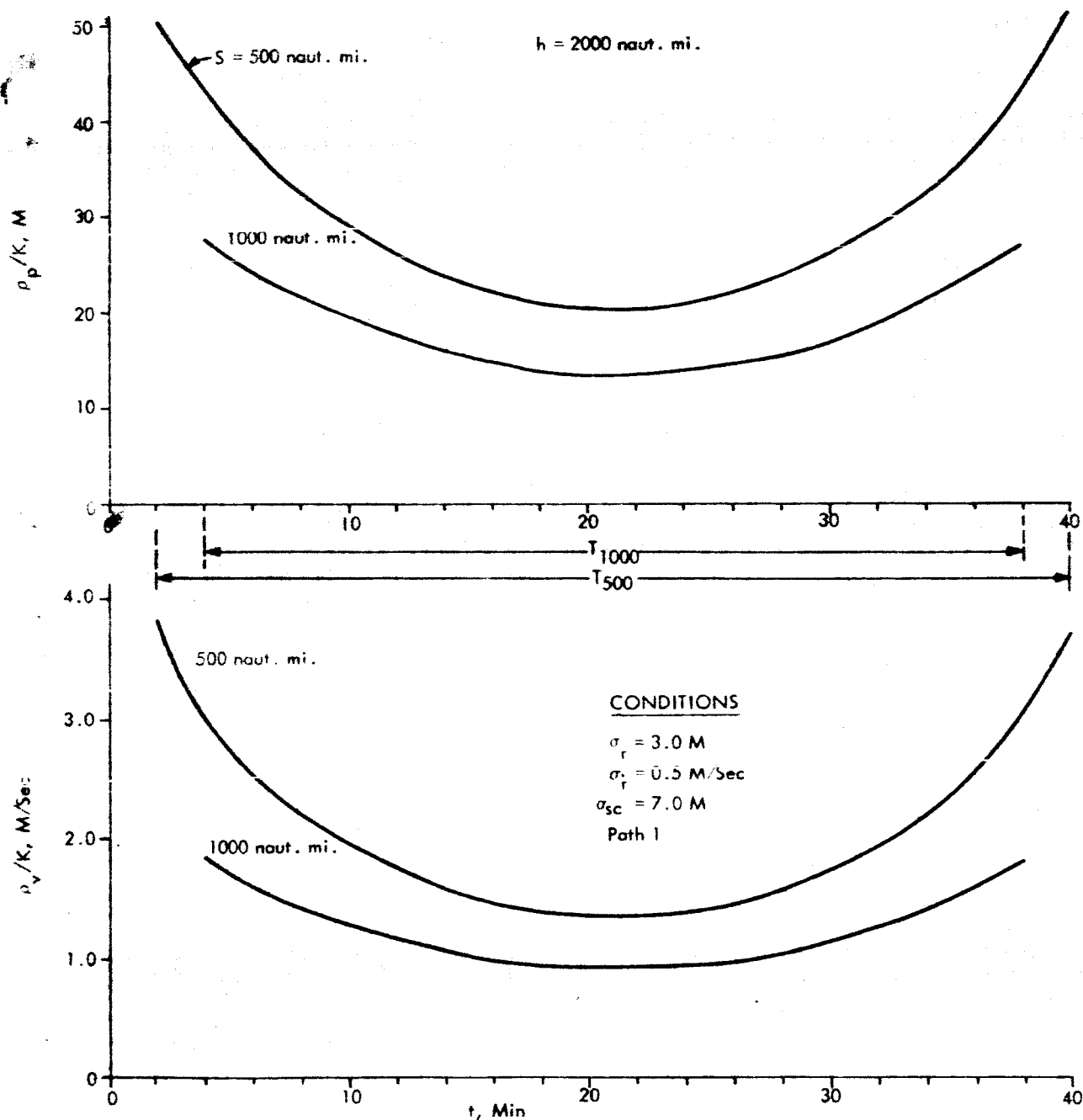


Figure A-15. Effects of Varying Station Separation Distance for Fixed Orbital Altitude ( $h = 2000$  nautical miles), (Runs 11, 6)

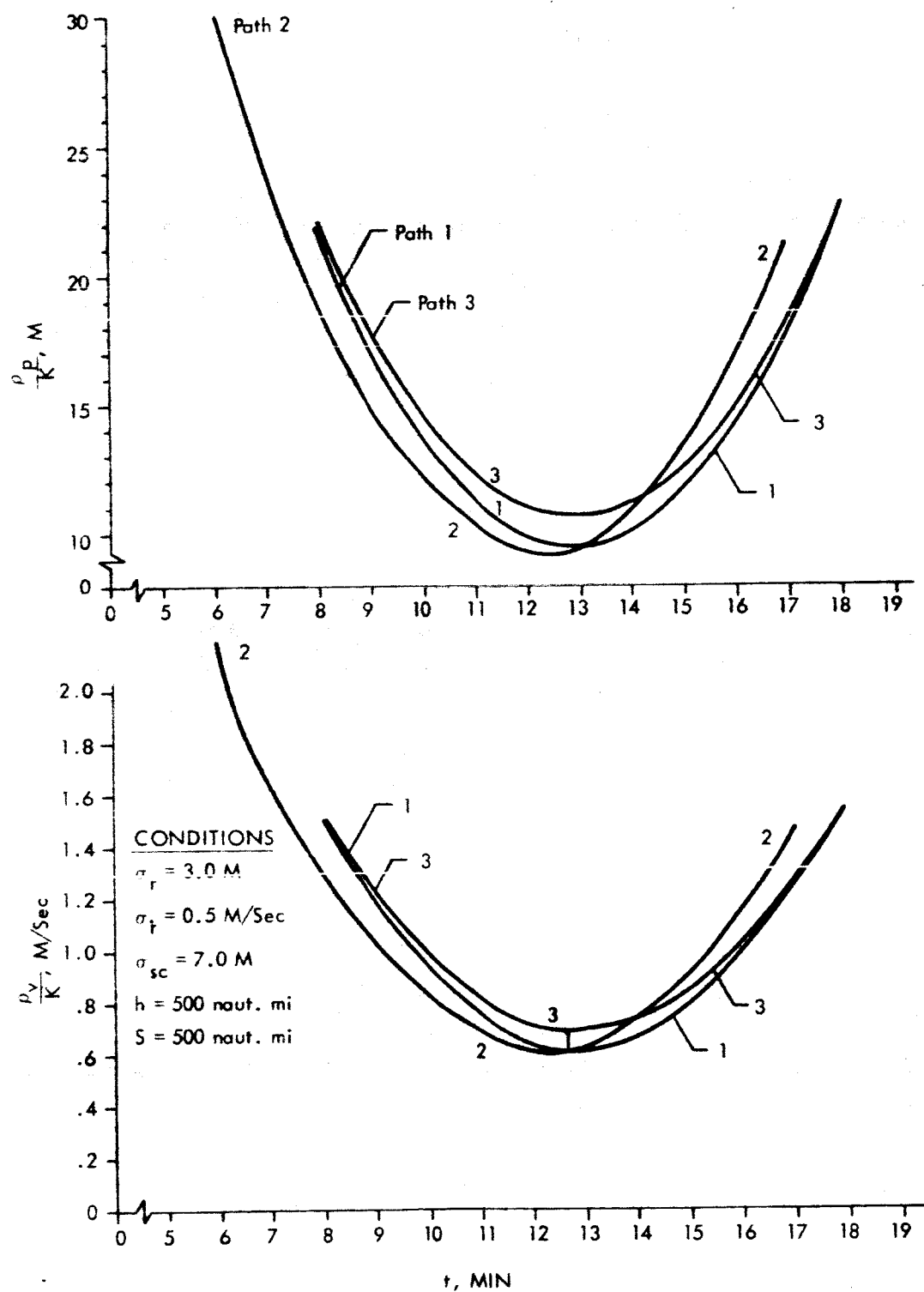


Figure A-16. Effect of Vehicle-to-Sections Relative Geometry (Runs 2, 5, 9)

orbital path (Path 2),  $(\frac{\rho_P}{K})_{\text{MIN}}$  and  $(\frac{\rho_V}{K})_{\text{MIN}}$  are 9.2 m and 0.6 m/sec, respectively, whereas for the worst orbital path (Path 3), these values are 10.8 m and 0.7 m/sec, respectively.

For the wide spectrum of missions anticipated for the AROD system, it is important to quantitatively determine the influence of geometry on system performance. Toward this end, the data of Figure A-16 (and similar data for other h and S combinations and orbital paths such as that contained in Section 2.2 in the main body of this report) will prove most useful.

To summarize, the preliminary computer results given in Figures A-6 through A-16 serve primarily to demonstrate the utility and flexibility of the AROD Error Evaluation Computer Program as a system planning and analysis tool. As the operational envelope and basic ground rules of the AROD system evolve, the computer program will prove an invaluable preliminary design, tactical evaluation, station site location, and overall systems analysis aid.

## Appendix B

### ERRORS INTRODUCED BY THE PROPAGATION MEDIUM

#### 1.0 INTRODUCTION

This appendix estimates the measurement errors introduced by the propagation medium through which the AROD transmissions pass. To accomplish this task, the following is discussed: a description of the Earth's atmosphere and its effects upon electromagnetic energy; equations for corrections to the range measurements; calculations of the magnitude of the corrections; estimates of the residual range errors after application of the corrections; and equations, corrections, and residual errors for the range rate measurements.

It must be emphasized that the magnitudes presented for the residual errors are only estimates. There exists only one set of data<sup>B-1</sup> in a form even approximating that required for AROD. Moreover, these data are based upon important assumptions, and reflect only the Washington, D. C. area. The validity of these assumptions, and the applicability of the data to tropical and sub-tropical climates must be investigated for the operational AROD equipment. However, for the purposes of this Feasibility Study, the assumptions made, and procedure followed by Counter<sup>B-1, B-2</sup> provide satisfactory estimates. Where available, experimental data have generally corroborated the theoretical estimates presented.

#### 2.0 GENERAL EFFECTS OF THE ATMOSPHERE

Propagation of electromagnetic energy through the earth's atmosphere (Figure B-1)<sup>B-3</sup> is affected by: the troposphere, which tends to bend the radiation down toward the horizon; the stratosphere, which has the same

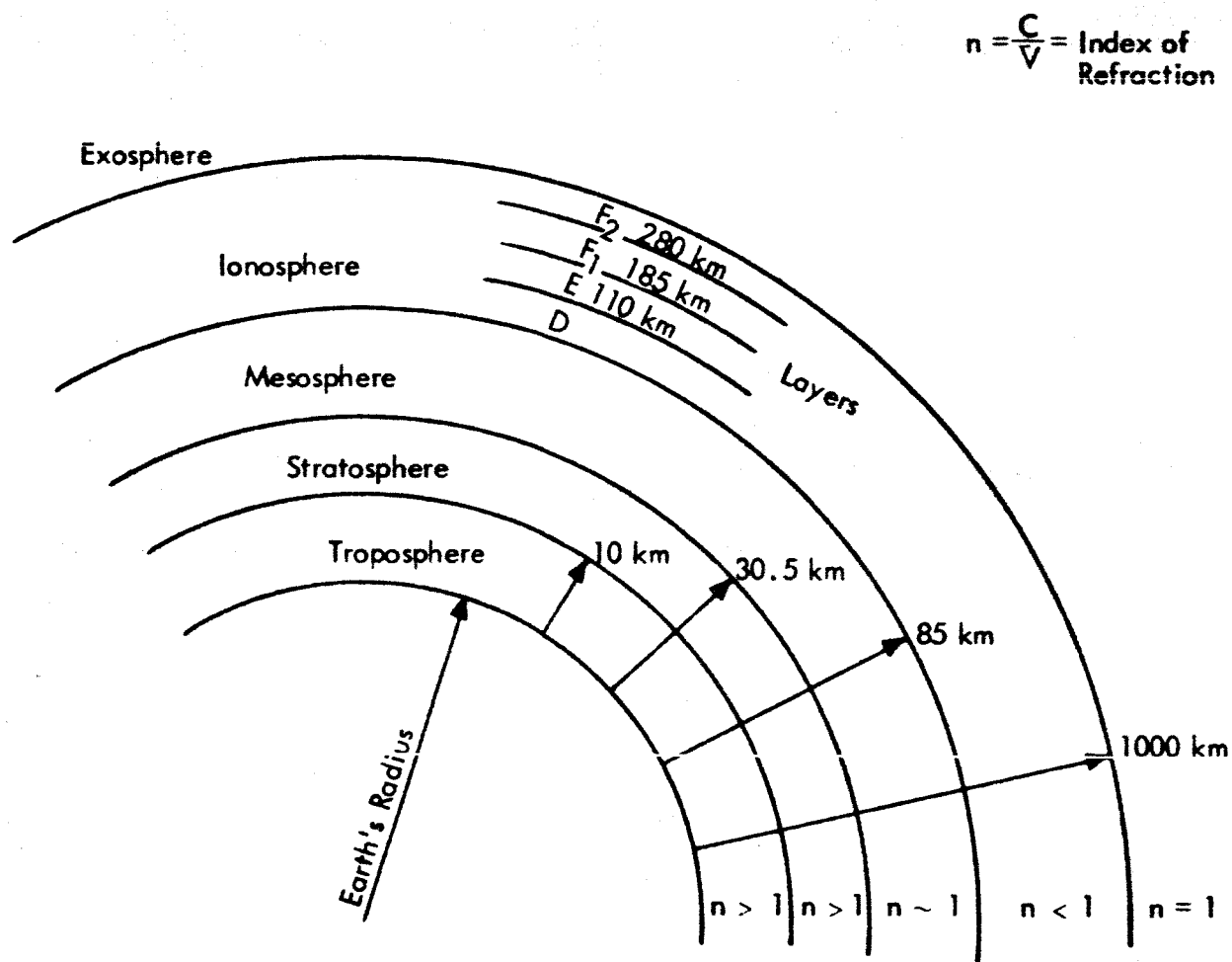


Figure B-1. Structure of the Atmosphere

effect as the troposphere but to a lesser extent; the mesosphere, which behaves quite like free space; the ionosphere, where the ray is bent downward and retarded below the peak index of refraction of the  $F_2$  Layer and bent upwards above the  $F_2$  Layer peak; and the exosphere, which includes the Van Allen belts and other factors with characteristics not well-determined.

The characteristics of the atmosphere have been measured at the surface and up to altitudes of about 100,000 feet by conventional weather observing facilities. Rocket and balloon exploration has been extensive for altitudes up to the ionosphere, while above the base of the ionosphere occasional rocket probes have been used and radio techniques have been in regular use to measure electron densities. Recent efforts to utilize radio transmissions from earth-orbiting satellites, have extended the observations of the ionosphere above the peak of the  $F_2$  Layer.

Table B-1 indicates the U. S. Standard Atmosphere proposed in 1962 for international use. Figure B-2 indicates the variation of index of refraction according to several popular tropospheric models. The 4/3 Earth model is conventionally used by radar engineers, the CRPL model is based on work by Bean and others at the NBS Central Radio Propagation Laboratory in Denver, and the Low Latitude model is based on a statistical study of refraction at tropical and semitropical radiosonde stations for Project Mercury. Figure B-3, Electron Density in the Ionosphere, is based on the Chapman distribution of electron densities<sup>B-3</sup>. Figure B-4, Index of Refraction in the Ionosphere, is derived from Figure B-3 by means of the equation,  $n = 1 - 40 D / f^2$ , where  $D$  is the electron density (electrons per cubic meter),  $f$  is the operating frequency and  $\sqrt{40 D}$  is the critical frequency. Other models of the ionosphere yield a somewhat different distribution of electron densities, particularly above the peak of the  $F_2$  layer (Figure B-5). Superimposed on these models is the seasonal variability (Table B-2) and the variation due to sunspot activity (Figure B-6).

From the foregoing tables and figures considerable uncertainty regarding the true nature of the ionosphere can be seen. In the estimates of range and range rate errors, this uncertainty will be reflected in a larger percentage of residual ionospheric errors remaining after the application of corrections based upon standard profiles.

Table B-1

U. S. Standard Atmosphere, 1962 B-4

	Geometric Height (km)	Geopotential Height (km)	Molecular Scale Temperature (T/M) M <sub>0</sub> (°K)	Temp. Gradient (dT/dh) (°K/km)	Mean Molecular Weight	Kinetic Temperature (°K)	Pressure (mb)	Density (g/M <sup>3</sup> )
TROPO- SPHERE	0.000	0.000	288.15	- 6.5	28.966	288.15	1013.25	1225.0
	11.019	11.000	216.65	0.0	28.966	216.65	226.32	363.92
STRATO- SPHERE	20.063	20.000	216.65	+ 1.0	28.966	216.65	54.747	88.033
	32.162	32.000	228.65	+ 2.8	28.966	228.65	8.6798	13.225
MESO- SPHERE	47.350	47.000	270.65	0.0	28.966	270.65	1.090	1.4275
	52.429	52.000	270.65	- 2.0	28.966	270.65	5.8997 x 10 <sup>-1</sup>	7.5939 x 10 <sup>-1</sup>
	61.591	61.000	252.65	- 4.0	28.966	252.65	1.8209 x 10 <sup>-2</sup>	2.5108 x 10 <sup>-2</sup>
	79.994	79.000	180.65	0.0	28.966	180.65	1.0376 x 10 <sup>-3</sup>	2.0009 x 10 <sup>-3</sup>
	90.000	88.743	180.65	+ 3.0	28.966	180.65	1.6437 x 10 <sup>-3</sup>	3.1698 x 10 <sup>-3</sup>
D LAYER	100.000	98.451	210.65	+ 5.0	28.88	210.02	3.0070 x 10 <sup>-4</sup>	4.9731 x 10 <sup>-4</sup>
	110.000	108.129	260.65	+10.0	28.53	257.00	7.3527 x 10 <sup>-5</sup>	9.8277 x 10 <sup>-5</sup>
	120.000	117.777	360.65	+20.0	28.07	349.49	2.5209 x 10 <sup>-5</sup>	2.4352 x 10 <sup>-5</sup>
	150.000	146.542	960.65	+15.0	26.92	892.79	5.0599 nb	1.8350 x 10 <sup>-6</sup>
	160.000	156.071	1110.65	+10.0	26.66	1022.20	3.6929 nb	1.1584 x 10 <sup>-6</sup>
E LAYER	170.000	165.572	1210.65	+ 7.0	26.40	1103.40	2.7915 nb	8.0330 x 10 <sup>-7</sup>
	190.000	184.485	1350.65	+ 5.0	25.85	1205.40	1.6845 nb	4.3450 x 10 <sup>-7</sup>
F <sub>1</sub> LAYER	230.000	221.968	1550.65	+ 4.0	24.70	1322.30	0.69572 nb	1.5631 x 10 <sup>-7</sup>
	300.000	286.478	1830.65	+ 3.3	22.66	1432.10	188.28 pb	3.5831 x 10 <sup>-8</sup>
F <sub>2</sub> LAYER	400.000	376.315	2160.65	+ 2.6	19.94	1487.40	40.278 pb	6.4945 x 10 <sup>-9</sup>
	500.000	463.530	2420.65	+ 1.7	17.94	1499.20	10.949 pb	1.5758 x 10 <sup>-9</sup>
	600.000	548.235	2590.65	+ 1.1	16.84	1506.10	3.4475 pb	4.6362 x 10 <sup>-10</sup>
	700.000	630.536	2700.65		16.17	1507.60	1.1908 pb	1.5361 x 10 <sup>-10</sup>

0 - 32 km Standard; international agreement

32 - 90 km Tentative; extensive rocket exploration

&gt; 90 km Speculative; additional study may result in significant changes

nb = 10<sup>-6</sup> mbpb = 10<sup>-9</sup> mb

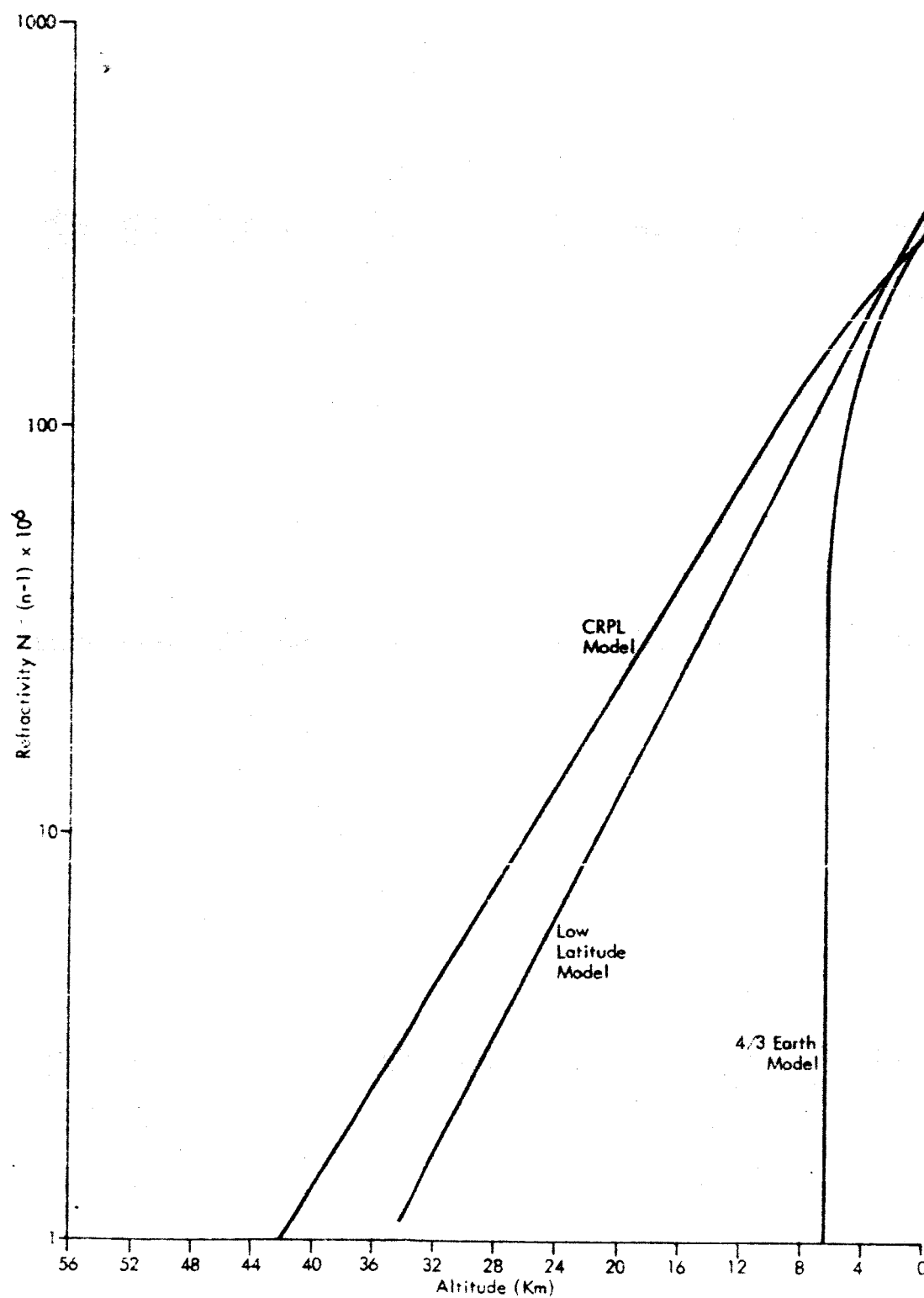


Figure B-2. Index of Refraction for Various Tropospheric Models

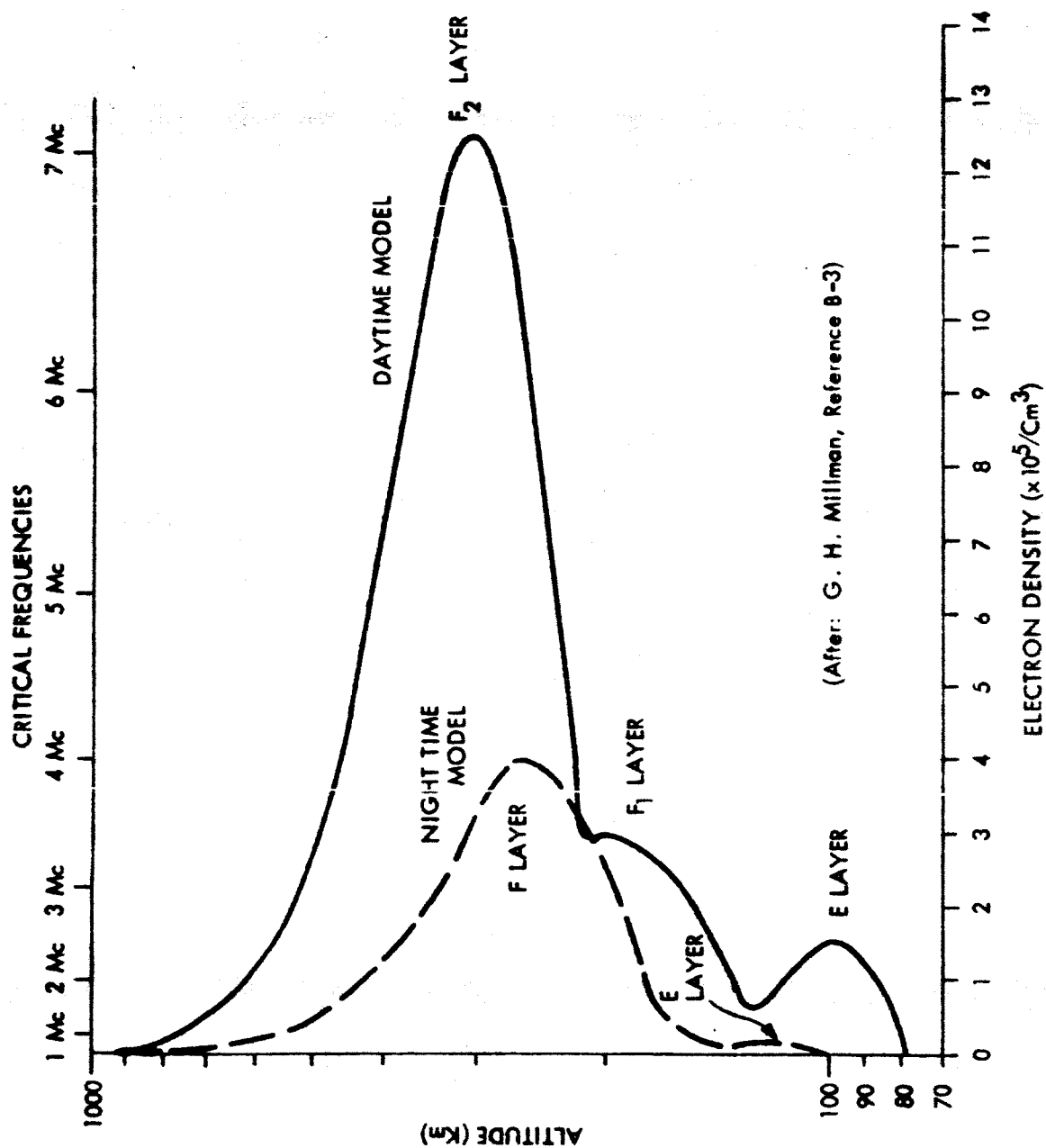


Figure B-3. Electron Density in the Ionosphere (Chapman Distribution)

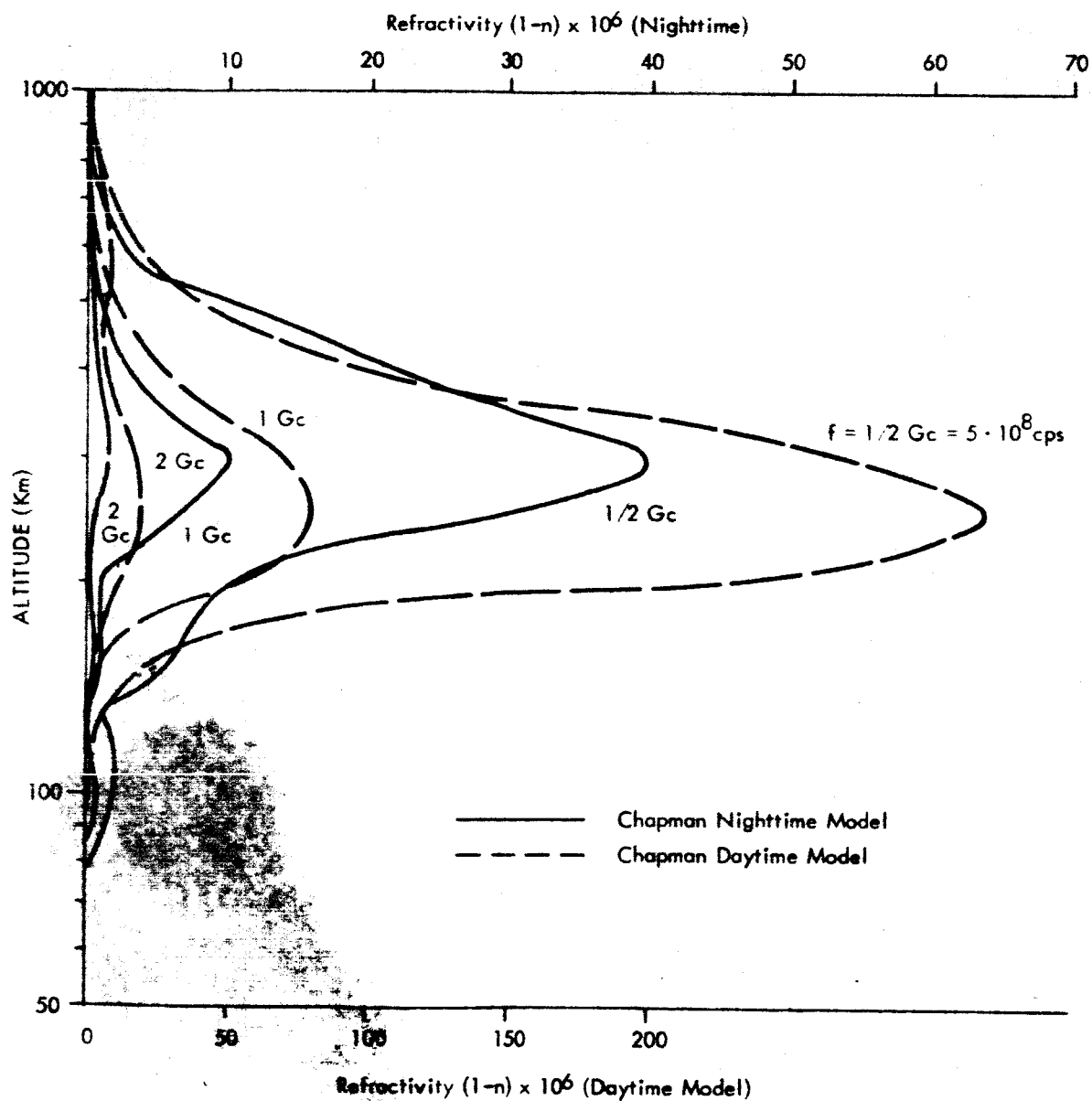


Figure B-4. Index of Refraction in the Ionosphere for Various Frequencies

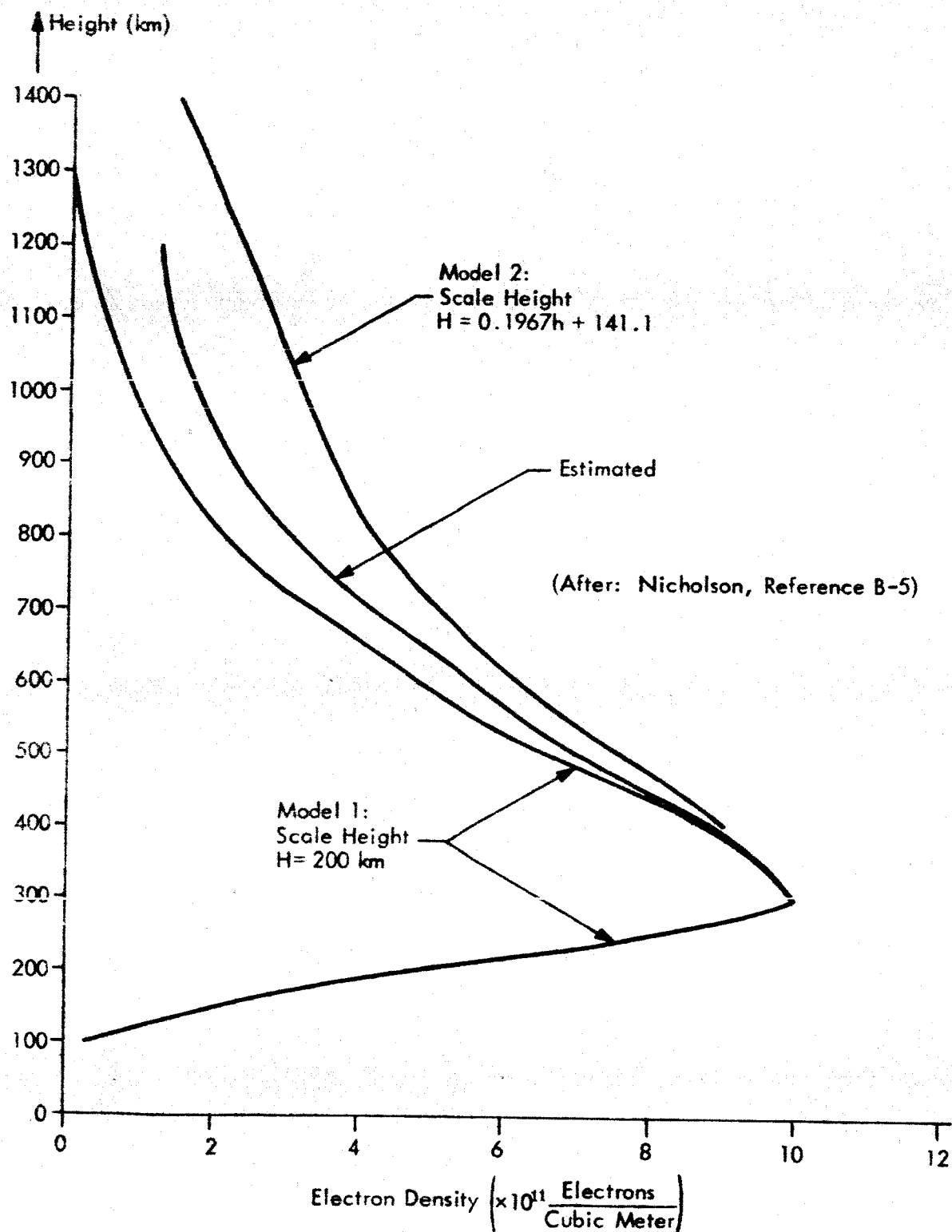


Figure B-5. Estimated and Theoretical Electron Densities in the Ionosphere

TABLE B-2

Mean Critical Frequencies at Washington, D. C. 1959 (Noon)<sup>B-5</sup>

Season	$f_c$ in Mc for $F_2$ Layer	$f_c$ in Mc for E Layer
Spring	12.20	4.00
Summer	7.20	4.80
Fall	9.80	3.80
Winter	13.20	3.28

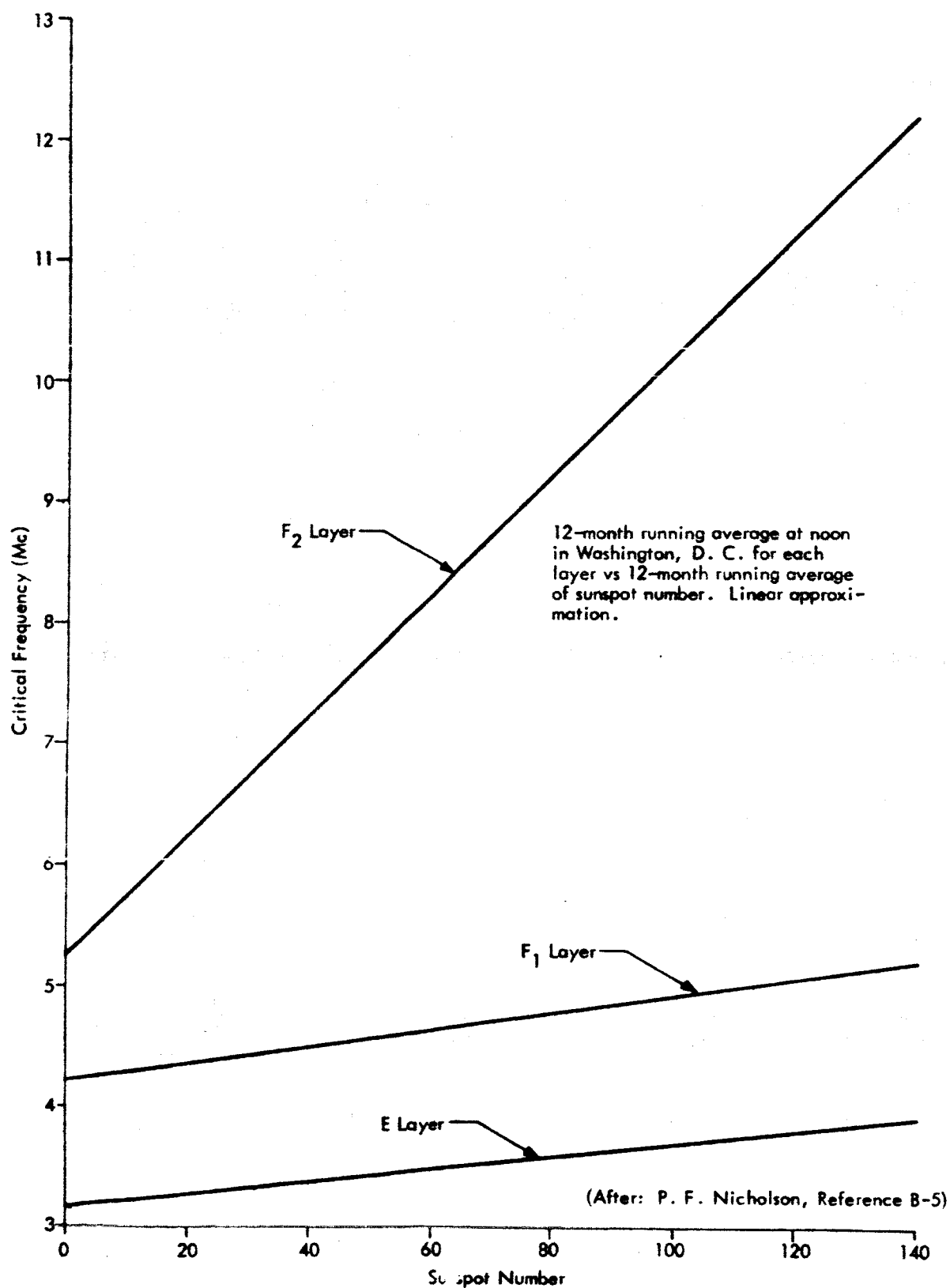


Figure B-6. Critical Frequency vs. Sunspot Number

### 3.0 RANGE ERRORS

#### 3.1 Lower Atmosphere

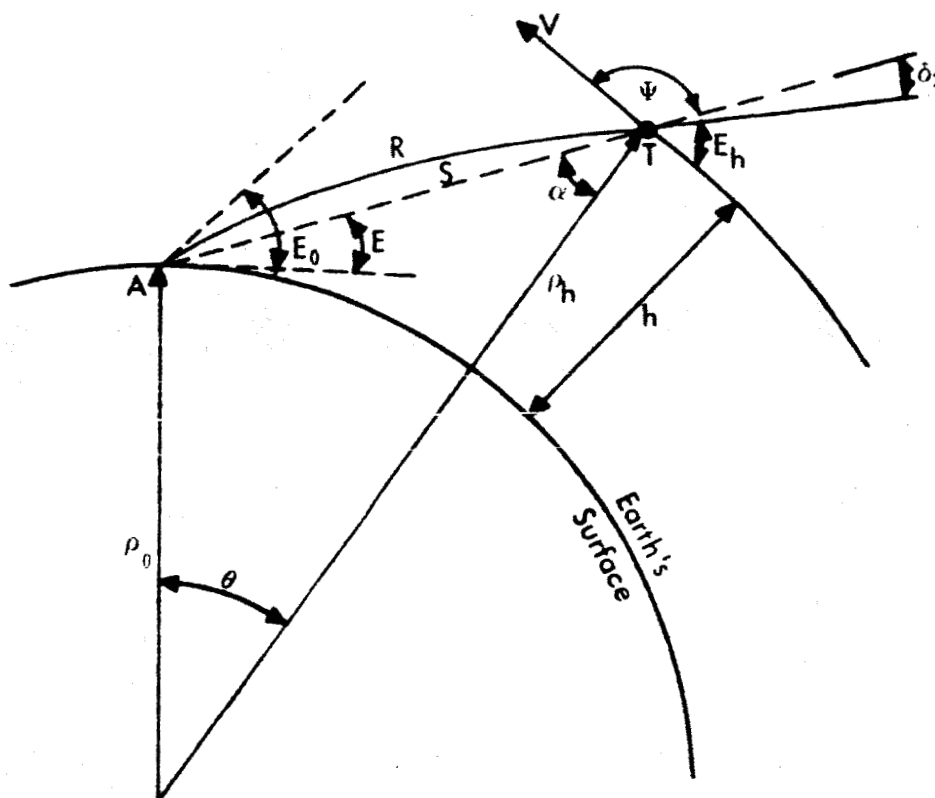
Two errors exist when assuming a range measurement represents the true distance to a given point. First, because of the bending, the energy must follow a curved path which is longer than the straight line path. Second, the energy is propagated through a medium with nonunity index of refraction so that the velocity of propagation is less than the vacuum velocity of light. Also, if the velocity of propagation has been assumed to be equal to the vacuum velocity of light, the apparent path length along the arc would seem to be greater than the true arc length.

It will now be shown that the elongation due to the curvature of the ray is negligible. Consider a ray being propagated through the lower atmosphere where most of the bending occurs in the lower layers. The lower the layer, the greater the bending or, equivalently, the smaller the radius of curvature,  $\frac{1}{K}$ , of the ray. We can get an upper bound on the curvature error of the range measurement by comparing the straight line distance through the first 10,000 ft. of atmosphere with the arc of a ray that has the same radius of curvature as that at the ground level where the curvature is greatest. Using the notation of Figure B-7, S is compared with R, where R is an arc on a circle of radius  $\frac{1}{K}$ . R in this example is an overestimation of the true arc length since the bending diminishes as the ray increases in altitude. In order to have a specific worst case, take a small elevation angle of  $3^\circ$ . From the notation of Figure B-7:

$$S^2 = h^2 + 2\rho_o \rho_h (1 - \cos \theta)$$

$$\theta = \int_{\rho_o}^{\rho_h} \frac{d\rho}{\rho \tan E_h} = 8.65 \text{ mr in this example for } E_o = 3^\circ.$$

Assuming  $h = 10^4$  ft. yields  $S = 17.96 \times 10^4$  ft. Let  $\psi_o$  be the angle subtended by the arc R and the line S in the circle of radius  $\frac{1}{K}$ . Then  $R = \frac{\psi_o}{K}$  and



- A is the ground station.  
 $\rho_0$  is the geocentric radius to the ground station.  
 $E_0$  is the observed elevation angle (arrival angle) of the spacecraft.  
 $h$  is the altitude of the spacecraft.  
 $E_h$  is the elevation angle of the ray path (R) at height  $h$ .  
 $E$  is the elevation angle of the direct line from A to T.  
 $S$  is the geometric length of the straight line  $\overline{AT}$ .  
 The index of refraction  $n = n(\rho)$

Snell's law for spherically symmetric index of refraction is

$$n\rho \cos E_h = l \text{ a constant.}$$

Fermat's rule yields the equation of the path R

$$d\rho/d\theta = \rho/l \sqrt{n^2\rho^2 - l^2}$$

- V is the velocity vector of the spacecraft.

*Figure B-7. Geometry for Ray Bending*

$S = \frac{2}{K} \sin^{-1} \frac{\psi_0}{2}$  or  $2 \sin^{-1} \left( \frac{SK}{2} \right) = \psi_0$  so that  $R = \frac{2}{K} \sin^{-1} \left( \frac{SK}{2} \right)$ . The elongation of the ray due to curvature is then:

$$R - S = \frac{2}{K} \sin^{-1} \left( \frac{SK}{2} \right) - S = \frac{2}{K} \left\{ \frac{SK}{2} + \frac{1}{6} \left( \frac{SK}{2} \right)^3 + \frac{3}{40} \left( \frac{SK}{2} \right)^5 + \dots \right\} - S = \frac{1}{3K} \left( \frac{SK}{2} \right)^3 + \frac{3}{20K} \left( \frac{SK}{2} \right)^5 + \dots$$

The radius of curvature is: <sup>B-6</sup>

$$\frac{1}{K} = \frac{\rho_n^2}{-1 \frac{dn}{d\rho}} = \frac{n_o}{\nu_o \cos E_o}$$

at the ground level for the index of refraction profile  $\nu = \nu_o e^{-\beta h}$  where  $n = \nu + 1$ .

Typical values for the parameters at tropical and semi-tropical latitudes are  $\nu_o = 361.8 \times 10^{-6}$ , and  $\beta = 51.5 \times 10^{-6}/\text{ft}$ . Thus  $\frac{1}{K} \approx 5.36 \times 10^7$  ft. which is about 2.5 times as large as the earth radius but appreciably smaller than the conventional radius of curvature of  $4\rho_o$  appearing in the 4/3 Earth model. This means that the bending is more pronounced than usual.

With the values for S and K fixed, the error due to bending can be computed as:

$$R - S = \frac{5.36 \times 10^7}{3} \left( \frac{17.96 \times 10^4}{2 \times 5.36 \times 10^7} \right)^3 + \left( \frac{3}{20} \right) \left( 5.36 \times 10^7 \right) \left( \frac{17.96 \times 10^4}{2 \times 5.36 \times 10^7} \right)^5 + \dots$$

$$= 0.166 \text{ ft.} + \text{terms of the order of } 10^{-6} \times \text{the first term.}$$

This error is on the order of two inches and can safely be ignored. It is greater than the true error since at 10,000 ft. the radius of curvature is 40% larger. At higher altitudes, the radius of curvature gets larger and the bending less so that the error due to curvature becomes smaller in each higher interval.

In the second source of range deviations, "slowdown" of the wavefront, the error associated with the longer path can be expressed as:  $\Delta R = \int_0^h n dS - \int_0^h dS$ , where dS is an increment of arc length and both integrations are over the Fermat path (Figure B-7). Using the definition  $n = \nu + 1$  and the notation of Figure B-7, we have:

$\Delta R = \int_{\rho_o}^{\rho_h} \frac{\nu d\rho}{\sin E_h}$ . This form is difficult to integrate so a number of simplifications have been tried. Bauer<sup>B-7</sup> suggested the formula:

$\Delta R = \csc E_0 \int_{\rho_0}^{\infty} \nu d\rho$ , since  $\nu$  gets quite small at high altitudes and the tropospheric index of refraction differs imperceptibly from unity. Bauer calls the integral  $T = \int_{\rho_0}^{\infty} \nu d\rho$  the "radio thickness" of the troposphere. With the refraction model  $\nu = \nu_0 e^{-\beta h}$  an integration yields  $T = \frac{\nu_0}{\beta}$ . Substituting "average" values for the lower latitudes it is found  $T = 7.0$  feet, directly overhead.

Using data obtained in a temperate maritime climate, Bauer determined some extremes for the radio thickness at the zenith.

<u>Season</u>	<u>Time of day</u>	<u>Radio Thickness</u>
Winter (March)	2 p.m.	8.44 ft.
Winter (February)	2 p.m.	8.50 ft.
Late Spring	4 a.m.	8.86 ft.
Summer	6:30 a.m.	8.99 ft.
Summer	10 p.m.	9.08 ft.

The extreme values available from low latitude refraction data for the zenith suggest the possible radio thickness range of 4.76 ft.  $< T < 9.85$  ft; however, these extremes have not been correlated and the range may be exaggerated. The extreme deviations from the mean for the low latitude data indicate that the atmospheric shape parameter ( $\beta$ ) contributes almost three times as much error as the surface refractivity ( $\nu_0$ ).

If real time radiosonde observations are available, Bauer (op. cit.) suggests that the variability of the radio thickness looking at the zenith can be reduced to 1/10 ft. At an elevation of  $10^\circ$  this suggests an uncertainty of 4 feet using the simplified formula.

The most extensive statistical analysis of the tropospherically induced range errors is contained in the work of Counter<sup>B-1, 2</sup>. The results of this work are discussed later because of their applicability to the total atmosphere. Counter also computes the "correctability" of the deviations and estimates the residual errors remaining after the application of standard corrections.

### 3.2 Ionosphere

As with other ionospheric effects, the range deviations are frequency-dependent. Observations of a 500 km high satellite at the horizon will yield deviations of the order of 100 meters at 1 Gc<sup>B-7</sup> with the deviation varying inversely with the square of the operating frequency. An observation at the zenith will have a deviation of the order of 10-30 meters at 1 Gc.

Standard corrections usually result in smaller decreases in the ionospheric induced errors than for the troposphere unless account is taken of predicted ionospheric conditions as a function of time of day, season and sunspot number. With these considerations, the range deviation should be reduced by a factor of 1/3 to 1/10<sup>B-7</sup>. If real time ionosondes are available, these deviations should be improved materially.

However, the incorporation of these real-time corrections into the spacecraft computer would result in an important penalty to the vehicle. The approach recommended, therefore, is the use of a standard correction (which takes into account the phase of the sunspot cycle) in conjunction with operation in the kilomegacycle region. (The analysis discussed in Section 3 of the main body of this report resulted in the selection of 2 Gc as the nominal AROD carrier frequency.)

The index of refraction in the ionosphere is given by  $n = 1 - 1/2 \left( \frac{f_c}{f} \right)^2$  where  $f_c$  is the critical frequency and  $f$  is the carrier frequency. The phase velocity  $v = c/n > c$  but the group velocity  $u = \frac{c^2}{v} = nc$ . The time delay in the ionosphere which is manifest as a range deviation is:

$$c\Delta t = \Delta R = c \int_{\text{Path}} \left( \frac{1}{u} - \frac{1}{c} \right) dS = \int \left( \frac{1}{n} - 1 \right) dS \sim \frac{1}{2f^2} \int f_c^2 dS$$

or

$$\Delta R = \frac{1}{2f^2} \int \frac{f_c^2 n r dr}{\sqrt{n^2 r^2 - 1^2}} = \frac{1}{2f^2} \int \frac{f_c^2}{\sin E_h} dr.$$

Snell's law for a spherically symmetric index of refraction will aid the numerical integration of this expression.

Counter<sup>B-1</sup> has determined a set of deviations for the ionosphere at Washington, D. C. (see later discussion), which differ noticeably from those estimated for the arctic ionosphere by Hay and Storey<sup>B-8</sup> (see Table B-3). However, recent experiments have indicated a greater electron density above the peak of the F2 layer than its assumed exponential shape. These experiments suggest that Counter's estimates have to be revised upwards by 30% which would bring his deviations more into line with Hay and Storey's.<sup>B-7</sup> Since additional tests currently underway or planned (e.g., ionospheric topside sounders) will greatly enhance our knowledge of the ionosphere, no revision of Counter's work was attempted at this time.

### 3.3 Range Errors in the Total Atmosphere

Counter<sup>B-1</sup> uses the formula

$$\Delta R = \int_{\rho_0}^{\rho_h} (n-1 + f \frac{\partial n}{\partial f}) \frac{\rho d\rho}{\sqrt{\rho^2 - \rho_0^2} \cos^2 E_0} \quad \text{to determine the range deviation in both the lower atmosphere (where } \frac{\partial n}{\partial f} = 0) \text{ and the ionosphere.}$$

The element of ray path length  $dS = \frac{\rho d\rho}{\sqrt{\rho^2 - \rho_0^2} \cos^2 E_0} \approx dR$  where  $dR$  is an element of chord. With this substitution, the range error becomes:

$$\Delta R = \int_{\rho_0}^{\rho_h} (n-1 + f \frac{\partial n}{\partial f}) dR$$

In the ionosphere  $n = 1 - \frac{f_c^2}{2f^2}$  and the range error is

$$\Delta R = \frac{1}{2f^2} \int_{\rho_I}^{\rho_h} f_c^2 dR$$

where  $\rho_I$  is the base of the ionosphere. Counter refers to this integral as:

$$Q = \int_{\rho_I}^{\rho_h} f_c^2 dR$$

From a statistical analysis of a variety of representative refraction profiles, Counter has indicated (for 1000 Mc) the following: the expected

**TABLE B-3****Range Deviations Caused by the Ionosphere<sup>B-8</sup>**

<b>E (degrees)</b>	<b>h (km)</b>	<b>Range Deviation (<math>\Delta R</math>) (meters)</b>	
		<b>at 500 Mc</b>	<b>at 50 Mc</b>
<b>0</b>	<b>200</b>	<b>4.1</b>	<b>410</b>
<b>0</b>	<b>920</b>	<b>86.8</b>	<b>8680</b>
<b>90</b>	<b>750</b>	<b>24.9</b>	<b>2490</b>
<b>90</b>	<b>1200</b>	<b>25.3</b>	<b>2530</b>

range deviation ( $\overline{\Delta R}$ ) for the total atmosphere (Figure B-8); a standard correction,  $\chi(\Delta R)$  (Figure B-9); the standard error,  $\sigma_s(\Delta R)$ , remaining after applying the standard correction (Figure B-10)\*; and the standard error,  $\sigma_m(\Delta R)$ , remaining after the use of the surface index of refraction ( $n_s$ ) in the correction (Figure B-11)\*. In addition, Counter has computed the effects of the troposphere on any frequency ( $x$  Mc) as shown in Figure B-12. Above 100 Mc, each of the range variables ( $\overline{\Delta R}$ ,  $\chi(\Delta R)$ ,  $\sigma_s(\Delta R)$ , or  $\sigma_m(\Delta R)$ ) can be expressed as:

$$V_f = V_x + (V_{1000} - V_x) \left( \frac{1000}{f} \right)^2$$

where:  $V_f$  is  $\overline{\Delta R}$ ,  $\chi(\Delta R)$ ,  $\sigma_s(\Delta R)$ , or  $\sigma_m(\Delta R)$  at a signal frequency  $f$  (in Mc); and  $V_x$  represents the same variable at  $x$  Mc.

From these formulas and Figures B-10 and B-12, residual range errors (after a standard correction that does not use the surface refractivity) introduced by the propagation medium have been computed for 2000 Mc.\*\* These errors are shown in Figure B-13 for vehicles at altitudes of 90,500, and 2000 naut. mi. to illustrate the extremes of the AROD operating envelope.

#### 4.0 RANGE RATE ERRORS

Because of the effects of the propagating medium, the measured value of doppler frequency will also differ from the true value. The principal cause of this difference is the angle ( $\delta_2$  in Figure B-7) between the line-of-sight from the spacecraft to the ground station and the (curved) path followed

\*The scales for the range error in Figures B-10 and B-11 differ from those in Counter because of an error in Reference B-1. This correction was obtained via a personal communication with Mr. Counter.

\*\*As discussed in more detail in Section 3 of the main body of this report, this frequency has been selected as the nominal AROD carrier frequency because it is the best compromise among propagation errors, vehicle equipment weight and efficiency, and ground station complexity.

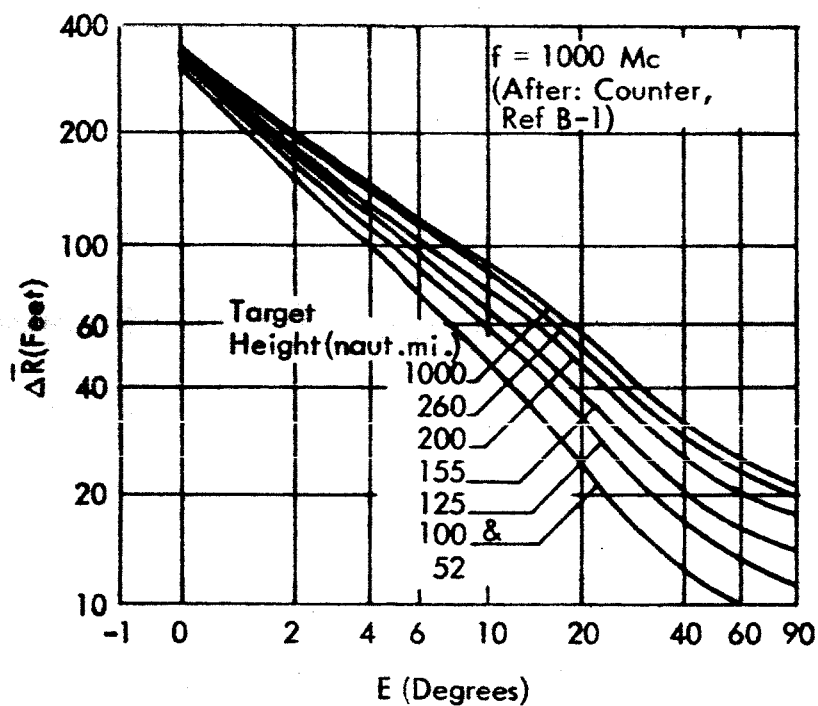


Figure B-8. Expected Range Deviation,  $\Delta \bar{R}$

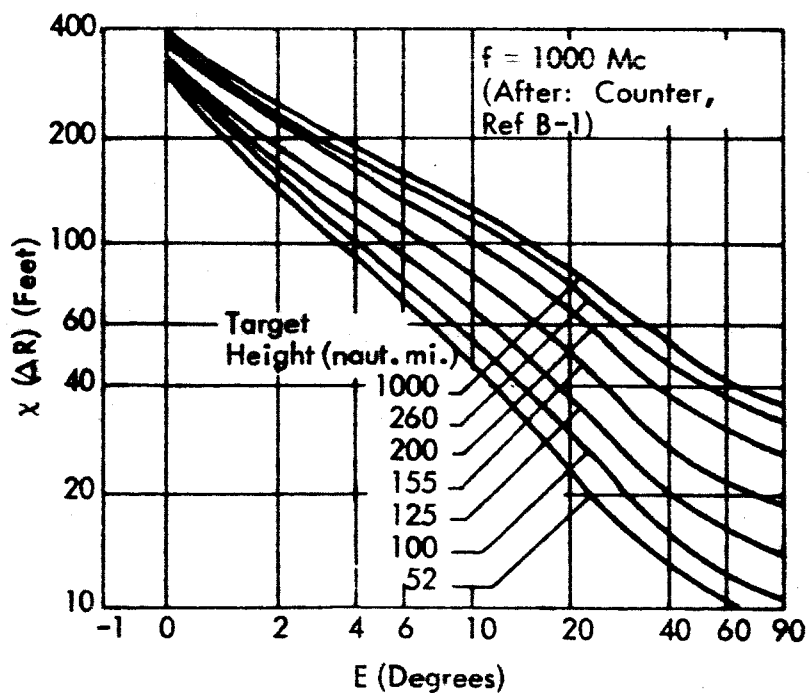


Figure B-9. Standard Correction  $\chi(\Delta R)$

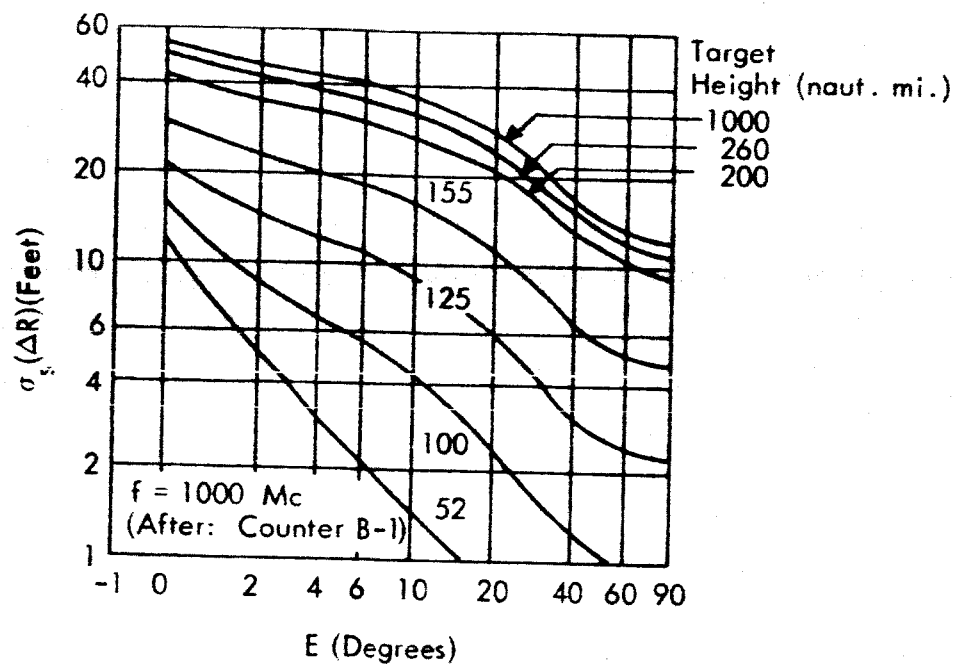


Figure B-10. Standard Error,  $\sigma_s(\Delta R)$

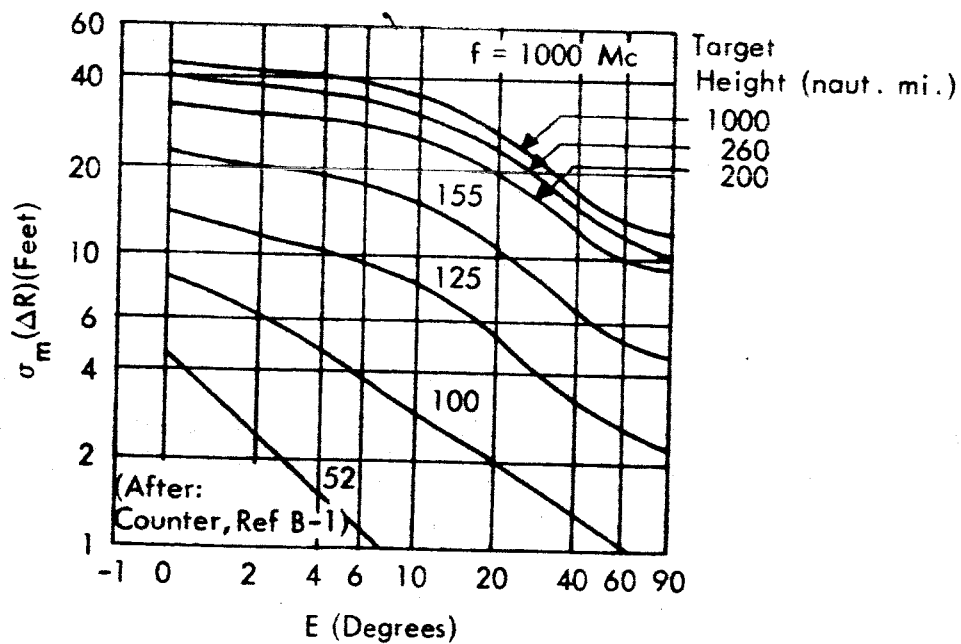


Figure B-11. Standard Error After Using  $n_s \sigma_m(\Delta R)$

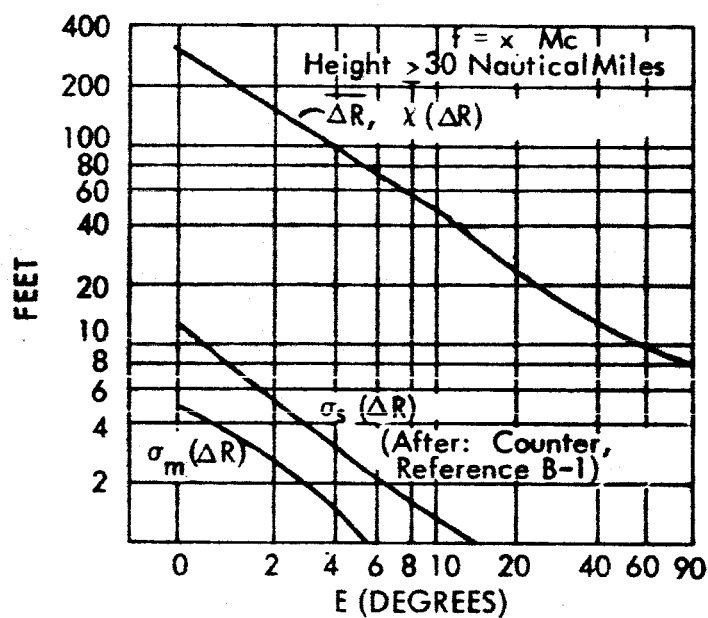


Figure B-12.  $\overline{\Delta R}$ ,  $\chi(\Delta R)$ ,  $\sigma_s(\Delta R)$  and  $\sigma_m(\Delta R)$

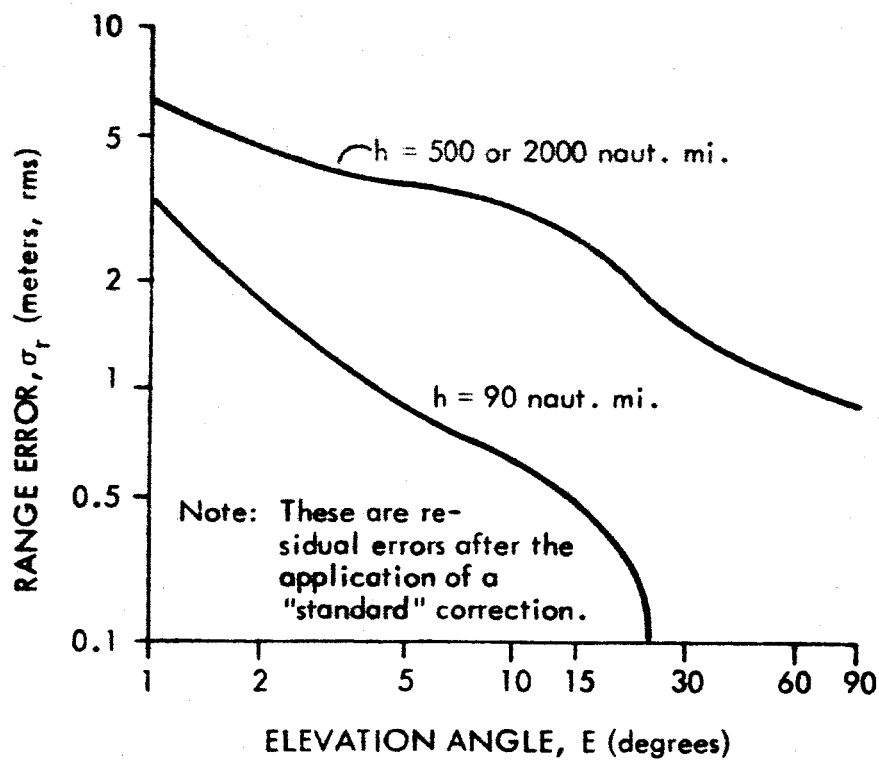


Figure B-13. Propagation-Induced Range Errors at 2 Gc

by the ray.\* Following Figure B-7, the difference between the true doppler velocity and the apparent doppler is:

$$\begin{aligned}\Delta \dot{r} &= V \cos (\psi + \delta_2) - V \cos \psi \\ &= V [\cos \psi \cos \delta_2 - \sin \psi \sin \delta_2 - \cos \psi] \\ &= V [\cos \psi (\cos \delta_2 - 1) - \sin \psi \sin \delta_2]\end{aligned}$$

Since the angle  $\delta_2$  will always be sufficiently small at the frequencies of interest to apply the small angle approximations,

$$\Delta \dot{r} \sim \delta_2 V \sin \psi.$$

$V$  and  $\psi$  will be fixed by the mission of the spacecraft and the ground station geometry, but  $\delta_2$  will be determined by the propagation medium. For a given spacecraft-ground station geometry,  $\delta_2$  will vary with variations in the atmosphere and therefore can be treated as a random variable in the same sense that the characteristics of the atmosphere can be (and have been) treated.

Again, the most useful source of information is the work of Counter (personal communication concerning data that will be published in the near future). In this work, the effects of the atmosphere on  $\delta_2$  are separated into tropospheric effects ( $\delta_{2t}$ ) and ionospheric effects ( $\delta_{2i}$ ), to provide a more general treatment. The data from which the statistical analyses were compiled are for Washington, D. C., and the nominal frequency used for the graphs of  $\delta_{2i}$  is 100 Mc. Some strong assumptions had to be made concerning the nature of the probability distributions involved, in order to permit computation of the required results, but the data will represent the most useful collection for the AROD study. It is hoped that later studies will provide more extensive data and delete some of the assumptions.

---

\*Near the maximum of the  $F_2$  layer in the ionosphere an additional effect must be considered. In this region an erroneous doppler measurement can result from the lack of knowledge of the true value of the index of refraction at the (moving) spacecraft. Since the error introduced by this cause is proportional to the uncertainty in  $n$ , the data in Figure B-4 and Table B-2 can be used to show that this effect is of second order, for most cases of interest to AROD, when compared with the angular deviations to be discussed. However, it may be necessary to include this effect if highly accurate propagation corrections are used.

The average value of  $\delta_2$  for any frequency can be obtained from Figures B-14 and B-16 as:

$$\bar{\delta}_2 = \bar{\delta}_{2t} + \left(\frac{100}{f}\right)^2 \bar{\delta}_{2i}$$

with the ionospheric effects again decreasing with the square of the transmitted frequency. The standard correction that could be applied to reduce this error is:

$$\chi(\delta_2) = \bar{\delta}_{2t} + \left(\frac{100}{f}\right)^2 \chi(\delta_{2i}),$$

where  $\chi(\delta_{2i})$  can be obtained from Figure B-17. After the application of this correction, which does not vary with season or time of day, the residual error (standard deviation) is approximately:

$$\sigma(\delta_2) = \left[ \sigma^2(\delta_{2t}) + 4 \left(\frac{100}{f}\right)^4 \sigma^2(\delta_{2i}) \right]^{1/2}$$

where  $\sigma(\delta_{2t})$  and  $\sigma(\delta_{2i})$  are the standard deviations for the troposphere and ionosphere, respectively, as shown in Figures B-15 and B-18.

It is important to note that Counter concludes that the residual error due to the troposphere cannot be appreciably reduced by the use of a correction based on the measured value of the index of refraction on the ground. This indicates that a more complex correction would be necessary to reduce the residual error beyond that determined by Figures B-15 and B-18.

When the data from these figures are combined with values for  $V$  and  $\psi$  obtained from standard tables,<sup>B-9</sup> the residual errors in range rate can be found from the relationship

$$\sigma_r = \sigma(\delta_2) V \sin \psi$$

for the missions and frequencies of interest. To cover the spectrum of spacecraft missions of interest to the AROD Feasibility Study, values for  $\sigma_r$  were computed for circular orbits of 90, 500, and 2000 naut. mi. altitudes. These values are presented in Figure B-19.

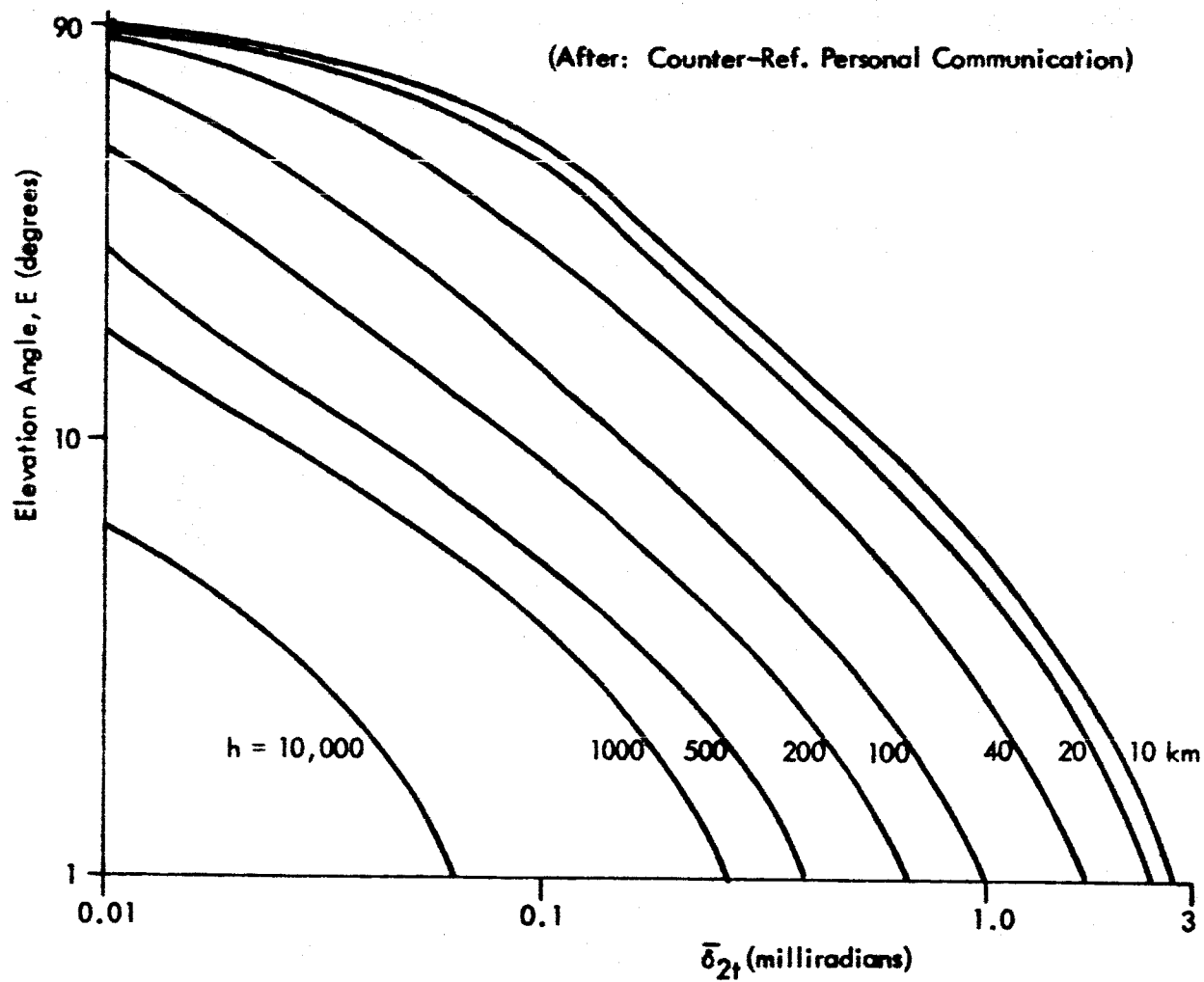


Figure B-14. Tropospheric Bending

(After: Counter-Ref. Personal Communications)

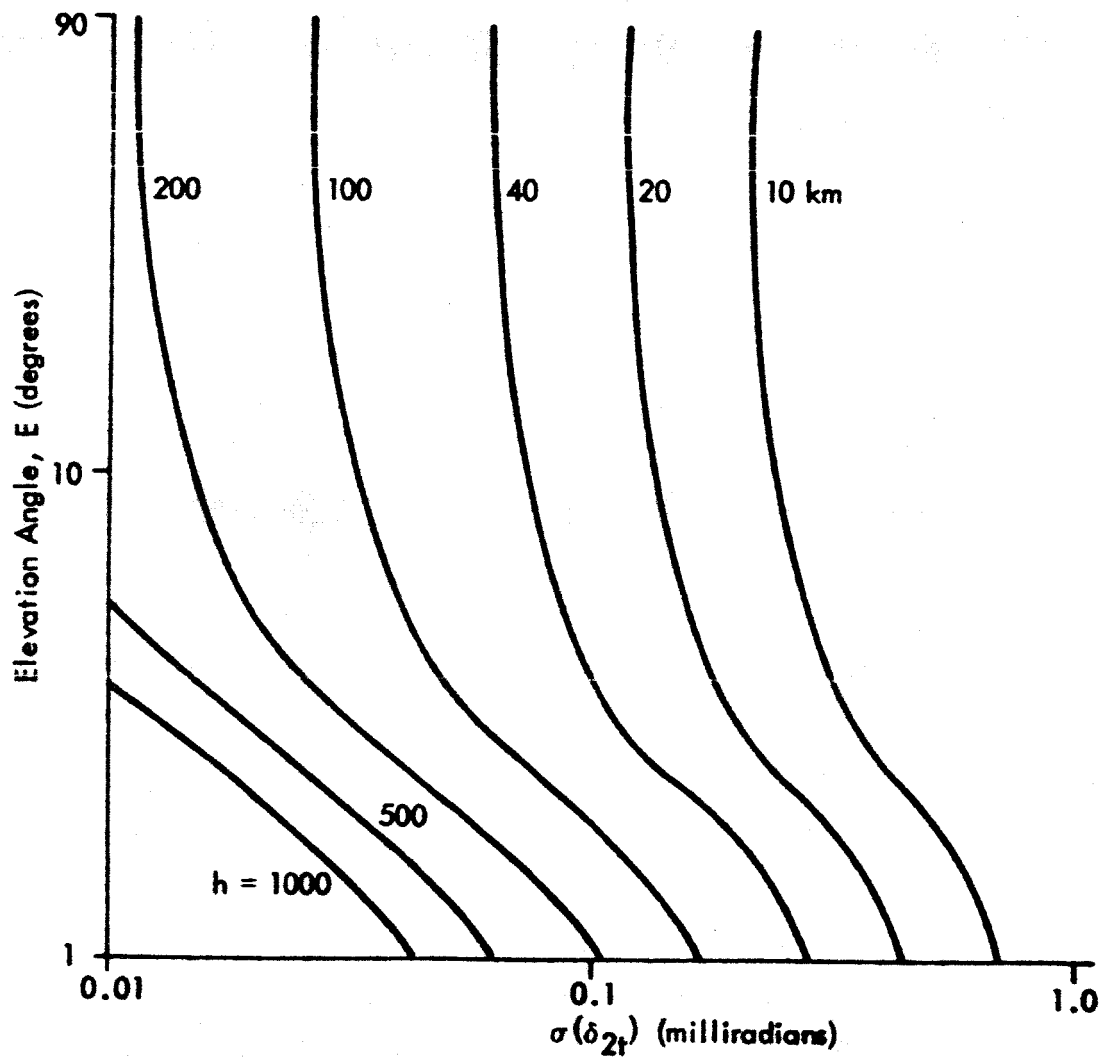


Figure B-15. Tropospheric Error

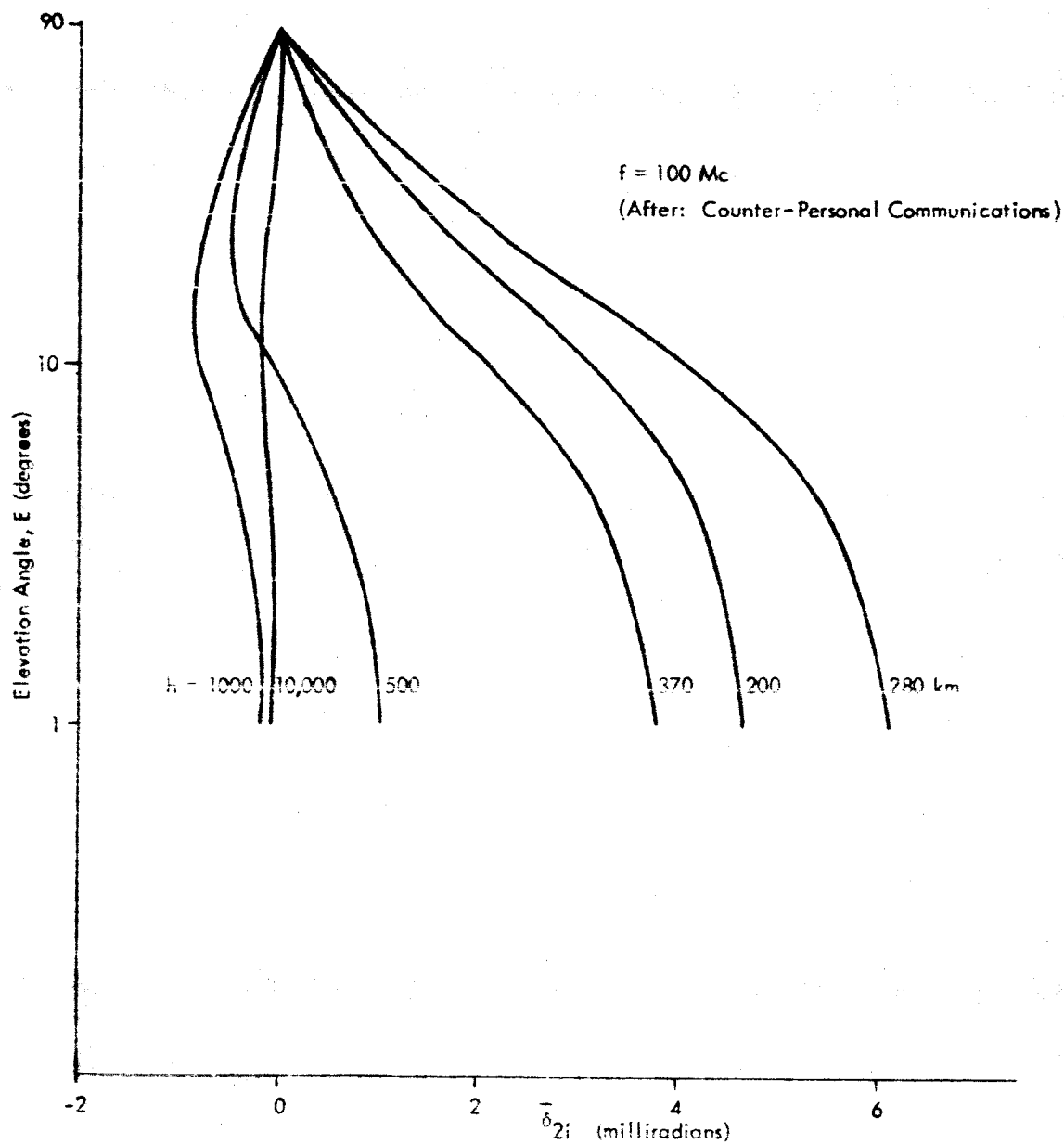
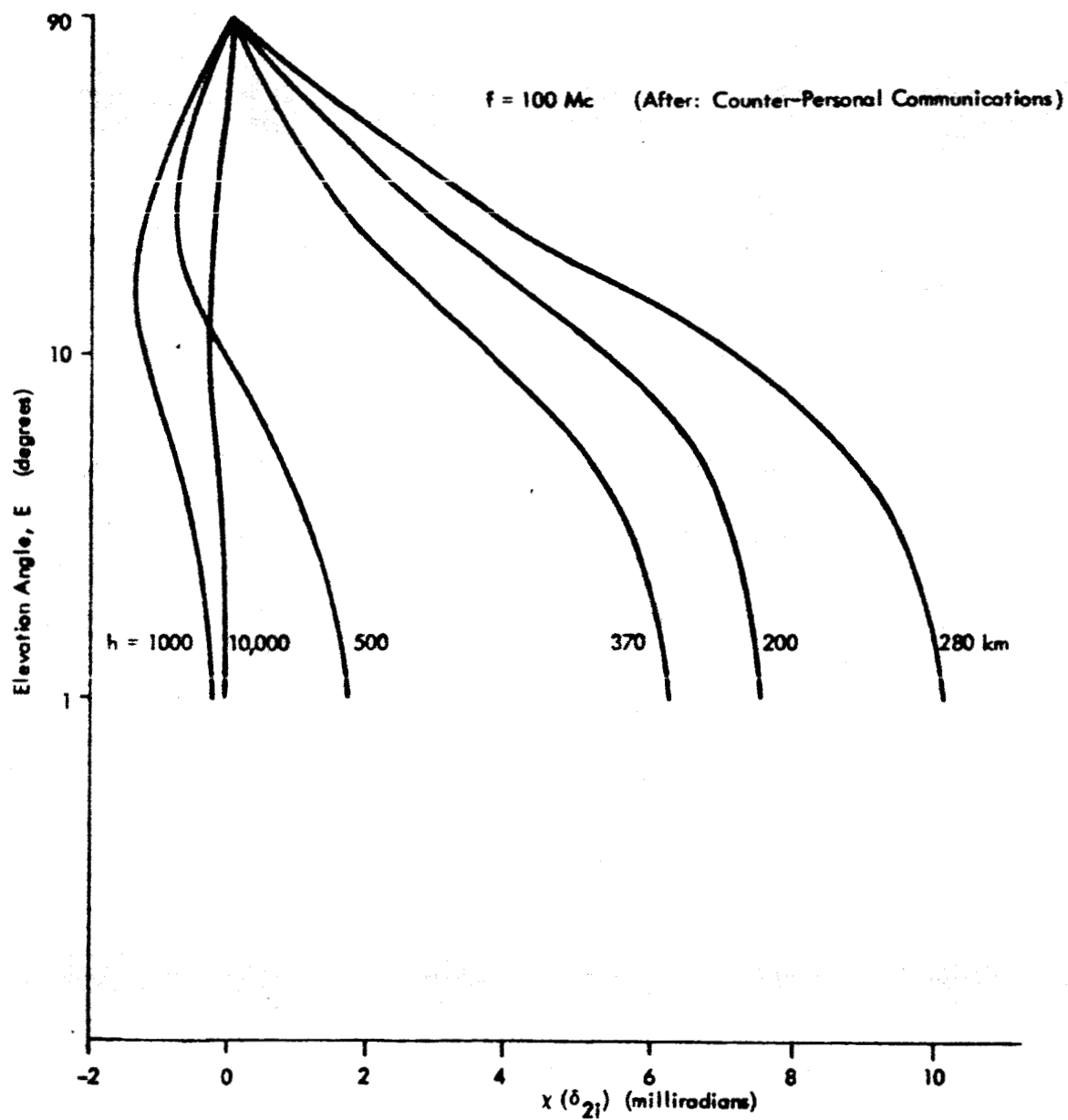


Figure B-16. Ionospheric Bending



**Figure B-17. Ionospheric Correction**

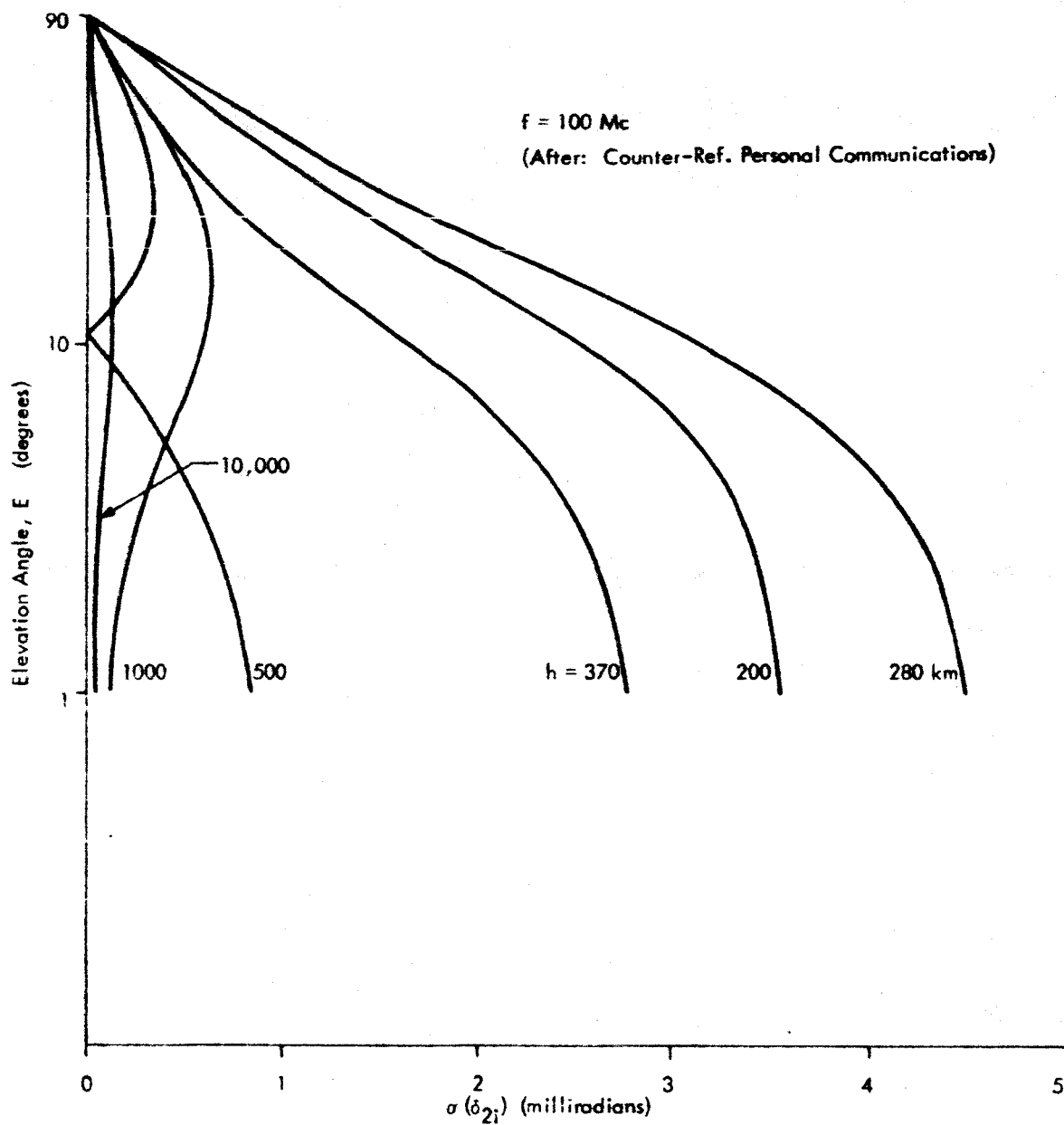


Figure B-18. Ionospheric Error

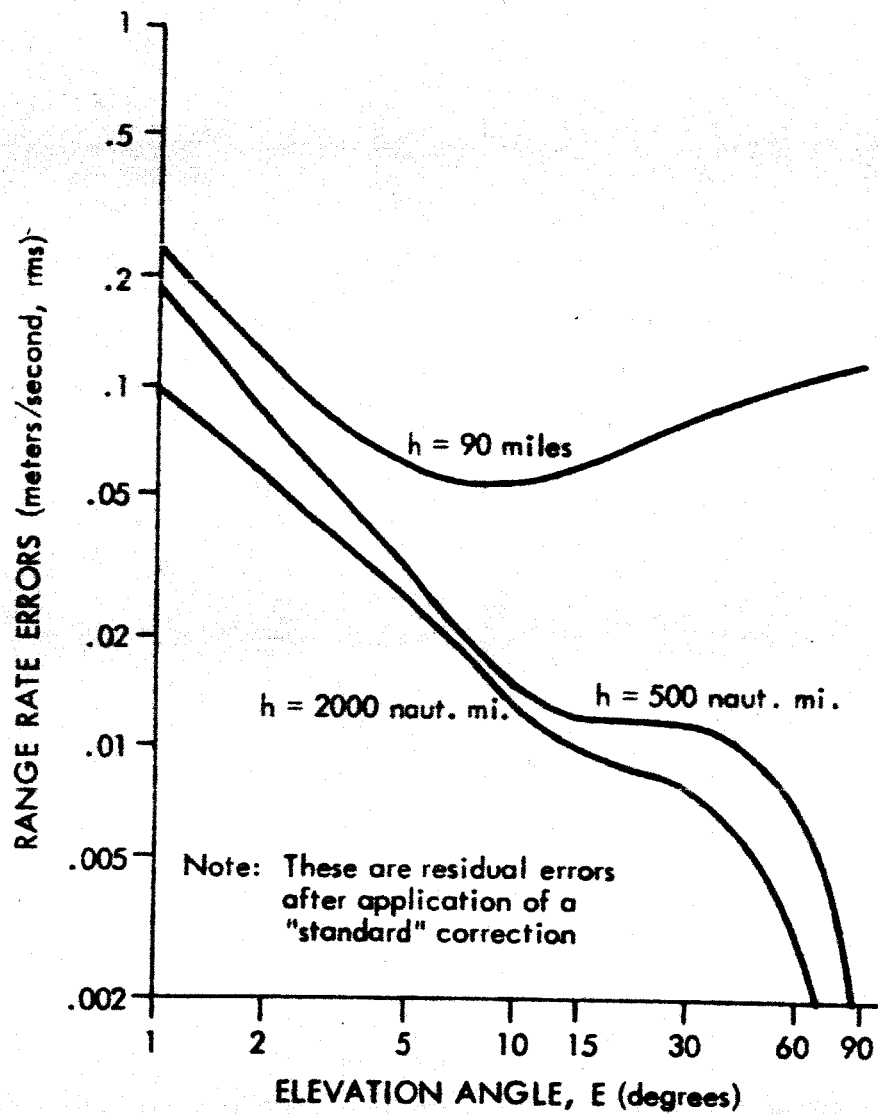


Figure B-19. Propagation-Induced Range Rate Errors at 2 Gc

## 5.0 CONCLUSIONS

The ideal form for propagation error statistics would include:

- a) The expected range and range rate errors as a function of:  
frequency, elevation angle, vehicle altitude, time of day, day of year, phase of the sunspot cycle, surface refractivity, tropospheric refractivity profile, ionospheric electron density profile, etc.
- b) The probability distribution of the residual errors remaining in the range and range rate measurements after the application of corrections of varying degrees of complexity based upon the above variables.
- c) The equipment and computations required to make the various corrections.

Unfortunately, data in this form are not available. However, Counter's work (References B-1, B-2 and personal communications) has provided estimates of residual errors (remaining after the use of a standard atmosphere) that are quite satisfactory for the purposes of the AROD Feasibility Study. These errors are graphed in Figures B-13 and B-19 for 2000 Mc.

The conclusions that have been reached from a study of Counter's work and many other sources are:

- a) If the vehicle's altitude (h) and elevation (E) are not taken into consideration, tropospheric-induced range errors in excess of 15 meters and 1 meter per second will be possible. Since these errors cannot be reduced by operating at higher frequencies, it is recommended that a correction based upon the computed altitude and elevation angle (or, equivalently, altitude and range) be incorporated in the vehicle computer.
- b) If a "standard" (i.e., worldwide) tropospheric model is employed to compute a correction for the errors introduced by the troposphere, the residual tropospheric errors left after the correction will usually be less than one meter and 0.1 meters/sec. for  $E \geq 5^\circ$ . Since propagation errors increase sharply for lower elevation angles, it is recommended that AROD measurements be restricted to  $E \geq 5^\circ$ .

- c) Measurement of the surface index of refraction at each ground station might reduce the residual tropospheric errors slightly. More complex measurements (e.g., radiosonde data) and computations might reduce the residual tropospheric error by a greater factor, but it is questionable whether the additional complexity is justified by the improvement.
- d) The content of the ionosphere varies more, and is less well-known, than that of the troposphere. Consequently, the residual errors will be a large percentage of the original errors.
- e) The errors introduced by the ionosphere can be reduced in several ways: operating at higher frequencies; computing correction factors; or transmitting on two different frequencies. The ionospheric errors vary inversely as  $f^2$ ; therefore, operating at 2 kMc reduces errors to one-fourth their magnitude at 1 kMc. Alternatively, if a correction based upon E, h, time of day, season, and phase of the sunspot cycle is computed in the vehicle and applied to the range measurement, it has been estimated that the residual error will be 10 to 30 per cent of the original error; the use of current ionogram data would result in substantial further reductions. Alternatively, transmission on two separate frequencies has been estimated to result in a residual error that is less than ten per cent of the original error. <sup>B-10</sup>
- f) The use of ionospheric corrections computed from local conditions seems unnecessarily complicated for a spacecraft on an extended mission, especially for unattended ground stations. The use of two separate frequencies to reduce ionospheric errors also seems to be too high a penalty for the spacecraft. It is recommended, therefore, that the required reduction in propagation errors be achieved through the use of frequencies in the kilomegacycle region. (Considerations discussed in Section 3 of the main body of this report have led to the selection of 2000 Mc as the nominal operating frequency.)

- g) It is recommended that a correction based on a standard worldwide atmospheric model (adjusted for the phase of sunspot cycle) be incorporated into the vehicle computer. The additional complexity of utilizing local conditions for the propagation corrections does not seem justified at this time.

## REFERENCES

- B-1 V. A. Counter and E. Paul Reidel, "Calculations of Ground-Space Propagation Effects, "Lockheed Aircraft Corporation Report No. LMSD-2461, 22 May 1958. Astia No. AD 162000.
- B-2 V. A. Counter, "Propagation of Radio Waves through the Troposphere and Ionosphere, "Lockheed Aircraft Corporation Report No. LMSD-2066-R1, 14 May 1958. Astia No. AD 211504.
- B-3 G. H. Millman, "An Analysis of Tropospheric, Ionospheric, and Extra-Terrestrial Effects on VHF and UHF Propagation," General Electric Report No. R56EMH31, 6 October 1956. Astia Document No. AD 137969.
- B-4 Sissenwine, Dubin, and Wexler, Bulletin of the American Meteorological Society, Vol. 43, No. 7, June 1962, p. 283-287.
- B-5 P. F. Nicholson, "Atmospheric Refraction of Radio Frequency Electromagnetic Waves," NRL Report 5607, April 6, 1961. Astia Document No. AD 256768.
- B-6 F. Ditto, "A Catalog of Tangent Rays," MIT Lincoln Lab Group Report 226-0005, Aug. 59.
- B-7 A. M. Peterson, J. R. Bauer, et. al., "Upper Atmosphere Clutter Research. Final Report. Part XIII: Effects of the Atmosphere on Radar Resolution and Accuracy," Stanford Research Institute Project 2225, April 1960. Astia No. AD 238407.
- B-8 D. R. Hay and L. R. O. Storey, "Propagation Factors Affecting Long Range UHF Radars at High Latitude," Defense Research Telecommunication Establishment (Ontario, Canada) Report 41-1-3. December 1958.
- B-9 "Space Communications Handbook," Philco Western Development Laboratories WDL-TR 1162, 15 September 1959.
- B-10 S. M. Harris, "Refraction Compensation in a Spherically Stratified Ionosphere," IRE Trans. on Antennas and Propagation AP-9(2): 207-210, March 1961.

## APPENDIX C

### GEODETTIC ASPECTS OF AROD

#### 1.0 INTRODUCTION

The performance of the AROD system, in terms of overall system accuracy, depends strongly upon the accuracy to which the locations of the ground transponders are known. For the purpose of the Feasibility Study, two important aspects of the general geodetic problem had to be studied. First, it was necessary to estimate the geodetic accuracies expected from the application of advanced surveying techniques to land-based stations in order to determine the AROD system performance. Second, it was necessary to estimate the accuracy with which the position and velocity of a moving ship could be determined, both for planning purposes of early AROD flight tests and to serve as a preliminary estimate for the station coordinate errors associated with "fixed" shipborne transponders for the determination of overall performance of the operational AROD system.

To provide as accurate an analysis of these aspects of the general geodetic problem as possible, a subcontract was awarded to Geonautics, Inc. The analysis to be performed was restricted to transponders located between  $\pm 40^{\circ}$  latitude with nominal baseline separation distances of 500 nautical miles. The feasibility of achieving a value of 10' - 50' for the standard deviation of the location of worldwide stations to a common datum was to be investigated under the subcontract.

This appendix summarizes the results of the Geonautics, Inc. subcontract. Section 2 presents a preliminary estimate of the accuracies of present and future geodetic techniques for establishing locations of AROD land-based stations to localized geoidal datums and tie-in of remote datum systems. Section 3 is concerned with two aspects of the shipborne station problem:

- a) A preliminary estimate of the accuracy with which the position and velocity may be obtained for a ship within the ocean area enclosed by latitudes  $40^{\circ}\text{N}$  and  $40^{\circ}\text{S}$  and longitudes  $15^{\circ}\text{W}$  and  $75^{\circ}\text{W}$ , using VLF transmissions from stations located at present and planned LORAN sites.
- b) A preliminary investigation of the feasibility of using satellites with well-defined orbits for determining a ship's position and velocity.

## 2.0 POSITIONING OF LAND-BASED AROD TRANSPONDERS

### 2.1 A UNIFIED GLOBAL GEODETIC NETWORK

A unified geodetic network extending around the world has until recently been of little practical value and of only academic interest. In the last two decades, however, unification of separate datums to ever increasing accuracies has been of mounting necessity.

The advent of the exploration of space has placed more difficult requirements upon such surveys. For example, unprecedented standards were formulated for the Cape Canaveral area, then recalled and changed several times to more exacting and expensive requirements. These demands have only lately been met.<sup>1</sup> and there is no reason to believe that even more rigorous requirements will not soon be necessary. The AROD system will probably pose even more stringent accuracy requirements on a vast scale not previously considered.

Existing surveys, which cover only 15-20% of the land area, were designed to meet the mapping and navigational requirements of a slower moving, more leisurely world. After 200 years of execution, they do not meet modern accuracy needs as to location, nor do they provide union of datums.

Gravimetry, a method that has received great practical and theoretical attention, provides a method of unifying all world datums to a deliberately smoothed first order approximation, in the distant future. Even when

combined, however, with relevant satellite data (which are ineffective in determining the fine gravitational structure) it offers only rough (but useful) approximations. This method does not meet the 10'-50' objective for the AROD system nor is it likely to do so, for the following principal reasons:

- a) It requires a worldwide knowledge of gravity (and geodetic position), which is known only for a small portion of the world at the present time.
- b) It determines only relative shape and, therefore, requires some other method to give scale; i.e., a measurement of equatorial diameter of the Earth. Such a scale can only be supplied to the accuracies desired for AROD by a surveying technique which will be good to the same accuracies.
- c) Satellite methods for determining the small scale structure of the geopotential will require a tremendous mass of observational material based upon a ground survey system of the AROD type. Indeed, satellite methods may never be capable of such results due to complications in resolving orbital parameters.

Great strides have been accomplished since World War II to unify the principal geodetic systems by direct geodetic methods, but none of these methods presently meet the accuracy objectives posed for the AROD system. In fact, it can be stated that all present geodetic systems except portions of the Atlantic Missile Range, will be of only minimal value in achieving these objectives.

In consideration of the accuracy desired for the worldwide AROD tracking network, accurate determination of positions appears to require departures from traditional position locating methods, to newer, largely untried methods, not yet fully developed, whose ultimate dependability and accuracy cannot be fully resolved at this time. Such approaches involve combinations of the roles traditionally belonging to the separate sciences of astronomy, geodesy and electronics. They would combine modern photogrammetric position astronomy, advanced geodetic triangulation and base measuring techniques, satellite ranging and range-rate measurements, and

accurate relative astronomic position location methods which are independent of gravity. Some of these methods are summarized in sections of this appendix which follow.

The most promising advanced geodetic methods at this time involve photogrammetric position astrometry as applied to satellite observations and flare triangulation<sup>2, 3</sup>. These methods are now capable of high accuracies and will probably be improved greatly. Since they are a developing art, the ultimate accuracy attainable is not known. In order to realize the potential of these techniques (and similar systems) methods are required for measuring long baselines to an accuracy commensurate with these advanced systems. The lengths of these baselines should be of the order of, or greater than, the length of the average triangulation sides in the space triangulation system. Because of the propagation of errors, a number of such bases should be observed on the various major land masses near the equator. Lengths and orientations should be chosen carefully to contribute the maximum strength to the results, consistent with other requirements, such as accessibility, terrain factors, vegetation, weather, political considerations, road nets, etc.

Of the two highly precise means presently available for measuring baselines of great length, only that based on Geodimeter observations is suitable.<sup>1</sup> Invar tape measurements are too laborious and time consuming to be employed to any extent. Taped bases have a higher reproducibility and would meet requisite accuracies, but are subject to systematic errors which are difficult to assess. Taping methods will be needed, however, for some minor measurements and, particularly, for calibrating Geodimeter equipment.

The Geodimeter system makes it possible for a few men to measure several highly accurate lines of up to 20 miles in length in the course of a night's work. Using this device, the U. S. Coast and Geodetic Survey is planning eight United States transcontinental traverses; four of these to be in North-South directions and four in East-West directions.

Although the extent of the work to provide the required number of baselines of the long lengths desired appears prodigious, such lines can

be measured. Some of the problems associated with their establishment have been previously investigated and a "leap-frog traverse" system using the Geodimeter has been proposed.<sup>4</sup> These investigations indicate that adequate methods can be established to provide accurate terrestrial baseline measurements to scale advanced geodetic systems that will be employed for inter-datum ties and final integration of a world geodetic network.

Although these paragraphs provide only a cursory outline of the geodetic problems in establishing a unified global network, it is evident that the desired objectives (less than 50') of the AROD tracking network are technically feasible, but their accomplishment will be tedious and their cost substantially increased due to measurement problems of accurate baselines.

## 2.2 USABLE METHODS FOR DETERMINATION OF GEODETIC POSITIONS

This section provides a brief summation of various techniques which are suitable for positioning stations separated by distances of 300-500 miles or more. The methods discussed are considered applicable to problems associated with positioning AROD ground transponders within localized datums, and also on a worldwide network basis. Suitability of the methods for meeting geodetic objectives of the AROD tracking network depends on the relative positional accuracies desired within individual datums, and the overall inter-datum relationships necessary for providing the desired accuracy of a global network. Individually, the methods are of little practical use in fulfilling positional requirements for a global reference network, but when used in combination and with precise baselines as discussed in the previous section, they can approach and possibly satisfy the accuracy objectives set for the AROD system. The capabilities and operational status of the various methods are outlined in the following paragraphs, and comparative accuracies of the systems are listed in Table C-1.

### 2.2.1 Hiran Trilateration

Hiran was developed specifically as an airborne electronic, first-order distance measuring instrument for use in establishing precise geodetic networks and photogrammetric control for mapping purposes.<sup>5</sup> The system is capable of measuring geodetic distances over ranges of 50 - 500 miles or more within an accuracy of  $\pm 0.0020$  to  $\pm 0.0025$  statute miles (probable error). Because of its long-range measurement capability, Hiran is suitable for geodetic ties over water, desert or rough terrain. Hiran trilateration has been extended over great distances, the most significant being the North American-European connection which achieved a relative accuracy of 1:314,000 or  $\pm 39$  feet over a net length of 2,330 miles.<sup>6</sup> Generally, Hiran trilateration is considered accurate to 1:150,000 - 1:250,000 (probable error) and perhaps better, depending on the geometry and number of measure lines within the network.

In recent years Hiran has been used extensively by the U. S. Air Force to obtain geodetic connections among insular groups in the Pacific and to extend horizontal control along the northeastern borders of South America. The latter project is scheduled for completion in early 1963 and will provide one of the longest trilateration networks - Cape Canaveral to Recife, Brazil. Hiran trilateration was recently completed throughout the Hawaiian Islands, and other surveys are underway to obtain geodetic connections between major insular groups in the Southwest Pacific.

### 2.2.2 Shiran Trilateration

Hiran equipment will be replaced eventually by the advanced Shiran (3000 mc-S band) system currently under development.<sup>7</sup> This system is expected to be operational by 1965 and will provide a capability for measuring lines up to distances of 900-1000 miles. Performance specifications for Shiran require air to ground slant range measurements to be within a standard error (standard deviation or rms error) of 2.8 meters for distances of 450 nautical miles, or approximately 1 part in 300,000.

Both Hiran and the advanced, longer-range Shiran are expected to be suitable for many of the early positioning problems of the AROD network, particularly for initial location of station facilities in remote areas. However, these systems will probably have only marginal utility for final position determination.

### 2.2.3 Photogrammetric Flash Triangulation

This method has been developed in recent years as an advanced geodetic tool for obtaining precise positional data over intermediate ranges (500-1500 miles) and over intercontinental distances.<sup>2</sup> Flash triangulation techniques are based on photographing rocket-ejected flares or satellite flashing lights against the star background from widely separated ground observation stations. Ultimate accuracy of triangulation is uncertain at this time as the techniques have had only limited operational use; however, instrumentation accuracies of 0.2" to 0.4" of arc for directional observations appear possible with advanced ballistic-type camera systems.<sup>4,8</sup> System accuracy is dependent on various factors including the focal length, aperture and calibration of the astro-camera, timing of the observations, accuracy of star catalogs, atmospheric effects, and the capabilities of the equipment used in reduction of astrographic plates. These error sources have been minimized or controlled to the point that flash triangulation now appears capable of attaining accuracies of 1 part in 1,000,000 under optimum operational conditions. In considering the precision necessary to achieve the objectives set for the AROD network, photogrammetric stellar triangulation offers at this time the most desirable means for positioning station facilities.

### 2.2.4 Geodetic Satellites

The use of geodetic satellites will facilitate making worldwide geodetic connections and obtaining certain geodetic quantities that will provide greater knowledge of the geophysical conditions and shape of the earth. Advantages of geodetic satellites have been enumerated in various reports

and already many contributions to geodesy have resulted from observations of early satellites.<sup>9,10,11</sup> Significant satellite programs in the immediate future which will be of interest to the AROD program are:

a) Secor. This system is to provide an electronic ranging capability for positioning remote stations on the earth's surface and for eventually establishing a worldwide geodetic datum for horizontal control.<sup>12</sup> Geodetic positioning will be accomplished by trilateration techniques using a minimum of four ground stations. Secor is a continuous wave, phase comparison system using three VHF/UHF bands—one for transmission to the satellite and two coherent frequencies for transmission from the satellite to the ground stations. Analysis of the difference in phase shift between the two returning frequencies permits corrections for ionospheric refraction effects. The equipment is expected to provide a ranging capability of 5000 miles or greater, with an instrumentation resolution of 1 to 2 feet. Secor is under development by the Army and is scheduled to be operational by mid-1963. Positioning accuracies of 30 feet or better (1:500,000+) over intercontinental distances are expected with the early operational system.

b) ANNA. This vehicle represents the first joint-service project for collection of worldwide geodetic data. The initial ANNA vehicle will be employed primarily to evaluate angle, range, and range-rate positioning techniques for intercontinental surveys.<sup>13</sup> The satellite will be instrumented with optical flashing beacons for photogrammetric stellar triangulation, a Secor transponder for ranging purposes, and a Doppler system of the Transit-type. Special ground facilities will be required for interrogation of the ranging transmitters and optical beacons. Because of power limitations, the satellite can be interrogated only six or seven times per 24 hour period for range and angle observations, which will limit optimization of geometric and operational conditions for any extensive intercontinental surveys. Accuracies of 1:500,000 using the electronic system and 1:1,000,000 using the flashing light are expected over intercontinental distances.

Comparative accuracies of the above systems are presented in Table C-1. These data were utilized to summarize the estimated geodetic errors in Section 2 of the main body of this report.

Table C-1

## Comparative Accuracies of Methods for Determination of Geodetic Positions Over Extended Areas

<u>Method</u>	<u>Estimated Accuracy</u> ( <u>Standard Error</u> )	<u>Remarks</u>
Hiran Trilateration (1962)	1:100,000 to 1:170,000 or 18' - 30' at 500 naut. mi.	Suitable for surveys over remote areas on localized datums. Limited intercontinental capability, 500 mile maximum range.
Shiran Trilateration (1965 est.)	1:300,000 to 1:500,000 or 12' - 20' at 1000 naut. mi.	System to be available in 1965. Expected to provide accurate control extensions over distances up to 1,000 miles or twice Hiran range.
Photogrammetric Flash Triangulation (1964 est.)	1:1,000,000 or better*	Additional development required to make fully operational.
Geodetic Satellites (1963-64 est.)	1:500,000 or better (electronic trilateration) 1:1,000,000 (photogrammetric stellar triangulation)	Under development, operational in 1963.

\*The time at which this accuracy will be achievable is strongly dependent on the effort expended in improving star catalogs.

### 3.0 POSITIONING OF SHIPBORNE TRACKING FACILITIES

Investigations of seaborne position determining capabilities were concerned with ships within the ocean area enclosed by latitudes  $40^{\circ}$  N and  $40^{\circ}$  S and longitudes  $15^{\circ}$  W and  $75^{\circ}$  W. This includes the Atlantic Missile Range and surrounding waters in the North and South Atlantic. As part of the study, preliminary comparisons were made of the suitability and expected accuracy of long range LF and VLF radio navigation systems for determining the position and velocity of a ship within this designated area.

In recent years, LF-VLF transmissions have been found to be relatively stable over long paths and, therefore, highly applicable for precise navigation purposes. The Loran C and Omega navigation systems were considered of primary interest, and a comparative evaluation was made of these systems to determine their suitability for use in the early AROD test flights and their possible applications to the operational AROD system. The positioning capabilities presented for the Loran C and Omega systems refer primarily to the repeatability of the systems not the absolute accuracy. Consideration was given also to the use of satellite techniques for determining position and velocity data for a vessel, and estimated accuracies of these methods were established. Results of the investigations are summarized in the following paragraphs.

#### 3.1 RADIO NAVIGATION

##### 3.1.1 Loran C

Loran-C is a pulsed hyperbolic radio navigation system operating at a frequency of 100 kcs. It utilizes phase-measuring and cycle identification techniques to obtain accurate measurements of the difference in times of arrival of radio signals from fixed transmitting stations. Groundwave propagation is utilized to provide accurate navigation over relatively long ranges to approximately 1400 nautical miles; skywave transmission, although less stable than groundwave propagation, is suitable for general navigation, from ranges of 800-2500 nautical miles or greater. Loran-C is of special interest to this study as it is capable of providing accurate radio navigation data for positioning tracking ships in the Atlantic Missile Range and surrounding ocean areas.

The accuracy of Loran-C is limited by several factors: (1) geometry of the hyperbolic lattice; (2) synchronization of the transmitting stations; (3) instrumentation accuracy of the receiver; and (4) propagation effects. Based on experimental and operational tests it has been found that synchronization errors can be maintained within 0.05 microseconds. Instrumentation accuracy of receivers is in the same order of accuracy. Propagation variations have been found to be less than 0.1 microsecond for groundwaves and nominally 1 to 1.5 microsecond for skywaves, excluding sunrise and sunset periods, and periods of high level radio interference. Considering all these errors, the total standard deviation of a single line of position when using groundwave propagation should not exceed 0.12 microsecond (115 feet on the baseline). Obviously, repeatability of a single determination of a position is affected by the geometry of the Loran-C net; i.e., the angle of intersection of the two lines of position and their degree of expansion due to distance from their respective baselines.

In considering performance capabilities of Loran-C, it is appropriate to summarize the engineering evaluation which was made of the U. S. East Coast Loran-C chain.<sup>14</sup> The master station for this chain is located at Cape Fear, N. C. with slave stations at Martha's Vineyard, Mass. and Jupiter Inlet, Florida. For the evaluation, a monitoring receiver was located at Bermuda to record time-differences of Loran-C transmissions from the master and slave stations. Data was recorded over long periods of time and statistically analyzed in various ways. For example, one analysis showed that position fixes obtained by averaging time difference readings over 8 hour periods from 0800 to 1600 during a year were within a CPE of 260 feet. In another analysis it was found that position fixes obtained by using 15 minute averages over a 38 1/2 hour period fell within a CPE of 105 feet. These results provide indication of the long term stability of the Loran-C system by averaging observations at a fixed location over a period of time.

The accuracy of position fixing, using single or instantaneous time difference observations is, of course, somewhat less than that obtained by averaging methods. During the Bermuda recording program it was found

that the probable error of instantaneous time differences between the master transmitter and the Florida slave station over a one year period was approximately 0.09 microsecond in the daytime and about 0.13 microsecond at night. In addition, it was found that during periods of a month or more the mean time difference varied from the yearly mean by as much as 0.2 microsecond. This latter deviation was attributed, in part, to long-term drifts in coding delays introduced at the slave stations.

Based on demonstrated performance using the Bermuda monitor and various theoretical considerations, the engineering evaluation concluded that it is feasible to obtain instantaneous position fixes at the extreme limits of the groundwave area with a probable error on each line-of-position of less than 0.1 microsecond plus a seasonal error of 0.1 microsecond or less for paths predominantly over water.

Data obtained with the East Coast Loran-C triad using skywave transmissions indicated that time difference measurements had a probable error of 1.0 to 1.5 microseconds. This corresponds to errors in line-of-position measurements on the baseline of approximately  $\pm 1000$  feet for 50 percent of the observations and  $\pm 3000$  feet for 95 percent of the observations. Although skywave accuracy obtained in these experiments was an order of magnitude less than that obtained by groundwaves, it is considered suitable for general navigation over relatively long ranges. For Loran-C stations having 100 kw radiated power, the maximum first-hop skywave range is approximately 1800 nautical miles. Second-hop waves have been observed as far away as 3400 nautical miles; however, at present the use of multi-hop skywaves is not recommended for any type of accurate navigation. In using skywave transmissions, corrections are applied to time difference measurements to reduce the skywave readings to equivalent groundwave readings. Corrections for these transmission delays are precomputed for Loran-C coverage areas based on the predictability of the ionospheric effects on the radio propagation. Skywaves are relatively stable over short periods of an hour or more, but they may vary considerably from day to day and from season to season. At present, there is not sufficient knowledge of the ionospheric effects to predict skywave corrections to better than a few microseconds.

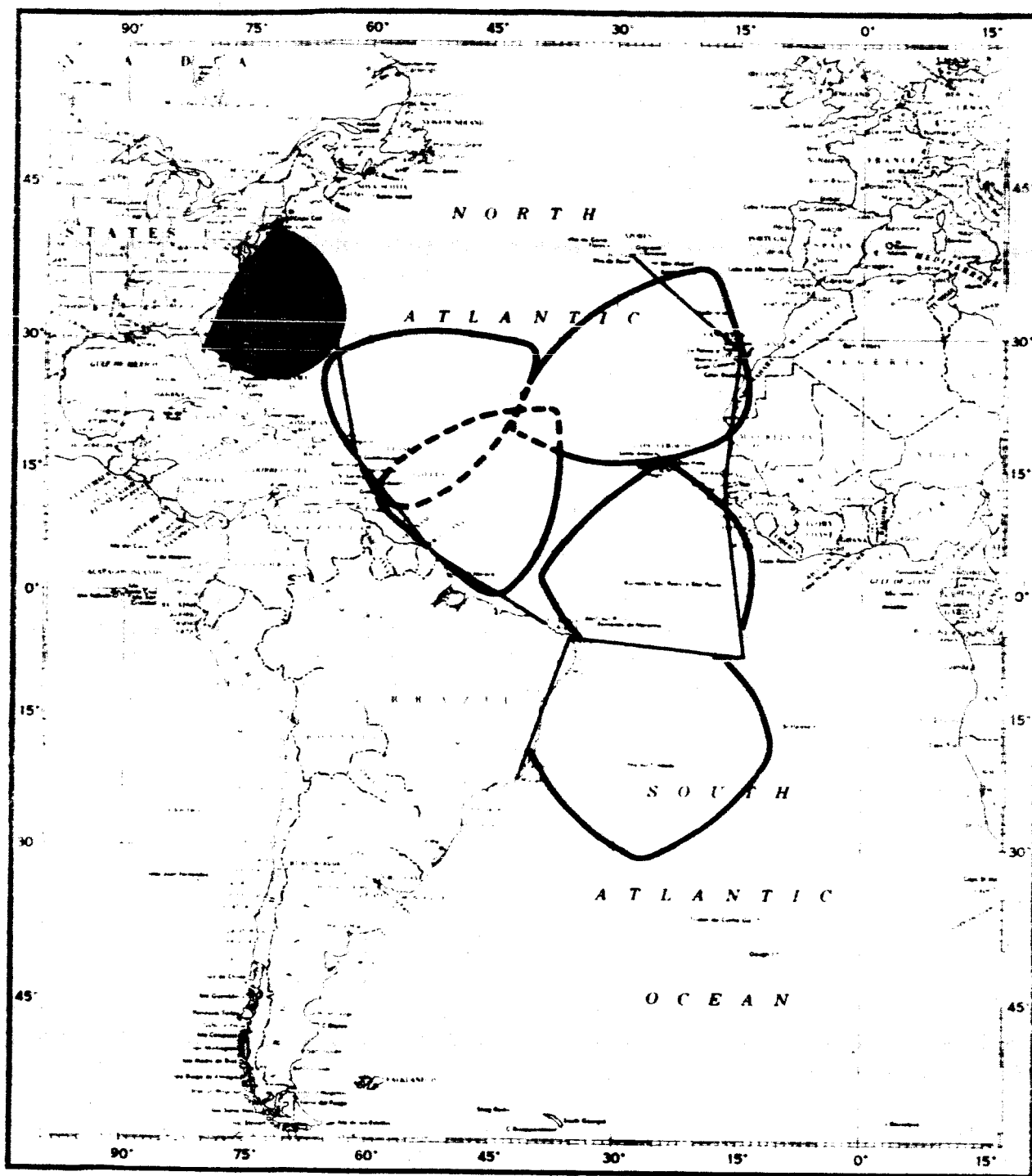
Figure 1 shows a coverage diagram for a preliminary Loran-C network in the area of interest. The coverages are based on systems of 1000 kw peak radiated power, which should provide suitable signal strengths of groundwave transmissions over ranges up to 1400 nautical miles. A total of 13 Loran-C stations were assumed, including the three stations of the existing East Coast chain, to obtain adequate ground-wave coverage through most of the operational area between  $\pm 40^\circ$  of the equator. The use of groundwave propagation should provide accurate position fixes within a standard deviation of approximately  $\pm 500$  feet under normal system operations. Loran-C coverage beyond groundwave range can be obtained throughout the remainder of the operational area by use of the first-hop skywave transmissions. Estimates indicate that these signals should be stable enough to give reliable position fixes within about 1 to 2 miles.

In preparing the coverage diagram of Figure 1, a total of 10 new Loran-C stations were considered. Equipment and installation costs for these new station facilities are estimated at \$20,000,000 or about \$2,000,000 per site.

### 3.1.2 Omega

Omega is a long-range, hyperbolic radio navigation system designed to operate in the Very Low Frequency navigation band of 10 to 14 kcs. The system utilizes phase comparison techniques with time-shared continuous wave transmissions to obtain phase difference measurements from two or more fixed stations. Omega is under final development and evaluation by the U. S. Navy, and is being considered as a global navigation system for multi-purpose marine operations. Experimental studies have shown that the system is capable of providing usable position fixes over ranges up to better than 6000 nautical miles; accuracy at long range being achieved by use of very long baselines between the Omega transmitters. The main advantage of the system is that a network of six transmitter stations separated by distances of about 6000 nautical miles can provide global navigation coverage.

Sufficient experimental data are not available at this time to fully assess positioning accuracy of the Omega system. The principal limiting



Existing LORAN-C network

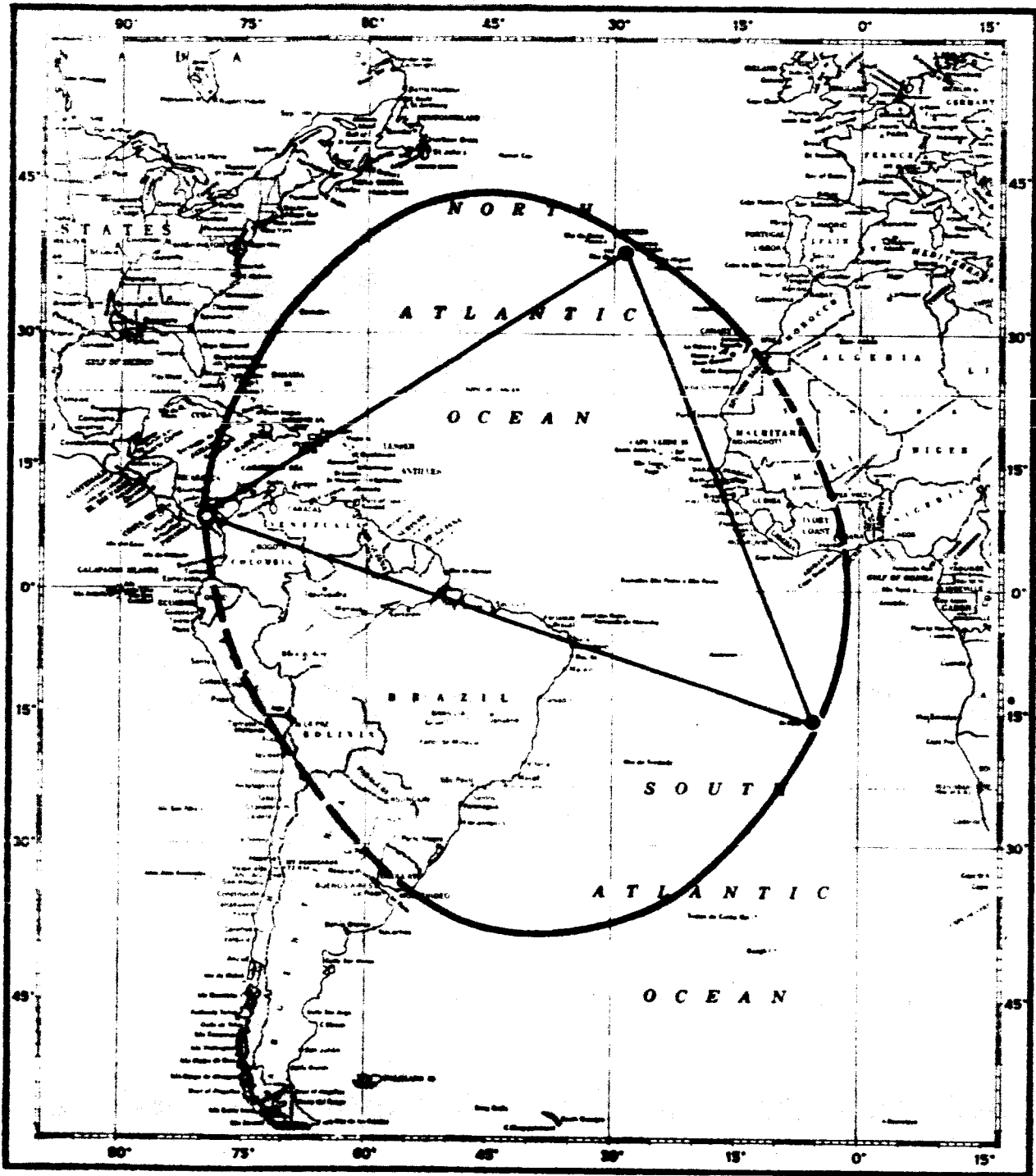
Limiting contour for 500-foot position accuracy (standard error) using ground-wave propagation from the proposed stations.

*Figure C-1. LORAN-C Coverage Diagram*

factor on system accuracy is the stability of propagation over long paths. Propagation measurements in the VLF spectrum have been limited; however, analyses have demonstrated that the propagation is relatively stable and that transmission time of the signal can possibly be predicted to a precision of 5 to 10 microseconds.<sup>15,16</sup>

Recent experimental tests were made by the U. S. Navy to obtain preliminary information concerning propagation characteristics and range capabilities of the Omega system in the arctic, temperate and tropical regions.<sup>17</sup> These tests were conducted using the experimental Omega transmitter network which is operating at a frequency of 10.2 kcs at Summit, Canal Zone; Haiku, Hawaii; and Forestport, New York. Results of these tests demonstrated that the system will be capable of providing position fixes within  $\pm 1.0$  nautical mile at distances of better than 6000 nautical miles. It was concluded from these experimental tests that propagation measurements are stable enough to provide a good potential system accuracy, and that it is possible to make qualitative predictions of the diurnal variation characteristics of the skywave transmissions. When Omega is fully developed, overall system accuracy is expected to be about  $\pm 0.5$  nautical miles within areas of good geometric coverage.

Omega coverage for the Atlantic area could be obtained by using a network of three transmitting stations similar to that shown in Figure 2. The geometry of this network would be very strong throughout the main areas of interest and navigational position fixes inside the triangle shown, would be expected to be within  $\pm 0.5$  nautical miles under favorable propagation conditions. Locations for the Omega transmitter stations were assumed in the Azores, St. Helena Island and at the existing experimental Omega station in the Canal Zone. It is assumed that this existing facility would be suitable for permanent Omega operations. Costs for station facilities at St. Helena and the Azores are estimated at approximately \$18,000,000 or \$9,000,000 per site.<sup>18</sup> Most of these costs involve equipment and installation of the antenna facilities as these are estimated at \$8,000,000 per antenna.



- O - Existing Omega experimental station using 100 kw, 9 to 40 kc transmitter.
- Area within the curve indicates approximate area for positioning accuracies of  $\pm 1$  nautical mile.
- Inside the triangle accuracies of  $\pm 0.5$  nautical miles may be achievable under favorable propagation conditions.

Figure C-2. Omega Coverage Diagram

### 3.1.3 Comparison of Omega and Loran-C Capabilities

Estimated navigation capabilities of Omega and Loran-C for use in determining the position, velocity, and track of a ship within the Atlantic area of interest are summarized as follows:

	Omega <sup>a</sup>	Loran-C
Position	+ 3000 feet (under optimum conditions of geometry and propagation stability)  + 1 naut. mi. (at 6000 naut. mi range)	+ 500 feet (groundwave) + 1 - 2 miles (skywave)
Speed <sup>b</sup>	5 - 10% or .25 - .75 m/sec.	1 - 2% or .05 - .15 m/sec.
Track <sup>b</sup>	2° - 4°	0.5°

<sup>a</sup> Sufficient data not available on VLF propagation stability to fully assess system accuracy.

<sup>b</sup> - Based on adjusted mean track from position observations over limited time periods (approximately 30 - 60 minutes).

All values should be considered as standard errors.

It must be recognized that the positioning capabilities listed above refer only to the repeatability of the navigation systems. Absolute accuracy of these systems in terms of geographic position (latitude and longitude to required degree of refinement) depends upon the geodetic coordinates of the reference stations, plus a system calibration throughout the coverage area of sufficient density to assure that secondary phase corrections are adequately known.

Based on preliminary comparisons of the navigation capabilities of these systems, the following conclusions are reached:

a) Low Frequency, long-range navigation has reached a high degree of development and has established operational capabilities; Very Low Frequency navigation is not fully developed nor is there sufficient knowledge of propagation characteristics to fully assess its potential positioning capabilities.

b) The Loran-C system, although limited in range and area coverage, is capable of providing more accurate position and velocity data for AROD shipborne tracking facilities in the Atlantic area than the VLF long-range Omega system.

c) Approximately 10 new Loran-C stations are required to provide precise navigation coverage in the Atlantic area. Estimated costs of these facilities are roughly equal to the cost of 2 Omega stations for navigation coverage of the area.

### 3.2 SUPPLEMENTARY NAVIGATIONAL METHODS

Excluding conventional means of navigation at sea, and in addition to the previously discussed Loran-C and Omega, several methods and techniques offer possibilities of determining position, and by further computation, course and speed, with reasonable accuracy. There are disadvantages to each with regard to their application to the singular problems of AROD. They are mentioned here as representative of back-up methods available in the event of loss of the basic navigation capability.

#### 3.2.1 Acoustic Positioning

Recently, developments in acoustical means have considerably increased the accuracy potential of ship positioning relative to fixed underwater objects. Each of the following has been used with some success:

##### a) Bathymetric Navigation.

Bathymetric navigation is by far the simplest of these acoustical means and requires the least amount of unusual equipment. It has been demonstrated that three techniques, profile-matching, line of sounding method, and contour advancing, may be successfully employed to position a ship relative to a unique bottom feature. Obviously, the "strength" of the feature affects the reliability of a fix, but recoveries with errors not larger than 500 feet are attainable under certain conditions, using a stabilized, narrow-beam echo-sounder of suitable depth range with a facsimile type expanded-scale recorder.

To establish the character and position of the bottom feature by survey methods, a good highly-repeatable external means of navigational control is required. The bathymetric navigation system is then applicable for positioning within the survey area if external navigational control is no longer available.

b) Underwater Trig Stations

The use of artificial undersea markers which would be used as underwater reference points or "trig stations" from which the position of a ship could be determined at sea offers further possibilities. The markers may be passive, as corner reflectors placed on the bottom in featureless terrain to provide a readily discernible target for ship-board sounding gear; or they may be transponders or active acoustic beacons, capable of detection at greater ranges, and coded for purposes of identification. The need for power for the active devices is an obvious disadvantage but must be weighed against a need for range, discrimination and identification.

One system of interest would consist of three units (active or passive) on the bottom in the form of a near-equilateral triangle.<sup>19</sup> If the triangle sides are held to such length that the transmitted sound enters the water nearly vertically, refractive errors are minimized. Unfortunately, the geometry of such a positioning system is poor and range measurements of high accuracy would be required. Under field conditions, acoustic range accuracies on the order of 1:10,000 are now attainable when the characteristics of the water column can be adequately defined. At present, accuracy of a fix relative to the submerged units is subject to improvement. As the ability to accurately establish acoustic ranges increases through further development, repeatabilities comparable to Loran-C should be attainable.

As a means of further reducing the effect of refraction and the non-homogenous medium, these units may be mounted in moored buoys submerged at a depth of several hundred feet beneath the water surface. At such depth, a greater degree of oceanographic stability

may be expected and the buoys will probably stabilize. Ranges in this case may be considered reliable, as above, but motion of the buoys must be determinable.

### 3.2.2. Geophysical Techniques for Navigation at Sea

The present state of the art of observing gravity and total magnetic intensity at sea lends itself to development of a means of positioning comparable in accuracy to bathymetric navigation (500 feet).<sup>20</sup> Most significant is the fact that these means are completely independent of emissions or reliance on external sources to recover a known position, after an initial survey has been conducted. Surveys at sea employing stabilized gravity meters and/or towed magnetometers must be carried out with external control to locate anomalies of suitable characteristics to permit recovery at a later date. The external control is necessary to achieve internal survey consistency and absolute position. Positioning at the time of recovery is simple in practice, requiring only manual matching of contours.

### 3.2.3 Flash Triangulation

Extension of the advanced geodetic tool described in Section 2 to positioning a ship at sea has been found feasible.<sup>21</sup> A properly stabilized camera aboard ship should be capable of providing the same accuracy of position (50-100 feet) as is possible on land. The use of the system is restricted by data reduction time, weather and sky brightness. However, when time is not critical, operations can be scheduled to take advantage of most favorable conditions.

It is apparent that flare triangulation in combination with acoustic or other means of relating the position of a ship at sea to a point on the ocean bottom may be used to establish the geodetic coordinates of that point. By reversing the procedure, the position of the ship may be established at a later date with a repeatability comparable to that of Loran-C.

### 3.3 SATELLITE METHODS

This section provides a preliminary investigation of the feasibility of using satellites with well-defined orbits in determining a ship's position and velocity. Consideration is given to the use of four observation techniques: 1) direction; 2) time rate of change in direction; 3) range; and 4) time rate of change in range. The conclusion on the suitability of these methods must be considered tentative because of the strong assumptions that had to be made concerning the satellite orbital characteristics and shipboard instrumentation capabilities.

#### 3.3.1 Necessity to Make Assumptions

In order to properly analyze the feasibility of using satellites with well-defined orbits for determining a ship's position and velocity, the answer to certain questions are required; or, for the lack of answers, certain assumptions must be made. The following questions are samples of those that need answers:

a) What means can be used to track or observe the satellite from shipboard? Photography of a sunlit satellite? Photography of a flashing-light satellite? Visual observations of either of these with an angle-measuring device? Radar ranging, with or without a satellite-borne transponder? Measurement of the Doppler shift of the frequency transmitted from a satellite-borne oscillator? Continuous measurements of the Doppler shifted frequency as a function of the time (during the course of a satellite pass)? Measurement of the integrated Doppler cycle count for a given time interval? Measurement of the time interval corresponding to a given pre-selected integral Doppler cycle count?

b) What information is available to the ship? Orbital elements of the "well-defined orbit" at some time  $t_0$  and their variation with time (including terms proportional to integral powers of the time interval from  $t_0$ , i.e., containing  $(t - t_0)^n$  as a factor, with  $n$  a positive integer), or periodic terms containing a factor of the type  $\frac{\sin}{\cos} 2\pi m(t - t_0)/T$ , where  $m$  is an integer and  $T$  is the satellite orbital period? Orbital

elements, updated at frequent intervals (like Transit)? An ephemeris of position and velocity?

c) What is meant by a "well-defined orbit?" What are the errors associated with tracking the satellite by the tracking stations on whose data the orbit is based? What perturbations are taken into account in computing the orbit? What non-negligible perturbations have been left out of account?

d) What computing facilities are contemplated, and where are they located? On board ship? At a distant land-based computing center? What sort of communications are available in the latter event?

e) How soon after observation of the satellite must the ship's position or velocity be computed from the tracking data? Seconds, minutes, hours, days later? With what precision must they be known?

The answers to the foregoing questions—either given or assumed—very much affect whether it is feasible to determine a ship's position and velocity. In the following, it will be made clear what assumptions are being made.

### 3.3.2 General Remarks on the Problem

In this discussion the errors arising from the fact that the geodetic locations of stations are not yet referred to a uniform worldwide geodetic datum for the entire surface of the Earth are ignored. Errors arising from this cause constitute a separate problem, (see Section 2 of this Appendix), and can be treated separately from the errors with which we are concerned here; namely, the errors of position and velocity of a ship as determined from observations of a passing satellite.

It is certainly feasible to obtain a ship's position from observations of a passing satellite. The equivalent has been carried out in the Transit satellite program, for which observational data consist of a "Doppler curve," that is, the observed frequency of a continuous-wave sinusoidal signal transmitted from a satellite in which the transmitted frequency is very accurately controlled, as a function of the time. Time signals are also transmitted by the satellite. Although some of the results of this program are still

classified, it is possible to say that the publicly announced objective of obtaining a terrestrial position with an accuracy of  $\pm 1/4$  mile has been achieved.

A position correct to  $\pm 1/4$  mile is good enough for most navigational purposes, but geodetic accuracy implies greater precision. In present practice, first-order geodetic surveys have an accuracy of 1 part in  $10^5$  or better. Over distances comparable to the North American continent (say, 4 to 6 thousand kilometers), this standard implies an error in the relative position of two stations at points well separated in the geodetic net of, say,  $\pm 40$  to  $\pm 70$  m. We shall therefore assume that to qualify as a geodetically valuable determination, a position must be determined with an error not exceeding  $\pm 100$  m.

a) Position

It is possible to improve on the quarter-mile accuracy quoted above—in fact, it is possible to achieve geodetic accuracy—from the observation of a passing satellite. This is especially true if all the methods listed under Section 3.3.1a are used and even more especially true if they are used together simultaneously.

Methods of determining a ship's position from satellite tracking data can logically be put into one of four classes:

- (1) Those using the direction of the satellite as seen from the ship, i.e., its elevation angle or azimuth, or both, its right ascension or declination, or both;
- (2) Those using the time rate of change of direction as seen from the ship;
- (3) Those using the (slant) range to the satellite from the ship;
- (4) Those using the time rate of change of the (slant) range.

Techniques for measuring the direction include photography of the illuminated satellite; visual measurement of the angular position of the satellite with optical devices of the theodolite family; electronic measurement of directions with radio interferometers, radar, directionally

sensitive antennas, etc. The only technique in this class which can yield a position with geodetic accuracy (i.e., with an error no greater than  $\pm 100$  m with respect to the same system of coordinates to which the satellite orbit is referred) from observations of a single pass is the photography of an illuminated satellite against a background of reference stars. Errors as small as 2" to 4" are already routine. For ground stations using cameras with focal lengths of the order of 1 m, single observations should be capable of yielding the angular position of the satellite with errors smaller than 1" of arc.

An angular error of 2" for a satellite 1000 km distant from the observer corresponds to an error of 10 m in his position, and an error of 1 msec in timing the observation corresponds to about 7 m. Although intrinsic accuracy of the photographic method is probably as high, if not higher, than any of the other methods (including those mentioned below), the photographs must be taken either from a stabilized platform (which may require special development) or with such short exposures that the ship's motion does not blur the star images. The method and its mathematics are conceptually simple, and have been used by astronomers for decades; on the other hand, the time required to process photographs, measure them and reduce the data, etc. can hardly be less than several hours.

Techniques currently available for measuring the rate of change of direction are the same as those for measuring direction itself, but more observations are required. Reductions are mathematically more complicated, accuracy is somewhat degraded, and nothing is gained over using the same data to obtain direction. Therefore, this method need not be considered further.

Techniques for measuring the range to a satellite measure either the travel time of a radio or light pulse (radar, maser-laser, etc.) or the phase of a signal returned from the satellite compared to the phase of an outgoing signal (phase comparison radar, transponders at the target, etc.). Precision of the first method is limited to the precision of measuring the length of short time-intervals. The best radars are capable of measuring

this interval with an error of the order of 0.03 microseconds corresponding to an error in the (round-trip) distance of 10 m. Phase-measurement methods are intrinsically capable of yielding even more accurate results—i.e., to a fraction of a wavelength of the radio-frequency radiation used, which can in principle be as little as a few centimeters—but to achieve this degree of precision, the total number of wavelengths between the station and the target must be known, so that phase lock must be maintained throughout the course of a run. Ordinary time-delay radars are used on shipboard, and there seems to be no reason why radars may not also be used in conjunction with transponder systems on a satellite.

Techniques for directly measuring the range rate, which depend on measurement of the Doppler shift of a signal transmitted from the satellite, are well developed in the Transit system. The Doppler curve for an entire pass of some minutes' duration contains a great deal of positional information, and the fitting of this curve with parameters that describe the position of the ship can, with certain ship-satellite geometries, yield these parameters with geodetic accuracy. The full equation representing the Doppler curve is very complicated and the fitting of the curve to the observed curve by adjusting the positional and other parameters requires a large computer if it is to be done in a short time. Differential correction methods are mathematically simple and easy, however, and will be used as the basis of discussion below.

All these methods require that the observer be able to record the time of his observations with an error not exceeding several milliseconds.

b) Ship's velocity

The ship's average velocity for a given time interval can naturally be determined from its position at the beginning and end of the interval. This interval may be quite short; e.g., two fixes, each having an accuracy of  $\pm 100$  m obtained one hour apart, would give the ship's average velocity with an accuracy of about  $\pm 0.04$  meter/sec or about  $\pm 0.1$  knot. The error in direction would depend on the speed of the ship: at 20 knots the error is of the order of 5 milliradians, or about  $0.3^\circ$ .

The only one of the previously mentioned tracking methods that allows the possibility of determining a ship's velocity from a single set of observations is the Doppler technique. The mathematical expression for the Doppler curve contains parameters expressing the ship's velocity in three dimensions. In fitting the theoretical curve to the observed curve, the ship's motion is usually treated as known, but it can in principle also be treated as unknown, and be derived from the curve. Whether there is any advantage in determining the ship's motion directly from the tracking data is a moot question, which is discussed in greater detail below. Suffice it to say for the present that: (1) simultaneous solution of Doppler curve data for position and velocity will degrade the accuracy of the position determination, apparently very seriously in some situations, and the velocity determined may not be much better than a velocity measured with respect to the water with due allowance for ocean currents and wind drift; (2) the velocity derived from a Doppler curve will in general be worse than one derived from two positional fixes separated by an interval of the order of an hour; (3) if a positional fix is obtained by some method other than the Doppler curve, the position coordinates can then be treated as known quantities and the velocity of the ship can be derived from the Doppler curve with a precision which might, under some circumstances, be worthwhile.

### 3.3.3 Mathematical Notes

In the following we use well known methods (see, e.g., S. Herrick, Astrodynamics, Van Nostrand 1961). We shall not go into any detail, but shall give a very brief sketch of how position and velocity might be determined from satellite tracking data obtained on shipboard.

We adopt the right-handed rectangular inertial coordinate system to which the satellite orbit is usually referred, with: (1) the origin at the center of gravitational attraction of the Earth; (2) the x-axis pointed toward the vernal equinox (right ascension  $\alpha = 0^{\circ}$ , declination  $\delta = 0^{\circ}$ ), (3) the y-axis pointed toward  $\alpha = 90^{\circ}$ ,  $\delta = 0^{\circ}$ ; and (4) the z-axis pointed

toward the north celestial pole,  $\delta = +90^\circ$ . The ship's rectangular coordinates are  $(X, Y, Z)$ . Capital letters refer to the ship, lower case to the satellite. The ship's spherical coordinates will also be useful. These are  $R$  (geocentric radius),  $\Theta$  (local sidereal time, or longitude measured eastward from the  $x$ - $z$  plane), and  $\Phi$  (geocentric latitude). Geocentric coordinates are easier to use in satellite problems, since, as noted above, the satellite's coordinates are already given in this system. For the ship's position, conversion backward and forward to ordinary geographic (geodetic) coordinates presents no problems. The ship's ordinary (geographic, geodetic, or geocentric) longitude measured eastward from the meridian of Greenwich will be denoted by  $\Lambda$ , and is related to  $\Theta$  by the equation

$$\Theta = \text{Greenwich Sidereal Time} + \Lambda \quad (1)$$

It is also convenient to denote the perpendicular distance of the ship from the Earth's axis of rotation by  $W$ , where

$$W = (X^2 + Y^2)^{1/2} \quad (2)$$

If the ship is stationary,  $W$  does not vary, although  $X$  and  $Y$  vary continuously because of the Earth's rotation.

Let the position vector of the ship be denoted by  $\underline{R}$ , and that of the satellite by  $\underline{r}$ . Let the position vector of the satellite as seen from the ship be  $\underline{\rho}$ . Then

$$\begin{aligned} \underline{\rho} &= \underline{r} - \underline{R} \\ &= \underline{r} - W (\underline{I} \cos \Theta + \underline{J} \sin \Theta) - \underline{K} Z. \end{aligned} \quad (3)$$

The position of the satellite is assumed to be given with a mean error (standard deviation) of  $\epsilon(\underline{r})$ , or to be calculated from a given set of orbital elements with or without their time variations, from which a set of errors  $\epsilon(\underline{r}, t)$  can be calculated as a function of the time.

The mathematical expressions needed to derive the position of a ship from satellite tracking data are naturally different for the three methods under consideration—direction, range, and range rate. For the first two

they are relatively simple and for the third very complicated. To avoid complications, we shall examine the expressions for the differential correction of an assumed position for the ship (and assumed velocity), which are very simple. The feasibility and accuracy with which a ship's position can be definitively obtained from the data are in no way diminished by this method. In fact, from the mathematical standpoint, such reductions are made more feasible, in the sense that they become so simple that most of them can be carried out without a large computer.

From (3) we see that the differentials are connected by the expression

$$\Delta \underline{\rho} = \Delta \underline{r} - \Delta \underline{R} \quad (4)$$

in which  $\Delta \underline{\rho} = \underline{\rho}$  (observed) -  $\underline{\rho}$  (computed from assumed position);

$\Delta \underline{r} = \underline{r}$  (observed) -  $\underline{r}$  (computed);

= 0, under the assumption that the satellite position is known;

and

$\Delta \underline{R} = \underline{R}$  (true) -  $\underline{R}$  (assumed).

The vector differential  $\Delta \underline{\rho}$  cannot be determined from any of the tracking methods used by itself, but one or more components of  $\Delta \underline{\rho}$  can be measured. A sufficient number of individual observations of the observable component of  $\Delta \underline{\rho}$  will yield a solution for the corresponding component of  $\Delta \underline{R}$ ; if a suitable time elapses (e.g., several minutes) between the individual observations in the same run, the components will be sufficiently different in direction to allow a three-dimensional determination of  $\Delta \underline{R}$ .

One other point should be mentioned. If the height of the geoid (sea-level surface) above or below the geodetic spheroid of reference is sufficiently well known, then only two coordinates for the ship will be required, its latitude  $\Phi$  and longitude  $\Lambda$ , since  $R$  is effectively known. Since the geoid height is known with an error which rarely exceeds 50 m, even in the open sea, the two-coordinate solution is applicable whenever errors of this order are allowable in the solution, or where other factors have already contributed to producing a larger error.

### 3.3.3.1 Three-Dimensional Solution from Direction Data

The observational data,  $\Delta\alpha_i$  and  $\Delta\delta_i$ , are the differences, observed minus computed, of the right ascension and declination of the satellite at a time  $t_i$ , as determined from shipboard observations. In other words we observe the two components of  $\Delta\rho$  perpendicular to the line of sight, and know nothing about the component along the line of sight. These two components are:

$$\begin{aligned}\Delta\rho_{\alpha} &= \rho \cos \delta \Delta\alpha = \Delta\rho \cdot \underline{A} , \\ \Delta\rho_{\delta} &= \rho \Delta\delta = \Delta\rho \cdot \underline{D}\end{aligned}\quad (5)$$

where  $\underline{A}$  and  $\underline{D}$  are two members of a triad of unit vectors forming a right-handed orthogonal matrix ( $\underline{L}$ ,  $\underline{A}$ ,  $\underline{D}$ ).  $\underline{L}$  is directed outward along the line of sight,  $\underline{A}$  is directed perpendicular to the line of sight eastward along the declination circle through the satellite, and  $\underline{D}$  is directed perpendicular to the line of sight northward along the hour circle through the satellite.

$$\begin{aligned}\underline{L} &= \begin{pmatrix} \cos\alpha \cdot \cos\delta \\ \sin\alpha \cdot \cos\delta \\ \sin\delta \end{pmatrix} , \\ \underline{A} &= \begin{pmatrix} -\sin\alpha \\ \cos\alpha \\ 0 \end{pmatrix} , \\ \underline{D} &= \begin{pmatrix} -\cos\alpha \cdot \sin\delta \\ -\sin\alpha \cdot \sin\delta \\ \cos\delta \end{pmatrix}\end{aligned}\quad (6)$$

We have also, (using equation 3):

$$\begin{aligned}\Delta\rho &= -\Delta R \text{ (since } \Delta r = 0) \\ &= -\Delta W (\underline{I} \cos\Theta + \underline{J} \sin\Theta) - W\Delta\Theta (-\underline{I} \sin\Theta + \underline{J} \cos\Theta) - \Delta Z \underline{K},\end{aligned}\quad (7)$$

where  $\underline{I}$ ,  $\underline{J}$ ,  $\underline{K}$  are unit vectors in the x, y, z directions. The bracketed vectors might be abbreviated  $\underline{F}$  and  $\underline{E}$ , with

$$\underline{F} = \begin{pmatrix} \cos \Theta \\ \sin \Theta \\ 0 \end{pmatrix} \quad \text{directed toward the intersection of the celestial equator and the local meridian}$$

and

$$\underline{E} = \begin{pmatrix} -\sin \Theta \\ \cos \Theta \\ 0 \end{pmatrix} \quad \text{directed eastward along the celestial equator at the local meridian,}$$

forming with

$$\underline{K} = \begin{pmatrix} 0 \\ 0 \\ 1 \end{pmatrix}$$

another orthogonal matrix of unit vectors.

When multiplied out, equation 5 gives the following pair of observation equations:

$$\begin{aligned} \Delta \rho_{\alpha} &= \Delta W \sin (\alpha - \Theta) - W \Delta \Lambda \cos (\alpha - \Theta) \\ \Delta \rho_{\delta} &= \Delta W \sin \delta \cos (\alpha - \Theta) + W \Delta \Lambda \sin (\alpha - \Theta) - \Delta Z \cos \delta. \end{aligned} \quad (8)$$

Since there are three unknowns,  $\Delta W$ ,  $\Delta \Lambda$  and  $\Delta Z$ , obviously a minimum of two complete observations will be required. Care should be taken to space these several minutes apart, so that the satellite will be viewed from quite a different direction, and the two lines of sight will cross at a sufficiently large angle so that the full accuracy of the method will not be degraded by poor geometry.

Assuming that  $\epsilon(\Delta \rho) \cong 10^{-4} \rho$  (20" of arc), that the trigonometric coefficients are of the order 0.1 to 1.0, that the satellite is of the order of 1000 km from the ship, and that the geometry has been used to best advantage to get an independent set of observation equations, then the errors of  $\Delta W$ ,  $W \Delta \Lambda$ , and  $\Delta Z$  will be of the order of 100 meters. Better observations (such as are now possible from land), or a least-squares solution of many more than two observations will improve this figure; a satellite slant range greater than 1000 km will worsen it.

### 3.3.3.2 Two-Dimensional Position from Directional Data

In the two-dimensional case, corresponding to the three-dimensional case with unknowns  $\Delta W$ ,  $\Delta\Lambda$  (or  $\Delta\Theta$ ) and  $\Delta Z$ , we now have:

$$\begin{aligned}\rho \cos \delta \Delta \alpha &= -R\Delta\Phi \{ \sin \Phi \sin (\alpha - \Theta) + \cos \Phi \} \\ &\quad + R\Delta\Lambda \cos \Phi \cos (\alpha - \Theta), \\ \rho \Delta \delta &= R\Delta\Phi \{ \sin \Phi \sin \delta \cos (\alpha - \Theta) + \cos \Phi \cos \delta \} \\ &\quad - R\Delta\Lambda \cos \Phi \sin \delta \sin (\alpha - \Theta)\end{aligned}\tag{9}$$

These are two observation equations in two unknowns  $\Delta\Phi$  and  $\Delta\Lambda$ .

The chief source of error here might be  $\epsilon(\rho)$ , which will be about as large as the error in the assumed position, i.e.,  $R\Delta\Phi$ , and  $R\cos\Phi\Delta\Lambda$ . If  $\epsilon(\rho)/\rho$  is about  $10^{-2}$  (which is easily possible), then  $\epsilon(\Delta\Phi)/\Delta\Phi$  will be of the order of  $10^{-2}$  on the average; or if  $R\Delta\Phi \cong 10$  km, then  $\epsilon(\Delta\Phi)R \cong 100$  meters. If the intrinsic errors of the original observations correspond to much less than 100 meters at the surface, then an iteration (using the improved position obtained from the first solution as an assumed position) would be worthwhile.

It will be noted that a mathematical solution for  $\Delta\Phi$  and  $\Delta\Lambda$  is now possible with only one observation in the two-dimensional case, which is intuitively obvious from the intersection of a determined line through a determined surface.

### 3.3.3.3 Three-Dimensional Position from Range Observations

The observed quantity is the component of  $\Delta\rho$  in the line of sight. We take as before:

$$\Delta\rho = -\underline{F} \cdot \Delta W - \underline{E}W\Delta\Theta - \underline{K}\Delta Z.\tag{10}$$

The component of  $\Delta\rho$  in the line of sight is

$$\Delta \rho \underline{L} = \Delta \rho \cdot \underline{L} = \Delta \rho (\text{range}). \quad (11)$$

Multiplying out gives linear scalar observation equations of the form

$$\Delta \rho (\text{range}) = -\Delta W \cos(\alpha - \theta) \cos \delta - W \Delta \Lambda \sin(\alpha - \theta) \cos \delta - \Delta Z \sin \delta, \quad (12)$$

with three unknowns  $\Delta W$ ,  $\Delta \Lambda$ , and  $\Delta Z$ . Thus one range observation of three different satellites (nearly) simultaneously, or three range observations of a single satellite separated in time sufficiently so that the directions will be different, will determine a fix. This is also easily deducible from the geometry of the situation. The errors in the three-dimensional fix will be of the same order as the range observations themselves, if the geometry is favorable; they will be worse if the geometry is unfavorable, and better if a solution is obtained from a least-squares solution of many individual observations. These errors of observation are of the order of 10 meters or better with present high-quality radars. It is worth mentioning that the solution of a set of equations becomes very weak if all the observations must be made near  $\delta = 0^\circ$  or  $\delta = +90^\circ$ . For instance, at  $\delta = 0^\circ$ , the coefficient of  $\Delta Z$  is very small and  $\Delta Z$  is nearly indeterminate.

#### 3.3.3.4 Two-Dimensional Case, Range Measurements

Here,  $\Delta \rho \cdot \underline{L}$  yields:

$$\Delta \rho (\text{range}) = -R (C_1 \Delta \Phi + C_2 \Delta \Lambda), \quad (13)$$

where

$$C_1 = \cos \delta \{ -\sin \Phi \cos(\alpha - \theta) + \cos \Phi \},$$

$$C_2 = \cos \delta \cos \Phi \sin(\alpha - \theta).$$

Two observations of range would give a solution for  $\Delta \Phi$  and  $\Delta \Lambda$ . The conditions for good and poor solutions are nearly the same as for the three-dimensional case discussed above.

For both cases, we have assumed that  $\alpha$  and  $\delta$  are known to about  $1:10^5$ , and  $\phi$  and  $\theta$  to about  $1:10^5$ , so that the errors of  $R\Delta\phi$  and  $R\cos\phi\Delta\lambda$  will be the same order of magnitude as the range observations. If the errors of  $\alpha, \delta, \phi$ , and  $\theta$  are worse, the error in  $\Delta\rho$  may become the predominant factor, in which case an iteration will be required.

### 3.3.3.5 Three-Dimensional Position Determined from Range-Rate Measurements

In order to use equation 3 in the range-rate method, we differentiate it with respect to time, and obtain:

$$\dot{\underline{\rho}} = \dot{\underline{r}} - W\dot{\theta} (-\underline{I}\sin\theta + \underline{J}\cos\theta). \quad (14A)$$

The foregoing equation is correct, strictly speaking, only for a fixed station. It should be slightly modified for a moving ship since an error in the ship's speed of one knot leads to an (average) error in position of about 400 meters. The equation must be modified if it is desired to solve for differential corrections to the ship's velocity as unknowns (see equation 18 below).

Equation 14A yields the following vector equation for the differential correction of position:

$$\Delta\dot{\underline{\rho}} = \Delta\dot{\underline{r}} + \dot{\theta}\Delta W (\underline{I}\sin\theta - \underline{J}\cos\theta) + W\Delta\lambda (\underline{I}\cos\theta + \underline{J}\sin\theta). \quad (14B)$$

We may set  $\Delta\dot{\underline{r}} = 0$ , under the assumption that we have perfect knowledge of the orbit. The left-hand side of (14B) represents the difference:

$$\Delta\dot{\underline{\rho}} = \dot{\underline{\rho}}(\text{observed}) - \dot{\underline{\rho}}(\text{computed}) \quad (15)$$

and is obtained from observation. In the range-rate method, we can measure only the absolute value of  $\Delta\dot{\underline{\rho}}$ , not its vector components. Forming the dot product of both sides of (15) with  $\dot{\underline{\rho}}(\text{observed}) + \dot{\underline{\rho}}(\text{computed})$ , and dropping terms of the order  $(\Delta\dot{\underline{\rho}})^2$  gives:

$$\Delta \dot{\rho} = [2 \dot{\rho} \text{ (computed)} \cdot \Delta \dot{\rho}] / [\dot{\rho} \text{ (observed)} + \dot{\rho} \text{ (computed)}] \quad (16)$$

Substitution of (15) into (16) gives the following linear scalar equation in the two unknowns  $\Delta W$  and  $\Delta \Lambda$  :

$$\Delta \dot{\rho} = \frac{2 \dot{\theta}}{\dot{\rho} \text{ (obs)} + \dot{\rho} \text{ (comp)}} \{ \Delta W (\dot{\rho}_x \sin \theta - \dot{\rho}_y \cos \theta) + W \Delta \Lambda (\dot{\rho}_x \cos \theta + \dot{\rho}_y \sin \theta) \} \quad (17)$$

This means that, in principle, two instantaneous observations of the range-rate of a passing satellite will supply two linear equations which can be solved simultaneously for  $\Delta W$  and  $\Delta \Lambda$ . Such a minimum set of observations, however, is likely to result in a rather inaccurate solution, so that a least-squares solution based on many observations (from a single run) is advisable. In general, such differential corrections can give the correct position with errors of the order of several tens of meters—better with some satellite-pass-versus-ship geometries, worse with others (see below). Furthermore, if the first assumed ship's position,  $W, \Lambda, Z$ , is very far off, it may be necessary to iterate through the differential correction procedure more than once. This process, however, converges rapidly.

Note that, in obtaining equation 14A, differentiation with respect to time had the effect of eliminating  $Z$  from all later equations. We are therefore dependent on  $W$  and  $\Lambda$  to fix a position. In principle, these are quite sufficient; but near the equator  $W$  is an insensitive function of the latitude ( $\cos \Phi = W/R$ ) and so does not give a very accurate fix in latitude.

To estimate the errors, we make the following assumptions:

- The standard error on the observed Doppler shift in frequency is 0.1 cps;
- The error in the computed Doppler-shifted frequency is 0;
- The error in the assumed value of the carrier frequency is not greater than 4 c/sec;
- The error in the velocity of light is 0.3 km/sec;

- The carrier frequency is of the order of 400 Mc/sec;
- The difference between the observed and computed Doppler frequency shift is not greater than 1 kc/sec.

If one substitutes reasonable and self-consistent values of the coefficients into equation 17, together with errors derived from the foregoing assumptions, the resulting solution for one of the unknowns (e.g.,  $\Delta W$ ) will have an error ranging from tens of meters (in the case of extremely favorable geometry) to  $\pm 1000$  meters or more (extremely unfavorable case). The estimated error is due in great measure to the first ingredient, i.e., the error in the measured Doppler shift. The error expected in practice might be greater than the 0.1 cps quoted above, so that the error in  $\Delta W$  would be correspondingly larger. On the other hand, the error in  $\Delta W$  can be reduced by making more than the minimum number of instantaneous observations necessary for an algebraic solution. One can think of the entire run of some minutes' duration being cut up into numerous samples (for example, 100), each a few seconds long, to give an equal number of observation equations. If the observed Doppler frequency curve is displaced point-by-point in a random way from the ideal curve, Gaussian statistics would apply and a least-squares solution could be made to give a much-improved result. In actual practice, ionospheric and tropospheric propagation effects displace the observed Doppler frequency systematically over the entire curve or parts thereof. These effects can be largely removed by suitable corrections, but the uncorrected remainder can still result in a small systematic error in the position derived from a single run (i.e., one satellite pass).

We quote recent estimates of the standard error for positions actually derived from single runs of a Transit satellite (oral communication with Applied Physics Lab.). The starred entries are relevant to the present discussions.

- \*  $\pm 40 - \pm 50$  meters - due to instrumental errors.
- \*  $\pm 50$  meters - tropospheric effects uncorrected.
- \*  $\pm 10$  meters - tropospheric effects corrected.

$\pm 400$  meters (day)      - ionospheric effects at 324 megacycles;  
 $\pm 150$  meters (night)      largely eliminated by the use of more  
    than one frequency.

$\pm 250$  meters - uncertainties in earth's gravitational field over  
 the orbit

This last entry may be regarded as another aspect of the problems associated with poor long-arc geodetic ties discussed under Section 2. Both problems - i.e., improvement of long-arc geodetic ties and the prediction of small but cumulative orbital perturbations produced by irregularities in the earth's gravitational field - could be solved by having a reasonably dense worldwide net of gravity data. Obviously all satellite orbits are affected by this error.

### 3.3.3.6 Two-Dimensional Case, Range-Rate Measurements

Putting

$$R = R (\underline{I} \cos \Phi \cos \theta + \underline{J} \cos \Phi \sin \theta + \underline{K} \sin \Phi)$$

and differentiating with respect to time, we obtain the vector equations:

$$\Delta \dot{R} = -R \begin{pmatrix} \dot{\theta} (\Delta \Phi \sin \Phi \sin \theta - \Delta \theta \cos \Phi \cos \theta) - \dot{\Phi} (\Delta \Phi \cos \Phi \cos \theta + \Delta \theta \sin \Phi \sin \theta) \\ \dot{\theta} (-\Delta \Phi \sin \Phi \cos \theta - \Delta \theta \cos \Phi \sin \theta) - \dot{\Phi} (\Delta \Phi \cos \Phi \sin \theta + \Delta \theta \sin \Phi) \quad \Phi \\ \cos \theta - \dot{\Phi} \Delta \Phi \sin \Phi \end{pmatrix} \quad (18)$$

In this equation the velocity components of the ship, expressed in rate of change of latitude and local sidereal time (the latter including change due to motion in longitude), are assumed to be known.

Substitution into equation 16 will yield in a straightforward way a linear scalar equation in the two unknowns  $\Delta \Phi$  and  $\Delta \theta$  ( $= \Delta \Lambda$ ). The errors of the solution are comparable with the three-dimensional case, with approximately the same restrictions.

### 3.3.3.7 Determining the Ship's Velocity from Satellite Tracking Data

As already mentioned, only Doppler data of the Transit system type are capable of giving a direct measure of the ship's velocity. For a given satellite pass, the ship's position has a much greater effect than the ship's velocity on the observed Doppler curve. ("Ship's velocity" here means the ship's motion through the sea, plus ocean current and wind drift effects; the motion due to the Earth's rotation has already been taken into account, since it applies equally to a fixed terrestrial station.) For this reason, it is foolish to consider trying to derive differential corrections to the ship's velocity with equations derived from equation 14B, unless either (a) the ship's position is already known with considerable precision, or (b) we derive equations for differential corrections for position and velocity simultaneously. We shall consider alternative (b) first.

Following procedures similar to those outlined above, one can obtain the following linear equation in the five unknown differential corrections: two for position, (only  $\Delta W$  and  $\Delta \Lambda$  since the third term corresponding to  $Z$  has dropped out, as before) and three for velocity ( $\Delta \dot{W}$ ,  $\Delta \dot{\Lambda}$ , and  $\Delta \dot{Z}$ ):

$$\Delta \dot{\rho} = \frac{2\dot{\rho} \text{ (comp)}}{\dot{\rho} \text{ (obs)} - \dot{\rho} \text{ (comp)}} \begin{pmatrix} -\Delta \dot{W} + W\dot{\theta} \Delta \Lambda \\ -W\Delta \dot{\Lambda} - \dot{\theta} \Delta W - W\Delta \dot{\Lambda} \\ -\Delta \dot{Z} \end{pmatrix} \cdot \begin{pmatrix} \dot{\rho}_x \cos \theta + \dot{\rho}_y \sin \theta \\ -\dot{\rho}_x \sin \theta + \dot{\rho}_y \cos \theta \\ \rho_z \end{pmatrix} \quad (19)$$

In principle, as before, we need a minimum of five observations of  $\Delta \dot{\rho}$  to furnish five linear equations to be solved simultaneously for the five unknowns. As before, a least-squares solution of a system of many more than five equations would give an improved solution.

In practice, these equations would probably still give an unsatisfactory result, for the following reason. The coefficients of the position terms contain either  $\dot{\theta}$  or  $W/W$ , which are of the order of  $10^{-4}$  or smaller, so that the position terms will be much more poorly determined than the velocity terms in the simultaneous solution. In fact, this natural internal weighting by the coefficients will have the effect of blaming almost the entire discrepancy between observed and computed range-rate on the velocity components, which will then receive large corrections, while the positions

remain virtually uncorrected. We therefore reject this method, and are left with alternative (a).

Alternative (a) presupposes that the ship's position is already known with considerable precision. One possibility would be to determine the ship's position from some method other than the range-rate method (e.g., from radar range measurements or angular position measurements). The differential correction equation for velocity components, analogous to equation 17 for position components, would then be:

$$\Delta \dot{\rho} = \frac{2}{\dot{\rho}(\text{obs}) + \dot{\rho}(\text{comp})} \begin{pmatrix} W \Delta \dot{\lambda} \\ \Delta \dot{W} \\ \Delta \dot{Z} \end{pmatrix} \cdot \begin{pmatrix} \dot{\rho}_x \sin \theta - \dot{\rho}_y \cos \theta \\ -\dot{\rho}_x \cos \theta - \dot{\rho}_y \sin \theta \\ \dot{\rho}_z \end{pmatrix} \quad (20)$$

Under favorable conditions (least-squares solution, good geometry, etc.), the accuracy of the velocity corrections may approach that of the left-hand side. Under fairly extreme but still reasonable assumptions, the error of measurement of  $\Delta \dot{\rho}$  might be as small as the order of 0.1 m/sec, which would give the ship's velocity to a fraction of a knot. Under average circumstances the result will probably not be that good. On the other hand, if the ship's velocity is already known from standard measurements, together with corrections for known currents or winds, to an accuracy of, say,  $\pm 1$  knot it would hardly be worthwhile to try to improve the velocity with satellite range-rate measurements.

### 3.3.4 Conclusions

Based on the preliminary considerations, on the assumptions made, and with the reservations given in specific cases, we conclude:

- That the determination of a ship's position with "geodetic accuracy" from satellite tracking data, is feasible;
- That under most circumstances the velocity can best be determined from two or more position fixes
- It appears that of the currently available satellite navigational techniques, the Transit system is the best developed and its use

would be more practicable than the others for the time-scale of the AROD flight test program (1964). Beyond this period more accurate position determinations may be achievable by the utilization of measurements from other types of satellites (with precisely-known orbits). Techniques such as flashing lights (e.g., ANNA) or transponders (e.g., SECOR) might reduce the Transit errors by more than an order of magnitude but would require much more shipborne equipment.

## REFERENCES

1. "A Singular Geodetic Survey," by L. S. Simmons. U. S. Coast and Geodetic Survey Technical Bulletin No. 13, dtd. September 1960.
2. "Photogrammetric Flare Triangulation—A New Geodetic Tool," by D. Brown. RCA Data Reduction Technical Report No. 46, dtd. December 1958.
3. "Satellite Triangulation," U. S. Coast and Geodetic Survey Information Bulletin, dtd. 1962.
4. "Results in Geodetic Photogrammetry II—A Study of the Feasibility of A Photogrammetric Survey of AMR to an Accuracy of 1 Part in  $10^6$ ," by D. Brown. RCA Data Processing Technical Report No. 65, dtd. September 15, 1960.
5. "The Progress of Hiran Surveying," by Carl I. Aslakson, Aero Service Corporation Report, dtd. May 1, 1957.
6. "Utilization of New Types of Distance Measuring Equipment in Integrated Military Surveys," by P. D. Thomas. Report on U. S. Coast and Geodetic Survey Project 40,000-849 (MIPR-ERDL 6-58) dtd. July 1958.
7. "Microwave, Digital, Geodetic, Survey Subsystem, Exhibit NR. WWDP-61-44A" dtd. June 26, 1961. Reconnaissance Systems Division, Wright-Patterson AFB, Ohio.
8. "The Role of Rocket-Flash Triangulation in World Geodesy," by O. W. Williams. Symposium, Geodesy in Space Age, February 1961. Institute of Geodesy, Photogrammetry and Cartography, Ohio State University Publication No. 15.
9. "The Geodetic Use of Artificial Earth Satellites," Final Report dtd. August 15, 1959, Parts I and II. AFCRC Report No. TR-59-276, PI. Systems Laboratories Corporation.
10. "Ellipsoid Parameters from Satellite Data," by J. A. O'Keefe, et al. Proceedings of a Conference on Contemporary Geodesy, Harvard College Observatory, 1958, American Geophysical Union, Geophysical Monograph 4:45-51, 1959.

11. "The Earth's Gravitational Potential Deduced from the Orbits of Artificial Satellites." *Geophysical Journal* 4:3-16, 1961.
12. "Army Map Service Mapping Activities in the Space Age," by Col. F. O. Diercks, AMS. *International Hydrographic Review*, Vol. 38, No. 1, dtd. January 1961.
13. "Project ANNA," by Cdr. M. M. Macomber. Paper presented at COSPAR Meeting, Washington, D. C., April 1962.
14. "Engineering Evaluation of the Loran-C Navigation System," Jansky & Bailey, Inc. dtd. September 30, 1959. U. S. Coast Guard Contract No. Tcg-40547 (CG-40,502-A).
15. "The Diurnal Carrier-Phase Variation of A 16-Kilocycle Transatlantic Signal," by J. A. Pierce. *Proceedings of the Institute of Radio Engineers*, Vol. 43, no. 5, May 1955.
16. "VLF Propagation Measurements for the Radux-Omega Navigation System," by C.J. Casselman, D.P. Heritage and M.L. Tibbals. *Proceedings of the Institute of Radio Engineers*, Vol. 47, No. 5.
17. "Omega Propagation Characteristics in the Arctic, Temperate and Tropical Regions," by L. Fletcher, U. S. Naval Research Laboratory Memorandum Report 1324, dtd. May 28, 1962.
18. "The Omega Long-Range Navigation System." U. S. Navy Electronics Laboratory, San Diego, California. Development Report No. 958, dtd. March 1, 1960.
19. "Some Aspects of Physical Geodesy," by Ewing, Worzel and Talwain. *Contemporary Geodesy*. American Geophysical Union, Geophysical Monograph No. 4. dtd. 1959.
20. "Geophysical Techniques for Precision Navigation at Sea," by Luskin and Davidson, Lamont Geological Observatory Technical Report No. 14, dtd. February 1957.
21. "A Photogrammetric Ship Positioning System," by N. C. Vance, U. S. Navy Oceanographic Office, Paper presented at 28th Annual Meeting of the American Society of Photogrammetry, March 1962.

## Appendix D

### MATHEMATICAL DERIVATIONS

This Appendix presents derivations of some important formulas used in various portions of the Feasibility Study. Two subjects are discussed herein—mixers and signal dynamics.

#### 1.0 MIXER ANALYSIS

Since mixers are used in many of the AROD circuits, equations for the signal-to-noise ratio of a mixed signal will be derived in this section. The inputs to the mixer are signals  $s_1(t)$  and  $s_2(t)$  which for mathematical simplicity will be considered as pure sine waves. However, the results are valid for all narrow band power spectra. The noises added to the input signals are represented as  $n_1(t)$  and  $n_2(t)$ . For mathematical simplicity it is assumed that both of these noises are white and the power densities are represented by  $N_{01}$  and  $N_{02}$ . The power spectra for the input signals and noise are shown in Figure D1. The output of the mixer is:

$$s(t) + n(t) = k[s_1(t) + n_1(t)][s_2(t) + n_2(t)] = k\{s_1(t)s_2(t) + s_1(t)n_2(t) + n_1(t)s_2(t) + n_2(t)s_2(t)\} \quad (1)$$

where  $k$  is a constant and has units of volts<sup>-1</sup>. For signal-to-noise considerations we can consider  $k = 1$  without loss of generality. The only term which is independent of noise is:

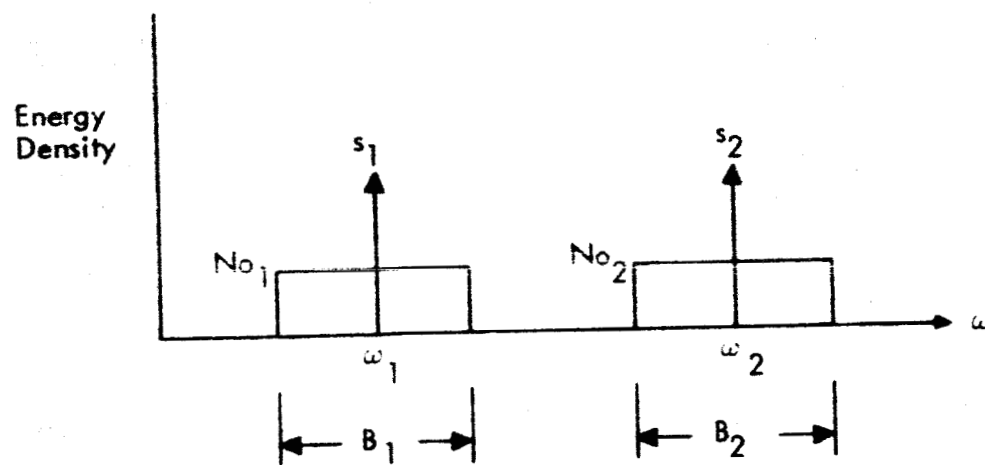
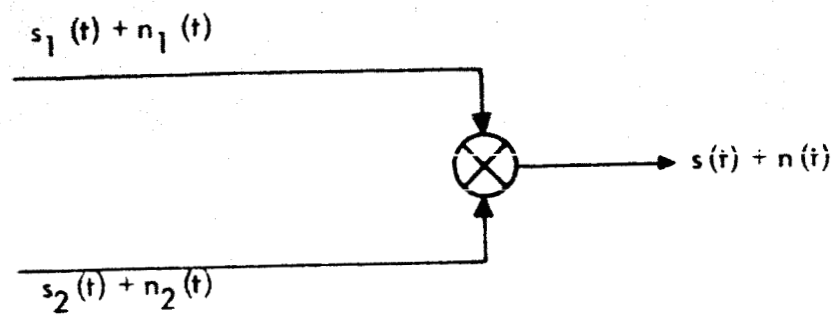


Figure D1. Mixer Parameters

$$s(t) = s_1(t)s_2(t) = [A_1 \cos \omega_1 t][A_2 \cos \omega_2 t] \quad (2)$$

$$s_1(t) = A_1 \cos \omega_1 t \quad s_2(t) = A_2 \cos \omega_2 t \quad (2a)$$

The output signal can be rewritten in the form:

$$s(t) = .5A_1A_2 \{\cos (\omega_1 - \omega_2)t + \cos (\omega_1 + \omega_2)t\} \quad (3)$$

The power spectrum of this signal is shown in Figure D2a.

The noise voltage in the output is given by:

$$n(t) = n_1(t)s_2(t) + n_2(t)s_1(t) + n_1(t)n_2(t). \quad (4)$$

The input noises can be written as Fourier integrals.

$$n_1(t) = \int_{\omega_1 - \frac{B_1}{2}}^{\omega_1 + \frac{B_1}{2}} \alpha_1(\omega) \cos \omega t d\omega \quad (5)$$

$$n_2(t) = \int_{\omega_2 - \frac{B_2}{2}}^{\omega_2 + \frac{B_2}{2}} \alpha_2(\omega) \cos \omega t d\omega \quad (6)$$

where  $\alpha_1(\omega)$  and  $\alpha_2(\omega)$  are random variables and  $B_1$  and  $B_2$  are the bandwidths of the white noise inputs which are centered at radian frequencies of  $\omega_1$  and  $\omega_2$ . In addition, since the noises are white with zero mean:

$$E[\alpha_1(\omega)] = E[\alpha_2(\omega)] = 0 \quad (7)$$

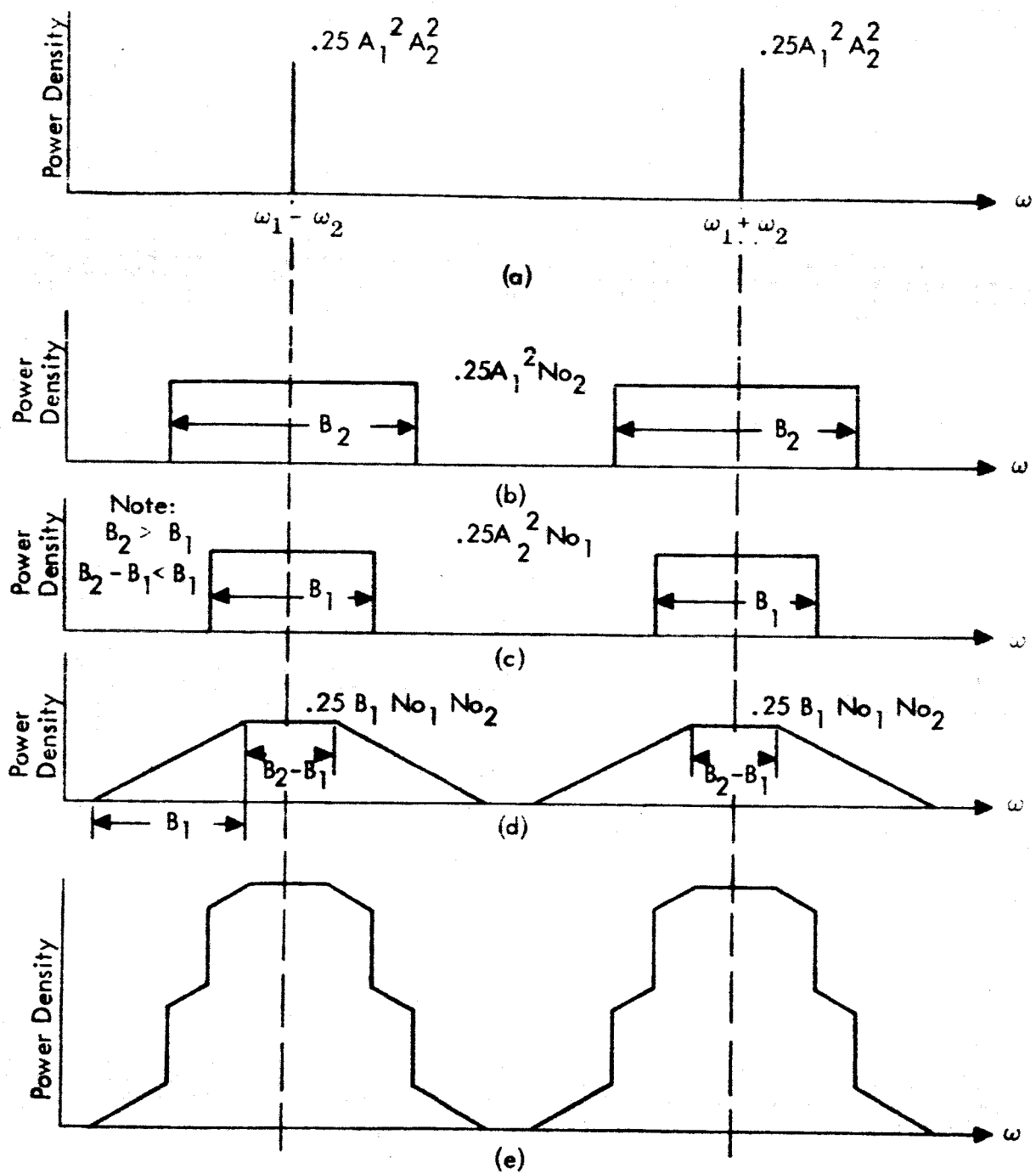


Figure D2. Mixer Output Spectra

$$E[\alpha_1^2(\omega)] = \begin{cases} 2 N o_1, & |\omega - \omega_1| < \frac{B_1}{2} \\ 0, & |\omega - \omega_1| > \frac{B_1}{2} \end{cases} \quad (8)$$

$$E[\alpha_2^2(\omega)] = \begin{cases} 2 N o_2, & |\omega - \omega_2| < \frac{B_2}{2} \\ 0, & |\omega - \omega_2| > \frac{B_2}{2} \end{cases} \quad (9)$$

It follows from Equations 2a and 6 that:

$$\begin{aligned} s_1(t)n_2(t) &= \left[ \int_{\omega_2 - \frac{B_2}{2}}^{\omega_2 + \frac{B_2}{2}} \alpha_2(\omega) \cos \omega t d\omega \right] A_1 \cos \omega_1 t \\ &= \frac{A_1}{2} \int_{\omega_2 - \frac{B_2}{2}}^{\omega_2 + \frac{B_2}{2}} \alpha_2(\omega) \cos (\omega - \omega_1) t d\omega + \\ &\quad \frac{A_1}{2} \int_{\omega_2 - \frac{B_2}{2}}^{\omega_2 + \frac{B_2}{2}} \alpha_2(\omega) \cos (\omega + \omega_1) t d\omega \end{aligned} \quad (10)$$

Hence, the spectrum of the  $s_1(t)n_2(t)$  is white in two separate frequency bands of width  $B_2$ ; one band is centered at  $(\omega_2 - \omega_1)$  and the other is at  $(\omega_2 + \omega_1)$ . This spectrum and the similar spectrum for  $s_2(t)n_1(t)$  are shown in Figures D2b and D2c.

The last noise term is:

$$n_{12}(t) \equiv n_1(t)n_2(t) = \left[ \int_{\omega_1 - \frac{B_1}{2}}^{\omega_1 + \frac{B_1}{2}} \alpha_1(\omega) \cos \omega t d\omega \right] \left[ \int_{\omega_2 - \frac{B_2}{2}}^{\omega_2 + \frac{B_2}{2}} \alpha_2(x) \cos x t dx \right]$$

$$= \frac{1}{2} \iint \alpha_1(\omega) \alpha_2(x) \{ \cos (\omega + x)t + \cos (\omega - x)t \} d\omega dx \quad (11)$$

In order to obtain the spectrum of  $n_{12}(t)$  it is convenient to first calculate its autocorrelation function:

$$R_{12}(\tau) \equiv \int_{-\infty}^{\infty} n_{12}(t)n_{12}(t + \tau) dt \quad (12)$$

Substitution of Equation 11 into 12 and integration over  $t$  yields:

$$R_{12}(\tau) = \frac{1}{4} \int_{y=\omega_1 - \frac{B_1}{2}}^{\omega_1 + \frac{B_1}{2}} \int_{x=\omega_2 - \frac{B_2}{2}}^{\omega_2 + \frac{B_2}{2}} \alpha_1^2(y) \alpha_2^2(x) \{ \cos (y + x)\tau + \cos (y - x)\tau \} dy dx \quad (13)$$

The spectral density  $S_{n_{12}}(\omega)$  is obtained by taking the Fourier transform of the autocorrelation function by use of the relationship:

$$S_{n_{12}}(\omega) = \int_{-\infty}^{\infty} R_{12}(\tau) e^{-j\omega\tau} d\tau \quad (14)$$

From Equations 13 and 14 we obtain:

$$S_{n_{12}}(\omega) = \frac{1}{4} \int_y \int_x \alpha_1^2(y) \alpha_2^2(x) \{ \delta(x + y + \omega) + \delta(x + y - \omega) + \delta(y - x + \omega) + \delta(y - x - \omega) \} dy dx \quad (15)$$

where  $\delta$  represents the Dirac delta function, which has the property,

$$\int_{\alpha_1}^{\alpha_2} f(x) \delta(x-a) dx = \begin{cases} f(a) & \text{if } \alpha_1 \leq a \leq \alpha_2 \\ 0 & \text{otherwise} \end{cases} \quad \alpha_1 < \alpha_2 \quad (16)$$

The expected value of the spectral density is obtained from Equation 15 and interchanging the order of the integrations over  $x$  and  $y$  with the expectation operation. The result is:

$$\bar{S}_{n_{12}}(\omega) = E[S_{n_{12}}(f)] = 1/4 \int \int E[\alpha_1^2(y) \alpha_2(x)] \left\{ \delta(x+y+\omega) + \delta(x+y-\omega) \right. \\ \left. + \delta(y-x+\omega) + \delta(y-x-\omega) \right\} dy dx \quad (17)$$

Since the input noises are independent substitution of Equations 8 and 9 into Equation 17 yields:

$$\bar{S}_{n_{12}}(\omega) = N_{o1} N_{o2} \int_{y=\omega_1-B_1/2}^{\omega_1+B_1/2} \int_{x=\omega_2-B_2/2}^{\omega_2+B_2/2} \left\{ \delta(x+y+\omega) + \delta(x+y-\omega) \right. \\ \left. + \delta(y-x+\omega) + \delta(y-x-\omega) \right\} dy dx \quad (18)$$

The integration yields the spectrum shown in Figure 2d.

Since the noise components are incoherent, the total noise power spectrum is obtained by adding the spectra shown in Figures D2a, 2b, and 2c. The resultant is shown in Figure D2e.

From Figures D2a and D2e it is obvious that the signal to noise ratio after passing the mixer output through a filter of bandwidth  $B_F$  and a center frequency of either  $(\omega_1 - \omega_2)$  or  $(\omega_1 + \omega_2)$  is:

$$(S/N)_0 = \frac{S_1 S_2}{S_1 N_{o2} + S_2 N_{o1} + B_1 N_{o1} N_{o2}} \frac{1}{B_F} \text{ if } B_F \leq (B_2 - B_1) \geq 0 \quad (19)$$

If  $B_F > B_2 - B_1$ , then the total noise power in  $B_F$  can be determined from Figure D2e.

An interesting case of Equation 19 results when  $(S_1/N_{o1}) = (S_2/N_{o2}) \gg B_1$  then Equation 19 reduces to:

$$(S/N)_0 = (S_1/2N_{o1}) (1/B_F) \quad (20)$$

In other words the signal to noise ratio of the mixed signal at the output of the filter is 3 db worse than the signal to noise ratio obtained by passing either input signal through a filter of bandwidth  $B_F$ .

Another case which is sometimes of interest is  $(S_1/No_1) \ll (S_2/No_2)$  and  $B_2 \ll (S_1/No_1)$ . Equation 19 then reduces to

$$(S/N)_0 = (S_1/No_1) (1/B_F). \quad (22)$$

## 2.0 SIGNAL DYNAMICS ANALYSIS

It is the purpose of this section to derive the equations determining the range of signal characteristics with which the phase-locked loops will have to operate. The operational envelope for the spacecraft is again assumed to be 90 - 2000 nautical miles, and it is assumed that circular orbits with altitudes between these limits are representative of the AROD missions. For these assumed characteristics then, the equations for the doppler frequency ( $f_d$ ) and rate of change of doppler frequency ( $\dot{f}_d$ ) are determined, and their maximum values calculated.

In Figure D-3 the geometry for the analysis to follow is shown. The expression for the rate of change of  $r$  with time and the second time derivative will be used to obtain and evaluate the equations for the doppler frequency and its rate of change.

At any point in time:

$$r^2 = (R_e + h)^2 + R_e^2 - 2R_e (R_e + h) \cos \theta$$

Differentiating with respect to time:

$$2r\dot{r} = 2R_e (R_e + h) \dot{\theta} \sin \theta$$

$$\dot{r} = \frac{R_e (R_e + h) \dot{\theta} \sin \theta}{r}$$

Once again:

$$\ddot{r} = \frac{r [R_e (R_e + h) \dot{\theta}^2 \cos \theta] - [R_e (R_e + h) \dot{\theta} \sin \theta] \dot{r}}{r^2}$$

since  $\dot{\theta}$  is constant for a circular orbit.

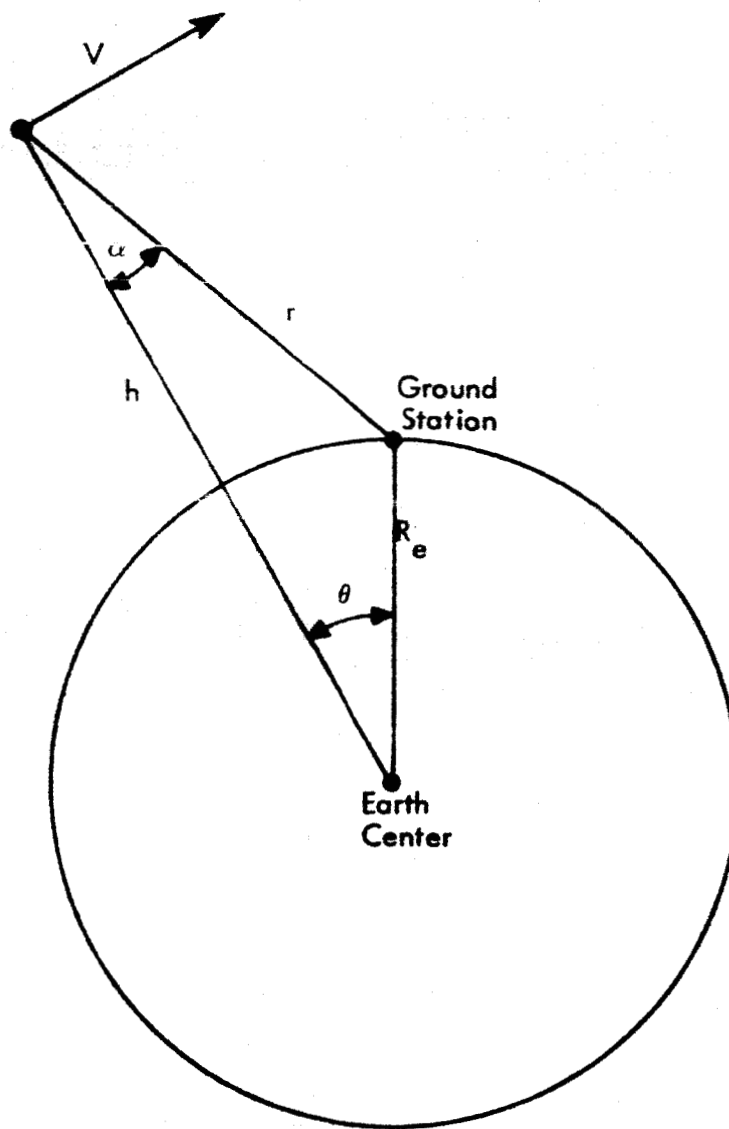


**Figure D-3. Geometry For The Analysis of Signal Dynamics**

These expressions can be evaluated at any point in an orbit by reference to tabulated data<sup>1</sup>.

The maximum values for  $f_d$  and  $\dot{f}_d$  determine the range of signal dynamics over which the phase-locked loops must operate. For a two-way signal:

$$f_d \approx \frac{2 \dot{r}}{\lambda}$$

and

$$\dot{f}_d \approx \frac{2 \ddot{r}}{\lambda}$$

The maximum value for  $f_d$  is at the horizon when  $\alpha$  and  $\dot{r}$  (or  $V \sin \alpha$ ) are maximum. That the maximum value of  $\dot{f}_d$  occurs at the zenith can be seen by simplifying the expression for  $\ddot{r}$ , then differentiating:

$$\ddot{r} = \frac{R_e(R_e + h)\dot{\theta}^2 \cos \theta - \dot{r}^2}{r}$$

$$\frac{d\ddot{r}}{d\theta} = \frac{-r[R_e(R_e + h)\dot{\theta}^2 \sin \theta + 2\dot{r} \frac{d\dot{r}}{d\theta}] - \frac{d\ddot{r}}{d\theta} [R_e(R_e + h)\dot{\theta}^2 \cos \theta - \dot{r}^2]}{r^2} = 0$$

at the zenith this equation is satisfied since:

$$\sin \theta = 0$$

$$\dot{r} = 0$$

$$\frac{d\dot{r}}{d\theta} = 2R_e(R_e + h) \sin \theta = 0.$$

The value for  $\ddot{r}$  at the zenith is:

$$\ddot{r} = \frac{R_e(R_e + h)\dot{\theta}^2}{h} = \frac{R_e V^2}{h(R_e + h)} = \frac{V^2}{h} - \frac{V^2}{R_e + h}$$

Values of  $f_d$  and  $\dot{f}_d$  are tabulated below for several points of interest in the AROD system at a carrier frequency of 2000 Mc.

h (naut. mi.)	Elevation Angle (degrees)	$f_d$ (cps) (two-way)	$\dot{f}_d$ (cps <sup>2</sup> ) (two-way)	r (naut. mi.)
90	5°	$1.0 \cdot 10^5$	68	600
90	90°	0	$4.8 \cdot 10^3$	90
500	23°	$7.9 \cdot 10^4$	82	1000
2000	5°	$5.3 \cdot 10^4$	1.7	3940
2000	90°	0	91	2000

<sup>1</sup>"Space Communications Handbook," Philco Western Development Laboratories Technical Report 1162, 31 August 1959.